DISS. ETH NO. 28056

SEDIMENT SUPPLY CONTROL ON RIVER WIDENING MORPHODYNAMICS AND REFUGIA AVAILABILITY

A thesis submitted to attain the degree of

DOCTOR OF SCIENCES of ETH ZURICH

(Dr. sc. ETH Zurich)

presented by

CRISTINA RACHELLY

MSc ETH Env Eng, ETH Zurich

born on *27.04.1990*
citizen of Geneva, Switzerland

accepted on the recommendation of

Prof. Dr. Robert M. Boes
Prof. Dr. Peter Molnar
Prof. Dr. Stuart Lane
Dr. David F. Vetsch
Dr. Volker Weitbrecht

2021

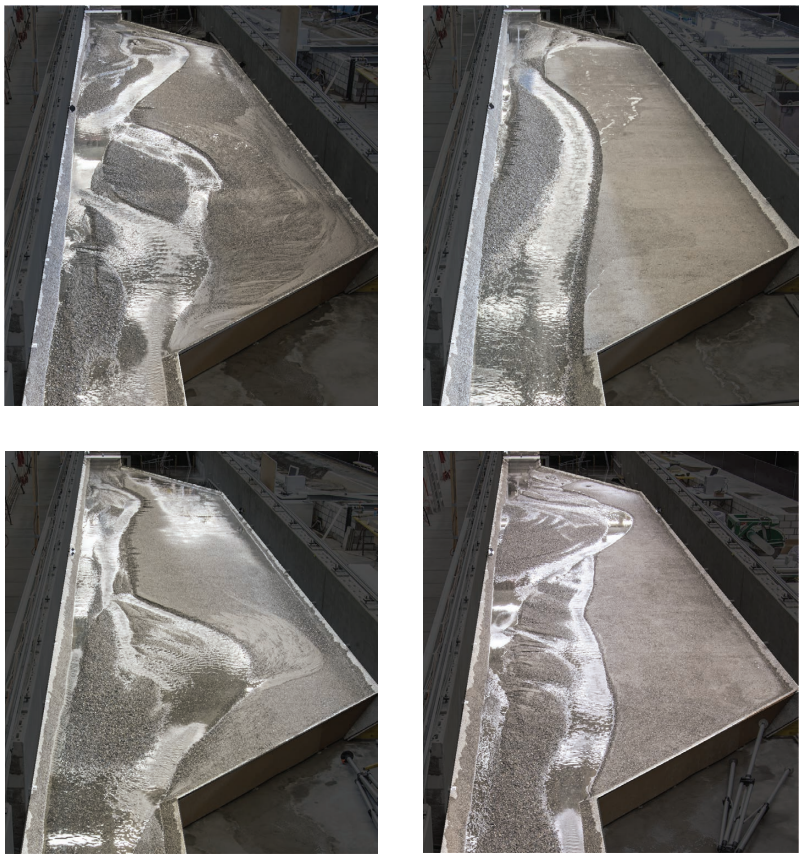

Channel patterns observed in mobile-bed laboratory experiments on dynamic river widening.

Acknowledgments

This doctoral thesis was written during my employment at the Laboratory of Hydraulics, Hydrology and Glaciology (VAW) at ETH Zurich. The project was funded by the Swiss Federal Office for the Environment (FOEN), Grant 16.0113.PJ/P501-1050, and was part of the interdisciplinary research program *Hydraulic Engineering and Ecology* in its fourth program phase *Riverscape - Sediment Dynamics and Connectivity*. The research program is funded by the Swiss Federal Office for the Environment (FOEN), the Swiss Federal Institute of Aquatic Science and Technology (Eawag), the Swiss Federal Institute for Forest, Snow and Landscape Research (WSL), the Platform of Hydraulic Constructions (PL-LCH) at EPFL, and the Laboratory of Hydraulics, Hydrology and Glaciology (VAW) at ETH Zurich. I want to thank all who contributed to the present work with particular acknowledgment to

- Prof. Dr. Robert Boes, VAW director and examiner, for his supportive guidance during my doctoral studies, many valuable discussions throughout the project, and his thorough review of all work related to this thesis.

- Dr. Volker Weitbrecht and Dr. David Vetsch, my supervisors and co-examiners, for their invaluable support, critical scrutiny, and stimulating discussions throughout this project. I immensely enjoyed working with you on both detailed questions and the bigger picture. I also highly appreciated your support in establishing valuable contacts in science and practice.

- The co-examiners Prof. Dr. Stuart Lane, University of Lausanne, and Prof. Dr. Peter Molnar, ETH Zurich, for their review of this thesis and valuable commentary on my work.

- All contributors to the research program *Hydraulic Engineering and Ecology* for interesting exchanges during our project meetings. I would especially like to thank Dr. Christine Weber and Dr. Kate Mathers for opening the field of fluvial ecology to me. I greatly appreciated our in-depth discussions and your willingness to advance interdisciplinary perspectives on river restoration.

- The Master and project theses students Anita Bianchi, Paul Demuth, Andreas Huwiler, Michel Nieto Medina, Patrik Stadtmann, and Barbara Stocker for their valu-

able contributions to this thesis.

- The technical infrastructure team of VAW, including mechanical and electronics workshop, photographer, and graphic designers, for their excellent work.
- All my VAW colleagues and friends, in particular Isabella Schalko, Claudia Beck, and Helge Fuchs, for their continuous encouragement, always helpful input, and a wonderful time at VAW.
- All my friends outside of VAW for their motivation, patience, and ability to take my mind off my thesis for a while.
- My entire family, especially my parents, Gaby and Charly, and my sister Fiona, for unconditionally supporting all my professional and personal endeavors.

Zurich, December 2021 Cristina Rachelly

Table of contents

Abstract

Reach-scale river widening is a restoration measure often implemented in channelized rivers with the aim of reactivating morphodynamic processes and increasing habitat heterogeneity. Following process-based restoration principles, widened reaches are increasingly implemented as dynamic widenings, where construction efforts are limited to the removal of bank protection and measures to locally initiate bank erosion. Despite significant advances in our understanding of fluvial processes, the interaction of sediment supply with river widening morphodynamics is still inadequately understood. In addition, the ecological assessment of reach-scale restoration measures often disregards the importance of certain habitats functioning as refugia for aquatic organisms during floods.

In this thesis, the morphological development of one-sided river widenings in channelized subalpine gravel-bed rivers in response to different sediment supply levels was studied using mobile-bed laboratory experiments. The initial experimental setup consisted of a straight channel with a longitudinal slope of around one percent and an adjacent floodplain 25 channel widths long and three wide. After removing the fixed bank, the floodplain was available for lateral erosion and channel shifting. Seven experimental series consisting of sequences of steady bed-forming discharge and unsteady larger flood hydrographs were conducted. Therein, different sediment supply scenarios with supply rates of 20%, 60%, 80%, and 100% of the transport capacity of the initial channel were tested. A combined analysis of the resulting widening topographies and the hydraulic conditions obtained from two-dimensional hydrodynamic numerical modeling allowed a detailed assessment of morphodynamic processes and potential refugia availability.

Sediment supply was found to exert fundamental control on the intensity of lateral erosion and sediment relocation processes in river widenings. Sediment supply rates close to the channel transport capacity were shown to promote channel widening and increase lateral channel-floodplain connectivity. In contrast, sediment supply considerably lower than the channel transport capacity resulted in a stable single-thread channel disconnected from its floodplain. Furthermore, the results indicate that morphodynamic processes can be reactivated by increasing sediment supply in previously sediment-starved reaches after a transition period of several years to decades. The hydro-morphological conditions in different widenings were also shown to be closely linked to potential flood refugia availability. Morphodynamically active widenings thereby generally offer more favor-

able conditions for aquatic organisms during high flows.

The present work highlights that sediment supply is a key driver of morphodynamic processes and adds to our understanding of how reach-scale river restoration may successfully increase the resistance and resilience of fluvial ecosystems during floods.

Kurzfassung

Flussaufweitungen werden häufig als Revitalisierungsmassnahme in kanalisierten Fliessgewässern umgesetzt. Ziel ist es, in einem begrenzten Perimeter naturnahe morphodynamische Prozesse zu reaktivieren und die Vielfalt und Qualität an Lebensräumen zu erhöhen. Entsprechend den Grundsätzen der prozessorientierten Fliessgewässerrevitalisierung werden Aufweitungen vermehrt eigendynamisch ausgeführt. Dabei werden bauliche Eingriffe auf die Entfernung des festen Uferschutzes und gegebenenfalls lokale Massnahmen zur Initiierung von Seitenerosion reduziert. Trotz erheblicher Fortschritte in den Kenntnissen fluvialer Prozesse ist die Interaktion zwischen Geschiebezufuhr und der morphodynamischen Entwicklung von Flussaufweitungen noch immer ungenügend erforscht. Zudem wird bei der ökologischen Beurteilung von Revitalisierungsmassnahmen die Verfügbarkeit von Refugien häufig ausser Acht gelassen. Refugien sind Lebensräume, die aquatischen Organismen während Hochwasserereignissen vorübergehend Schutz bieten.

In der vorliegenden Arbeit wurde mit Hilfe von Laborexperimenten mit beweglicher Sohle die morphologische Entwicklung von einseitigen eigendynamischen Aufweitungen in voralpinen Kiesflüssen in Abhängigkeit der Geschiebezufuhr untersucht. Der Versuchsaufbau bestand aus einem geraden Kanal mit einem Längsgefälle von einem Prozent und einem angrenzenden Vorland mit einer Länge von rund fünfundzwanzig Kanalbreiten und einer Breite von etwa drei Kanalbreiten. Nach Entfernung des festen Uferschutzes zwischen Kanal und Vorland wurde die Erosion des Vorlands zugelassen. Insgesamt wurden sieben Versuchsreihen, bestehend aus Sequenzen von stationären und instationären Abflüssen, durchgeführt. Dabei wurden verschiedene Geschiebeszenarien mit Zugaberaten von 20%, 60%, 80% und 100% der Transportkapazität des Kanals geprüft. Die kombinierte Auswertung der resultierenden Topographien und der mittels zweidimensionaler numerischer Simulationen ermittelten hydraulischen Verhältnisse ermöglichte eine detaillierte Betrachtung der morphodynamischen Prozesse und Refugienverfügbarkeit.

In den Experimenten zeigte sich, dass der Geschiebezufuhr eine zentrale Bedeutung für die Intensität der Seitenerosions- und Geschiebeumlagerungsprozesse zukommt. Zugaberaten nahe der Transportkapazität im Kanal führten zu einer kontinuierlichen Gerinneaufweitung und einer Erhöhung der lateralen Vernetzung von Hauptgerinne und Vorland. Im Gegensatz dazu blieb das Einzelgerinne bei geringerer Geschiebezufuhr sehr

stabil. Es resultierte ein vom Vorland abgekoppelter Hauptkanal mit relativ homogenen Fliessverhältnissen. Die morphodynamischen Prozesse in einer geschiebearmen Aufweitung können durch eine Erhöhung der Geschiebezufuhr wieder reaktiviert werden. Allerdings hat sich gezeigt, dass es mehrere Jahre oder Jahrzehnte dauern kann, bis sich eine ähnliche morphodynamische Aktivität wie bei hoher Geschiebezufuhr einstellt. Die hydro-morphologischen Verhältnisse wirken sich zudem stark auf die potentielle Refugienverfügbarkeit während Hochwasserereignissen aus. Die Bedingungen für aquatische Organismen sind dabei in morphodynamisch aktiven Flussaufweitungen generell besser als in morphodynamisch inaktiven Abschnitten.

Die vorliegende Arbeit unterstreicht die zentrale Bedeutung der Geschiebezufuhr für morphodynamische Prozesse, die ihrerseits als wesentliche Voraussetzung für Habitatvielfalt und -qualität gelten. Die gewonnenen Erkenntnisse tragen zudem zu unserem Wissen bei, wie Revitalisierungsmassnahmen die Resistenz und Resilienz aquatischer Populationen während Hochwasserereignissen erhöhen können.

1 Introduction

1.1 Motivation

Fluvial landscapes are shaped by interacting hydrological, geological, and biological processes (Castro and Thorne 2019). The varied interactions between these driving processes generate a wide range of river types. They host fluvial ecosystems that are characterized by a small-scale and intricate mosaic of habitat patches that is reorganized episodically (Stanford *et al.* 2005). This patchy and dynamic nature of fluvial ecosystems fosters an extraordinary biodiversity (Dudgeon *et al.* 2006).

Besides their remarkable ecological significance, fluvial systems are also of high socio-economic importance. The history of human interaction with rivers is long and includes both their utilization for society's benefit and the protection of society against the destructive forces of flood hazards. Rivers are used as transport routes, freshwater and sediment sources, to produce hydropower, and as recreational areas. Expanding agriculture adjacent to rivers and increased population pressure has moved settlements and infrastructure closer to rivers, thus necessitating protection against flood hazards. While these forms of river utilization have massively contributed to the establishment of our modern societies, the ecosystem health of many river systems has been severely compromised by significant anthropogenic modification and over-exploitation (Schinegger *et al.* 2012; Downs and Piégay 2019). In Switzerland, for example, 22% of aquatic and riparian plant, animal, and fungal species are extinct or threatened with extinction (Cordillot and Klaus 2011), and floodplain areas were reduced by 36% between 1900 and 2010 (Lachat *et al.* 2010).

The realization that the ecological state of rivers is critical for the delivery of ecosystem goods and services to society (Böck *et al.* 2018) has led to the development of the discipline of river restoration over recent decades (Bernhardt *et al.* 2005; Palmer *et al.* 2005; Wohl *et al.* 2015b). River restoration science and practice pursues the goal of improving the ecological state of fluvial systems to ensure a sustainable delivery of ecosystem goods and services (Dufour and Piégay 2009). Reflecting the wide range of human modifications of river systems, restoration efforts can focus on various river characteristics such as channel geometry, the hydrological and sedimentological regime, or water quality (Bernhardt *et al.* 2005; Woolsey *et al.* 2005; Roni *et al.* 2008; Kurth and Schirmer 2014). They also act on various spatial scales, from the localized re-establishment of certain habitats to restoration

strategies targeting entire watersheds. Many countries and regions are now pursuing river restoration strategies based on regulations such as the EU Water Framework Directive 2000 or the Swiss Water Protection Act of 1991 and 2011. Swiss restoration efforts include (i) spatial planning elements to secure room for rivers, (ii) measures at hydropower plants to re-establish sediment continuity and fish migration as well as mitigate hydropeaking, and (iii) reach-scale restoration of 4,000 km or 6.3% of the country's river network (e.g., Bammatter *et al.* 2015).

One example of a reach-scale restoration measure focusing on channel geometry is artificial *river widening* (Figure 1.1). Locally increasing river width is a response to the extensive historical channelization and narrowing of river courses (e.g., Hohensinner *et al.* 2021). In Switzerland, the first river widening was realized in 1991/92 at the Emme River (e.g., Zarn 1992; Rohde *et al.* 2005; see Section 2.6). It was implemented by active floodplain lowering to create an approximately 85 m wide channel of almost 500 m length. The goal was to replace transversal bed sills installed for erosion control with a more near-natural river reach while maintaining a certain bed elevation. Laboratory experiments investigating this first river widening were performed at the Laboratory of Hydraulics, Hydrology and Glaciology (VAW) at ETH Zurich (Zarn 1992). More research on river widenings has since been conducted at VAW. Hunzinger (1998) carried out systematic laboratory experiments to develop design guidelines for mechanically excavated river widenings, that is, river widenings implemented by active floodplain lowering. He found that the stabilizing effect of river widenings only fully develops if the river widening is long enough for the hydraulic conditions to fully adapt to the increased river width. Given the increasing number of implemented river widenings in Switzerland and the entire Alpine region, the associated opportunities and limitations were the topic of a workshop held at VAW (VAW 2006). The finding that widenings in eroding rivers are not able to stabilize the bed or may even aggravate the erosional state contributed an important clarification to the question of their stabilization potential (Requena *et al.* 2005; VAW 2007). In addition, experiments conducted by Marti (2006) suggested that low sediment supply may impact the morphology within the widening by favoring single-thread channels over more complex channel patterns.

While the first artificial river widenings were implemented by active excavation of the adjacent floodplain, the focus later shifted to dynamic river widening, that is, enabling

channel widening by lateral erosion within a defined perimeter. Requena (2008) conducted laboratory experiments to strengthen the process understanding of lateral erosion. It was recognized that lateral erosion is also fundamentally connected to sediment transport restoration efforts such as sediment replenishment (Friedl *et al.* 2015; Friedl 2017). Finally, numerical modeling of river widenings using one- and two-dimensional morphodynamic models was studied by Berchtold (2015). Examples of implemented reach-scale river widenings can also be found in neighbouring countries (e.g., Habersack *et al.* 2000; Klösch *et al.* 2011; Hafner *et al.* 2012) and internationally (e.g., Williams *et al.* 2020).

Figure 1.1 (a) Lateral erosion in the river widening Schäffäuli, Thur River (Orthophoto and data: geotopo ag, Frauenfeld), (b) pioneer vegetation in the river widening Augand, Kander River (Photo: Tiefbauamt des Kantons Bern, Oberingenieurkreis I, 2006) and (c) eroded riverbanks in the river widening Augand, Kander River. Both Thur and Kander River are gravel-bed rivers in Switzerland.

Over the past years, the question of how channel widening interacts with sediment supply and associated transport processes both on the regional and local scale has emerged as a central research topic, especially in the context of the Swiss bed-load restoration strategy (Schälchli and Kirchhofer 2012). Our understanding of how channel geometry interacts with sediment supply remains limited despite extensive previous research activity. This lack of knowledge is especially problematic in the case of heavily modified rivers where

limited space is available and the flood hazard potential is usually high. Also, increasing attention is paid to the effectiveness of restoration efforts. The ability to design restoration concepts that decrease the vulnerability of fluvial systems to disturbances has gained importance, especially in the face of increasing occurrence of extreme hydrological conditions due to climate change (e.g., Schmocker-Fackel *et al.* 2021). Given that reach-scale river widening as well as the restoration of the sediment regime are central to many restoration strategies, further research on the interaction of widening morphodynamics and sediment transport as well as on the ecological benefits of widenings is crucial.

1.2 Objectives

This work aims to improve the understanding of sediment supply interactions with morphodynamic processes, specifically in widened reaches of heavily impacted gravel-bed rivers. Large-scale laboratory experiments were conducted at the Laboratory of Hydraulics, Hydrology and Glaciology (VAW) at ETH Zurich and combined with hydrodynamic numerical simulations. The following research questions were addressed:

- How does sediment supply influence the morphodynamic development of one-sided dynamic river widenings?
  It was hypothesized that low sediment supply conditions may lead to higher lateral channel stability with reduced morphodynamic activity compared to conditions where sediment supply and transport capacity are roughly balanced. Low sediment supply could lead to inactive widenings despite the absence of fixed bank protection.

- If low sediment supply restricts morphodynamic activity within the widening, is the process reversible by once again increasing sediment transport or applying structural bank erosion initiation measures?
  It was hypothesized that a certain degree of recovery towards near-natural morphodynamic processes may be achieved by such measures.

- Does sediment supply affect the ecological effectiveness of dynamic river widenings, specifically the availability of aquatic flood refugia?
  It was hypothesized that conditions where sediment supply and transport capacity are roughly balanced may be favorable in terms of potential refugia availability due to higher hydro-morphological variability and stronger channel-floodplain connectivity associated with overall higher morphodynamic activity. While bed-load

transport is itself a disturbing force, it is hypothesized that conditions with artificially reduced sediment supply and conveyance are overall more detrimental to fluvial ecosystem resistance and resilience.

This study is part of the interdisciplinary research program *Hydraulic Engineering and Ecology* in its fourth program phase *Riverscape - Sediment Dynamics and Connectivity* (Vetsch *et al.* 2018). The research program is funded by the Swiss Federal Office for the Environment (FOEN), the Swiss Federal Institute of Aquatic Science and Technology (Eawag), the Swiss Federal Institute for Forest, Snow and Landscape Research (WSL), the Platform of Hydraulic Constructions (PL-LCH) at EPFL, and the Laboratory of Hydraulics, Hydrology and Glaciology (VAW) at ETH Zurich.

1.3 Outline

This doctoral thesis is divided into eight chapters. Chapter 2 establishes the context of this research project by outlining the practice and challenges of river restoration in general and river widening in particular. The literature review in Chapter 3 focuses on fluvial morphology and morphodynamic processes relevant for river widenings. The concept of aquatic refugia is introduced, which is of relevance for the ecological assessment of river widenings. Chapter 4 details the experimental setup and procedure of the laboratory experiments and numerical simulations. The results of the laboratory experiments and hydronumerical simulations are presented and discussed with regard to sediment supply control on morphodynamics (Chapter 5) and refugia availability (Chapter 6). Finally, management implications (Chapter 7) and conclusions (Chapter 8) are presented.

2 Background

2.1 Overview

This chapter contains background information on the science and practice of river restoration. Section 2.2 outlines the characteristics of natural river systems, while Section 2.3 describes the ways in which humans have impacted them. Section 2.4 contains general information on river restoration. The specific restoration measure of river widening is explained in Section 2.5. Finally, selected examples of river widenings are portrayed in Section 2.6.

2.2 The natural riverscape

Natural fluvial landscapes result from hydrological, geological, and biological conditions and their complex interactions (Castro and Thorne 2019). More tangibly, the main physical processes that shape riverscapes are the flow regime (Poff *et al.* 1997), sediment regime (Wohl *et al.* 2015a), and large wood regime (Wohl *et al.* 2019). A regime thereby collectively describes entrainment and transport processes as well as their magnitude, frequency, duration, timing, and rate of change (cf. Poff *et al.* 1997). These processes act and interact on various spatio-temporal scales, creating a patchy, dynamic landscape referred to as a *shifting habitat mosaic* (Stanford *et al.* 2005). The commonly high habitat heterogeneity of natural riverscapes hosts a biota of extraordinary diversity.

Another defining feature of fluvial environments is their directed network structure. The river network structure features various longitudinal gradients, for example, the increase in discharge and stream dimensions and simultaneous decrease in slope and grain diameter in downstream direction. Similarly, many biological and chemical processes show a longitudinal gradient such as the ratio of solute to particulate organic matter increasing in downstream direction. This fundamental quality of longitudinal connectivity was first introduced as the *River Continuum Concept* (RCC; Vannote *et al.* 1980). While the RCC represents a central framework for stream ecology, it is important to note that natural river systems are not typically continuous gradients along their entire length. Rather, changes in large-scale geological conditions or tributaries (e.g., Scorpio *et al.* 2018) can reset the river continuum locally, resulting in unique river system configurations. While the original RCC primarily focused on mainstem rivers, more recent concepts aim at providing a more holistic view including local conditions and the network structure of entire

river ecosystems (see Doretto *et al.* 2020 for a recent review).

Longitudinal connectivity may be the most apparent feature of natural fluvial environments, but their lateral, vertical, and also temporal connectivity is in fact just as relevant. These dimensions of connectivity were conceptualized by Ward (1989) as the *four-dimensional nature of lotic ecosystems* (see also Wohl 2017 for a recent review). Riverscapes are characterized by a strong lateral gradation from the baseflow channel to the outermost boundaries of the fluvial corridor. Habitats closer to the baseflow channel are generally more often inundated or subject to scouring, and support pioneer macrophyte vegetation that is adapted to rapid establishment on bare surfaces. The decreasing inundation and scouring frequency with increasing distance to the channel generates a lateral gradient of environmental conditions that supports a wide variety of biota (e.g., Tockner and Stanford 2002). For example, natural riparian vegetation shows a clear lateral succession pattern (e.g., Hohensinner *et al.* 2011). Likewise, fluvial environments show high degrees of vertical connectivity with the hyporheic zone. The interactions are thereby driven by spatially and temporally variable infiltration and exfiltration processes (Stanford and Ward 1993; Dole-Olivier *et al.* 1997).

2.3 Anthropogenic modifications of fluvial systems

Anthropogenic interaction with and modification of fluvial environments goes far back in history, however, pressures have significantly increased in recent decades to centuries (e.g., Downs and Piégay 2019). The timelines of anthropogenic river modifications differ globally, but as this thesis focuses on conditions in Alpine gravel-bed rivers, the historical development is hereafter outlined for the case of Europe. Starting in the 19th century, many river systems were subject to systematic channelization and straightening to yield agriculture and settlement land, protect it against floods, and enable navigation. Among the 143 largest rivers of the European Alps, multi-channel patterns declined by 56%, and 33% of their total length is now channelized (Hohensinner *et al.* 2021). Simplification of channel geometry caused more homogeneous flow fields with uniformly elevated bed shear stresses during high flows, prompting bed incision and channel narrowing (e.g., Surian and Rinaldi 2003; Scorpio *et al.* 2018). The resulting decrease in lateral channel-floodplain connectivity led to significant terrestrialization of riparian habitats and the deactivation of the floodplain as major sediment source (Tockner and Stanford 2002; Hohensinner *et al.* 2011; Janssen *et al.* 2020). Besides detrimental effects of channeliza-

tion on river ecosystem health such as that of macroinvertebrate communities (Blake and Rhanor 2020), channel incision also causes structural problems at bridges, reduced stability of bank protection, and lowering of groundwater tables. To counteract problematic channel incision, sequences of lateral bed sills were often built that now contribute to the longitudinal fragmentation of rivers.

During the 20th century, rivers were further impacted by the construction of dams and other transversal structures. Dams are especially disruptive to the natural longitudinal connectivity of rivers (Stanford and Ward 1983). Depending on their design and operation, dams can severely alter various river characteristics upstream and especially downstream of their location. Changes of the hydrological regime are common, for example, alterations of flow seasonality, reduction of peak flows, or water diversion into other catchments. The aspect most relevant to this thesis is their disruptive effect on the sediment regime associated with the interruption of sediment conveyance and possible alterations of the flow regime. In the impoundment zone of dams and other transversal structures, sediment can be partially or fully retained, causing a deficit in the downstream reach (Kondolf 1997). The imbalance between sediment supply and transport capacity in downstream reaches is further aggravated in channelized reaches. In contrast, Alpine water intakes may lead to excess sediment delivery in comparison to the transport capacity due to water abstraction (Gabbud and Lane 2016). In many rivers, gravel was also extracted to be used as construction material (Kondolf 1997; Moretto *et al.* 2014). Furthermore, the dangers due to excessive sediment transport during floods were met with the construction of sediment traps (e.g., Piton and Recking 2016; Mathers *et al.* 2021). Collectively, dam construction, sediment extraction, and land use changes (e.g., afforestation) further intensified channel narrowing and incision by reducing sediment supply to the channel and obstructing downstream sediment conveyance (Syvitski *et al.* 2005).

These modifications have significantly degraded many river systems worldwide resulting in a dramatic decline in freshwater biodiversity and a threat to freshwater ecosystem services societies rely on (Dudgeon *et al.* 2006; Böck *et al.* 2018). River systems are often affected by multiple stressors, including flow abstraction and regulation, water quality deterioration, habitat degradation, and sediment retention and extraction (Schinegger *et al.* 2012; Downs and Piégay 2019; Janssen *et al.* 2020). According to Schinegger *et al.* (2012), 59% of European rivers are impacted in terms of water quality, 41% in terms of

their hydrological regime and 38% in terms of their morphology. Considering only the Alps, morphological pressures are most common (70%), but also water quality and hydrological impacts (40%) and connectivity impairments (50%) are widespread (Schinegger *et al.* 2012).

2.4 River restoration

2.4.1 Restoration approaches and challenges

Mainly since the 1990s, a growing number of river restoration measures are implemented to mitigate the severe degradation of river systems (National Research Council 1992; Woolsey *et al.* 2005; Kurth and Schirmer 2014). As river systems differ widely, so do restoration measures. The analysis of a database of 37,099 restoration projects in the U.S. showed the most common goals to be (i) enhancement of water quality, (ii) management of riparian zones, (iii) improvement of instream habitat, (iv) fish passage, and (v) bank stabilization (Bernhardt *et al.* 2005). Further goals can be floodplain reconnection, aesthetics / recreation / education, instream species management, or dam removal (Wohl *et al.* 2015b; see also Roni *et al.* 2008 for a global overview on restoration techniques).

On a conceptual level, two main strategies can be identified: *reconnection* versus *reconfiguration* projects (Wohl *et al.* 2015b). These strategies are based on the distinction of three kinds of restoration intervention (McDonald *et al.* 2004):

- Field of dreams: *structure-based* or *form-based*, focus on the re-establishment of a past form to achieve a desired consequence (e.g., re-meandering)
- System function: *process-based*, focus on the re-establishment of desired processes
- Keystone approach: hybrid approach, restoration of some essential structural keystones in order to enable the re-establishment of desired processes

While the field of dreams approach was and is widely used in restoration practice, a growing scientific community argues that this approach is too short-sighted and anthropocentric, and process-based restoration should be pursued instead (Kondolf *et al.* 2006; Beechie *et al.* 2010; Polvi *et al.* 2020). Several studies have found no positive correlation between increased structural diversity and invertebrate or fish biodiversity thus challenging the *habitat heterogeneity paradigm* (i.e., habitat variability seen as the limiting

factor for fluvial ecosystem health) that informs most of restoration practice (e.g., Palmer *et al.* 2010; Wohl *et al.* 2015b). Examples of processes that should instead be restored are the flow regime (Poff *et al.* 1997), sediment fluxes (Wohl *et al.* 2015a), and the establishment and removal of vegetation (Hohensinner *et al.* 2011; Wohl *et al.* 2019; see also Section 2.2). The demand for more process-based restoration also indirectly calls for larger-scale restoration projects instead of the often implemented reach-scale projects (Gurnell *et al.* 2016; Polvi *et al.* 2020).

To set either structure-based or process-based restoration goals, some type of reference system is needed. Often, a historical or natural state is used although it is generally questionable whether we even know this state and whether it can be reinstated (e.g., Dufour and Piégay 2009). In light of the many constraints that current societies impose on restoration feasibility, more pragmatic approaches might be necessary in order to achieve progress. Instead of aiming for a natural state, an approach to move towards the least degraded and most ecologically dynamic state is suggested by Palmer *et al.* (2005). Dufour and Piégay (2009) propose to let the maximization of human benefit inform river restoration. Applied to sediment transport, Wohl *et al.* (2015a) distinguish a natural from a balanced sediment regime and argue that a recreation of a natural sediment regime may neither be feasible nor desirable.

A further challenge in river restoration concerns the monitoring of restoration success. If specific and measurable restoration goals are formulated, the impact of restoration measures can be assessed before and after the restoration, or at a control and the impact site. Pre-restoration and control site monitoring thereby provides the baseline data against which the success of a restoration project is measured (Jungwirth *et al.* 2002). Although there is a general consensus that monitoring is essential to the improvement of restoration practice, it is often neglected. Bernhardt *et al.* (2005) criticize that only 10% of 37,099 US restoration projects were monitored and that this omission impairs the restoration community's collective learning process about the effectiveness of different restoration measures (cf. Weber *et al.* 2019). The lack of quantitative data to enable broad, comparative studies on the success of restoration projects also contributes to the unresolved controversy over form versus process (Lave 2009).

2.4.2 River restoration in Switzerland

Starting in the 1950s, Switzerland has gradually incorporated more stringent water quality protection into its legislation (Eawag 2021). In the 1990s, the structural integrity of waters and floodplains also came into focus. Following the implementation of the Swiss Waters Protection Act (WPA) in 1991, a mission statement (BUWAL/BWG 2003) identified three main fields of action: (i) sufficient space for water, (ii) sufficient water supply, and (iii) sufficient water quality. Kurth and Schirmer (2014) reported a steady increase of cumulative restored river length starting in 1990. They name habitat provision, channel bed remodeling, and deculverting as the most common restoration measures implemented in Switzerland between 1979 and 2012. Woolsey *et al.* (2005) note that measures to improve structural variability and lateral connectivity were most common at the time, while measures to improve large-scale processes such as sediment connectivity were still rare.

In 2011, a major revision of the Swiss Waters Protection Act (WPA) formalized the restoration efforts initiated in prior years. It states that all restoration efforts must be directed towards sustainable freshwater management, which has ecological, economic, and societal dimensions (cf. BUWAL/BWG 2003; Woolsey *et al.* 2005). Sustainable freshwater management therefore includes the protection of freshwater ecosystems, the protection of society against (flood) hazards, and the protection of socio-economic benefits of rivers and lakes.

The Swiss river restoration strategy can be broadly divided into three parts (details refer to fluvial systems only):

- *Spatial planning*: Area along flowing waters is newly designated as riparian zone in spatial planning. The width of the riparian zone is thereby defined in relation to the natural bed width free of vegetation, and is thus greater for larger water bodies. Two relations between bed width and riparian zone width were defined. The minimum requirement for riparian width is thought to be sufficient to ensure flood protection and basic ecological functions. The maximum requirement is assumed to promote biodiversity and is mainly applied in conservation zones. Within the riparian zone, new construction is limited to site-specific projects of public interest (e.g., bridges), and the use of fertilizer and pesticides is prohibited.

- *Reach-scale restoration*: Of roughly 65,000 km flowing waters in Switzerland,

14,000 km were identified to be eco-morphologically heavily impacted. 4000 km thereof are planned to be restored by the year 2090, amounting to a restoration rate of 50 km/a (Bammatter *et al.* 2015). This restoration strategy thus focuses on reach-scale measures to restore typical fluvial processes and structures, increase connectivity, and provide suitable habitat to lotic biota.

- *Mitigation of negative hydropower impacts*: This restoration strategy is linked to specific, mostly transversal structures in rivers such as hydropower plants or sediment traps. Mitigation focuses on (i) fish passage, (ii) hydropeaking, and (iii) sediment continuity. Roughly (i) 1000, (ii) 100, and (iii) 500 structures were identified to require mitigation measures until 2030, respectively (Bammatter *et al.* 2015).

Recent developments include the introduction of a standardized impact monitoring concept to allow the comparison of different restoration approaches and the identification of particularly effective measures (Weber *et al.* 2019). Restoration and hazard protection planning also continuously incorporates more knowledge on climate change impacts including the increased risk for prolonged low flow periods, higher water temperatures, and more frequent extreme floods (Schmocker-Fackel *et al.* 2021).

2.5 River widening

2.5.1 Terminology

River widening refers to the reach-scale removal or setback of bank protection structures to create a wider channel section with a potentially more complex morphology. The morphological development of river widenings and their impact on the upstream and downstream river reaches strongly depends on the construction method. Although the specific construction method is often a combination of techniques and reflects local circumstances, two general methods can be identified, hereafter referred to as *excavated* and *dynamic* river widening (Figure 2.1). Both excavated and dynamic river widenings can be implemented with a two-sided, one-sided, or alternating planform.

- *Excavated river widening* is defined as the local removal of bank protection and the lowering of the surrounding terrain within a predefined perimeter (Figure 2.1a; Hunzinger 1998). The bed elevation in the widening can be equal to the former

channel bed, or a vertical bed offset can be anticipated (Hunzinger 1998; see Section 2.5.3).

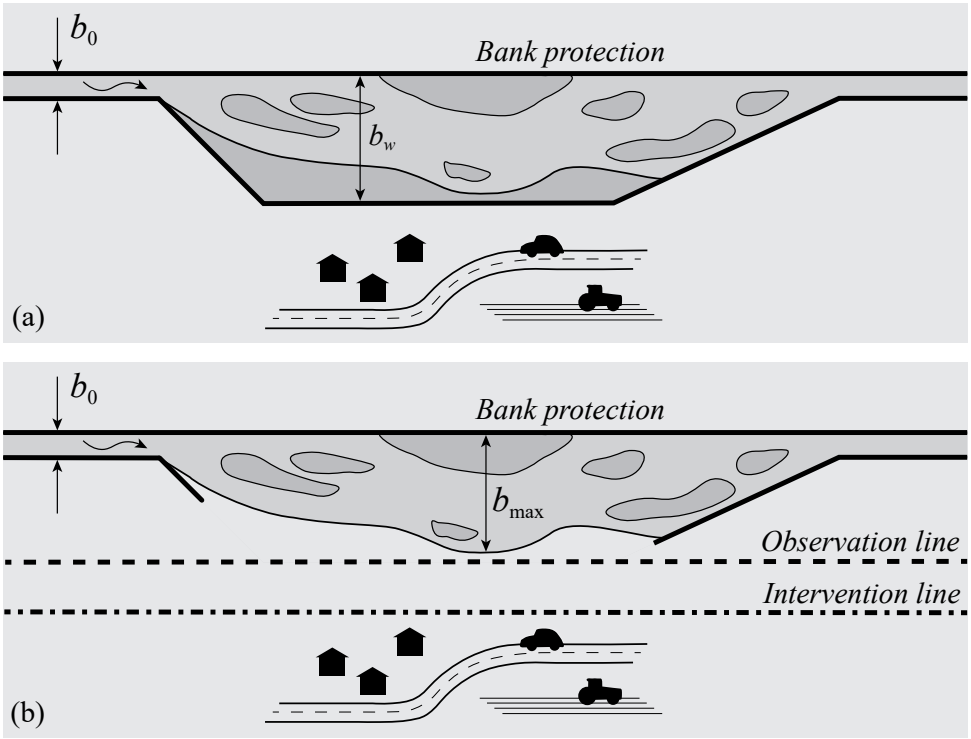

Figure 2.1 Schematic illustration of a one-sided (a) excavated river widening and (b) dynamic river widening. The concepts can be transferred to other planform configurations.

- *Dynamic river widening* takes advantage of lateral erosion and sediment redistribution processes during floods (Figure 2.1b). For this purpose, bank protection is removed or set back along a predefined length to enable lateral erosion of the floodplain (Requena 2008; Williams *et al.* 2020; Addy and Wilkinson 2021). In many cases some type of erosion initiation measure will be necessary. Examples of initiation measures are excavated secondary channels in the floodplain, flow deflectors on one river bank (Die Moran *et al.* 2013; Friedl 2017), or localized floodplain lowering. Depending on the local settings, the widening perimeter must be spatially limited. In Switzerland, the definition of an observation and intervention line is customary (Figure 2.1b; Künzi and Kimmerle 2017). The observation line delineates the perimeter where bank erosion and channel shifting are allowed without intervention. Should lateral erosion pass the observation line, possible interventions to prevent further lateral erosion will be evaluated. The outermost boundary of the widening, defined by the intervention line, may be secured by bank protec-

tion structures hidden in the floodplain where necessary (Requena 2008; Künzi and Kimmerle 2017).

2.5.2 River widening as a restoration measure

River widening is a widely used measure to restore channelized rivers at the reach scale (e.g., Habersack *et al.* 2000; Rohde *et al.* 2005; Habersack and Piégay 2007; Weber *et al.* 2009; Klösch *et al.* 2011; Aufleger *et al.* 2012; Habersack and Klösch 2012; Hengl *et al.* 2012; Hunziker 2012). Early river widenings were often of the excavated type while more recent projects tend towards dynamic river widening or some kind of mixed implementation. River widenings have been associated with rejuvenation of riparian vegetation (Martínez-Fernández *et al.* 2017), re-establishment of riparian semi-terrestrial habitats (Rohde *et al.* 2005; Jähnig *et al.* 2009), and greater habitat heterogeneity (Weber *et al.* 2009; Klösch *et al.* 2011; Williams *et al.* 2020). However, positive effects on the fluvial ecosystem cannot always be demonstrated. For example, Weber *et al.* (2009) reported only a weak response of fish assemblages to river widening.

River widening as described here is similar to restoration concepts such as the *erodible river corridor* (Piégay *et al.* 2005) or *freedom space* (Biron *et al.* 2014) but the perimeter is usually more limited in length and width (cf. Rohde *et al.* 2005). Limited land availability in heavily built-up areas often makes it virtually impossible to implement widenings that are longer than several hundred meters despite indications that longer river widenings would generate greater ecological benefits (Rohde *et al.* 2005; Weber *et al.* 2009).

The interaction of the widened reach and the bed-load balance on a larger scale is often mentioned as a central challenge related to river widening (e.g., Habersack *et al.* 2000; Habersack and Klösch 2012; Hengl *et al.* 2012; Hunziker 2012; Berchtold 2015). As described in Chapter 1, a widening in a river with sufficient bed-load transport can be expected to have a stabilizing effect on the bed elevation. However, river widenings are not fixpoints built from concrete but instead dynamic systems that react to varying hydrological and sedimentological conditions (Habersack *et al.* 2000). As a consequence, the stabilizing effect of a river widening is absent or bed erosion may even be aggravated in eroding rivers (Requena *et al.* 2005; Hafner *et al.* 2012; Berchtold 2015).

River widenings may also significantly impair sediment supply to the downstream reach. Whereas excavated river widenings may cause a temporary sediment deficit (see Section 2.5.3), dynamic river widenings likely promote a more gradual morphological

adjustment to increasing channel width and, therefore, a less severe disruption of sediment continuity (Klösch *et al.* 2011; Rachelly *et al.* 2018). Overall, sediment transport emerges as a central topic related to river widenings.

2.5.3 Morphological development of excavated river widenings

Hunzinger (1998) has conducted systematic laboratory experiments on symmetrical excavated river widenings. The following five phases describe the general morphological development of a widening after implementation and for sediment supply that is balanced with the transport capacity of the initial channel (Figure 2.2). Note that these phases refer to a widening where excavated sediment was removed, that is, no vertical offset was anticipated (Figure 2.2, ①).

- Phase ①: The hydraulic conditions adjust to the widened channel. The flow accelerates upstream of the channel expansion and decelerates at the downstream widening end due the flow constriction at the transition to the channelized reach.
- Phase ②: At the upstream end, flow acceleration leads to a higher transport capacity causing local bed degradation. The eroded sediment is deposited at the upstream end of the widening, where transport capacity is abruptly reduced. Bed-load is not transported through the widening at this point. This temporary sediment deficit leads to erosion in the downstream reach. A constriction scour just downstream of the widening is superimposed on this general erosion tendency.
- Phase ③: The upstream flow acceleration is counteracted by the growing sediment wedge within the widening. The erosional tendency in the upstream channel is thus reversed into aggradation. The slope of the aggradation in the widening S_w is steeper than the channel slope S_{ch}. It follows that bed elevation in the upstream channel will rise above the initial bed profile. Downstream of the widening, the erosion is ongoing because there is still no substantial bed-load transport through the widening. The maximum scour depth $t_{s,\max}$ is reached during this phase.
- Phase ④: The sediment wedge in the widening has grown to reach the downstream widening end and now enables bed-load to be transported through the widening perimeter. This leads to a reversal of the erosion tendency downstream while the upstream bed further aggrades.

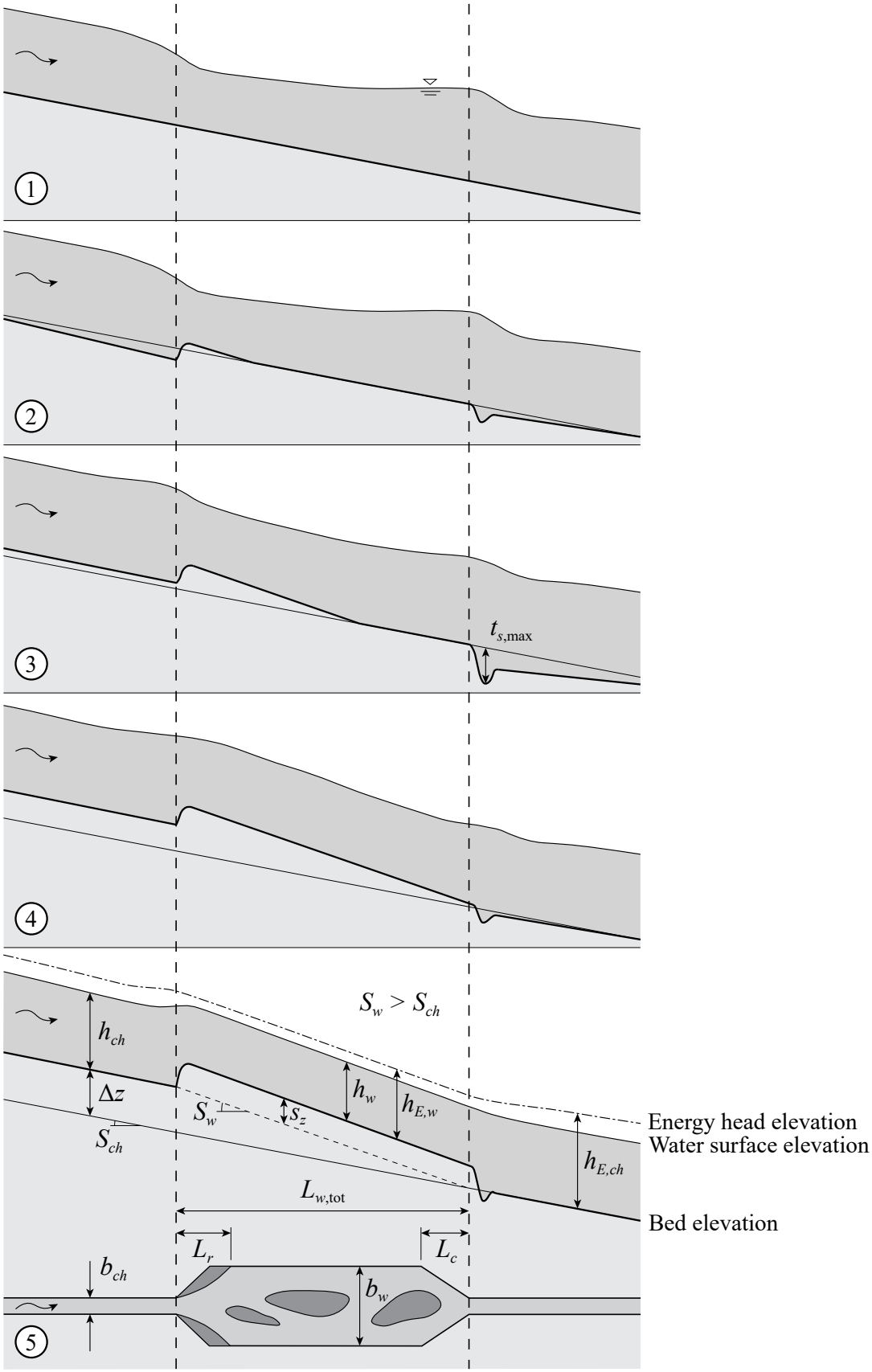

Figure 2.2 Morphological development of excavated river widenings (adapted from Hunzinger 1998)

- Phase ⑤: The flow conditions of all reaches are roughly corresponding to uniform flow. Within the widening perimeter, the uniform flow depth h_w and energy head elevation $h_{E,w}$ are thereby smaller than in the channelized reach (h_{ch}, $h_{E,ch}$). In the downstream reach, the initial bed elevation is re-established with only the constriction scour maintained. Within the widening, a steeper slope $S_w > S_{ch}$ has developed. In addition, the bed is vertically offset by s_z as a result of the hydraulic conditions. Due to the steeper widening slope, the bed of the upstream reach is raised by Δz relative to the initial channel bed. A river widening can thus be assumed to replace a transversal sill with a height of Δz.

Based on his experiments, Hunzinger (1998) recommends a two-stage design process to first determine the necessary width and length of the widening and to then plan the individual elements of the widening based on these dimensions. He derived the following design guidelines for excavated river widenings (see also Hunzinger 2004):

- *Widening width* b_w: Aspect ratio, that is, width relative to flow depth b/h, exerts the main control on the morphology in a given river with a characteristic grain size D (see Section 3.3). The design width b_w thus depends on the current and future morphology within the reach of interest. As a first approximation, a morphological classification may be applied to the widening reach (e.g., Jäggi 1983; Ahmari and da Silva 2011). It must be noted, however, that these considerations are only valid for channels with a balanced sediment supply. If the channel is in a state of sediment deficit, the flow within a river widening may not occupy the entire width and develop a simpler morphology, that is, single-thread instead of multi-thread (e.g., Marti 2006).

- *Widening length* L_w: The length of the widening exerts additional control over the morphological development within the widening. Hunzinger (1998) distinguished *short* from *long* widenings with long widenings having a total length $L_{w,\text{tot}}$ of

$$L_{w,\text{tot}} \geq 2L_r + L_c \tag{2.1}$$

where L_r is the length of recirculation zone, and L_c is the length of constriction zone (see Figure 2.2, ⑤). Only long channel widenings can develop the morphology predicted by their relative width. If the total length is shorter, the morphology within

the widening remains influenced by the transition zones and uniform flow is not established within the widening. For two-sided channel widenings in straight rivers, the recirculation length L_r depends on the widening ratio with

$$L_r = \frac{b_w - b_{ch}}{2} \left[2.21 - 2.81 \ln (1 - F)\right] \tag{2.2}$$

$$F = \left(\frac{v_w^2}{v_{ch}^2}\right)^{1.1} \left(\frac{h_w - s_z + dz_{bw}}{h_{ch}}\right)^{2.1} \tag{2.3}$$

where b_w is the widening width, b_{ch} is the channel width, v_w is the mean flow velocity in the widening, v_{ch} is the mean flow velocity in the channel, h_w is the mean flow depth in the widening, h_{ch} is the mean flow depth in the channel, s_z is the height of the vertical offset (see next point), and dz_{bw} is the difference between mean and wetted bed elevation. For $b_w/h_w > 30$, dz_{bw} can be described with

$$dz_{bw} = -0.62he^{\frac{-159.23h_w}{b_w}} \tag{2.4}$$

where h_w is the mean flow depth in the widening and b_w is the widening width.

- *Vertical bed offset* s_z: The vertical bed offset s_z is exclusively governed by the hydraulic conditions and therefore by the geometry of the widening with

$$s_z = h_{E,ch} - h_{E,w} + \Delta H \tag{2.5}$$

where $h_{E,ch}$ is the energy head elevation above the channel bed, $h_{E,w}$ is the energy head elevation above the widening bed, and ΔH are the energy losses due to changes in cross-section. An anticipation of the vertical bed offset s_z by distributing the excavated floodplain sediment in the widening perimeter is recommended to counteract the temporary sediment deficit in the downstream reach (see Figure 2.2, ② and ③; Hunzinger 1998, 2004; Klösch *et al.* 2011).

- *Upstream bed aggradation* Δz: If a channel widening is long enough, the reach upstream of the widening is subject to net aggradation Δz given by

$$\Delta z = \left(L_{w,\text{tot}} - L_r - \frac{L_c}{2}\right)(S_w - S_{ch}) + \Delta H \tag{2.6}$$

where $L_{w,\mathrm{tot}}$ is the total widening length, L_r is the recirculation length, L_c is the constriction length, S_w is the widening slope, S_{ch} is the channel slope, and ΔH are the energy losses due to changes in cross-section. For example, a 500 m long and 70 m wide river widening in a 25 m wide channel with a slope of 0.01 can be expected to replace a transversal sill with a height Δz of roughly 1 to 1.5 m. Note that this assumption is only valid if bed-load transport is more or less balanced with the transport capacity of the channel (see Section 2.5.2).

- *Constriction scour depth* $t_{s,\mathrm{max}}$: The maximum scour depth caused by the downstream flow constriction $t_{s,\mathrm{max}}$ (see Figure 2.2, ③) is given by

$$t_{s,\mathrm{max}} = h_{ch} - h_w \left(2.70 K_\delta \ln \omega + 1\right) \tag{2.7}$$

$$\omega = \left(\frac{b_w}{b_{ch}}\right)^{0.36} \left(\frac{h_w}{h_{ch}}\right)^{-1.78} \tag{2.8}$$

where h_{ch} is the mean flow depth in the channel, h_w is the mean flow depth in the widening, $K_\delta = 1$ for a constriction angle of 45° and $K_\delta = 0.7$ for a constriction angle of 25°, b_w is the widening width, and b_{ch} is the channel width.

2.6 Selected examples of river widenings

Figure 2.3 shows a map of Switzerland with a collection of 100 implemented or planned river widenings and 212 floodplains in the Federal Inventory of Floodplains of National Importance (FOEN 2017). As of 2017, the floodplain inventory contains 326 objects. For the analysis herein, only riverine floodplains were considered, reducing the data set to 212 objects (see also Bianchi 2018). The information on the degree of bed-load deficit was aggregated by Hanus *et al.* (2021) and refers to a percentage of the natural bed-load that was estimated for the unimpaired river systems (Schälchli and Kirchhofer 2012). Note that the value reported as natural bed-load is not equal to the transport capacity of channelized rivers, a value that is denoted by $Q_{s,0}$ throughout this thesis.

The river reaches contained in the floodplain inventory are of particular interest for restoration projects because residuals of valuable floodplain habitat are present and their ecological potential is thus high. Figure 2.3 shows that the inventoried floodplain reaches cover the entire range of bed-load deficit. Based on this compilation, a reference reach and a typical widening were identified as basis for the experimental design of this thesis.

The collection of river widenings in Figure 2.3 is by no means exhaustive but provides a valuable overview of Swiss river widening practice. The evaluation of widening configuration revealed that 65% of widenings in the collection are one-sided, which is reflected in the design of the laboratory experiment (see Section 4.3). The mean widening length is 908 m (derived from a subset of 74 objects).

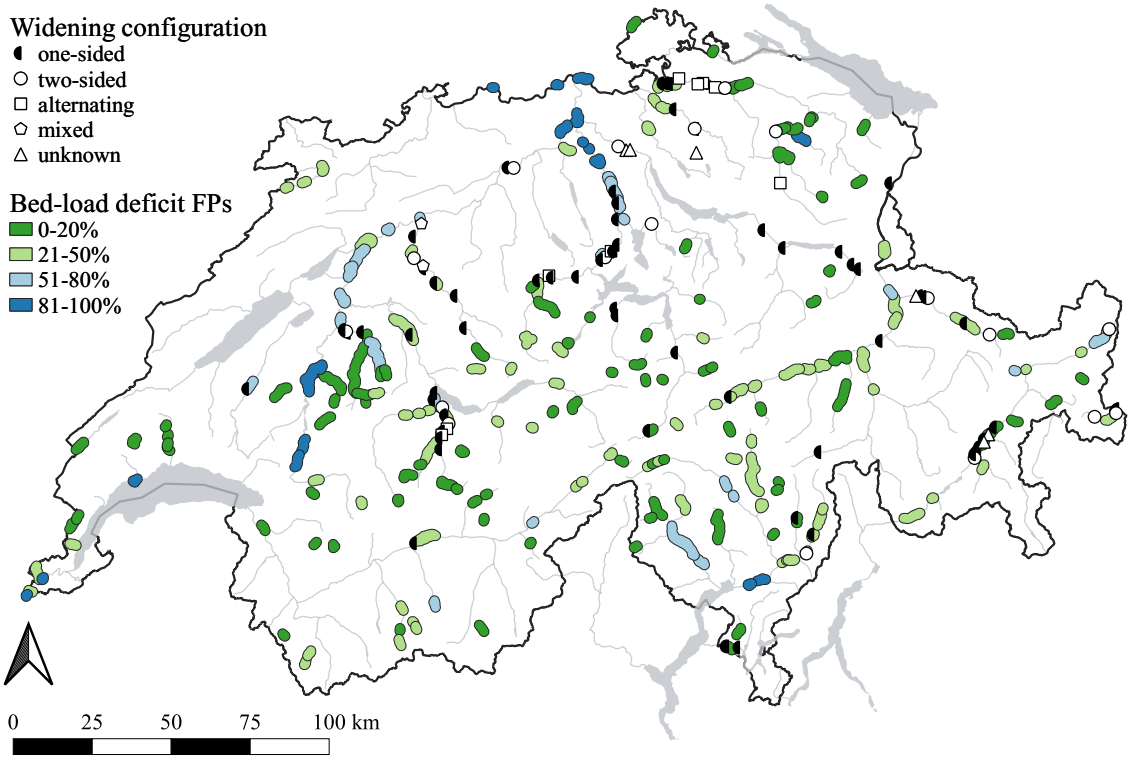

Figure 2.3 Map of Switzerland showing 100 implemented or planned river widenings and their configuration and 212 riverine floodplains (FPs) of the Federal Inventory of Floodplains of National Importance colored by bed-load deficit. The floodplains are displayed with a buffer of 1500 m. (Data: FOEN 2014, 2017; Bianchi 2018; swisstopo 2018; Hanus *et al.* 2021)

This chapter is concluded with a more detailed look at selected Swiss river widenings (see Appendix for more examples). For each widening, a collection of orthophotos and the corresponding discharge data are provided. Further information on the degree of bed-load deficit and the impairment of the natural discharge regime as well as a few notes on the widening morphodynamics are provided. Note that the morphodynamic assessment is based on the presented data alone. A more detailed analysis would require further information on local conditions and geomorphic history. Also, the inference of the ecological state of a specific river widening is not possible based on the presented data.

Thur River, Schäffäuli

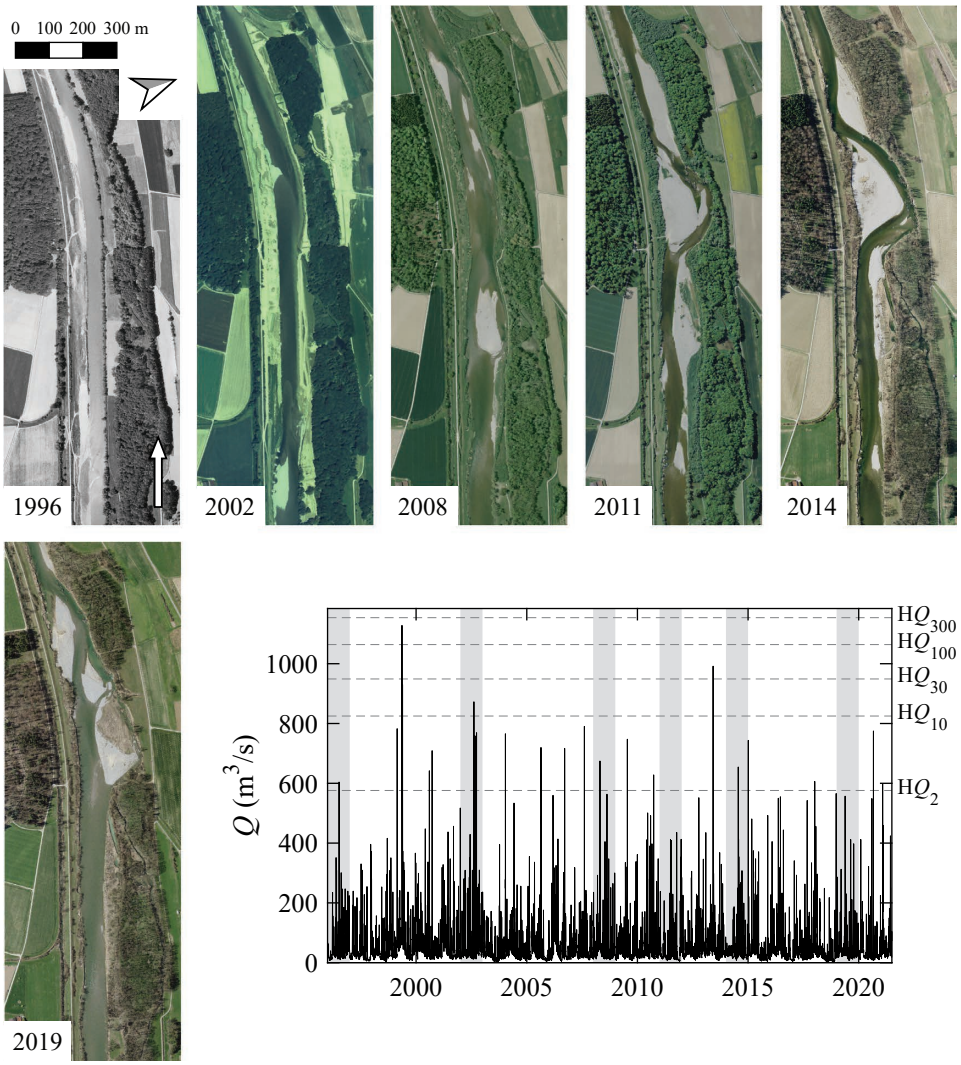

Figure 2.4 Temporal evolution of the river widening Schäffäuli, Thur River (47°35′33.748″N 8°45′51.829″E), and discharge time series with orthophoto acquisition years marked in gray (Photos: Federal Office of Topography; discharge data: Federal Office for the Environment)

Table 2.1 Characteristics of the river widening Schäffäuli, Thur River

Width (channel → widening)	46 m → 170 m
Slope	0.0016
D_m, D_{90} *	2.2 cm, 5.3 cm
Discharge+	no specifications
Bed-load[x]	> 80% of the natural bed-load remaining
Morphodynamics	Intensive channel widening and shifting, meandering tendency, evidence of erosion of vegetated areas

*VAW (2007), +HADES (2021), [x]Schälchli and Kirchhofer (2012)

Emme River, Aefligen-Utzenstorf

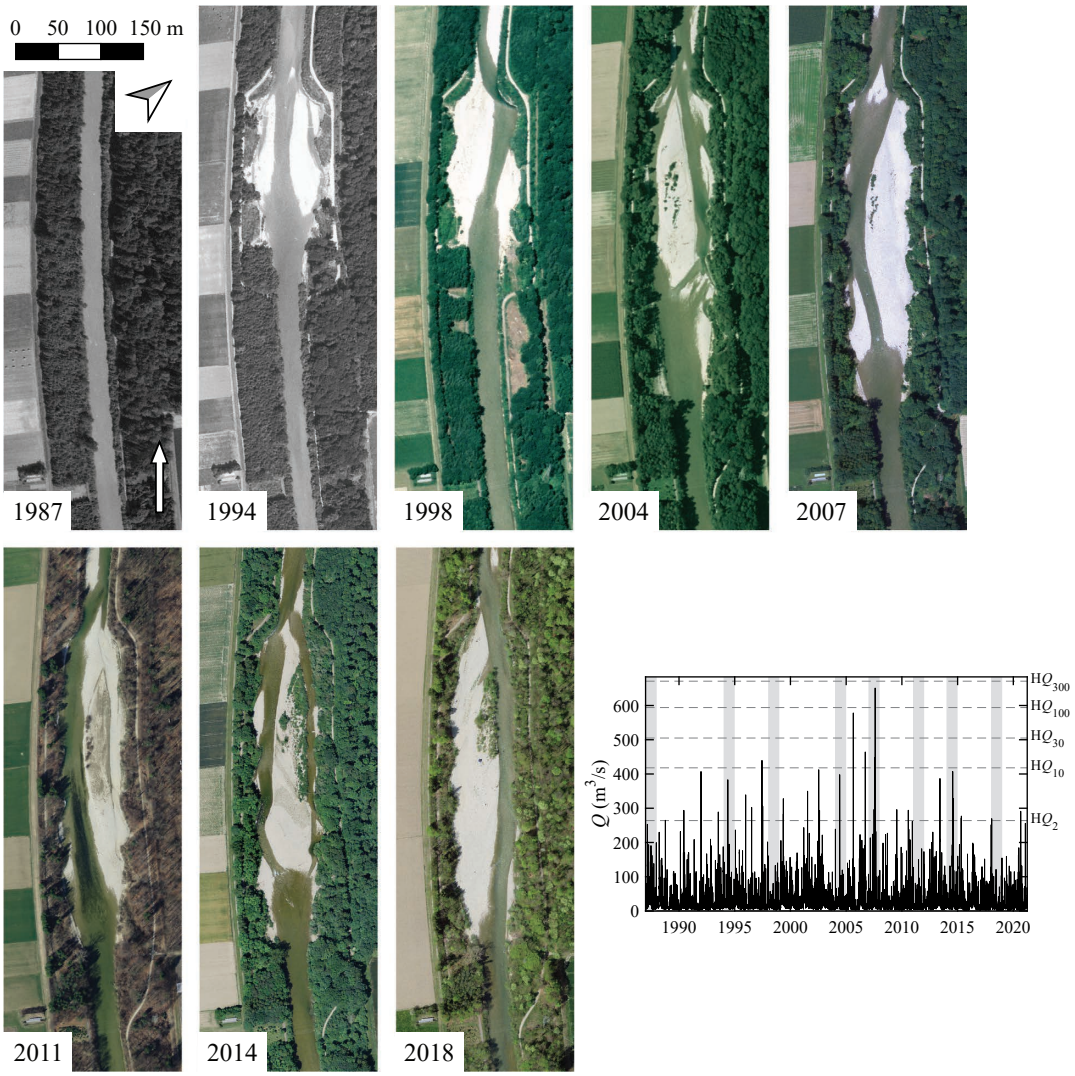

Figure 2.5 Temporal evolution of the river widening Aefligen-Utzenstorf (*Emme-Birne*), Emme River, implemented in two stages (47°06′08.166″N 7°32′52.138″E), and discharge time series with orthophoto acquisition years marked in gray (Photos: Federal Office of Topography; discharge data: Federal Office for the Environment)

Table 2.2 Characteristics of the river widening Aefligen-Utzenstorf (*Emme-Birne*), Emme River

Width (channel → widening)	30 m → 75 m
Slope	0.0045
D_m, D_{90} *	3.2 cm, 9.0 cm
Discharge+	no specifications
Bed-load[x]	50-80% of the natural bed-load remaining
Morphodynamics	Regular channel shifting, mostly maintaining a single-thread morphology

*Zarn (1992), +HADES (2021), [x]Schälchli and Kirchhofer (2012)

Alpine Rhine, Felsberg

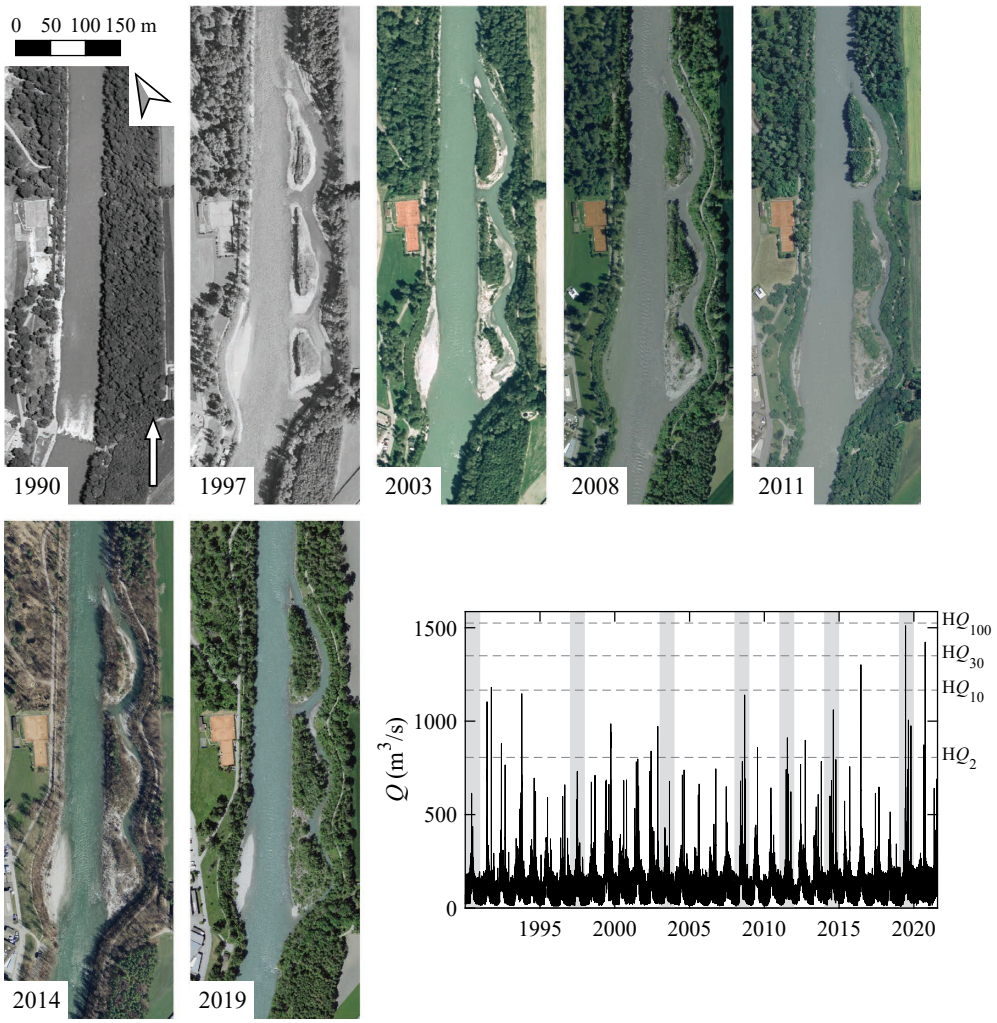

Figure 2.6 Temporal evolution of the river widening Felsberg, Alpine Rhine (46°50′54.495″N 9°29′22.970″E), and discharge time series with orthophoto acquisition years marked in gray (Photos: Federal Office of Topography; discharge data: Federal Office for the Environment)

Table 2.3 Characteristics of the river widening Felsberg, Alpine Rhine

Width (channel → widening)	65 m → 120 m
Slope	0.0025
D_m, D_{90} *	8.2 cm, 19.6 cm
Discharge+	> 80% of natural yearly discharge remaining; at least 20% discharge increase in winter; hydropeaking
Bed-loadx	20-50% of the natural bed-load remaining
Morphodynamics	High morphological stability, vegetation growth on stable islands

*Zarn *et al.* (1995), +HADES (2021), xSchälchli and Kirchhofer (2012)

Kander River, Heustrich (reference reach)

Figure 2.7 shows the river widening Heustrich on the Kander River. It originates from flood damage during a 50-year flood in 2005. It was decided not to reconstruct the channel because planning of several river widenings along the Kander River was ongoing at the time. This widening was used as a reference reach for the laboratory experiments (see Chapter 4). The widening dimensions can be found in Table 2.4, and characteristic discharges for the reference reach are listed in Table 4.4.

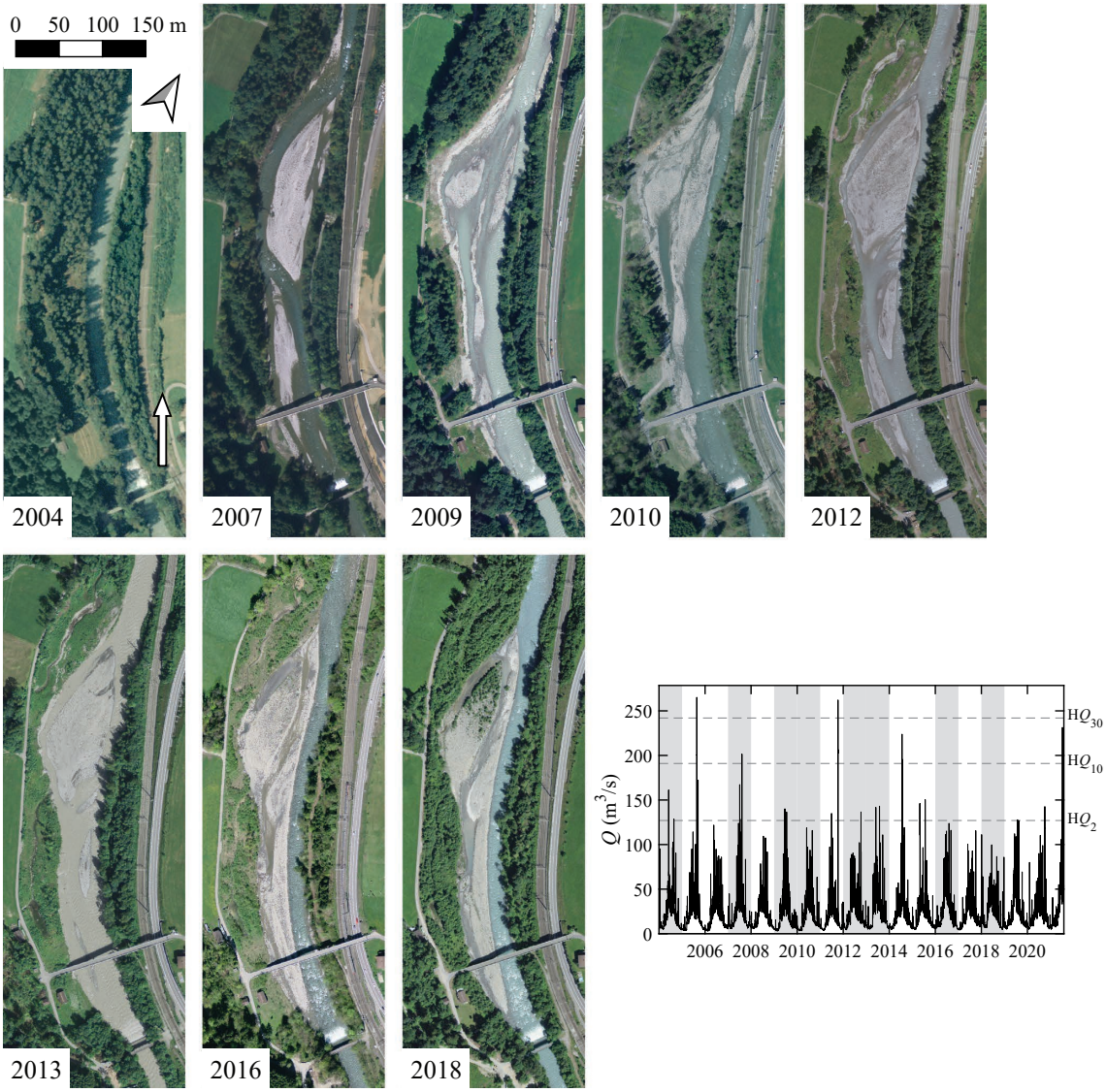

Figure 2.7 Temporal evolution of the river widening Heustrich, Kander River (46°39′14.755″N 7°40′49.398″E), and discharge time series with orthophoto acquisition years marked in gray (Photos: Federal Office of Topography; discharge data: Federal Office for the Environment)

Table 2.4 Characteristics of the river widening Heustrich, Kander River

Width (channel → widening)	27 m → 90 m
Slope	0.01
D_{50}, D_{90} *	4.6 cm, 18.7 cm
Discharge+	no specifications
Bed-loadx	20-50% of the natural bed-load remaining
Morphodynamics	Relatively active channel shifting until 2012, increasing stability of a single-thread channel during the following years potentially due to the absence of large floods except 2014 (see Figure 2.8 for recent impressions)

*Section 4.3.3, +HADES (2021), xSchälchli and Kirchhofer (2012)

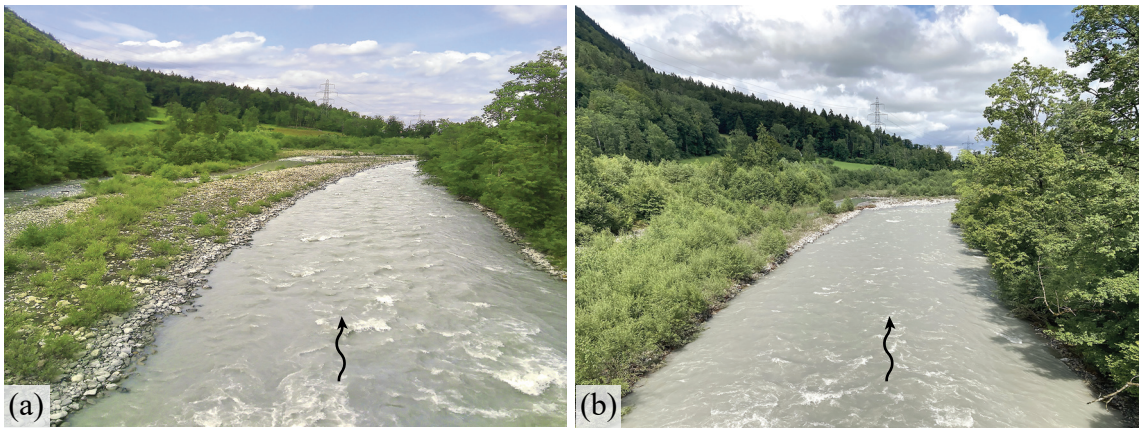

Figure 2.8 View from the bridge across the Heustrich widening, Kander River on (a) July 13, 2019 and (b) August 8, 2021. Note the increasingly dense vegetation growth on the left side of the widening that presumably contributes to the stability of the single-thread channel.

3 Fluvial morphodynamics and sediment supply: a review

3.1 Overview

This chapter provides the reader with an overview of the most relevant literature related to fluvial morphology and morphodynamics. Section 3.2 introduces the wide range of fluvial channel patterns and Section 3.3 presents selected pattern discriminators. The fundamental importance of channel width and selected width predictors are discussed in Section 3.4. Section 3.5 outlines channel adjustments in response to boundary condition changes. The influence of variable sediment supply on channel pattern, width, bars, and substrate is described in Section 3.6. Section 3.7 summarizes literature on aquatic refugia and Section 3.8 summarizes this and the previous chapters and identifies existing research gaps.

3.2 Fluvial morphology

A wide range of fluvial channel patterns (or planforms) occurs in response to different environmental conditions. In their fundamental work, Leopold and Wolman (1957) have distinguished *braided*, *meandering*, and *straight* rivers. Further classic channel patterns are *anastomosing* and *wandering* channels as well as *step-pool cascades*. Channel pattern is fundamentally a result of stream power (product of slope and discharge; Ferguson 1987) and sedimentological characteristics such as transported grain size or cohesiveness of the river banks. In addition, biological processes such as vegetation growth can strongly influence channel pattern by modifying river bank erodibility (Tal and Paola 2010; Bertoldi *et al.* 2015; Castro and Thorne 2019).

Figure 3.1 presents an overview of alluvial channel patterns specifically focusing on sediment supply as an influencing factor (Church 2006). In the vertical direction, it shows a gradient from bed-load dominated streams typical for headwaters with steep slopes to wash-load dominated streams typical for lowland rivers with small slopes. The change in sediment transport mode is related to decreasing sediment caliber (grain size). Channel stability increases from headwaters to lowland rivers. Headwaters are frequently restructured by typical flashy floods while the meander migration of a lowland river usually progresses rather slowly.

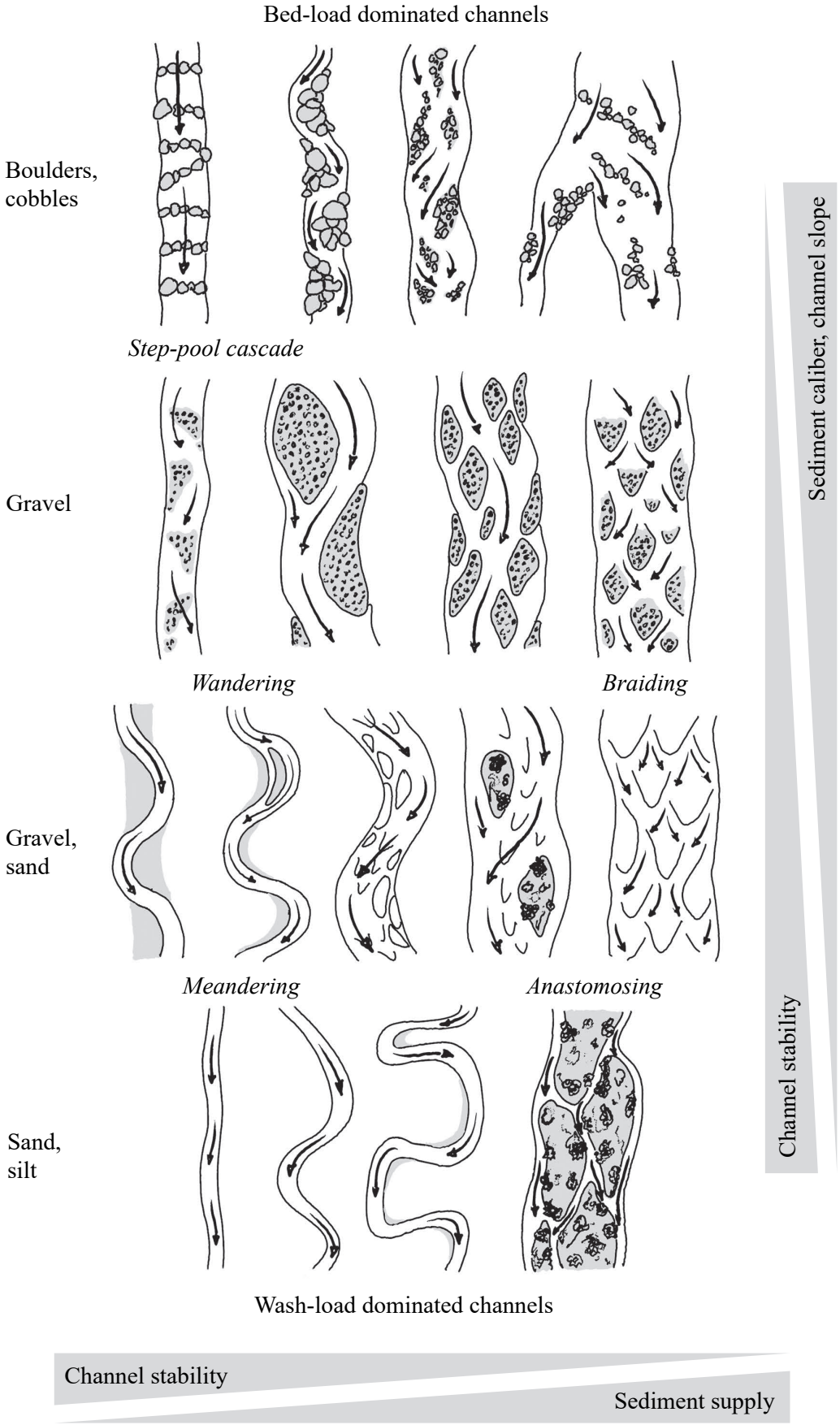

Figure 3.1 Alluvial channel patterns (or planforms) and their primary control factors. Classic channel patterns are written in italic (adapted from Church 2006).

In the horizontal direction, the influence of sediment supply on channel stability is shown for the main groups of channel patterns. Increasing sediment supply thereby decreases channel stability. For example, a gravel-bed river showing signs of alternate bars may be transformed into a wider braiding river if sediment supply significantly increases.

3.3 Channel pattern discriminators

The description and prediction of channel pattern is a central topic of fluvial geomorphology and also of fundamental importance for river engineering. A large number of channel pattern discriminators have been developed based on the elementary distinction of braided, meandering, and straight rivers. Most of them are empirical relations, but some mechanistic approaches have also been developed. It is important to note that an entire spectrum of channel patterns exists. Proposed thresholds, therefore, never represent sharp limits between different channel patterns but rather fuzzy transitions.

Leopold and Wolman (1957) related the occurrence of the primary channel patterns mainly to bankfull discharge Q by defining an empirical meandering-braiding threshold slope S^*_{bm} as

$$S^*_{bm} = 0.0125 Q^{-0.44}. \tag{3.1}$$

Following previous work (e.g., Henderson 1966; Ferguson 1987), a similar relation was proposed by van den Berg (1995), additionally taking the median grain diameter D_{50} into account to discriminate between meandering and braiding as

$$S^*_{bm} = 0.273 Q^{-0.5} D_{50}^{0.42}. \tag{3.2}$$

Alternatively, the relation by van den Berg (1995) can be formulated as a stream power ($\omega = \rho g Q S / b$) threshold

$$\omega^*_{bm} = 900 D_{50}^{0.42}. \tag{3.3}$$

To take a greater variety of channel patterns into account, this threshold can be complemented by a threshold separating meandering rivers with scroll bars (curvilinear ridge along the inner meander bend) from moderately braiding and meandering rivers with chute bars (forming at the downstream end of a chute channel) ω^*_{sc} (Kleinhans and van den Berg

2011) and an inactive-active threshold ω_{ia}^{*} (Makaske *et al.* 2009) given by

$$\omega_{sc}^{*} = 285 D_{50}^{0.42} \tag{3.4}$$

and

$$\omega_{ia}^{*} = 90 D_{50}^{0.42}. \tag{3.5}$$

Inactive channels are thereby defined as immobile channels showing no lateral migration (Makaske *et al.* 2009).

A well-known channel pattern classification scheme was developed by Yalin and da Silva (2001) and extended by Ahmari and da Silva (2011). According to Yalin and da Silva (2001), large-scale horizontal turbulence structures in open-channel flows are a function of the aspect ratio b/h and relative submergence h/D. As bar occurrence is controlled by these large-scale turbulence structures, the region plan of Ahmari and da Silva (2011) broadly distinguishes straight, meandering, alternate bar, and braided planforms based on b/h and h/D (Figure 3.2).

According to Ahmari and da Silva (2011), the alternate bar and meandering region are separated from the braiding region by

$$\left(\frac{b}{h}\right) = 25\left(\frac{h}{D}\right)^{1/3} \qquad \text{for } \frac{h}{D} \leq \approx 200 \tag{3.6}$$

$$\left(\frac{b}{h}\right) = 146 \qquad \text{for } \frac{h}{D} > \approx 200. \tag{3.7}$$

The alternate bar and meandering region is separated from the meandering and plane bed region by

$$\left(\frac{b}{h}\right) = 25\left(\frac{h}{D}\right)^{-0.55} \qquad \text{for } \frac{h}{D} \leq \approx 25 \tag{3.8}$$

$$\left(\frac{b}{h}\right) = \frac{2}{13}\left(\frac{h}{D}\right) \qquad \text{for } \approx 25 < \frac{h}{D} \leq \approx 130 \tag{3.9}$$

$$\left(\frac{b}{h}\right) = 20 \qquad \text{for } \frac{h}{D} > \approx 130. \tag{3.10}$$

The lower limit for meandering is given by

$$\left(\frac{b}{h}\right) = 4 \qquad \text{for } \frac{h}{D} >\approx 25. \tag{3.11}$$

Based on his own and other experiments, Zarn (1997) suggested an adjustment of the line separating alternate bar from plane bed region (Figure 3.2) as

$$\left(\frac{b}{h}\right) = 5.5\left(\frac{h}{D}\right)^{1/3} \qquad \text{for } \frac{h}{D} \leq\approx 100. \tag{3.12}$$

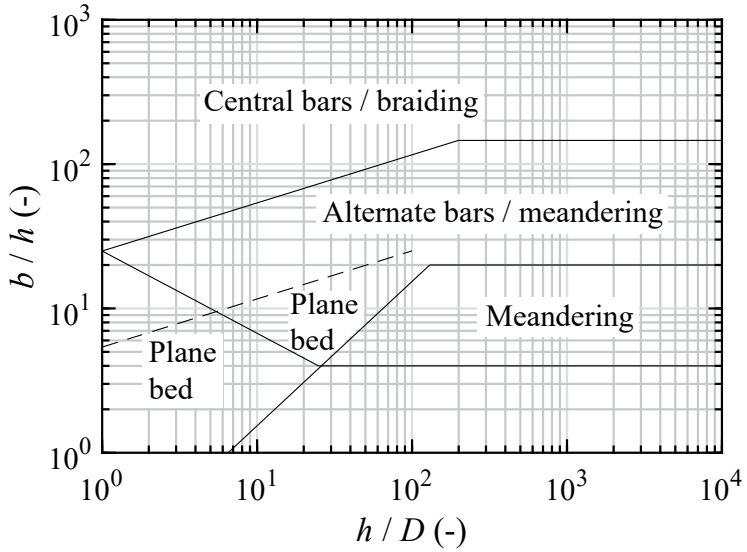

Figure 3.2 Morphological classification system based on aspect ratio b/h and relative submergence h/D (adapted from Ahmari and da Silva 2011 and Zarn 1997)

Crosato and Mosselman (2009) propose a mechanistic approach based on a linear model for bed topography to estimate the most likely number of bars to occur in the transverse direction. The bar mode predictor m after Crosato and Mosselman (2009) is defined as

$$m^2 = 0.17g\frac{(B-3)}{\sqrt{(s-1)D_{50}}}\frac{b^3 S}{C_f Q} \tag{3.13}$$

where g is the gravitational acceleration, B is the degree of nonlinearity of sediment transport versus depth-averaged flow velocity (recommended values are $B = 10$ for gravel-

bed rivers and $B = 4$ for sand-bed rivers), s is the relative sediment density, D_{50} is the median grain diameter, b is the channel width, S is the channel slope, C_f is the Chézy coefficient, and Q is the discharge. Alternate bars occur for $0.5 \leq m < 1.5$, central bars for $1.5 \leq m < 2.5$, and braiding for $m \geq 2.5$.

Bars can be divided into *forced* and *periodic* bars (e.g., Vonwiller 2018; Crosato and Mosselman 2020). Forced bars occur locally, triggered by channel curvature, flow separation zones behind obstacles, or changes in channel geometry. Periodic bars occur due to morphodynamic instabilities of the bed. They can be divided into *free* migrating bars and *steady* bars. Free bars are generally shorter with wavelengths L_B/b of 6 to 10 and wavenumbers $\lambda_B = (\pi b)/L_B$ of 0.35 to 0.5. Steady bars have typical wavelengths L_B/b of 15 to 20 and wavenumbers λ_B of 0.15 to 0.2.

A fundamental difference between the presented empirical approaches (Equations 3.1 to 3.5), and those by Ahmari and da Silva (2011) and Crosato and Mosselman (2009) is that the former are based on parameters independent of channel geometry (bankfull discharge or annual flood and grain size), while channel geometry has to be known for the latter. In a river engineering context, channel geometry is often subject to modifications. Heavily impacted rivers deviate from the alluvial rivers most morphological classifications are based on due to fixed bank protection or vertical erosion control structures. Classification approaches that take channel geometry into account are therefore of central importance, and channel width b thereby emerges as the main parameter controlling morphology (Zarn 1997; Siviglia *et al.* 2008; Garcia Lugo *et al.* 2015). Taking the example of the classification scheme after Ahmari and da Silva (2011) and assuming that grain size composition and the hydrological regime of a certain river reach cannot be altered, channel width b is the only parameter that can be influenced by river engineering measures. As is detailed in Section 3.6, sediment supply is another important controlling factor for channel width and pattern. However, in a channelized river, no significant morphological adjustments can be expected from varying sediment supply because the primary control is exerted by the limited channel width (e.g., Eaton and Church 2009; Rachelly *et al.* 2021a).

3.4 Channel width

The description and prediction of channel width is a fundamental problem of fluvial geomorphology and river engineering. *Channel width* describing the width of a single channel must thereby be distinguished from the *total wetted width* in case of multi-thread

morphologies (see Equation 3.17).

The intensity of bed-load transport is relevant for single-thread channel geometry. *Threshold channels* are stable channels with no or a negligible amount of bed-load transport (Church 2006). Their cross-section is rounded and controlled by the balance between gravity and fluid friction. In *active channels*, the critical bed shear stress for grain motion is exceeded in the channel center, causing bed-load transport there, while the banks remain stable. The bed elevation of the active transport zone is flat (see, e.g., Abramian *et al.* 2020), and they are wider than threshold channels. It has to be assumed that most equations describing channel width based on field data refer to active channels but this is not always clearly stated.

Various empirical approaches called *regime* equations were formulated to relate channel geometry to parameters such as discharge, slope, bed material, and bank strength. Lacey (1930) studied irrigation canals and found that their width b scales with the square root of discharge Q as

$$b = 2.67Q^{0.5}. \tag{3.14}$$

Many similar relations were proposed with slightly varying exponents and factors depending on local conditions (e.g., Leopold and Maddock 1953).

Parker (1979) included the median grain size diameter of the armor layer $D_{50,A}$ in his approach to determine the width of active alluvial gravel-bed channels as

$$b = 4.4\frac{Q^{0.5}}{\sqrt{(s-1)gD_{50,A}}} \tag{3.15}$$

where Q is the discharge, s is the relative sediment density, g is the gravitational acceleration, and $D_{50,A}$ is the median grain diameter of the armor layer. Parker (1979) noted that in the channels he studied, bed-load transport is low but nonzero, and the banks are stable.

Relative bank strength was taken into account by Millar (2005), who presented a set of regime equations based on the assumption that alluvial channels assume a geometry that allows maximum transport capacity. Their width b is defined as

$$b = 16.5D_{90}\left(\frac{Q}{\sqrt{(s-1)gD_{50,A}}D_{50,A}^2}\right)^{0.7} S^{0.6}\mu'^{-1.1} \tag{3.16}$$

where D_{90} is the 90$^{\text{th}}$ percentile of the bulk grain size distribution, Q is the discharge, s is the relative sediment density, g is the gravitational acceleration, $D_{50,A}$ is the median grain diameter of the armor layer, S is the longitudinal channel slope, and μ' is the relative bank strength. Millar (2005) recommends using a relative bank strength μ' of 1.0 to 1.2 for bank material with similar erosion resistance as the channel material. Higher values represent increased erosion resistance, for example by vegetation or cohesive bank material.

For braided rivers, the total wetted width is of interest. According to Ashmore (2001), it is

$$b = 0.0098(\rho g Q S)^{0.777} D_{50}^{-0.7} \tag{3.17}$$

where ρ is the density of water, g is the gravitational acceleration, Q is the discharge, S is the longitudinal slope, and D_{50} is the median grain size diameter. Total wetted width thereby has to be distinguished from the active width (Ashmore *et al.* 2011). The active width is the lateral extent of bed-load flux and short-term morphological change at any moment. According to Ashmore *et al.* (2011) it increases with stream power and normally occupies between 10% and 40% of the wetted width. There is also evidence that active transport width may be related to sediment supply (see Section 3.6).

3.5 Channel adjustments

The description and prediction of channel adjustment in response to natural or anthropogenic variations of environmental conditions is of central importance. Lane (1955) formulated the qualitative relation $Q_s D \propto QS$ with sediment load Q_s, grain size diameter D, discharge Q, and channel slope S. It states that a river *at grade* adjusts its slope so that the imposed sediment load of a certain grain size distribution can be transported by the available discharge in a stable channel. The concept of grade provides a helpful conceptual model of stream response to hydrological and geomorphic changes that was refined in many variations of regime theory (Eaton and Millar 2017). For example, Eaton and Church (2011) extended the original formula by Lane (1955) with the mean flow depth h and the dimensionless critical shear stress θ_c as

$$\frac{Q_s}{QS} \propto \left[\frac{hS}{D\theta_c}\right]^{(3/2)x_1} \tag{3.18}$$

$$x_1 = \frac{4.28}{\left[\log\left(\omega^*/\omega_0^*\right) + 1.54\right]^{2.41}} \tag{3.19}$$

where ω^* is the dimensionless stream power and ω_0^* is the critical dimensionless stream power computed for a given critical bed shear stress θ_c. The dimensionless stream power is defined as

$$\omega^* = \frac{\omega}{\rho\left[g(s-1)D\right]^{3/2}} = \frac{v}{U_*}\theta^{3/2} \tag{3.20}$$

where ω is the specific stream power, ρ is the density of water, g is the gravitational acceleration, s is the relative sediment density, D is a characteristic grain size diameter, v is the flow velocity, U_* is the shear velocity, and θ is the dimensionless bed shear stress.

Equation 3.18 identifies the various possibilities of channel adjustment in response to a change in Q or Q_s:

- Changes in channel geometry are described by the mean flow depth h.
- Aggradation, degradation, and changes in sinuosity are described by the stream slope S.
- The degree of armoring is described by the surface grain size D (Parker and Klingeman 1982).
- Surface structures are described by the dimensionless critical shear stress θ_c (Church 2006).

Figure 3.3 shows a graphical representation of these channel responses. The exponent x_1 (Equation 3.19) decreases for higher relative stream power, which indicates that the relative importance of surface grain size, surface structure, and channel shape is more pronounced for gravel-bed rivers with low relative stream power as compared to sand-bed rivers with high relative stream power (Eaton and Church 2011).

A similar regime approach was formulated by Eaton *et al.* (2004) following the premise that alluvial systems will maximize their system flow resistance f_{sys}, which is the sum of the grain resistance f', the within-channel form resistance f'', and the reach-scale form resistance due to sinuosity f'''. It follows that a river generally has three degrees of freedom to adjust to any changes in flow regime and sediment supply. The following section describes channel response to variations in sediment supply in more detail.

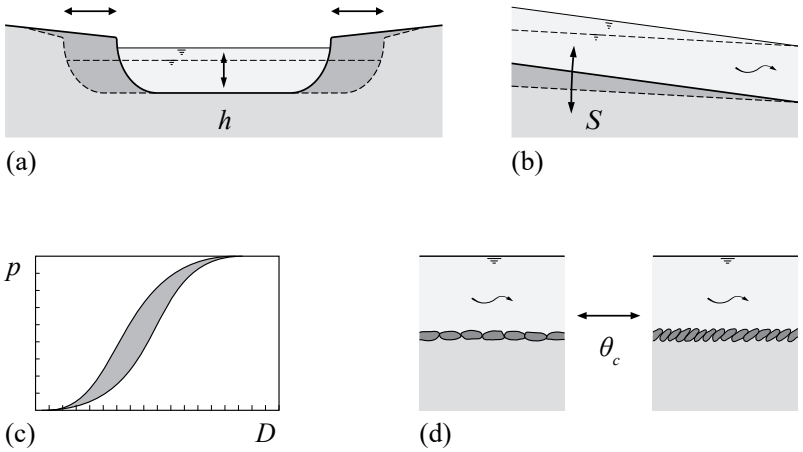

Figure 3.3 Possible channel adjustments to variable discharge Q and sediment supply Q_s according to Eaton and Church (2011) with (a) mean flow depth h, (b) channel slope S, (c) surface grain size D, and (d) dimensionless critical shear stress θ_c.

Note that although these regime approaches allow a fundamental understanding of channel responses, their simplicity and integrative nature cannot fully represent the large variability in many parameters and the multiple interacting and dynamic processes (Eaton and Millar 2017). Variations in bank stability due to variable grain sizes, cohesion, and vegetation are usually not included in these models, regardless of their importance in channel formation (e.g., Tal and Paola 2010; Bertoldi *et al.* 2015).

3.6 Variable sediment supply

3.6.1 Effects on river planform and width

The insight that sediment supply may be a central driver of morphodynamic processes mainly originates from field observations of river systems where sediment supply was drastically reduced due to natural causes or - more often - due to anthropogenic modifications (Kondolf 1997). Reported channel responses include planform simplification, channel narrowing, incision leading to floodplain disconnection, and substrate coarsening (Kondolf 1997; Surian and Rinaldi 2003; Marti 2006; Moretto *et al.* 2014). Although the relation is often obscured by further modifications such as channelization (e.g., Scorpio *et al.* 2018) or changes in the flow regime, the central importance of sediment supply has been well established.

Opposite processes, that is, increases in morphological complexity, channel widening, aggradation leading to floodplain reconnection, and substrate fining after substantial increases in sediment supply have also been observed in the field. Some studies have inves-

tigated this relation for sediment supply fluctuations caused by larger-scale geomorphic processes such as increased landslide activity that triggered mid-channel bar formation (Madej *et al.* 2009). Smith and Smith (1984) describe how large sand inputs by an adjacent dune field caused the William River to change its morphology from single-thread to braided and increase its channel width by a factor of five over a short distance. Other studies focused on the effects of targeted sediment management. Moretto *et al.* (2014) describe that channel widening occurred in a previously heavily impacted reach after upstream gravel mining activity decreased. Even vegetated patches were eroded. Dam removal can release large quantities of trapped sediment over a short time and has been reported to increase braiding, channel sinuosity, and bar growth (Ritchie *et al.* 2018). These geomorphic responses are often especially pronounced during transport-limited conditions right after dam removal, and diminish later when supply-limited conditions have re-established (East *et al.* 2018; Ritchie *et al.* 2018).

In recent years, larger data sets have been analyzed with regard to sediment supply conditions and channel width. For example, Pfeiffer *et al.* (2017) have elaborated the relation between bankfull geometry and sediment supply for U.S. rivers. They found that for bankfull discharge, some rivers accommodate far greater bed shear stresses than necessary to initiate motion of D_{50} grains, thus deviating from the theory of threshold channels (see Section 3.4). These channels were more common on the U.S. West coast where erosion rates and thus sediment supply to rivers is greater. Based on field data of meandering and braiding rivers, Métivier *et al.* (2016) also reached the conclusion that bed-load transport generates wider individual channels than predicted by threshold theory. A positive relation between sediment supply and channel width has also been established for mixed gravel-bedrock and bedrock channels (Baynes *et al.* 2020).

The difference between threshold channels and channels with active sediment transport has further been established in laboratory experiments. According to Métivier *et al.* (2017), channels actively transporting sediment can accommodate more sediment until they have reached 1.7 times the threshold channel width. If sediment transport increases beyond this threshold, the channels destabilize into braiding and each braid is again a channel with active sediment transport. They formulated a threshold to assess the stability of channels with active bed-load transport in the form of the detrended channel width b_* defined as

$$b_* = \frac{b}{C_W D_{50} \sqrt{Q_*}} \tag{3.21}$$

$$Q_* = \frac{Q}{\sqrt{g D_{50}^5}} \tag{3.22}$$

$$C_W = \frac{\pi}{\sqrt{\mu}} \left[\theta_c (s-1)\right]^{-\frac{1}{4}} \sqrt{\frac{3C}{2^{\frac{3}{2}} \mathcal{K}\left[\frac{1}{2}\right]}} \tag{3.23}$$

where b is the channel width, D_{50} is the median grain diameter, Q is the discharge, g is the gravitational acceleration, μ is the friction angle, θ_c is the critical dimensionless bed shear stress, s is the relative sediment density, C is the turbulent friction coefficient, and $\mathcal{K}\left[\frac{1}{2}\right] \approx 1.85$ is a transcendental integral. Métivier *et al.* (2017) propose to use $\mu = 0.7$, $\theta_c = 0.05$, and $C = 0.1$. A value of $b_* = 1$ represents threshold channels (no sediment transport), while $b_* = 1.7$ was identified to be the stability threshold for active channels. These channels are about to destabilize into braiding.

Abramian *et al.* (2020) suggest that channel width is in fact not the most suitable predictor of sediment supply. This is linked to their observation that sediment transport is responsible for two counteracting processes that distinguish channels with active sediment transport from threshold channels: (i) widening of the active transport width, and (ii) narrowing of the bank zone. They suggest that the aspect ratio b/h is instead a suitable predictor of sediment supply.

3.6.2 Effects on bars

The fundamental importance of sediment supply for morphodynamic processes can also be demonstrated at the scale of river bars. Upon sediment supply termination, alternate bars were eliminated in two sets of laboratory experiments conducted by Venditti *et al.* (2012). Free non-migrating bars began to migrate out of the flume without being replaced, and steady bars were progressively eroded, which also resulted in a plane bed. Conversely, sediment supply reduction in laboratory experiments with free non-migrating bars by Lisle *et al.* (1993) caused progressive thalweg incision leading to a reduction in longitudinal slope and concurrent emergence of the bars. Thalweg incision and lateral bar degradation was also reported by Bankert and Nelson (2018). Their experiments focused on bar stratigraphy included several cycles of sediment supply variation. During the degra-

dational cycle, the lateral erosion of bars ceased as soon as the coarse layer of previously present bars was exposed. Numerical experiments by Vonwiller (2018) also support the observation that bars tend to emerge when sediment supply is reduced. As discussed by Venditti *et al.* (2012), their specific initial conditions with higher relative submergence and a greater portion of the bed experiencing bed-load transport compared to the experiments by Lisle *et al.* (1993) may have caused bars to disappear rather than emerge. However, the conditions leading to either bar degradation or emergence in response to reduced sediment supply have not yet been conclusively described. In contrast to free and steady bars, forced point bar geometry does not significantly change in response to sediment supply termination (e.g., Friedl 2017; Rachelly *et al.* 2021a).

The effect of increasing sediment supply on bedforms has also been reported in several studies. When Venditti *et al.* (2012) increased sediment supply again in their experiments, bars reformed. However, they only reappeared after the original channel slope was re-established (cf. Vonwiller 2018). When sediment supply was increased beyond the transport capacity of a channel with free migrating bars, an increase in bar celerity was observed (Nelson and Morgan 2018). In a channel with steady bars, an increase of sediment supply beyond the channel transport capacity caused transient migrating bedforms of a shorter wavelength to appear (Podolak and Wilcock 2013). These migrating bars disappeared after the transitional phase and the original steady bars reappeared at the new equilibrium slope. Podolak and Wilcock (2013) quantified the trapping efficiency of the aggrading sediment wedge as 40%, that is, 2.5 times the theoretical minimum duration was necessary to establish the steeper slope. Similar transitory behavior was reported by Bankert and Nelson (2018), where increased sediment supply temporarily caused steady bars to migrate before they stabilized again. In settings where bedforms are forced by planform variations, they are not affected by sediment supply and the primary response is limited to channel slope adjustment (Nelson *et al.* 2015; Morgan and Nelson 2021).

3.6.3 Effects on bed structure and composition

Reducing the observation scale further, impacts of sediment supply on bed structure and composition have also been described. Upon sediment supply reduction, the active sediment transport zone was progressively confined to a narrow band both for plane beds (Dietrich *et al.* 1989) and alternate bar morphologies (Lisle *et al.* 1993). In both studies, coarse, inactive zones expanded at the expense of the active transport zone, and migrating

bed-load sheets disappeared. Bed-load sheets were shown to reappear for sufficiently high sediment supply (Madej *et al.* 2009). Nelson *et al.* (2009) described these sorting processes as a balance of free, forced, and fixed patches. Accordingly, sediment supply reduction causes fixed patches to expand on the expense of free patches. Venditti *et al.* (2017) have created a conceptual bedform phase diagram relating the appearance of bed structures to bed-load discharge and mobility conditions. For example, bed-load sheets appear for medium to high sediment supply and selective transport conditions, whereas transverse ribs and stone cells tend to form in low sediment supply and partial mobility conditions.

Venditti *et al.* (2012) reported reduced surface grain size heterogeneity with slight coarsening following sediment supply reduction. Conversely, Podolak and Wilcock (2013) documented increased surface grain size variability for increasing sediment supply. Increasing sediment supply thus seems to be related to decreasing surface armoring (e.g., Pfeiffer *et al.* 2017). Buffington and Montgomery (1999) point out that surface D_{50} asymptotically approaches bulk D_{50} for increasing sediment supply.

3.7 Aquatic refugia

3.7.1 Disturbance

When biotic or abiotic processes in fluvial ecosystems (see Section 2.2) assume exceptional values, this is referred to as a *disturbance*. More precisely, ”a disturbance is any relatively discrete event in time that is characterized by a frequency, intensity, and severity outside a predictable range, and that disrupts ecosystem, community, or population structure and changes resources or the physical environment.” (Resh *et al.* 1988, p.1; based on the definition by Pickett and White, 1985).

Lake (2000) identified three main types of fluvial disturbance distinguished by different temporal variations of the disturbance intensity (Figure 3.4). Pulses are short, sharply delineated events such as floods (e.g., Lepori and Hjerdt 2006). Press events have an instantaneous start with the pressure subsequently maintained and are often caused by human modifications such as channelization (e.g., Blake and Rhanor 2020). An example of a natural press disturbance is excessive sedimentation of a river system after a landslide (e.g., Madej *et al.* 2009). Ramp events are characterized by a steadily increasing disturbing force such as droughts (e.g., Wood *et al.* 2010). The level of disturbance can then either

be maintained (e.g., establishment of neobiota) or decrease again (e.g., normalization of water availability after a drought).

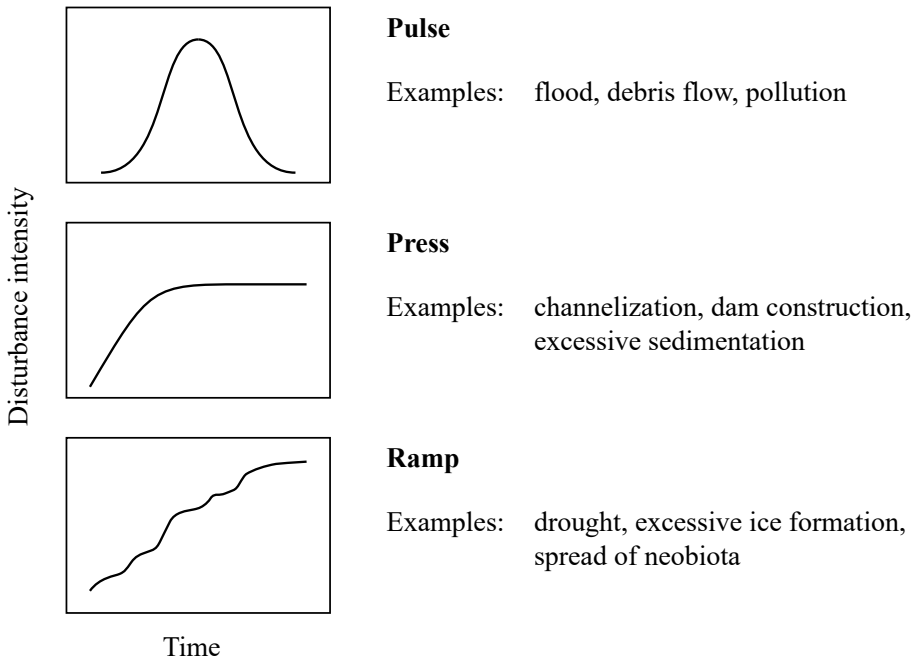

Figure 3.4 Disturbance types with examples for fluvial environments (adapted from Lake 2000)

Natural ecosystems may experience various disturbance types acting on different spatio-temporal scales (Townsend 1989; Naiman *et al.* 1993). The entirety of disturbance events in any environment can be aggregated to the disturbance regime. The disturbance regime can be conclusively described by the five components (i) magnitude, (ii) frequency, (iii) duration, (iv) timing or predictability, and (v) rate of change or flashiness (cf. Poff *et al.* 1997). Disturbance regimes of natural ecosystems vary widely. For example, tidal environments exhibit a naturally higher disturbance level than spring-fed environments (Ward and Stanford 1983). Ward and Stanford (1983) applied the intermediate disturbance hypothesis to lotic environments, stating that river systems with a disturbance level that is neither too intense nor too weak support the most diverse biotic communities.

Human modification of river systems often causes the disturbance regime to change in either direction. For example, storage hydropower plants may strongly increase the discharge variability and rate of change on a diurnal scale due to hydropeaking (e.g., Vanzo *et al.* 2016). The floodplains along channelized rivers, however, are disconnected from the main channel and the flood disturbance level therefore strongly decreases in these habitats, potentially disrupting vegetation succession (e.g., Hohensinner *et al.* 2011). According

to the intermediate disturbance hypothesis, both trends decrease the biotic diversity due to local extinction and increasing dominance of few species. The non-equilibrium communities of moderately disturbed lotic systems thereby experience a shift towards more stable and less diverse communities (Ward and Stanford 1983; Naiman *et al.* 1993).

This thesis focuses on floods, a major form of pulse disturbance. Floods commonly induce high hydraulic stress as well as sediment and large wood transport in the affected rivers (e.g., Sedell *et al.* 1990; Lake 2000; Lepori and Hjerdt 2006; Czuba *et al.* 2018). During a flood, aquatic organisms may be displaced, injured, or killed (Lake 2000). To assess the disturbance impact on specific organisms, it is important to consider the disturbance characteristics relevant to the organism of interest (Townsend *et al.* 1997). For example, a small flood with only minor bed-load transport activity may not be problematic for macroinvertebrates able to retreat to the interstitial space, but may be devastating for organisms living on the river bed surface.

However, stream communities usually recover fairly rapidly (e.g., Lake 2000; Gjerløv *et al.* 2003; Lepori and Hjerdt 2006) indicating that a certain number of organisms can resist the disturbing force. In addition, aerial or aquatic dispersal of organisms may play an important role in the recolonization of disturbed habitats (e.g., Williams and Hynes 1976). Townsend (1989) describes how during low and intermediate flow, lost individuals are quickly replaced by general redistribution of organisms among different habitats. After extreme events such as floods or droughts, however, recolonization may happen primarily from refugia, that is, habitats less affected by the disturbance event (see Section 3.7.3). Spotlighting the impact on biota, Townsend (1989, p.38) defines disturbance as ”any relatively discrete event in time that removes organisms and opens up space which can be colonized by individuals of the same or different species”. Despite the apparent adverse effects of hydrological disturbance events for stream organisms, high magnitude flood events and disturbances in general are inherent features of lotic ecosystems and vital for maintaining healthy ecosystem functioning (Townsend *et al.* 1997; Lepori and Hjerdt 2006).

3.7.2 Refuge function of habitats

Disturbance intensity may vary widely between habitats due to their spatial arrangement, substrate characteristics, or the acting hydraulic forces (e.g., Weber *et al.* 2013). ”Places (or times) where the negative effects of disturbance are lower than in the surround-

ing area (or time)" are referred to as *refugia* (Lancaster and Belyea 1997, p.222). Refugia are, among others, habitats that mitigate the effects of a disturbance on the biota and enable organisms to resist the disturbance (Lake 2000). Following disturbance events, refugia are sources of recolonization (Townsend 1989). Lotic community structure is therefore a result of the interaction of long-term adjustments to hydraulic habitat available at baseflow and the short-term availability of refugia during disturbance events. Species that find their preferred habitat in both conditions are most likely to be abundant (Lancaster and Hildrew 1993). Allan and Castillo (2007) conclude that the severity of a disturbance event is not only defined by the disturbance parameters, but by the availability of refugia.

Refugia exist at various spatial and temporal scales (e.g., Sedell *et al.* 1990; Lancaster and Belyea 1997; Lancaster 2000), and their refuge function depends on various factors such as the disturbance type (e.g., Lake 2000), organism characteristics (e.g., Pearsons *et al.* 1992; Weber *et al.* 2013; Sueyoshi *et al.* 2014), substrate composition (e.g., Sedell *et al.* 1990; Mathers *et al.* 2019, 2021), and hydro-morphological conditions (e.g., Lancaster and Hildrew 1993; Rice *et al.* 2007). This thesis specifically focuses on habitats that assume refuge function during floods.

3.7.3 Aquatic flood refugia

Aquatic flood refugia are, among others, habitat patches that are not exposed to severe hydraulic conditions and bed-load transport during floods (Lancaster and Belyea 1997). Examples of flood refugia can be found at different spatial and temporal scales (Sedell *et al.* 1990; Lancaster and Belyea 1997; Lancaster 2000; Allan and Castillo 2007). Figure 3.5 shows examples of aquatic refugia types sorted by their spatial scale.

On a reach-scale, tributaries (Figure 3.5a) and less impacted side channels (Figure 3.5b) may serve as refugia. For example, Sueyoshi *et al.* (2014) identified a small spring-fed tributary as valuable refuge for invertebrates in a field study during a seasonal snowmelt flood. The hyporheic zone (Figure 3.5c) and floodplain (Figure 3.5d) are important flood refugia in the vertical and lateral dimension, respectively. Dole-Olivier *et al.* (1997) conducted field experiments on the hyporheic invertebrate refuge finding that downwelling zones were a more effective refuge than upwelling zones unless the threshold for sediment motion was exceeded (see also Stubbington 2012 for a review of the highly variable refuge function of the hyporheic zone). Matthaei and Townsend (2000) documented the lateral movement of invertebrates onto the floodplain during a flood but express concerns about

its real refuge function due to adverse conditions on the floodplain and in the main channel during receeding flow. Fish have also been shown to move into floodplain habitats available only during high flow conditions (Schwartz and Herricks 2005). Hydraulically dead zones in backwaters (Figure 3.5e) can also function as refugia (Reynolds *et al.* 1991; Lancaster and Hildrew 1993).

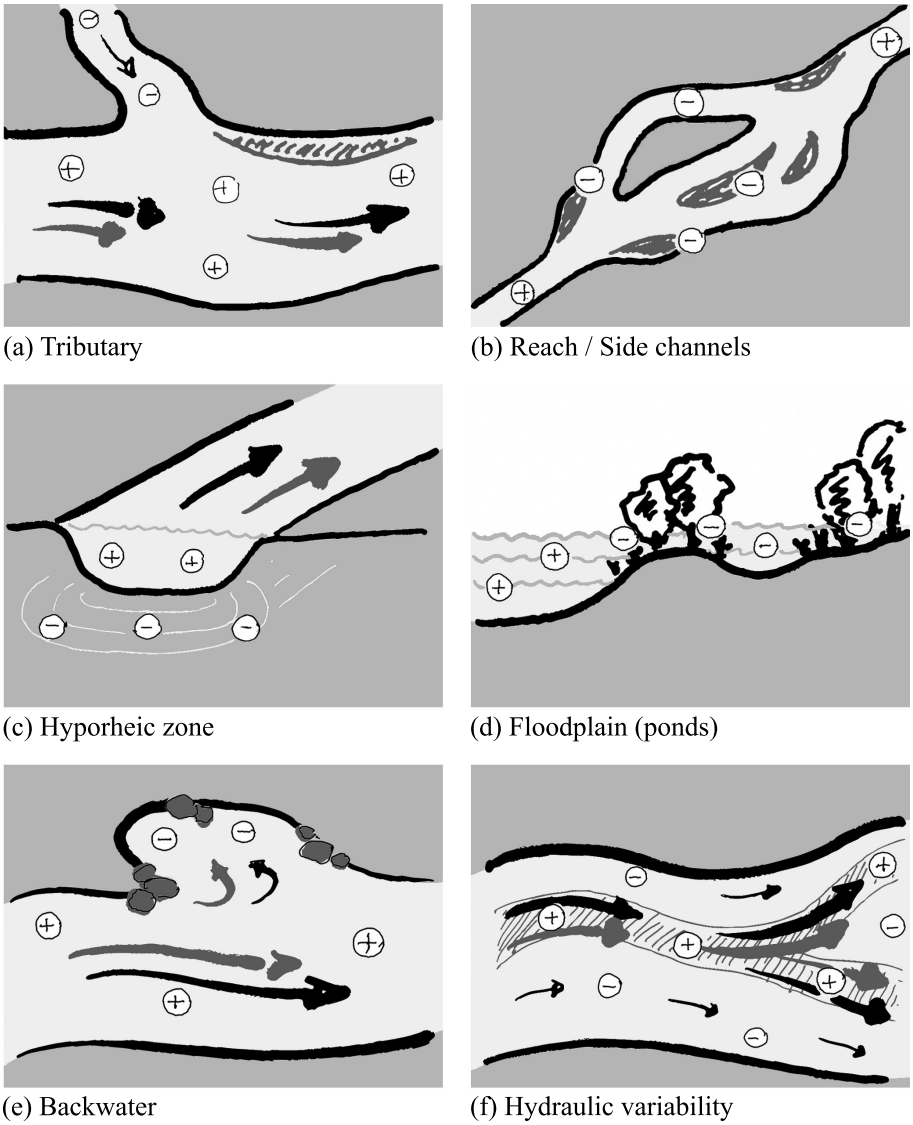

Figure 3.5 Schematic visualization of aquatic refugia types sorted by their spatial scale from reach-scale to patch-scale. The black and gray arrows visualize the flow field and their size indicates the intensity of hydraulic stress and bed-load transport, respectively, with larger arrows representing higher intensity. In addition, plus and minus signs signal the overall disturbance intensity.

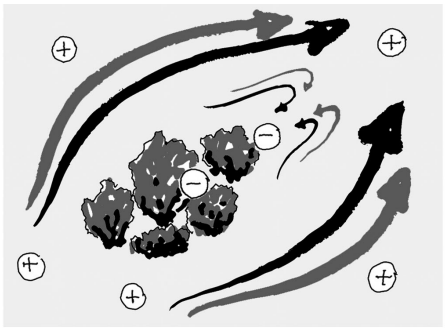

(g) Vegetation

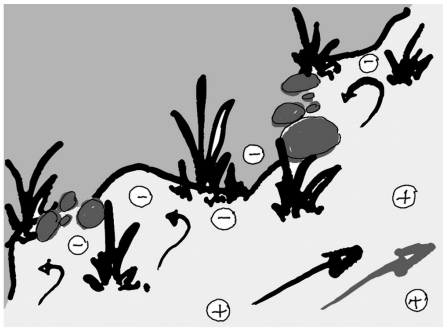

(h) Complex shoreline

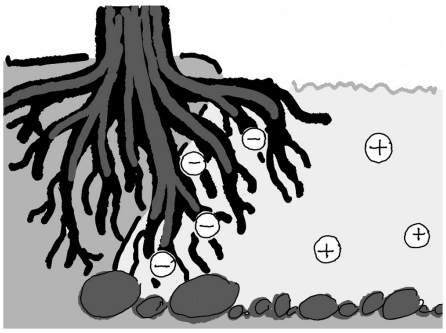

(i) Undercut banks / Roots

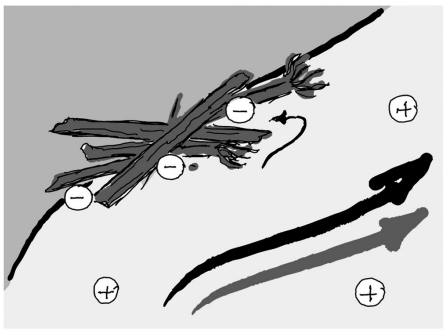

(j) Large wood accumulations

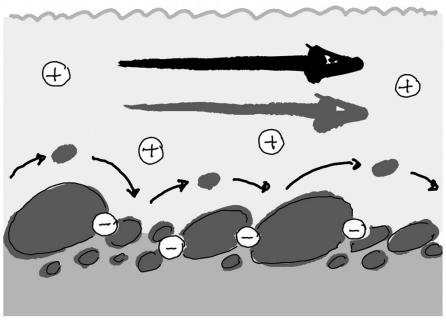

(k) Interstitial space

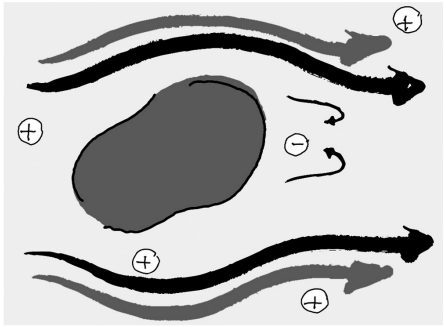

(l) Boulders

Figure 3.5 (continued)

Hydraulic variability (Figure 3.5f) describes the degree to which a river reach is well-structured and thus provides a high degree of hydro-morphological diversity. It is commonly assumed that the closer a reach is to its natural state the more heterogeneous its habitats will be, thereby providing ample refugia opportunities under a range of hydrological conditions (Sedell *et al.* 1990; Pearsons *et al.* 1992; Gjerløv *et al.* 2003). In particular, a more morphologically and hydraulically complex reach will likely preserve low bed shear stress zones during periods of elevated discharge (Pearsons *et al.* 1992; Lancaster and Hildrew 1993; Winterbottom *et al.* 1997; Lancaster 2000). Lancaster and Hildrew (1993) identified low shear stress refugia for benthic invertebrates in a field study and connected the results to tracer experiments that identified hydraulic dead zones such as

backwaters (Reynolds *et al.* 1991). Streams with a persistent high proportion of low shear stress refugia during floods also show higher dispersive fractions, that is, a high ratio of hydraulic dead zones to total reach volume. Based on these results, Lancaster and Hildrew (1993) distinguished three types of bed shear stress shifts in response to increasing discharge: type I from unimodal skewed to bimodal, type II from unimodal skewed to unimodal bell-shaped, and type III from bimodal to unimodal bell-shaped (Figure 3.6). Lancaster and Hildrew (1993) concluded that a type I shift in bed shear stresses holds the highest potential for refugia, because low bed shear stress zones persist throughout the discharge range associated with the main channel being most affected by a disturbance event (Lepori and Hjerdt 2006).

On a smaller scale, vegetation patches (Figure 3.5g), well-structured shoreline areas (Figure 3.5h), and undercut banks (Figure 3.5i) may provide shelter from flood disturbance (e.g., Rempel *et al.* 1999; Schwartz and Herricks 2005). Large wood accumulations generally reduce disturbance inside the accumulation and in their wake (e.g., Schalko *et al.* 2021). Finally, organisms may move into low-velocity crevices of the interstitial space (Figure 3.5k) or retreat behind or below boulders (Figure 3.5l) as reported in a field study by Matthaei *et al.* (2000).

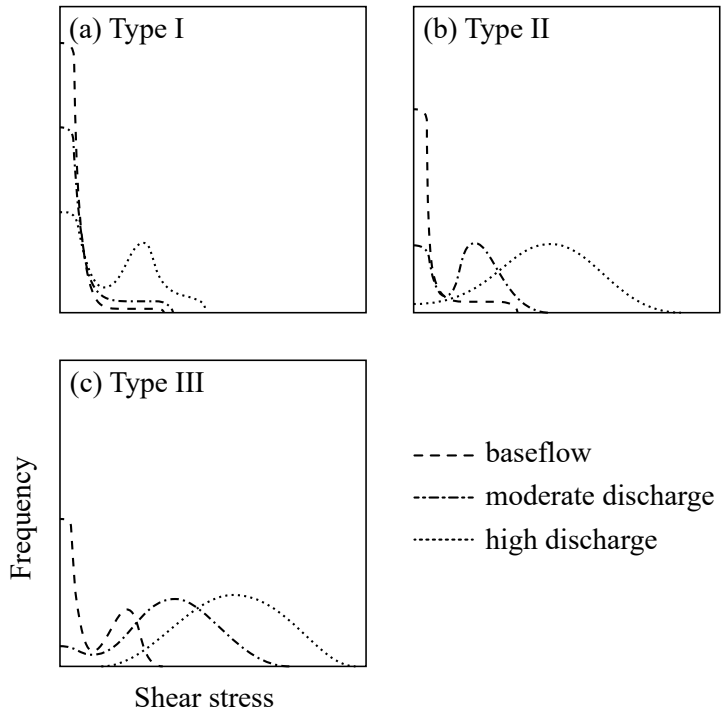

Figure 3.6 Shifts of bed shear stress frequency distributions in response to increasing discharge: (a) type I: unimodal skewed to bimodal, (b) type II: unimodal skewed to unimodal bell-shaped, and (c) type III: bimodal to unimodal bell-shaped (adapted from Lancaster and Hildrew 1993)

3.8 Summary and identified research gaps

River widening is a widely used reach-scale restoration measure applied in channelized systems. Many examples of implemented widenings can be found in literature and their effectiveness in increasing habitat heterogeneity, albeit within a limited perimeter, is widely documented. Dynamic river widening is presented as a method that focuses on re-establishing near-natural morphodynamic processes and thus is in line with the postulation to prefer process-based over structure-based restoration approaches. However, several aspects that deserve further research emerge from the presented literature.

Sediment supply has been recognized as a primary control on river morphodynamics. It acts on multiple spatial and temporal scales and may influence river planform, channel width, bedforms, and bed surface composition. Its relative importance compared to flow magnitude may vary depending on the geological, hydrological, and biological characteristics of a river but its significance for morphodynamic processes cannot be contested.

Evidence for the importance of sediment supply mainly originates from field observations. Where it was possible to disentangle the multiple anthropogenic modifications of river catchments, it became evident that decreasing sediment supply and transport led to substantial channel narrowing and simplification, incision, and substrate coarsening. Conversely, observations of channel response to increased sediment supply, for example from landslides, documented channel widening and destabilization, aggradation, and substrate fining. These processes have also repeatedly been studied in the laboratory and, to a lesser extent, in numerical models. However, many laboratory studies were conducted in fixed width flumes, thus disregarding planform changes. As the concept of dynamic river widening relies on active morphological processes and sediment supply has been shown to be a main driver thereof, this thesis aims at applying this knowledge to the rather technical setting of river widenings along channelized rivers (Rachelly *et al.* 2018).

Although a growing body of literature examines the links between morphodynamic processes and the ecological state of river reaches, our knowledge in this regard remains highly limited. These links are especially difficult to establish for extreme conditions such as floods. The assessment of restoration success is, therefore, often limited to the survey of morphological indicators and habitat analyses for mean flow conditions (but see Gabbud *et al.* 2019). This thesis aims at expanding this view by explicitly considering the effects of floods on aquatic organisms in river widenings established under variable sediment

supply conditions. The availability of refugia, that is, habitats that are less impacted by the flood disturbance, is studied via several metrics characterizing hydro-morphological conditions and sediment transport.

As river restoration projects require substantial public investments, financial means should ideally be allocated to the most effective measures for each specific case. It is therefore a key objective of this thesis to identify the necessary boundary conditions for sustained morphodynamic activity in a widened river reach. If these conditions are not met, the pursuit of a different restoration approach might be more worthwhile. Where dynamic river widening is an appropriate restoration measure, an optimization of the construction process can result in less expenses and limit the disturbance of the ecosystem during the construction period.

These identified research gaps are mainly addressed by laboratory experiments combined with 2D hydrodynamic numerical modeling. The laboratory experiments thereby serve as calibration data for the numerical model.

4 Methodology

4.1 Overview

The primary method used in this study was a mobile-bed laboratory experiment combined with hydrodynamic numerical simulations. Scaling of the laboratory experiment is discussed in Section 4.2, and the details of the experimental setup and procedure are described in Section 4.3. Section 4.4 presents the 2D hydrodynamic simulations performed to investigate the flow field in detail. Finally, the data analysis is explained in Section 4.5.

The geometric, hydrological, and sedimentological characteristics of the laboratory experiments were adapted to a section of the Kander River in Switzerland, a typical channelized subalpine gravel-bed river, where dynamic river widening is a valid restoration measure. See Section 2.6 for the characteristics of the Heustrich widening, the primary reference reach used in this study.

4.2 Scaling

Hydraulic model experiments allow the investigation of a prototype situation at a smaller scale. The ratio between field-scale and model-scale values is described by the scale factor

$$\lambda = \frac{\text{Field-scale length}}{\text{Model-scale length}}. \tag{4.1}$$

To be completely similar, a model would need to satisfy geometrical, kinematic, and dynamic similarity to the prototype (Heller 2011):

- *Geometric similarity*: similarity of shape (i.e., length, area, and volume)
- *Kinematic similarity*: similarity of motion (i.e., velocity, time, acceleration, and discharge)
- *Dynamic similarity*: identical ratios of all forces

Forces can be combined as force ratios (ASCE 2000; Heller 2011). Relevant forces for fluid mechanics are inertial, gravitational, and viscous forces, among others. Their force ratios are called Froude number F and Reynolds number R

$$\mathsf{F} = \sqrt{\frac{\text{Inertial force}}{\text{Gravitational force}}} = \frac{v}{\sqrt{gL}} \tag{4.2}$$

$$\mathsf{R} = \frac{\text{Inertial force}}{\text{Viscous force}} = \frac{Lv}{\nu} \tag{4.3}$$

where v is the flow velocity, g is the gravitational acceleration, L is the characteristic length (flow depth h in open channel flow), and ν is the kinematic viscosity of the fluid. To ensure complete (mechanical) similitude, all force ratios would need to be equal at field and model scale, effectively meaning that model tests would need to be conducted in a ”miniature universe” where all physical properties are to scale (Heller 2011). As dynamic similitude cannot realistically be achieved, model similitude is usually ensured for only the most relevant force ratio. The deviation in the remaining force ratios introduces scale effects that may lead to significant differences between model and field scale. These *scale effects* generally increase with increasing scale factor but it is not possible to define a limiting scale factor independent of the specific conditions to be modeled (Heller 2011). The careful consideration of possible scale effects is thus necessary to determine whether they can be neglected.

Open channel flow models are commonly scaled according to Froude similitude, thus ensuring an equal Froude number at field and model scale (Equation 4.2). Table 4.1 lists the scale factors used in this thesis where Froude scaling with $\lambda = 30$ was applied.

Table 4.1 Scale factors according to Froude similitude for $\lambda = 30$.

Parameter	Unit	Scale factor	
Length	m	λ	30
Area	m^2	λ^2	900
Volume	m^3	λ^3	27,000
Time	s	$\lambda^{1/2}$	5.5
Velocity	m/s	$\lambda^{1/2}$	5.5
Discharge	m^3/s	$\lambda^{5/2}$	4,930

Scale effects in Froude scale models are typically expected due to deviations in the Reynolds (inertia versus viscosity) and Weber (inertia versus surface tension) numbers (Heller 2011). The Reynolds numbers calculated for the experiments presented here place them in the turbulent flow regime ($\mathsf{R} > 10^4$) (ASCE 2000). This matches field-scale conditions, because it can be assumed that virtually all open channel flows relevant to

river engineering are turbulent.

Further, the flow conditions can be described by the grain Reynolds number R_*

$$\mathsf{R}_* = \frac{U_* D}{\nu} \tag{4.4}$$

$$U_* = \sqrt{g R_h S} \tag{4.5}$$

where U_* is the shear velocity, D is the grain diameter, ν is the kinematic viscosity, g is the gravitational acceleration, R_h is the hydraulic radius, and S is the longitudinal slope. Assuming $D = D_{90}$ (i.e., the 90$^{\text{th}}$ percentile of the grain size distribution), grain Reynolds numbers for the presented experiments are $\mathsf{R}_* > 10^2$, indicating hydraulically rough flow conditions (ASCE 2000). Therefore, scale effects due to viscosity are assumed to be negligibly small. Similarly, the initial flow depths in the laboratory experiments are $h > 0.02$ m, a lower limit suggested by ASCE (2000) to avoid non-negligible surface tension effects.

Two corrections were applied to the field-scale grain size distribution (GSD) when transferring it to model scale (see Figure 4.5 in Section 4.3.3). First, a correction to grains with grain Reynolds numbers $\mathsf{R}_* < 70$ was applied to correctly reproduce critical shear velocities for their movement (Jäggi 1986; Zarn 1992). Second, grains smaller than 0.25 mm were excluded from the model GSD to prevent cohesive effects (similar to suggestions in Heller 2011). Whether the first correction was in fact necessary cannot be conclusively assessed here, because the difference in GSD is in the range of the scatter of grain size samples obtained in the field (compare field and laboratory GSDs in Figure 4.5; Jäggi 1986). The formation of small bedforms (i.e., ripples) described as an undesirable effect of GSD scaling (Jäggi 1986) was not observed to be a dominant bed feature in the laboratory experiments presented here.

As channel morphology continuously changes during mobile-bed laboratory experiments, zones with shallow flow depths and low Reynolds numbers are expected to occur in some places. Therefore, it cannot be completely ruled out that non-negligible scale effects occur. However, the evaluation of the flow conditions just described permits the assumption that scale effects are largely negligible and the observed processes are thus broadly representative of field-scale fluvial processes.

4.3 Laboratory experiments

The laboratory experiments are the central element of this investigation on river widening morphodynamics under different sediment supply levels. To further expand our understanding of the relevant processes, they are combined with hydrodynamic numerical modeling (see Section 4.4).

The experiments were partially conducted within the scope of two Master theses by Stocker (2019) and Demuth (2020).

4.3.1 Experimental setup

The laboratory experiments were performed in a 31.6 m long and 4 m wide straight flume with a longitudinal slope of 0.01 at VAW (Figure 4.1). Within the flume, a simplified one-sided river widening surrounded by fixed banks with a slope of 2:3 (v:h) was built. Bank roughness was approximated by applying a fixed cover of grains with diameters D of 5 to 6 mm to the banks. The bed consisted of mixed-grain mobile sediment (see Section 4.3.3).

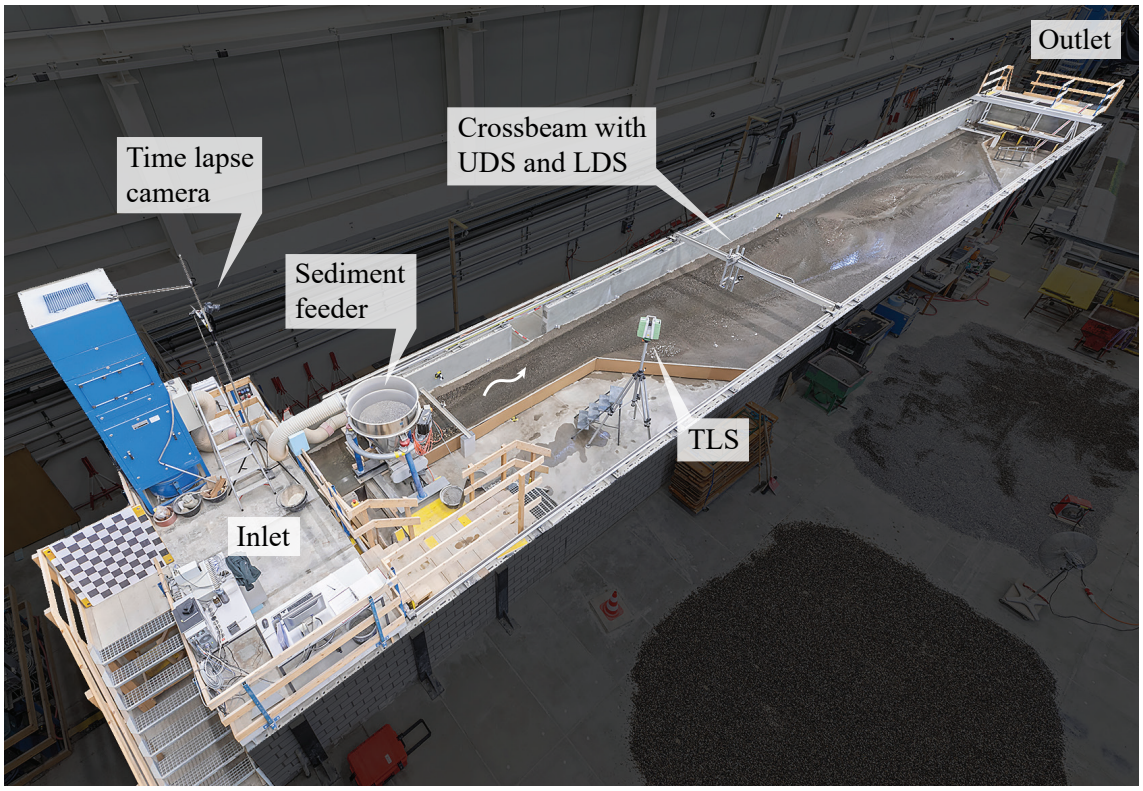

Figure 4.1 Experimental flume at VAW with its main components (UDS = ultrasonic distance sensor, LDS = laser distance sensor, TLS = terrestrial laser scanning).

Figure 4.2 shows the experimental setup and notation for the laboratory experiments. During the first phase of each experiment (see Section 4.3.4 for detailed experimental procedure), channel widening was prevented by thin panels placed between channel and floodplain with a slope of 2:3 (Figure 4.2a). After removing the panels (fixed bank) along the widening (Figure 4.3), floodplain erosion was possible during the remaining experimental duration (Figure 4.2b).

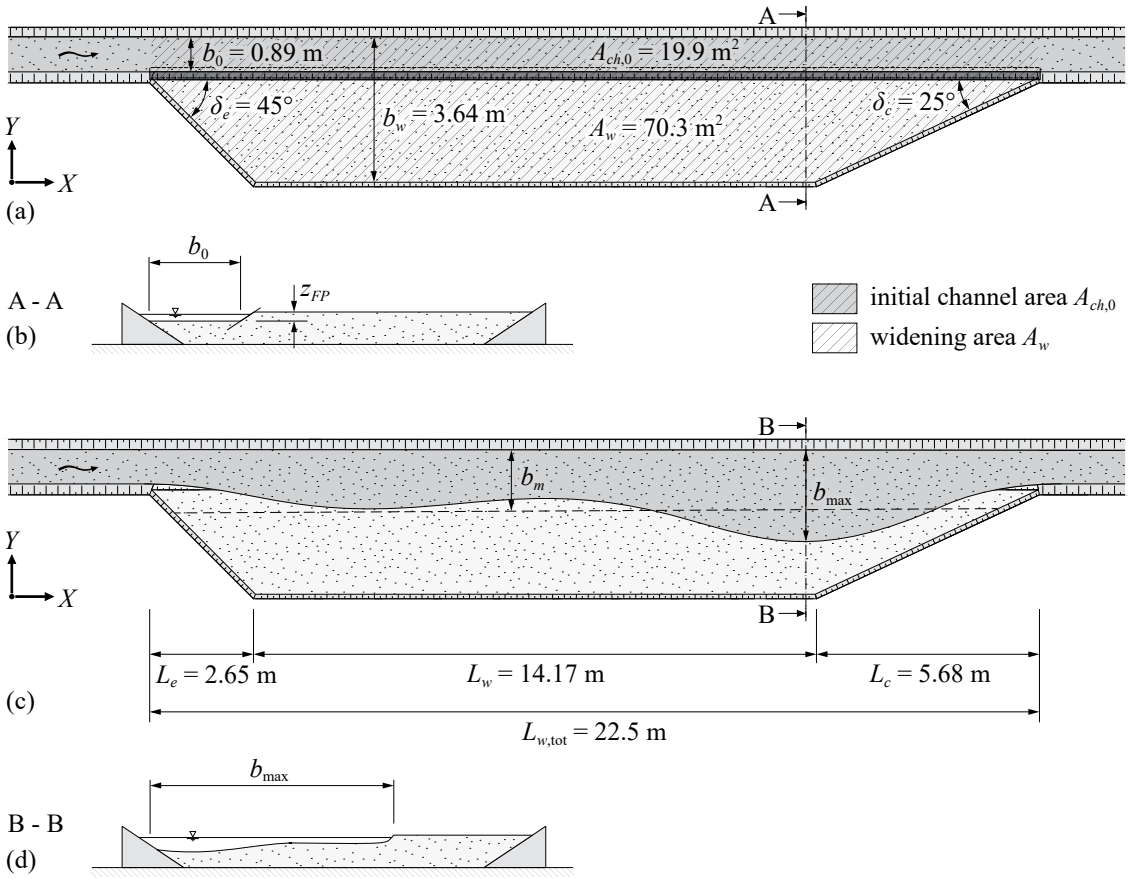

Figure 4.2 (a) Planform geometry and (b) cross-section of the experimental setup during the channelized phase (all banks are fixed), and (c) planform geometry and (d) cross-section when floodplain erosion is possible (right channel bank is erodible).

The length of the widening perimeter was $L_{w,\mathrm{tot}} = 22.5$ m on the longer side (25 channel widths) and $L_w = 14.17$ m on the shorter side (Figure 4.2). The maximum width was $b_w = 3.64$ m resulting in a widening ratio of $b_w/b_0 = 4.1$. The upstream expansion angle and downstream contraction angle were chosen as $\delta_e = 45°$ and $\delta_c = 25°$, respectively, following recommendations by Hunzinger (1998). The initial longitudinal slope of both channel and floodplain was $S_0 = 0.01$ with an initial vertical floodplain offset $z_{FP} = 0.07$ m. The floodplain elevation approximately corresponded to the water surface

elevation (WSE) of a 30-year flood in the reference reach. The total widening area excluding the channelized inlet and outlet sections was A_w = 70.3 m^2. $A_{ch,0}$ = 19.9 m^2 thereof were occupied by the initial channel. The initial channel width b_0 and area $A_{ch,0}$ are used as reference metrics for the comparison of the widened to the channelized configuration throughout this text.

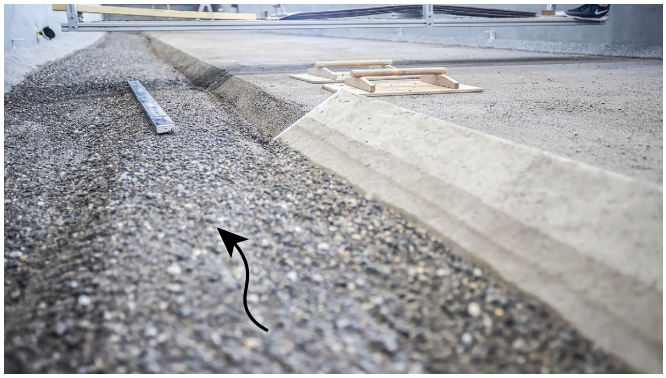

Figure 4.3 Channel after removal of the fixed bank panels to allow lateral erosion of the adjacent floodplain.

4.3.2 Instrumentation

Figure 4.4 shows a detailed layout of the experimental flume with the measurement equipment used during the laboratory study. Unless stated otherwise, measured variables were recorded at a sampling rate of 1 Hz.

The flume is equipped with two pumps with a total discharge capacity of up to 400 l/s, only one of which was used for the experiments described here. A magnetic inductive discharge meter (MID; Endress+Hauser) is installed to gauge inflow. The inlet basin and rounded inflow ramp ensure symmetrical inflow into the flume. In the outlet basin, an ultrasonic distance sensor (UDS; UNAM 30, Baumer) is linked to a gate valve to control the WSE within the basin and maintain nearly uniform flow conditions across the fixed bed sill at the downstream end of the flume. During the experiment, WSEs were measured with two fixed UDSs close to the inlet and outlet as well as a UDS mounted on a movable horizontal cross-beam. The movable UDS recorded point measurements by averaging the signal during 10 s.

Sediment was supplied using a sediment feeder (K-Tron Soder K-ML-S-510-10D) positioned directly after the inflow ramp. Sediment outflow was collected in a filtering basket suspended from load cells (SSM-AJ-10KN, Interface Inc.) and submerged in the outlet basin.

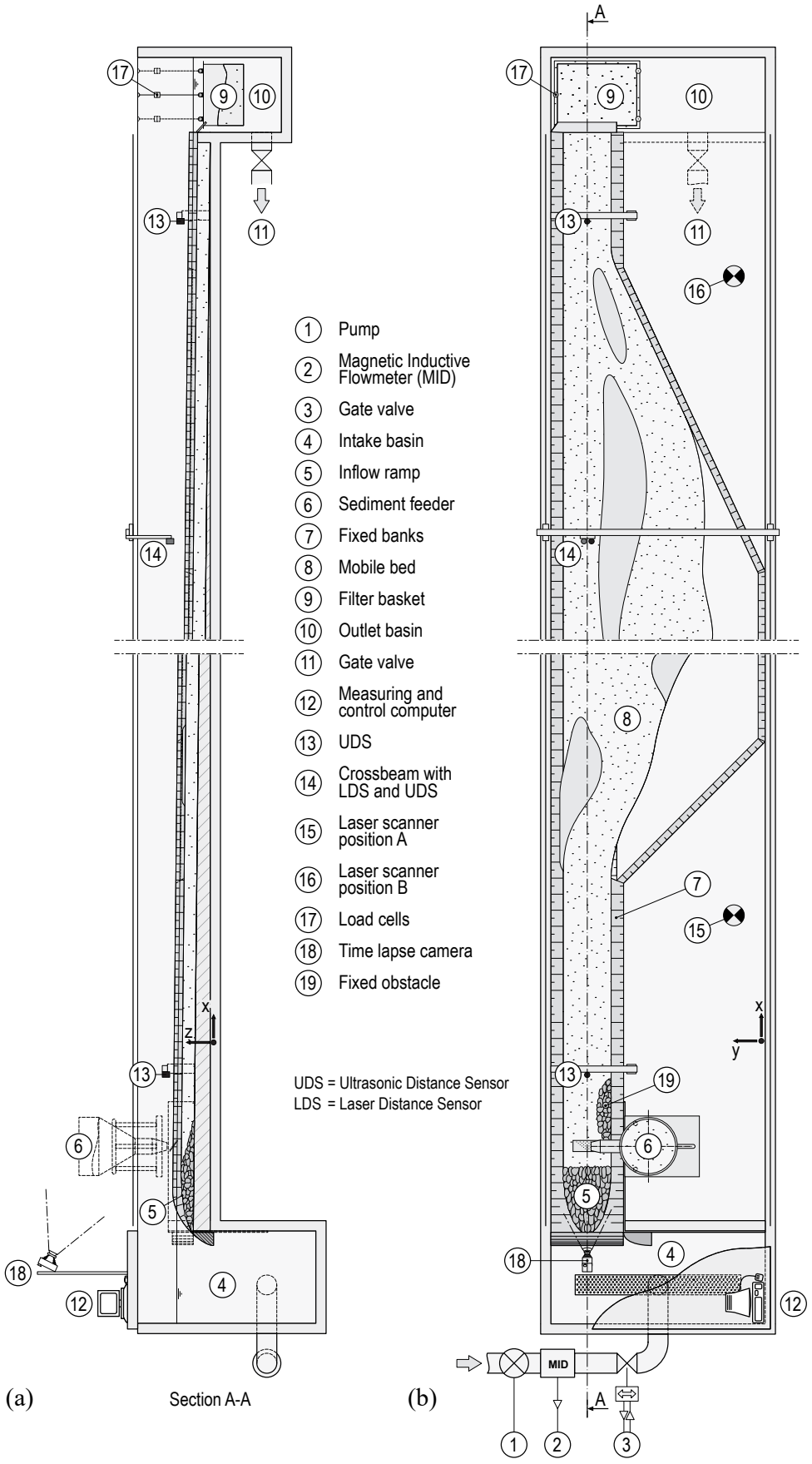

Figure 4.4 (a) Longitudinal section and (b) plan view of the experimental flume at VAW.

Both sediment inflow and outflow rates were continuously recorded during all experiments. Sediment was not recirculated and according to visual observation, all sediment was transported as bed-load.

Dry topography was recorded with the Leica ScanStation P15 terrestrial laser scanning (TLS). Point clouds from two scanning positions were merged to cover the entire flume (Figure 4.4). The density of the resulting point clouds is spatially variable with a mean of 74 pt/cm^2, $P_{5\%}$ = 10 pt/cm^2, and $P_{95\%}$ = 270 pt/cm^2. In addition to laser scanning, a laser distance sensor (LDS; OADM 21, Baumer) mounted on the movable cross-beam was used for point measurements.

4.3.3 Model sediment

Figure 4.5 shows the grain size distribution (GSD) used as bed material of the initial channel and initial floodplain as well as for the sediment feed throughout the experiments. Repeated square-hole sieve analyses of 2500 g samples ensured GSD consistency throughout the experimental period. Figure 4.5 displays a total of 39 samples and their mean GSD. The mean characteristic bulk grain sizes (± standard deviation) were D_{50} = 1.9±0.1 mm (±σ), D_m = 2.5±0.1 mm (±σ; equivalent to D_{61}), and D_{90} = 5.9±0.2 mm (±σ). Figure 4.5 also shows six line samples and six BASEGRAIN (Detert 2020) samples obtained from the reference reach of the Kander River. GSD scaling from field to model scale is described in Section 4.2.

4.3.4 Experimental program and procedure

Seven experimental *series* with eleven to twenty-nine separate *intervals* were conducted (Figure 4.6). The intervals are separated into up to five *phases* which are explained below. Between intervals, the flume was drained and filled carefully to avoid sediment relocation. Where sharp topographic features developed within the flume, small-scale sediment movement on a scale of a few cm^2 during drainage could not always be prevented. After drainage, the filtering basket in the outlet basin was emptied and its content was thoroughly mixed, weighed, and dried. The GSD of the output sediment was determined by square-hole sieving a 2500 g sample. Finally, the dry bed topography was recorded with TLS from two locations (Figure 4.4) and LDS point measurements were recorded at the same locations as the WSE measurements (UDS) were conducted during the experiments.

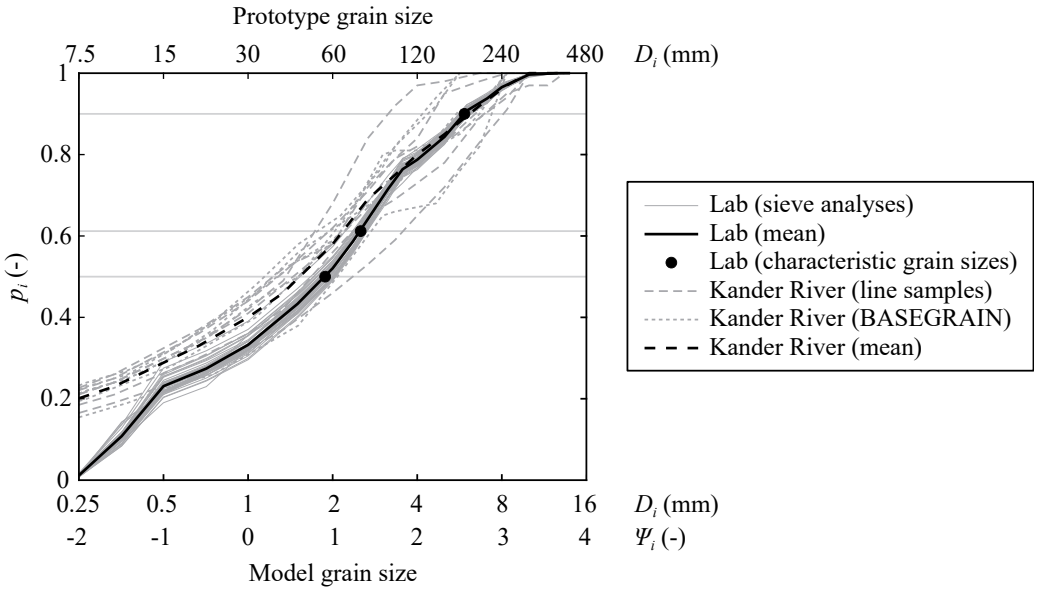

Figure 4.5 Grain size distribution (GSD) of the laboratory sediment with characteristic bulk diameters and field samples from the reference reach of the Kander River shown on the logarithmic Ψ-scale (Bunte and Abt 2001).

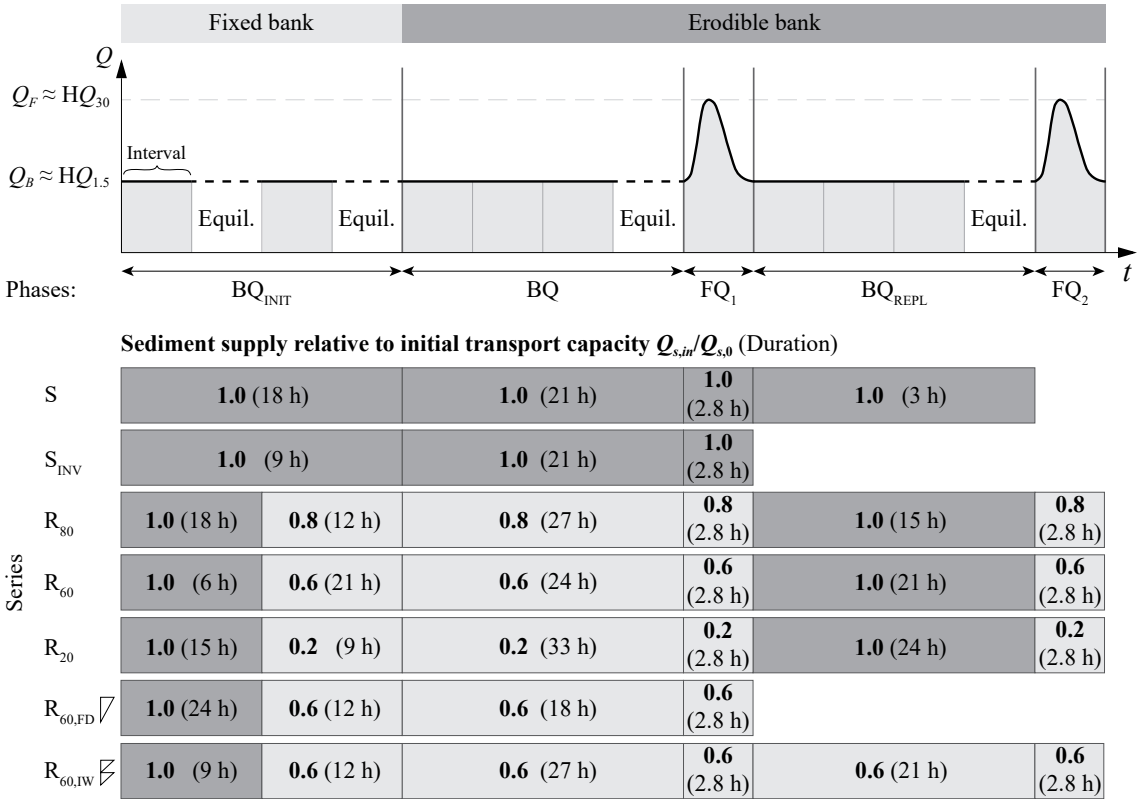

Figure 4.6 Experimental program with seven experimental series of up to five phases. Each phase consists of one or more intervals. During S (*standard*) series, sediment supply was always equal to the channel transport capacity, while R (*reduced*) series also contain intervals with reduced sediment supply. The subscript numbers thereby refer to the percentage of the channel's transport capacity, that is, R_{80} refers to a supply of 80% of the transport capacity. The subscripts INV, FD, and IW refer to *inverse initial topography*, *flow deflector*, and *initial widening*, respectively.

The experimental intervals were of two types:

- ***BQ intervals*:** 3-hour long interval with steady discharge Q_B = 23.7 l/s and steady sediment supply with different supply rates. Q_B roughly corresponds to a *bed-forming* discharge with a return period of 1.5 years in the reference reach (FOEN 2019). The duration of BQ intervals was limited by the capacity of the filtering basket at the highest sediment supply rate, and the interval duration was not adjusted for lower sediment supply rates.

- ***FQ intervals*:** 2.8-hour long interval with an unsteady *flood* hydrograph with a peak flow of Q_F = 49.5 l/s ≈ $2Q_B$ and unsteady sediment supply (Figure 4.7). The hydrograph shape and peak flow roughly correspond to a 30-year flood event in the study system (FOEN 2019). The FQ interval duration was determined by the duration of the hydrograph truncated for discharges $Q < Q_B$.

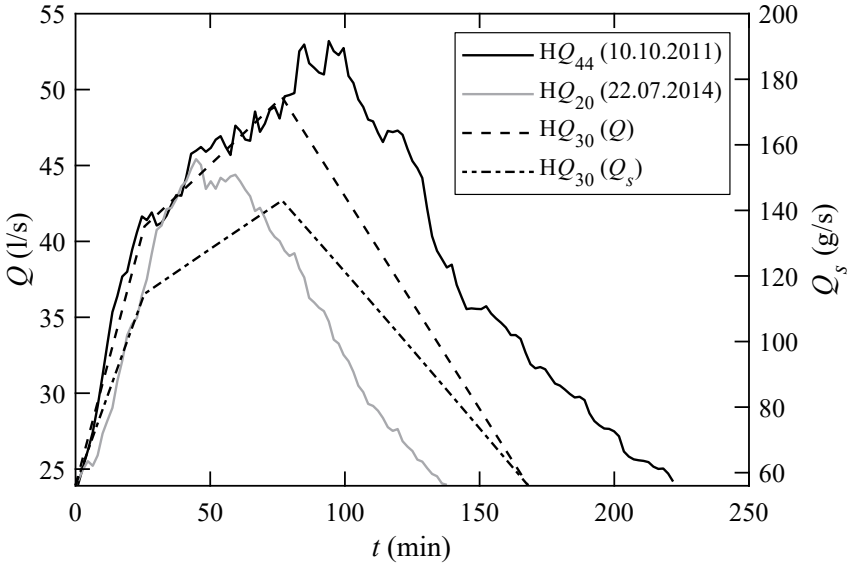

Figure 4.7 Derivation of a simplified hydrograph (Q) and sedimentograph (Q_s) with a 30-year flood peak flow (HQ_{30}) based on two flood events with return periods of 20 and 44 years recorded in the Kander River reference reach (Discharge data: FOEN 2019).

The experimental series were designed to examine the effects of sediment supply as the main variable. The sediment supply rate was thereby defined relative to the transport capacity of the initial channel as $Q_{s,in}/Q_{s,0}$. The transport capacity of a channelized reach is a useful metric in this context because it can be estimated with reasonable certainty given the reach geometry, discharge, and bed-load material.

The transport capacity $Q_{s,0}$ of the initial trapezoidal channel with slope S_0 = 0.01 and bed width b_0 = 0.89 m was determined experimentally for the bed-forming discharge Q_B = 23.7 l/s. The resulting $Q_{s,0}$ = 62.5 g/s corresponds reasonably well to Q_s = 66.8 g/s calculated after Wong and Parker (2006) for a rectangular channel of the same bed width b_0. All intervals of the S (*standard*) series were run with a sediment supply of $Q_{s,in}/Q_{s,0}$ = 1, while the supply was reduced during some phases of the R (*reduced*) series (Figure 4.6; e.g., reduction to $Q_{s,in}/Q_{s,0}$ = 0.2 or $Q_{s,in}$ = 12.5 g/s). During the unsteady FQ phases, sediment supply was also unsteady. The instantaneous rates corresponding to $Q_{s,in}/Q_{s,0}$ = 1 were calculated after Wong and Parker (2006) and for lower sediment supply levels, the rates were reduced accordingly.

Each series started with a flat bed in the initial channel (see Figure 5.1a in Section 5.2). A fixed obstacle covering one third of the channel width b_0 was installed in the flume inlet to trigger the formation of steady alternate bars (see description of phase BQ_{INIT} below; Figure 4.4). Mean values (± standard deviation) of the initial conditions of all series were bed slopes of $S_{b,0}$ = 0.0100±0.0002 (±σ), bed widths of b_0 = 0.89±0.01 m (±σ), flow depths of h_0 = 0.040±0.004 m (±σ), flow velocities of v_0 = 0.64±0.06 m/s (±σ), Froude numbers of F_0 = 1.03±0.15 (±σ), and Reynolds numbers of R_0 = $6.1 \cdot 10^5 \pm 5.7 \cdot 10^4$ (±σ). The measured values match well with a uniform flow calculation for a corresponding rectangular channel.

The experimental series were divided into a maximum of five phases described below (Figure 4.6). Phases BQ_{INIT}, BQ, and BQ_{REPL} were repeated until a sediment transport equilibrium was reached, or, in selected cases during BQ and BQ_{REPL}, until at least five intervals were completed.

- ***Phase BQ_{INIT}*:** The purpose of phase BQ_{INIT} was the formation of the initial channel topography under steady conditions. For all series, the phase began with a sediment supply of $Q_{s,in}/Q_{s,0}$ = 1 that was maintained until a sediment transport equilibrium was reached. For R series, sediment supply was then reduced to $Q_{s,in}/Q_{s,0}$ = 0.8, 0.6, or 0.2, causing rotational erosion around the fixed outlet sill in some series. The phase was continued until a new sediment transport equilibrium was reached for reduced sediment supply. In agreement with well-known morphological predictors (see Section 3.3), steady alternate bars developed during phase BQ_{INIT} of all series. The relative width b_0/h_0 = 23 and relative submergence h_0/D_{50} = 20 place the

channel in the alternate bar region (Ahmari and da Silva 2011), and the bar mode predictor m = 1.33 lies between $0.5 \leq m < 1.5$, the range of alternate bar formation (Crosato and Mosselman 2009). The bar pattern was very similar for all series except S_{INV} where the bar pattern was inverse (see Chapter 5).

- ***Phase BQ*:** Following the removal of the fixed bank along 22.5 m of the right channel side (Figures 4.2 and 4.3), the purpose of phase BQ was to study lateral erosion and channel widening under steady conditions with different sediment supply rates. Structural initiation measures to promote bank erosion were placed in series $R_{60,FD}$ and $R_{60,IW}$ (Figures 4.8 and 4.9). For $R_{60,FD}$, a fixed flow deflector of triangular shape was positioned on the left channel side at the upstream end of the widening (Figures 4.8a and 4.9a). The triangular structure was $2b_0$ long and $0.5b_0$ wide and made up of angular grains with diameters of 20 to 32 mm. Its height H_{FD} was chosen so that it was completely submerged for Q_F, but not for Q_B. For $R_{60,IW}$, the floodplain was lowered to the mean bed elevation Z_m in two consecutive triangular zones at the upstream end of the widening (Figures 4.8b and 4.9b). The planform dimensions of one initial widening triangle were identical to the flow deflector.

- ***Phase FQ$_1$*:** During phase FQ_1, the morphological effect of a single large flood peak on the widening developed under bed-forming discharge was studied. The same relative sediment supply levels as in phase BQ were applied.

- ***Phase BQ$_{REPL}$*:** Imitating sediment replenishment activities, the sediment supply level was increased to $Q_{s,in}/Q_{s,0} = 1$ in series R_{80}, R_{60}, R_{20} and the further development of the widening under steady conditions was studied. Series $R_{60,IW}$ presents an exception and was continued with $Q_{s,in}/Q_{s,0} = 0.6$.

- ***Phase FQ$_2$*:** Finally, the effect of a second large flood peak on the widening morphology was studied. The sediment supply levels were again reduced assuming that even with replenishment measures in place, sediment input during larger floods may still be reduced due to hillslope stabilization, check dams in headwaters, etc. This is especially true if the restoration of sediment transport is achieved with active (e.g., repeated gravel placement) rather than passive measures (e.g., removal of sediment barriers or discontinuation of gravel extraction).

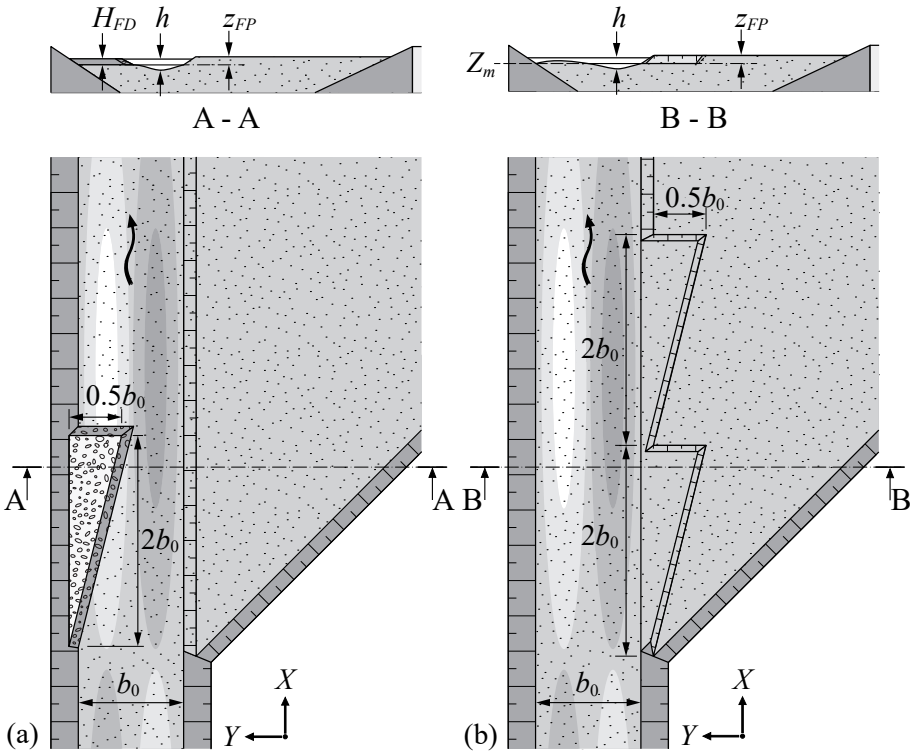

Figure 4.8 Plan view and cross-section of the (a) flow deflector (FD) and (b) initial widening (IW).

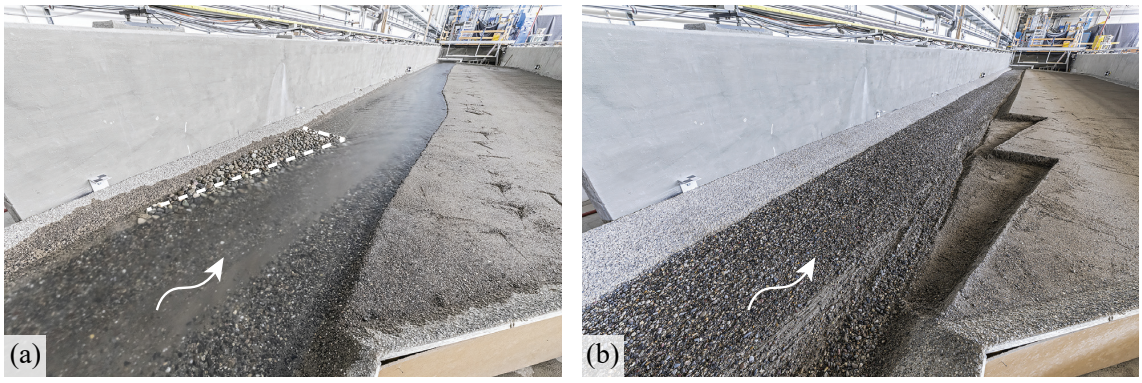

Figure 4.9 Photos of the implemented initiation measures (a) flow deflector (FD) and (b) initial widening (IW).

4.3.5 Measurement accuracy and error estimation

The laboratory experiments are subject to systematic and random errors. Table 4.2 lists the measurement accuracy for the instrumentation used in the experiments. Maximum systematic errors were determined based on the largest values measured during all experiments. The systematic error of the TLS refers to the maximum point cloud registration error based on eight fixed targets. Reported sediment output rates may be slightly underestimating true sediment output due to small quantities of fine grains carried past the

filtering basket at high filling levels.

The consistency of all elevation measurements (TLS, LDS, UDS) was checked by comparing repeated measurements of 53 points along the channel centerline. The overall deviation of LDS values from laser scan values was -0.0002±0.0055 m ($\pm\sigma$) and the deviation of UDS values from laser scan values was 0.0001±0.0064 m ($\pm\sigma$). No temporal trends in these deviations were observed throughout the experimental period.

Table 4.2 Measurement accuracy of the instrumentation used in the laboratory experiments and maximum systematic errors occurring for the measured value range.

Instrument	Parameter	Measurement accuracy	Systematic error (max.)
Magnetic inductive discharge meter MID	Q	±0.5%	±0.25 l/s
Ultrasonic distance sensor UDS	Z_{wse}	±1%	±6 mm
Laser distance sensor LDS	Z	±1%	±7 mm
Terrestrial laser scanning TLS	X, Y, Z	±3 mm at 40 m	±2 mm
Sediment feeder	$Q_{s,in}$	±0.5%	±0.7 g/s^{+}
Load cells filtering basket	$Q_{s,out}$	±5%	±3.4 g/s*

$^{+}$manual calibration measurements resulted in errors of ±0.1 and ±0.4 g/s

*based on the uncertainty of the maximum cumulated output weight of one interval recorded in this study (±37 kg within three hours)

4.4 Hydrodynamic numerical model

To obtain detailed data regarding the hydraulic conditions generated by different widening topographies and assess potential refugia availability, 2D hydrodynamic simulations were combined with results of the laboratory experiments described in Section 4.3 (cf. MacKenzie and Eaton 2017; Bankert and Nelson 2018).

The numerical simulations were performed with BASEMENT (version 3.1), a freeware simulation tool for hydro- and morphodynamic modeling developed at VAW (Vanzo *et al.* 2021). The two-dimensional model based on the depth-averaged shallow water equations was used for the hydrodynamic simulations. Morphodynamic processes were not modelled, thus a fixed bed was assumed for all simulations.

4.4.1 Model setup

The topographies obtained in the laboratory were transformed to individual computational meshes for fixed bed simulations. To reduce potential rounding errors due to small flow depths and grid units (cf. MacKenzie and Eaton 2017), the simulations were set up

at field scale (Froude scaling, $\lambda = 30$). Preliminary tests showed that differences between simulations at field and laboratory scale are in fact minimal (see Section 4.4.2). Nevertheless, the simulation setup is hereafter described at field scale with laboratory-scale values in brackets.

Each topography obtained in the laboratory (see Section 4.3) was transformed into an individual computational mesh using the BASEmesh plugin (BASEmesh 2021) for QGIS (QGIS 2021). The numerical model perimeter is, therefore, identical to the laboratory perimeter (see Section 4.3). To remove grain-scale roughness from the digital elevation models (DEMs), they were first smoothed with the SAGA (Conrad *et al.* 2015) tool *Mesh denoise* ($T_{\mathrm{SAGA}} = 0.7$, $n_{\mathrm{SAGA}} = 20$, $v_{\mathrm{SAGA}} = 50$) integrated in QGIS. The tool is based on an algorithm by Sun *et al.* (2007), which removes noise without the loss of sharp topographic features (Stevenson *et al.* 2010). The filtered DEMs were subsequently interpolated onto an unstructured computational mesh of up to 238,967 elements. The element sizes are distributed homogeneously across the entire perimeter, with a minimum element size of 0.11 m^2 (1.2 cm^2), a mean element size of 0.32 m^2 (3.6 cm^2), and a maximum element size of 0.5 m^2 (5.6 cm^2).

The hydrodynamic simulations were started from an initially dry domain. Uniform flow was assumed at both the upstream and the downstream model boundary. To robustly distinguish between wet and dry cells, a threshold of $h_{\mathrm{dry}} = 0.1$ m (0.003 m) was used (Toro 2001), which lies between the D_{50} and D_{90} of the bed material (see Section 4.3.3). A reduced threshold of $h_{\mathrm{dry}} = 0.01$ m (0.0003 m) was only used for runs with the lowest discharge Q_m (see Sections 4.4.2 and 4.4.3).

4.4.2 Model calibration

The quantitative comparison of simulation and laboratory results was mainly achieved by comparing the root mean square error (RMSE) of simulated and measured WSEs. The RMSE values were calculated at 53 points with 0.5 m spacing along the centerline of the initial channel where WSE elevation was measured during the laboratory experiments. The WSE measurements used for this comparison were obtained during the last 12 minutes of each experimental interval, thus ensuring that the observed water table matches the recorded topography used to set up the numerical model.

Bed roughness height was used as the main calibration parameter. The dimensionless friction coefficient c_f was determined following the Chézy approach (cf. Vetsch *et al.*

2021). It uses a logarithmic friction law, and the dimensionless friction coefficient c_f is calculated as

$$\begin{cases} c_f = 5.75 \log\left(12\dfrac{R_h}{K_s}\right) & \text{for } R_h \geq K_s \\ c_f = 5.75 \log\left(12\right) & \text{for } R_h < K_s \end{cases} \tag{4.6}$$

where R_h is the hydraulic radius and K_s is the bed roughness height.

The optimal parametrization of bed roughness was determined by varying the bed roughness height K_s used in the Chézy approach. Bed roughness of gravel-bed rivers is usually linked to a characteristic grain size, and K_s was thus varied in relation to the field-scale $D_{90} \approx 0.188$ m (see Figure 4.5). Figure 4.10 presents the RMSE values resulting from variable bed roughness heights K_s for eleven randomly selected topographies. The RMSE values obtained for widening topographies (Figure 4.10b) had higher scatter than RMSE values derived for channel topographies (Figure 4.10a). This is likely due to more complex topography and thus more variable flow depths in the widened configuration. Armoring may also play a role with stronger armoring potentially increasing the bed roughness height. This tendency is visible in Figure 4.10b but was not further investigated. Overall, a uniform bed roughness height of $K_s = 0.188$ m $\approx D_{90}$ was determined suitable and was used for all further simulations.

Note that the power law based Strickler approach (Strickler 1923; Vetsch *et al.* 2021) with $k_{st} = 31$ m$^{1/3}$/s $\approx 23.5 D_{90}^{-1/6}$ also produced satisfactory but more ambiguous results in that the optimal roughness value was less evident (cf. Rachelly *et al.* 2021b).

In addition to bed roughness height, several other parameters were varied in preliminary runs (see summary in Table 4.3). The 2D Courant-Friedrichs-Lewy (CFL) criterion is defined as (Vetsch *et al.* 2021)

$$\text{CFL} = \frac{\left(\sqrt{v_x^2 + v_y^2} + c\right)\Delta t}{r_i} \tag{4.7}$$

where v_x, v_y are the flow velocity components in x- and y-direction, $c = \sqrt{gh}$ is the shallow water wave celerity, and r_i is the radius of the element incircle. CFL = 0.95 was used for all hydrodynamic simulations.

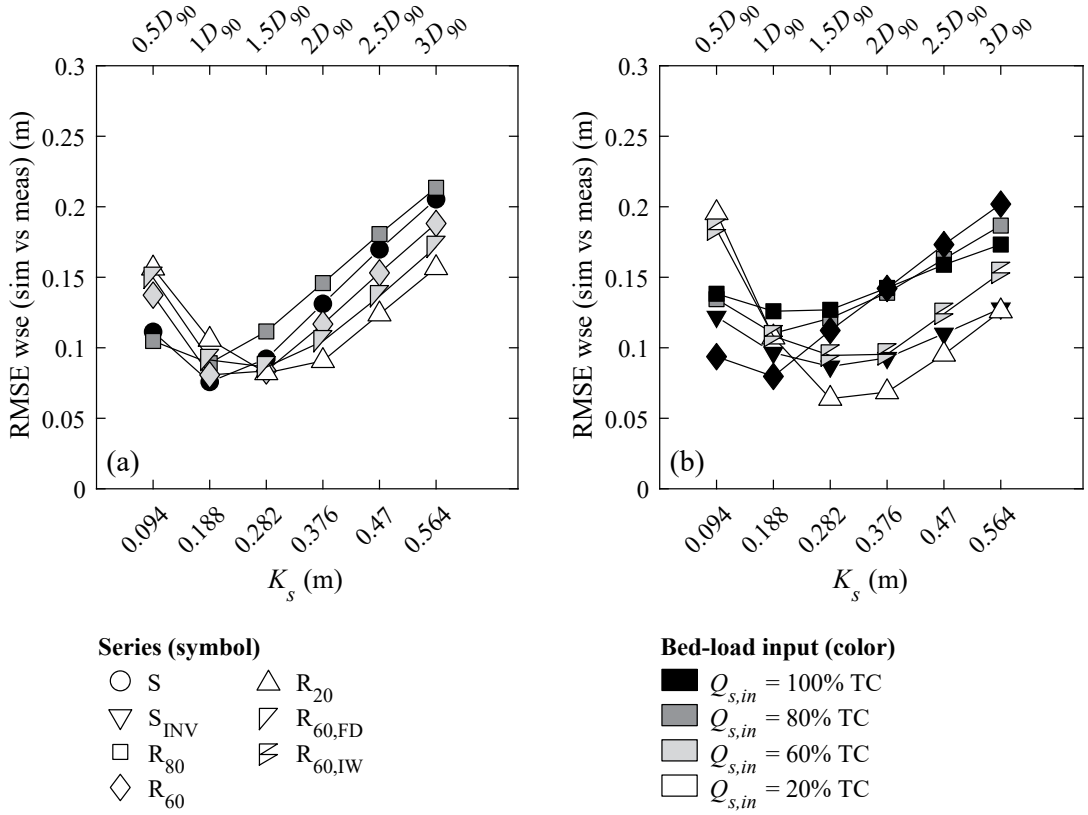

Figure 4.10 RMSE values for simulated versus measured WSEs resulting from variation of uniform bed roughness height for (a) five channel and (b) six widening topographies.

Table 4.3 Summary of calibration results for parameters other than bed roughness.

Parameter variation (number of tested topographies)	Summarized results
Field vs. model scale (3)	Maximum RMSE deviation of 3.3%
CFL = [0.1,1] (1)	No RMSE deviations
h_{dry} = [0.01;0.1] m (3)	h_{dry} = 0.1 m identified as more suitable value in qualitative analysis of floodplain inundation

4.4.3 Test program

Steady state simulations were performed for discharges Q_B and Q_F and further characteristic discharges ranging from mean annual flow Q_m = 20.4 m^3/s (4.1 l/s) to a 100-year flood HQ_{100} = 313 m^3/s (63.5 l/s) (Table 4.4). The simulation time was 50 min (9 min) or longer if a steady state was not yet reached. The steady state was verified by ensuring flow retention (inflow – outflow) and changes in wetted area were below 0.1% between time steps (Figure 4.11).

Table 4.4 Characteristic discharges of the Kander River used in the hydrodynamic simulations listed as absolute values at field and laboratory scale and as multiples of the mean annual discharge Q_m (data series 1981-2018; FOEN 2019). Simulations with Q_B ($HQ_{1.5}$) were performed for all topographies, while simulations with all listed discharges were only performed for the topographies of the final interval of each experimental phase.

		Q Field (m^3/s)	Q Lab (l/s)	Q/Q_m (-)	Relevance
Mean annual discharge	Q_m	20.4	4.1	1	Baseflow conditions
Discharge reached or exceeded on 3 days per year	Q_3	71	14.4	3.5	High flow conditions
Discharge reached or exceeded on 1 day per year	Q_1	88.1	17.9	4.3	High flow conditions
Flood with a return period of 1.5 years	$HQ_{1.5}$ | Q_B	118.3	24	5.8	Bed-forming discharge; corresponds to steady bed-forming discharge (Q_B) in the laboratory experiments
Flood with a return period of 2 years	HQ_2	128	26	6.3	Bed-forming discharge
Flood with a return period of 5 years	HQ_5	163	33.1	8	Bed-forming discharge
Flood with a return period of 10 years	HQ_{10}	193	39.2	9.5	Medium flood
Flood with a return period of 30 years	HQ_{30} | Q_F	244	49.5	12.0	Large flood; corresponds to the peak flow of the flood hydrograph (Q_F) in the laboratory experiments
Flood with a return period of 100 years	HQ_{100}	313	63.5	15.3	Very large flood

Note that for many simulations, the simulated discharge is higher than the formative discharge of the topography, for example, when a HQ_{30} discharge is run on topographies obtained during a BQ phase in the laboratory. This might lead to some unrealistic flow

conditions, as the topography would continually adjust to the imposed discharge under natural conditions. However, these deviations are assumed to be small compared to the general trends in hydraulic variability that are observed when subjecting different topographies to a wide range of discharges (e.g., Reid *et al.* 2020).

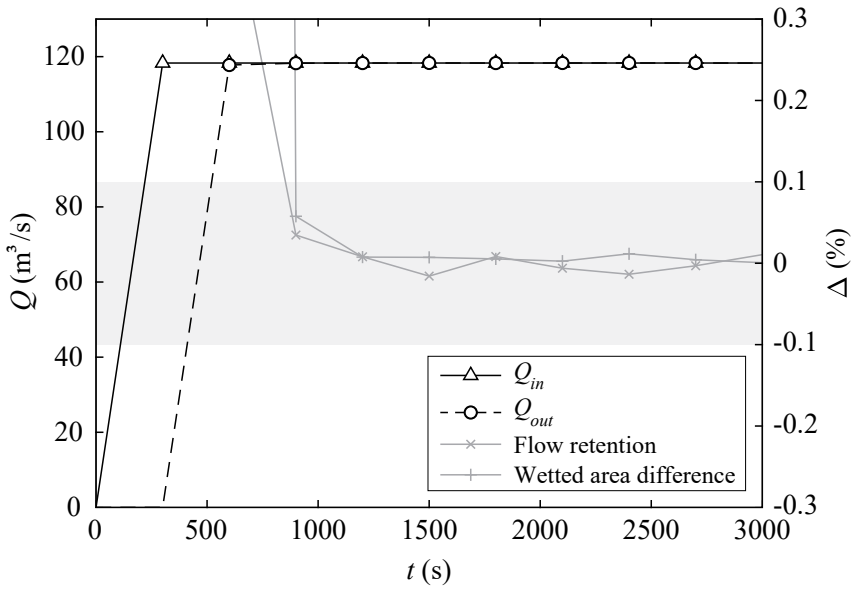

Figure 4.11 Example steady state check for a hydrodynamic simulation. Flow retention and wetted area differences between time steps below ±0.1% were judged to be sufficiently low to qualify as steady state.

4.5 Data analysis

In this section, the basic analysis of topographic data and flow field characteristics are described. Based both on data obtained from the laboratory experiments and the hydrodynamic numerical simulations, several other variables were derived.

4.5.1 Bed elevation and sediment relocation

Figure 4.12 presents the analysis of the topographic data obtained from the laboratory experiments. The laser scanning point clouds were linearly interpolated onto a 0.01x0.01 m grid to obtain digital elevation models (DEMs) (Figure 4.12a,b). The DEM of difference (DoD) was obtained by subtracting one DEM from another (Figure 4.12c). The DoD error quantified by linear error propagation of the laser scan registration error of ±0.002 m results in $\delta_{DOD} = (\delta_{DEM1}^2 + \delta_{DEM2}^2)^{0.5} = (0.002^2 + 0.002^2)^{0.5} = 0.0028$ m. Probabilistic thresholding with a Student's t-test and a confidence level of 95% was applied to identify areas of true bed elevation change (Figure 4.12d; Lane *et al.* 2003). Figures 4.12e

and 4.12f show the elevation distribution for the unthresholded and thresholded DoDs corresponding to Figures 4.12c and 4.12d, respectively.

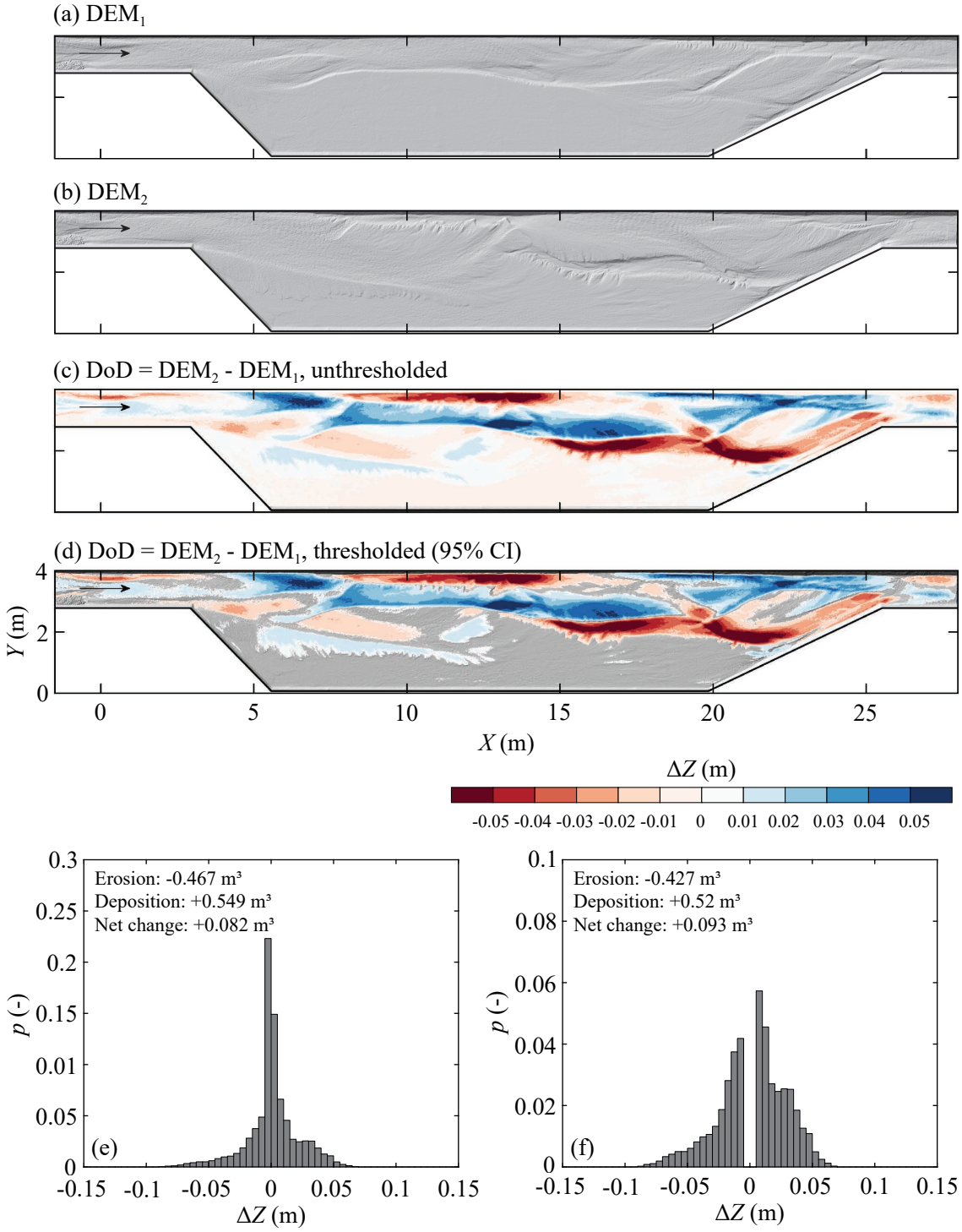

Figure 4.12 Example topographic analysis with (a) digital elevation model DEM_1, (b) DEM_2, (c) unthresholded DEM of difference (DoD), (d) thresholded DoD (95% confidence interval; Lane *et al.* 2003), (e) bed elevation distribution of the unthresholded DoD, and (f) bed elevation distribution of the thresholded DoD. Note the different ordinate scaling in (e) and (f).

Erosion and deposition areas and volumes within the widening perimeter were identified from the DoDs. The total sediment relocation area A_{reloc} is defined as the sum of erosion and deposition areas.

4.5.2 Alternate bar characteristics

For phase BQ_{INIT} (see Section 4.3.4), alternate bar characteristics were extracted from the DEMs by evaluating cross-sectional bed elevation statistics in streamwise direction. The mean bed elevation in every cross-section is $Z_{m,i}$, the 95$^{\text{th}}$ percentile is $Z_{95,i}$, and the 5$^{\text{th}}$ percentile is $Z_{5,i}$. Riffles are located at local minima of $Z_{95,i} - Z_{m,i}$, and the deepest scours η_B at local minima of $Z_{5,i} - Z_{m,i}$. Bar height H_B was defined as $Z_{95,i} - Z_{5,i}$ at the location of the deepest scour η_B (Figure 4.13; cf. Ikeda 1984).

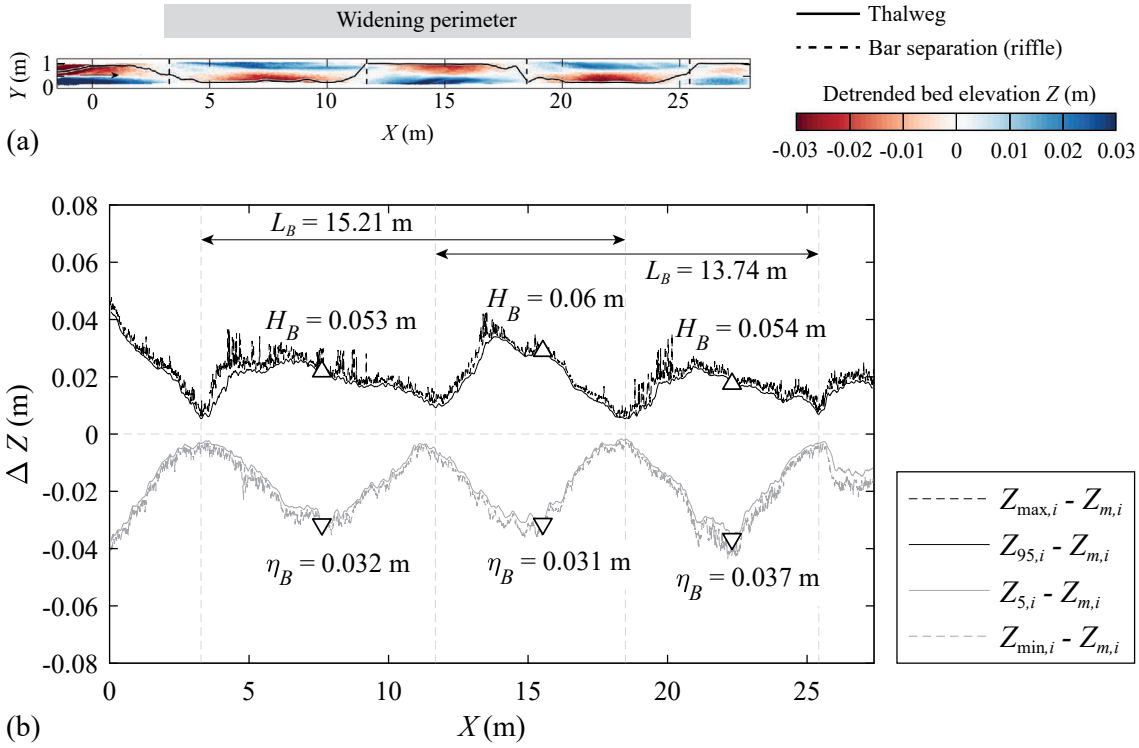

Figure 4.13 Example (a) detrended bed elevations and (b) longitudinal profiles of detrended maximum, 95$^{\text{th}}$, 5$^{\text{th}}$, and minimum percentile bed elevations for the determination of alternate bar characteristics. The 95$^{\text{th}}$ and 5$^{\text{th}}$ percentiles are shown as moving averages (window size of 0.1 m). The vertical bar separation lines (location of riffles) at the local minima of $Z_{95,i} - Z_{m,i}$, scour depths η_B, bar heights H_B, and bar lengths L_B are shown.

4.5.3 Flow field

The primary flow field variables that were extracted from the numerical simulations include flow depths h, depth-averaged flow velocities v, and bed shear stresses τ_b (Figure 4.14).

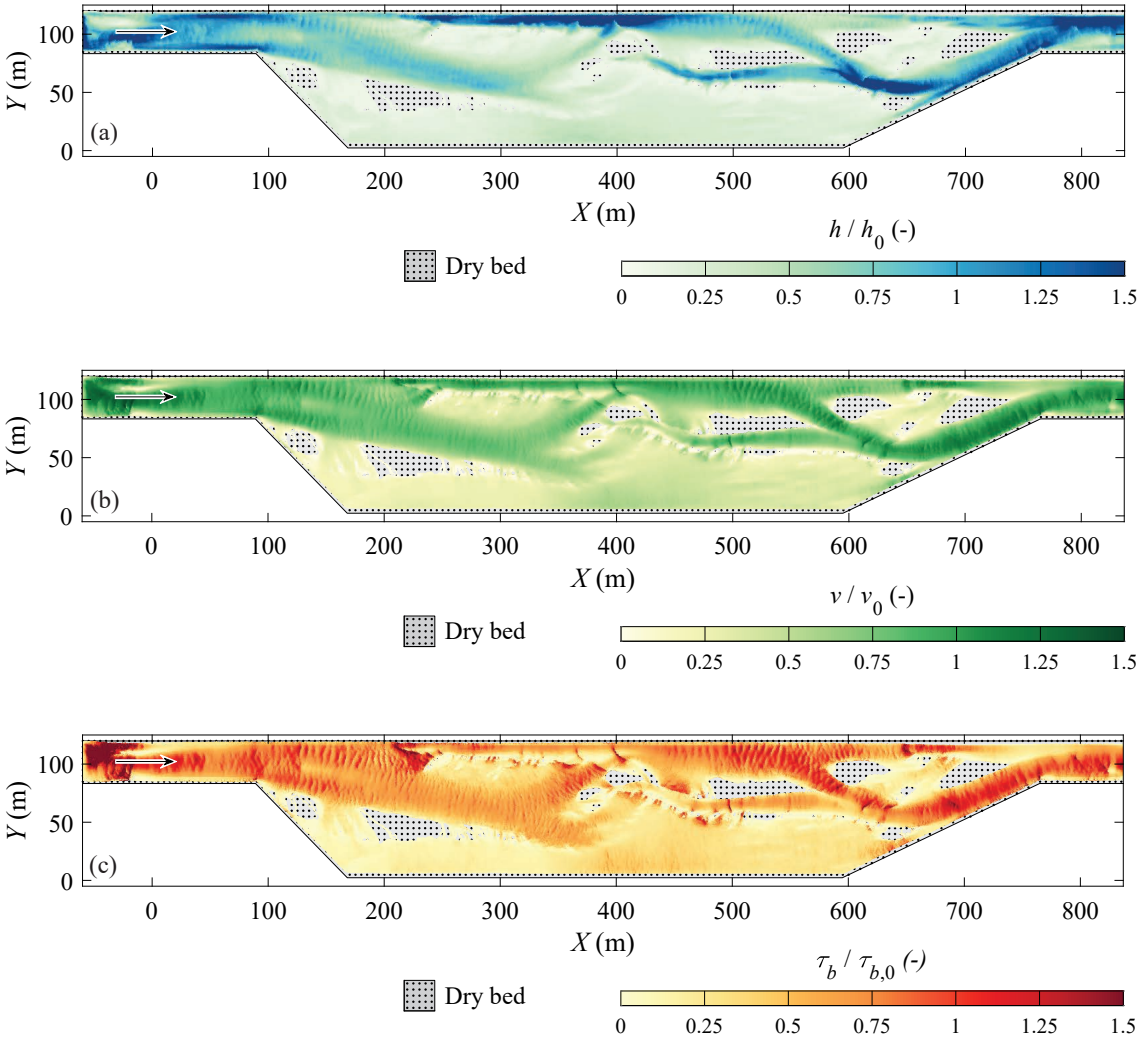

Figure 4.14 Exemplary flow field with relative (a) flow depth, (b) flow velocity, and (c) bed shear stress. The variables are presented relative to their mean value in the initial channel (subscript 0).

Applying the quadratic friction law (see, e.g., Chow 1959 for an overview), bed shear stress τ_b was calculated as

$$\tau_b = \left(\left(\frac{\rho v_x |v|}{c_f^2} \right)^2 + \left(\frac{\rho v_y |v|}{c_f^2} \right)^2 \right)^{0.5} \tag{4.8}$$

where ρ is the density of water, v_x is the velocity component in x-direction, v_y is the

velocity component in y-direction, $|v| = \sqrt{v_x^2 + v_y^2}$ is the velocity magnitude, and c_f is the dimensionless Chézy coefficient. Dimensionless bed shear stress θ was calculated for the median grain diameter D_{50} (see Section 4.3.3) as

$$\theta_{D50} = \frac{\tau_b}{(g(\rho_s - \rho)D_{50})} \tag{4.9}$$

where g is the gravitational acceleration, and ρ and ρ_s are the densities of water and sediment, respectively.

4.5.4 Geometric and hydraulic characteristics of the widening

Table 4.5 shows metrics characterizing the river widening. Most of them were derived from the numerical simulations. The reason for not using the topographical data to define channel width was the significant channel bed aggradation observed in some experiments making it difficult to distinguish channel from floodplain. Instead, a definition based on hydraulic characteristics ($\theta_{D50} > 0.03$) was assumed to generate more reliable results. The same threshold was also used to define mean flow depth with the intention to exclude shallow and slow flowing floodplain areas from the mean flow depth calculation.

Table 4.5 Metrics characterizing the river widening perimeter. All metrics except S_{wse} were derived from the numerical simulations.

Notation	Metric	Definition
A_{wet}	Wetted area (m^2)	Total area of wetted cells
$A_{\theta>\theta c}$	High bed shear stress area (m^2)	Total area of cells where $\theta > \theta_c$ with $\theta_c = 0.03$ or 0.06
h_m	Mean flow depth (m)	Mean flow depth of cells where $\theta_{D50} > 0.03$
b_m	Mean channel width (m)	Mean cross-section widths where $\theta_{D50} > 0.03$
b_{max}	Maximum channel width (m)	99^{th} percentile of cross-section widths where $\theta_{D50} > 0.03$
S_{wse}	WSE slope (-)	Linear regression of point measurements along the centerline of the initial channel during the last 8.5 min of each interval

High bed shear stress areas $A_{\theta>\theta c}$ were used to characterize the potential bed-load transport conditions. A critical Shields parameter of $\theta_c = 0.03$ was assumed for partial transport and $\theta_c = 0.06$ for full transport (Buffington and Montgomery 1997). The dimensionless bed shear stress θ can be calculated for a certain grain diameter, usually the

median grain diameter D_{50} (see Eq. 4.9). See Figure 4.15 for an example flow field with binned critical bed shear stresses related to certain intensities of bed mobility.

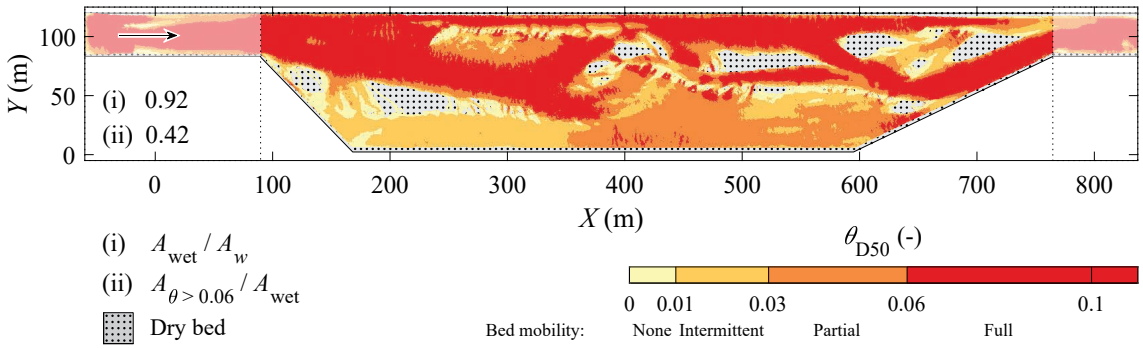

Figure 4.15 Example of wetted areas colored by dimensionless bed shear stress. 92% of the widening area are wetted, and 42% of the wetted area experience dimensionless bed shear stresses $\theta_{D50} > 0.06$.

4.5.5 Shoreline length

The shoreline length relative to the channel length (km/km) was calculated based on the wetted area A_{wet} (Tockner and Stanford 2002). Shoreline length is a measure of complexity of the marginal zones and lateral connectivity between aquatic, semi-terrestrial, and terrestrial habitats (Ward *et al.* 1999). It is discharge-dependent and can assume values from 2 km/km for straight channels up to 25 km/km for braided morphologies such as the Tagliamento River in Italy (Tockner and Stanford 2002). To compute the shoreline length, flow depths obtained from the numerical simulations were interpolated onto a 0.01x0.01 m grid as binary data (1 = wet, 0 = dry), and wet patches were delineated. To prevent overestimation of the shoreline length, identified boundaries with a length below 300 grid elements or 3 m (90 m at field scale) were discarded. The threshold was set based on a comparison of total shoreline length to minimum boundary length of individual patches (Figure 4.16). The remaining smoothed boundary lengths (window length 21) were then summed and divided by the streamwise length of the river widening 22.5 m (675 m at field scale, see Figure 4.2c).

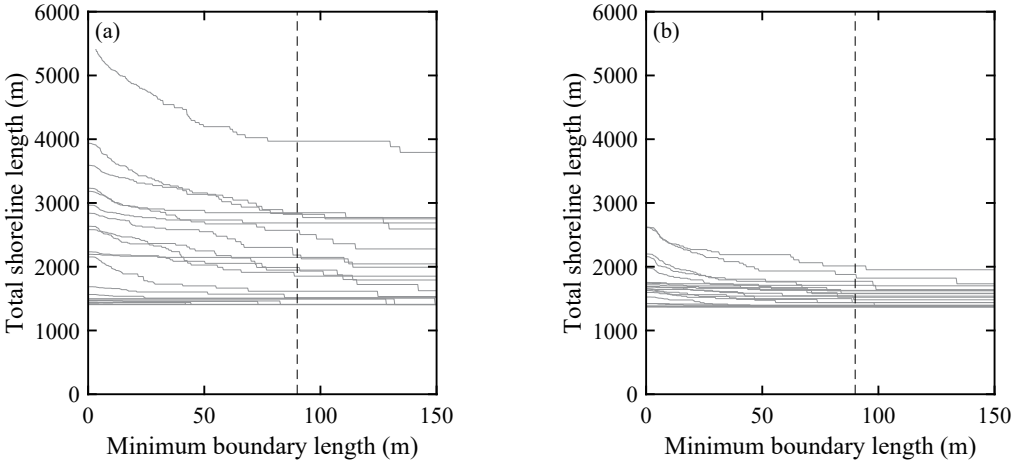

Figure 4.16 Total shoreline length (field scale) for (a) a topography of series S and (b) a topography of series R_{20} as a function of minimum boundary length. The different curves represent discharges from 40-320 m^3/s (8-65 l/s at model scale). A threshold boundary length of 90 m (3 m at model scale) was defined for this study. Note that the minimum determined shoreline length is 1377 m in (b). Divided by the widening length of 675 m, the resulting 2.04 km/km are close to the theoretical minimum value of 2 km/km.

4.5.6 Hydro-morphological diversity

Flow depth and velocity as the basic flow field descriptors can be used to assess the hydro-morphological conditions within the widening perimeter. Here, the dimensionless hydro-morphological index of diversity (HMID; Gostner *et al.* 2013) was calculated as

$$\mathrm{HMID} = \left(1 + \frac{\sigma_v}{\mu_v}\right)^2 \cdot \left(1 + \frac{\sigma_h}{\mu_h}\right)^2 \tag{4.10}$$

where μ_v is the mean flow velocity, σ_v is the standard deviation of flow velocities, μ_h is the mean flow depth, and σ_h is the standard deviation of flow depths. Here, μ_v and μ_h refer to spatially averaged values within the widening perimeter. The higher the HMID the closer the hydro-morphological conditions are to natural conditions, independent of the specific morphology present. Gostner *et al.* (2013) introduced the classification (i) channelized and morphologically heavily altered for HMID < 5, (ii) lightly modified with limited hydraulic variability for 5 ≤ HMID ≤ 9, and (iii) morphologically pristine for HMID > 9. Note that the HMID was originally defined for mean flow conditions and its value is discharge-dependent.

4.5.7 Refugia availability

Aquatic flood refugia availability was assessed using several hydro-morphological characteristics that can be linked to potential refugia provision by identifying habitats

subject to reduced disturbance intensities (Table 4.6; see Section 3.7). Quantitative values associated with these characteristics (e.g., HMID) were compared across a wide range of discharges to identify discharge-dependent patterns in refugia availability associated with different widening topographies (see Table 4.4).

Table 4.6 Hydro-morphological characteristics related to the potential availability of aquatic flood refugia. All characteristics except for the active bed-load transport zone were derived from the numerical simulations.

Hydro-morphological characteristic	Relevance
Hydro-morphological diversity	Hydro-morphologically more complex reaches potentially provide more habitats that function as refugia (e.g., Pearsons *et al.* 1992; Gjerløv *et al.* 2003; see Section 4.5.6).
Floodplain inundation	Shallow, slow flowing habitats become accessible once the floodplain is inundated (e.g., Negishi *et al.* 2002; Schwartz and Herricks 2005; see Section 4.5.4).
Shoreline length	High shoreline length implies high complexity of the marginal zones, potentially providing marginal refugia (see Section 4.5.5).
Bed shear stress distribution	Low bed shear stress zones that persist during high flows provide potential refugia where disturbance intensity is reduced (e.g., Lancaster and Hildrew 1993; Winterbottom *et al.* 1997; see Section 4.5.4)
Active bed-load transport zone	Habitats subject to excessive scouring or burial are not suitable refugia (e.g., Matthaei and Townsend 2000; see Section 4.5.1).

The hydraulic and geomorphic conditions could further be linked to habitat suitability data for different organism groups, such as relationships between near-bed shear stress and macroinvertebrate densities (e.g., Gabbud *et al.* 2019). However, this project does not include such analyses since it is not concerned with a specific case study. In addition, residential habitat suitability must not necessarily coincide with the refuge function of a particular habitat. The application of habitat suitability data for flood refugia assessment thus requires detailed knowledge of the biota at a specific site. Instead, the focus of the refugia analysis herein was on the discharge-dependent dynamics of hydro-morphological conditions and the identification of gradual versus abrupt responses to increasing disturbance intensity.

5 Sediment supply control on widening morphodynamics

Parts of this chapter are submitted for publication:

- *Rachelly* et al. *(2022) Sediment supply control on morphodynamic processes in gravel-bed river widenings.*

Accompanying data can be found in Rachelly et al. *(2021c)*.

5.1 Overview

This chapter presents the results of the laboratory experiments. In Section 5.2, photographic impressions of different morphodynamic processes observed during the experiments are provided, and morphodynamic activity is defined. Section 5.3 summarizes all experiments as time series of several metrics. In the sections that follow, the experimental series are analyzed in more detail. The formation of alternate bars in the initial channel is examined in Section 5.4. The widening response to variable sediment supply rates and bank erosion initiation measures is presented in Section 5.5. Different morphodynamic trajectories are identified in Section 5.6, and finally, the results are discussed and summarized in Sections 5.7 and 5.8, respectively.

5.2 General process observations

The aim of this section is to provide the reader with visual impressions of typical channel patterns and morphodynamic processes observed in the laboratory experiments (Figures 5.1 to 5.8). The processes are not discussed in detail at this point. Where appropriate, the following sections refer back to these figures. With the exception of Figure 5.1a, the photographs show a discharge of 1 l/s (4.9 m^3/s at field scale). This discharge was applied solely for visualization purposes and roughly corresponds to the Q_{347} of the reference river reach, that is, the discharge reached or exceeded on 347 days (95%) of the year (FOEN 2019). The shoreline is emphasized by a white dashed line where relevant and the black arrows schematically visualize the main flow paths.

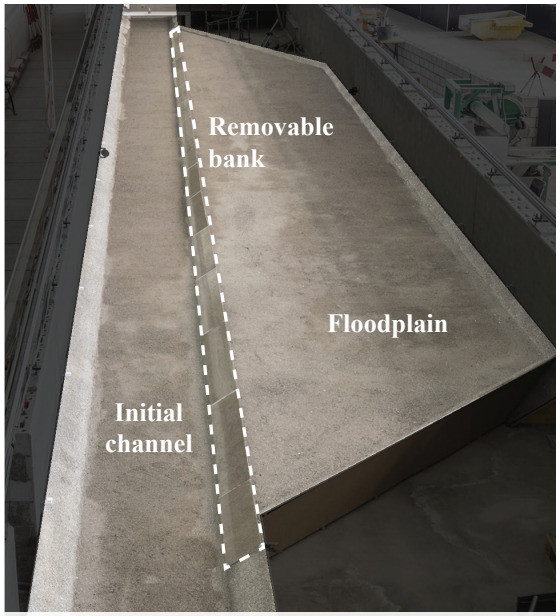

(a) Series S | Phase BQ_{INIT} (start)

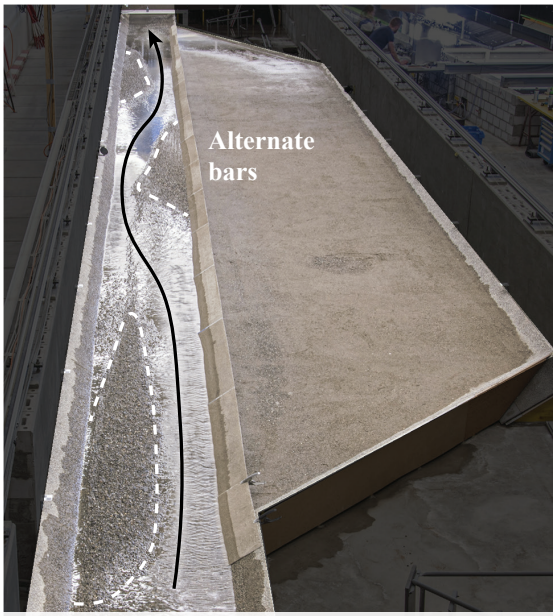

(b) Series S | Phase BQ_{INIT} (4/7) | $Q_{s,in}/Q_{s,0} = 1$

Figure 5.1 Alternate bar formation: Initial channelized configuration with (a) the plane bed separated from the floodplain by removable bank panels at the start of each experiment and (b) alternate bars formed during the experimental phase BQ_{INIT}.

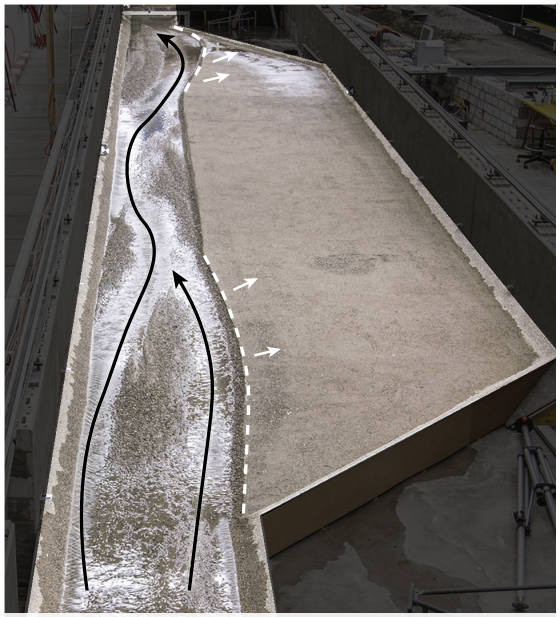

(a) Series S | Phase BQ (2/7) | $Q_{s,in}/Q_{s,0} = 1$

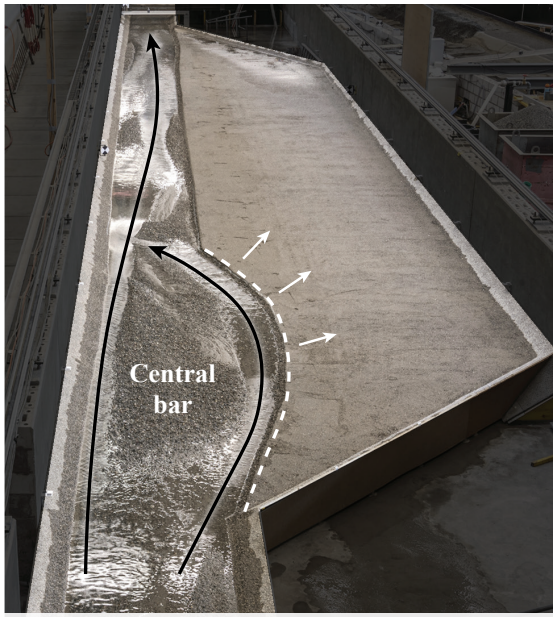

(b) Series $R_{60,IW}$ | Phase BQ (3/9) | $Q_{s,in}/Q_{s,0} = 0.6$

Figure 5.2 Initiation of lateral erosion: Two examples of lateral floodplain erosion initiation (a) at the location of the alternate scours formed during phase BQ_{INIT} and (b) at the location of the initial floodplain lowering in series $R_{60,IW}$. Note the central bars that formed concurrently with lateral erosion.

(a) Series R_{20} | Phase BQ_{REPL} (end) | $Q_{s,in}/Q_{s,0} = 1$ (b) Series R_{20} | Phase FQ_2 (end) | $Q_{s,in}/Q_{s,0} = 0.2$

Figure 5.3 Channel disconnection: (a) The main channel flowing through the former floodplain was (b) filled and shifted towards its initial course. The side channel was abandoned for low flows.

(a) Series R_{80} | Phase BQ_{REPL} (1/5) | $Q_{s,in}/Q_{s,0} = 1$ (b) Series R_{80} | Phase BQ_{REPL} (2/5) | $Q_{s,in}/Q_{s,0} = 1$

Figure 5.4 Channel reconnection: (a) A disconnected side channel on the former floodplain was (b) reconnected resulting in two channels of similar size.

(a) Series $R_{60,IW}$ | Phase BQ (7/9) | $Q_{s,in}/Q_{s,0} = 0.6$

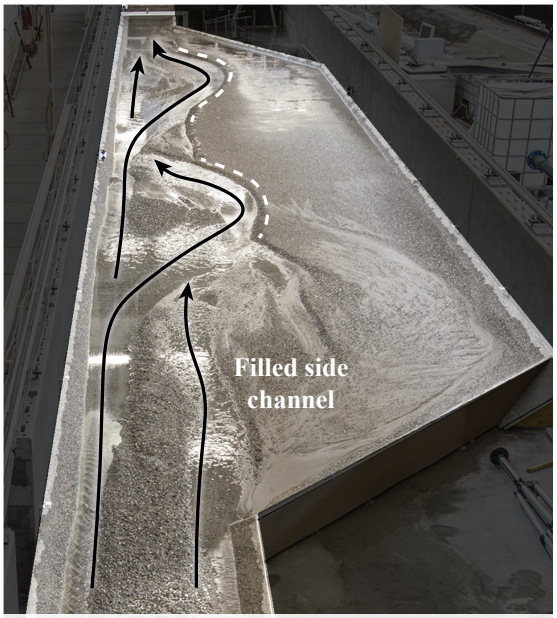

(b) Series $R_{60,IW}$ | Phase BQ (9/9) | $Q_{s,in}/Q_{s,0} = 0.6$

Figure 5.5 Downstream shifting of erosion zones: (a) Two lateral erosion zones were (b) shifted downstream and changed their dimensions. The former side channel at the upstream end of the widening was filled with sediment.

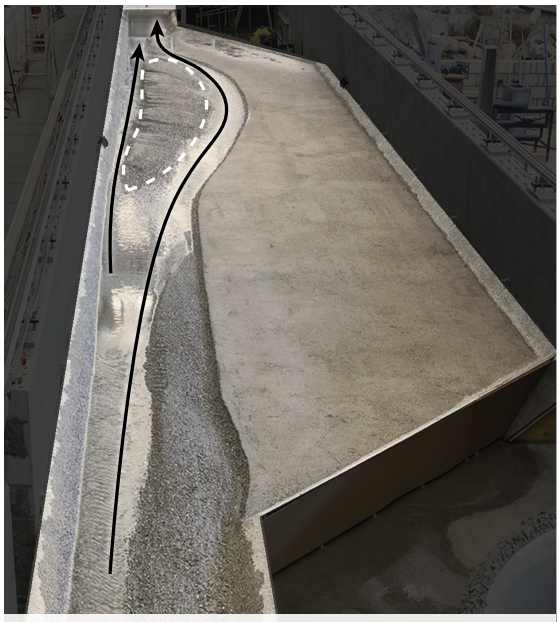

(a) Series S_{INV} | Phase BQ (2/7) | $Q_{s,in}/Q_{s,0} = 1$

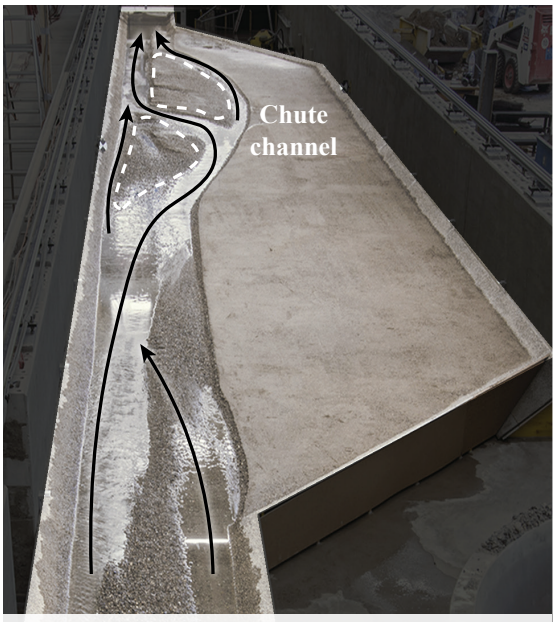

(b) Series S_{INV} | Phase BQ (3/7) | $Q_{s,in}/Q_{s,0} = 1$

Figure 5.6 Chute channels: (a) A large bar at the downstream end of the widening was (b) cut through by a chute channel.

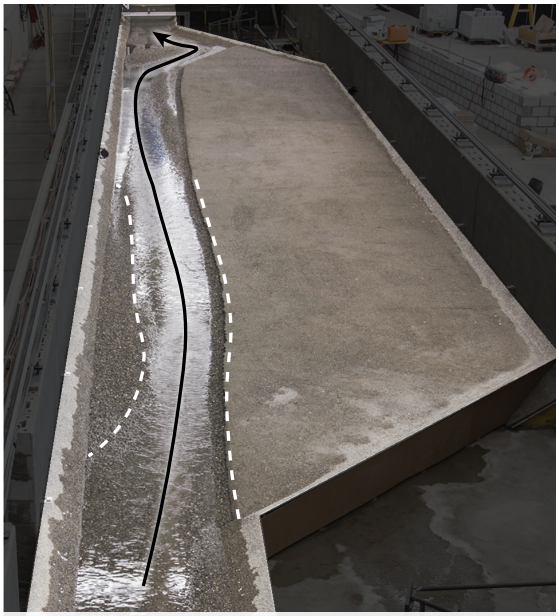

(a) Series R_{20} | Phase BQ (end) | $Q_{s,in}/Q_{s,0} = 0.2$

(b) Series R_{20} | Phase FQ_1 (end) | $Q_{s,in}/Q_{s,0} = 0.2$

Figure 5.7 Channel shifting during flood hydrograph: Starting from (a) an almost conserved channel with alternate bars, the flood hydrograph of phase FQ_1 caused (b) channel shifting into the floodplain combined with a pronounced increase in alternate bar wavelength. This process was primarily observed for low sediment supply rates.

(a) Series S | Phase BQ (end) | $Q_{s,in}/Q_{s,0} = 1$

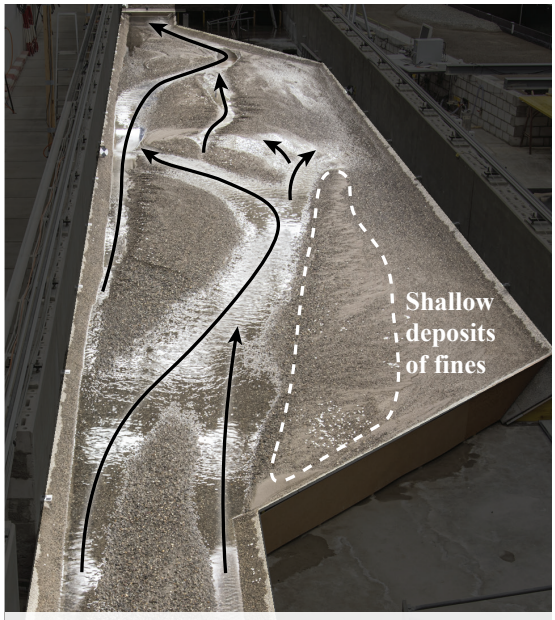

(b) Series S | Phase FQ_1 (end) | $Q_{s,in}/Q_{s,0} = 1$

Figure 5.8 Complete restructuring during flood hydrograph: Starting from (a) a partly multi-channel widening with traces of a former side channel at the upstream end, the flood hydrograph during phase FQ_1 caused (b) a complete restructuring of the widening with substantial lateral erosion and channel shifting. This process was primarily observed for high sediment supply rates. Note also the shallow deposits of fine sediment on the floodplain.

Morphodynamic activity

To facilitate the description of widening morphodynamics, the term *morphodynamic activity* is introduced here. Two morphodynamic states are distinguished:

- A *morphodynamically active* reach can be subject to *channel widening*, *channel shifting*, or substantial *sediment relocation* (and therefore topographic changes). These processes do not necessarily need to occur simultaneously.
- A *morphodynamically inactive* reach undergoes neither significant widening nor substantial sediment relocation or channel shifting. Bed-load transport can occur but it is mostly routed through the reach without substantial morphodynamic interaction.

The laboratory experiments are discussed with regard to morphodynamic activity in Section 5.7.

5.3 Experimental series at a glance

Figures 5.9 to 5.15 provide the reader with time series of several metrics for all experimental series. From these metrics, a first impression of morphodynamic effects of variable sediment supply levels can be gained. The following sections will refer to these time series for more detailed descriptions of the presented metrics.

Additional visual material on the laboratory experiments can be found in Rachelly *et al.* (2021c):

- Timelapse videos
- Hillshade topography animations
- Hillshade topography animations with a DEM of difference (DoD) overlay

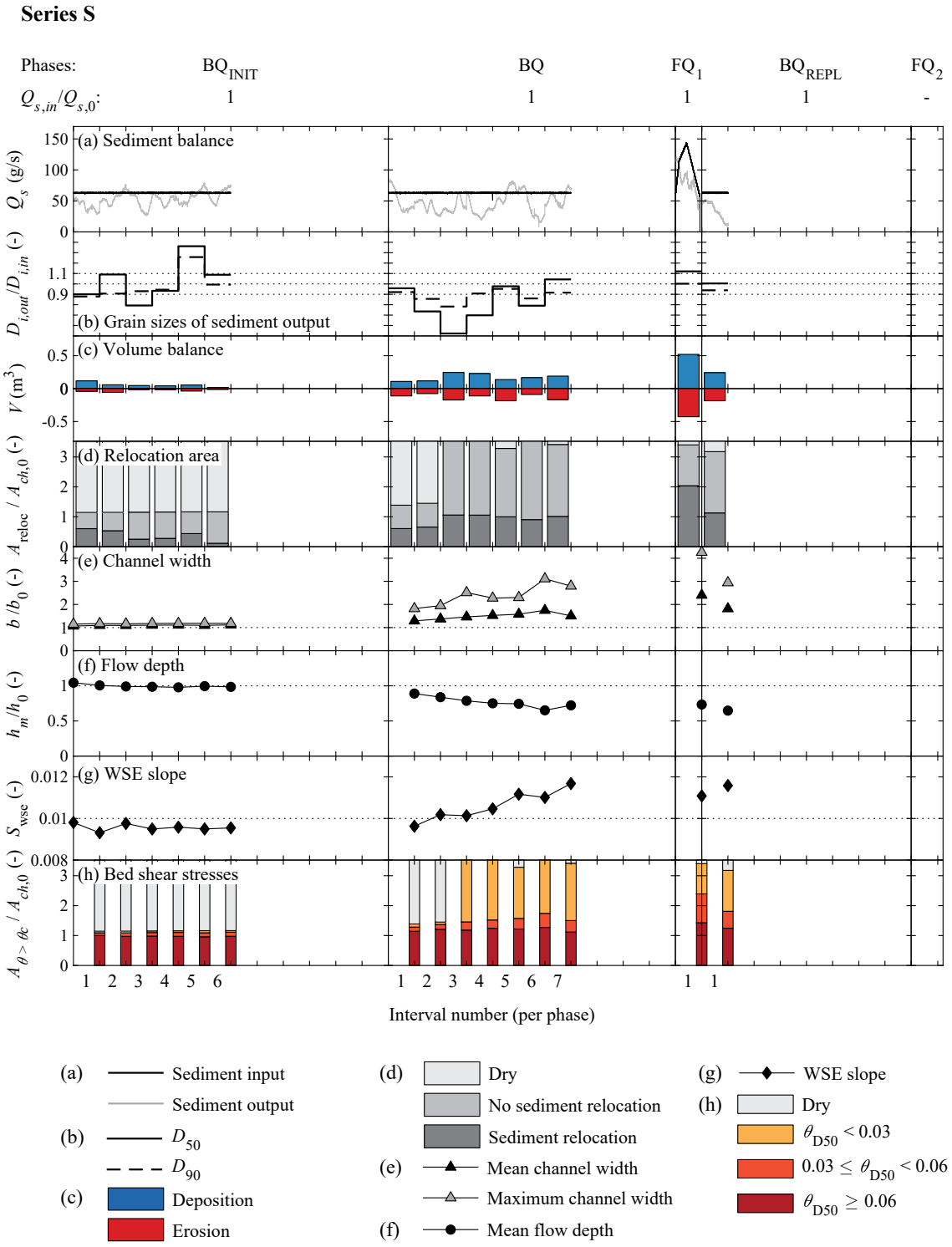

Figure 5.9 Series S with a sediment supply of $Q_{s,in}/Q_{s,0} = 1$.

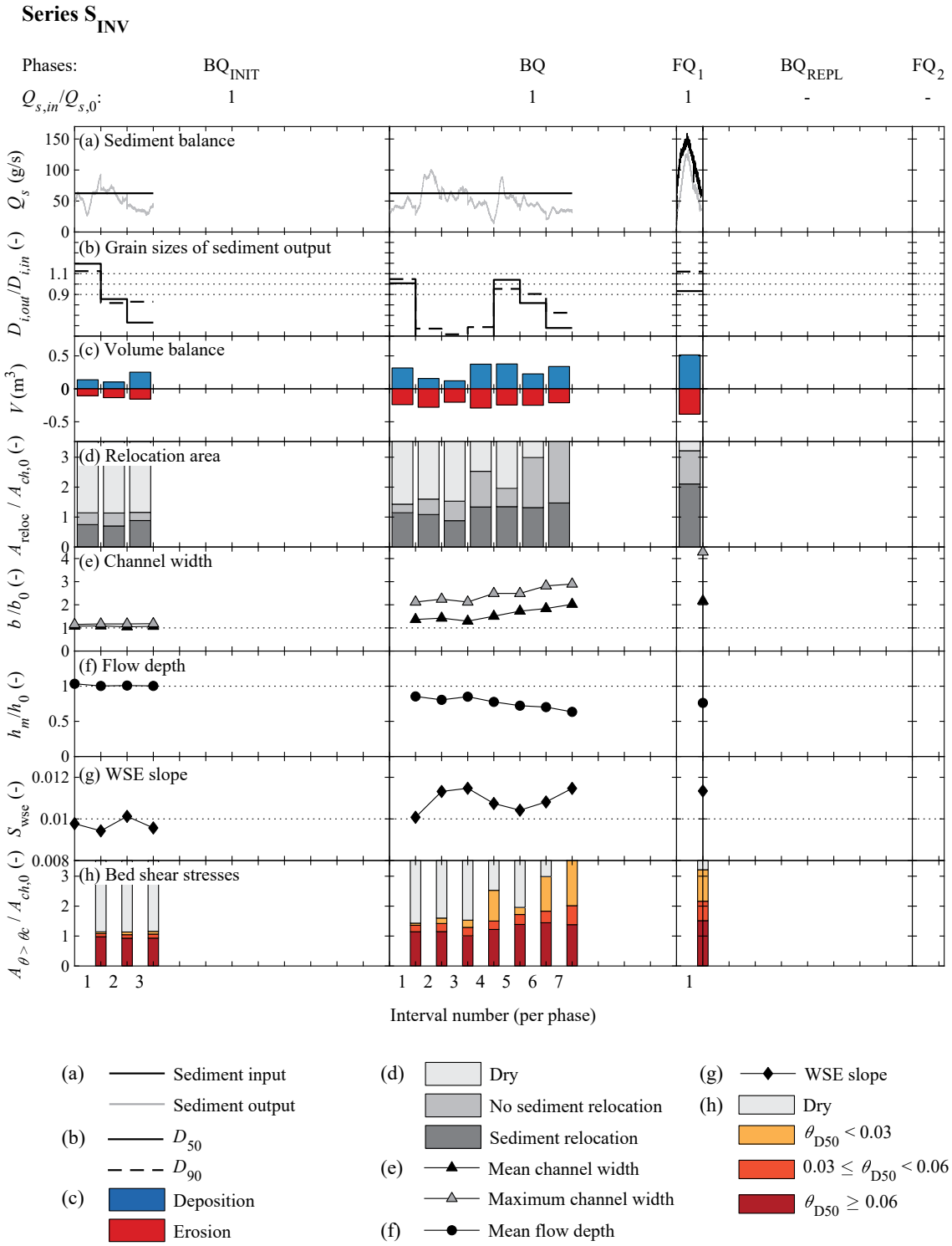

Figure 5.10 Series S_{INV} with a sediment supply of $Q_{s,in}/Q_{s,0}$ = 1 and an inverse alternate bar pattern after phase BQ_{INIT}.

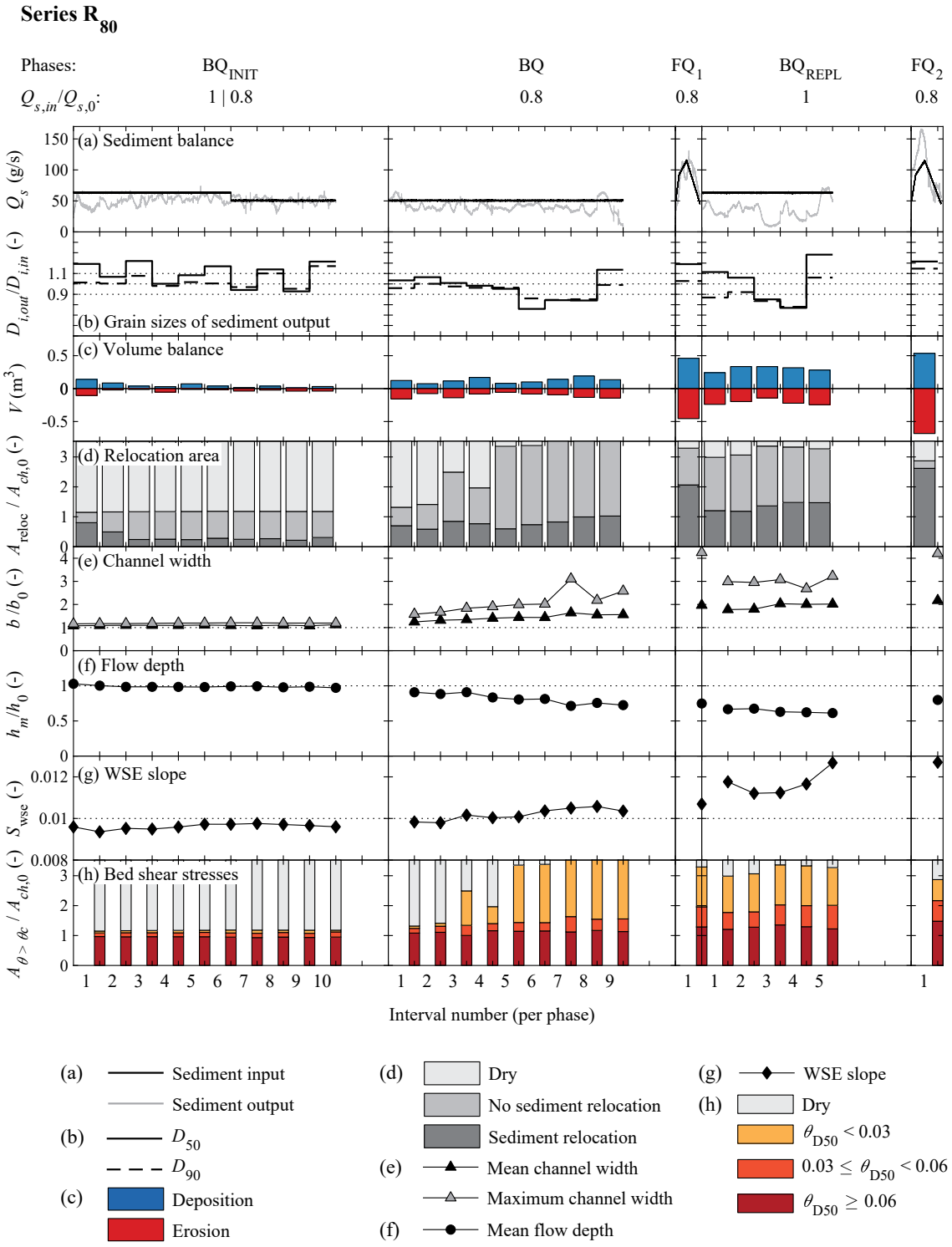

Figure 5.11 Series R_{80} with a sediment supply of $Q_{s,in}/Q_{s,0}$ = 1 and 0.8.

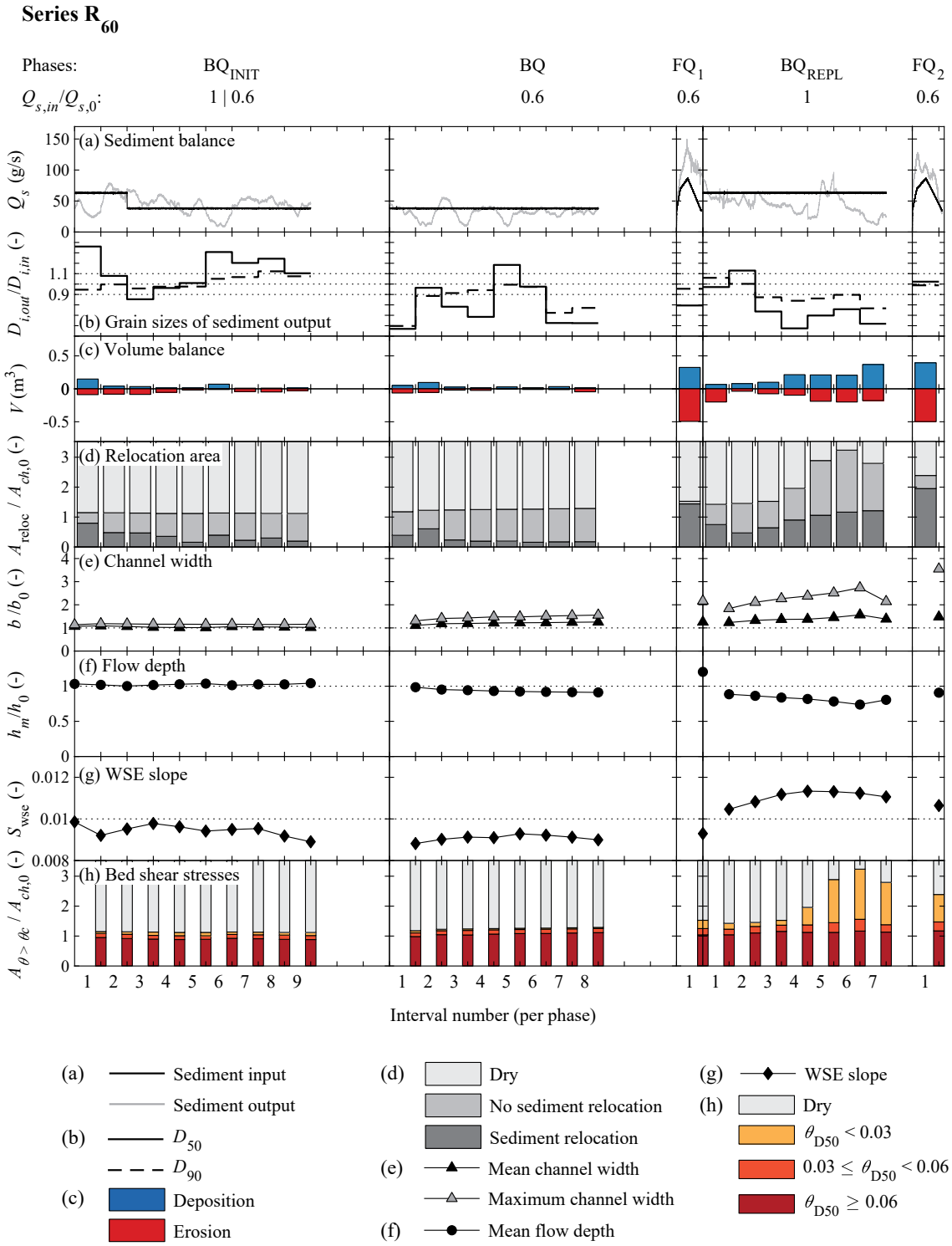

Figure 5.12 Series R_{60} with a sediment supply of $Q_{s,in}/Q_{s,0}$ = 1 and 0.6.

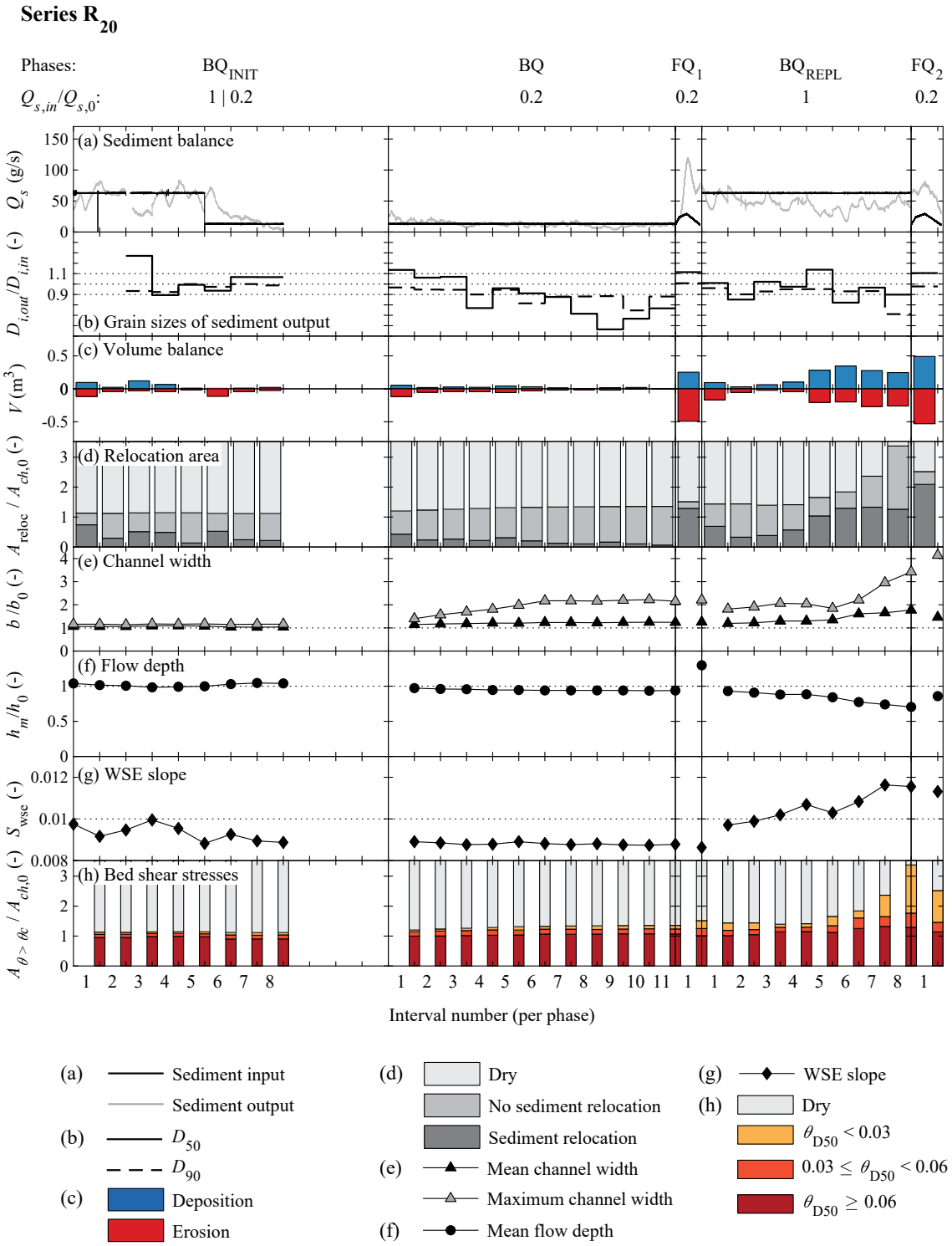

Figure 5.13 Series R_{20} with a sediment supply of $Q_{s,in}/Q_{s,0}$ = 1 and 0.2.

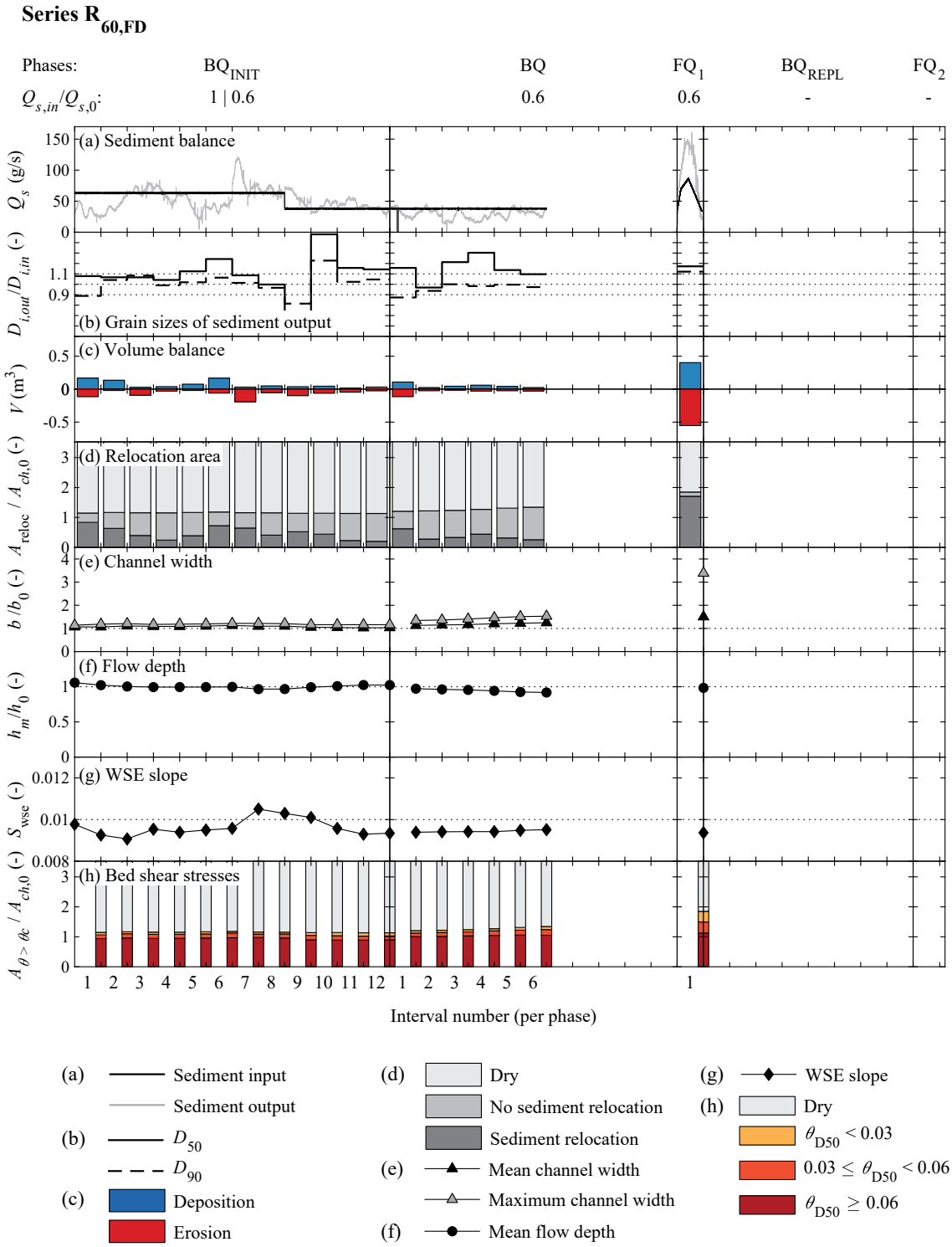

Figure 5.14 Series $R_{60,FD}$ with a sediment supply of $Q_{s,in}/Q_{s,0}$ = 1 and 0.6 and a flow deflector as bank erosion initiation measure at the start of phase BQ.

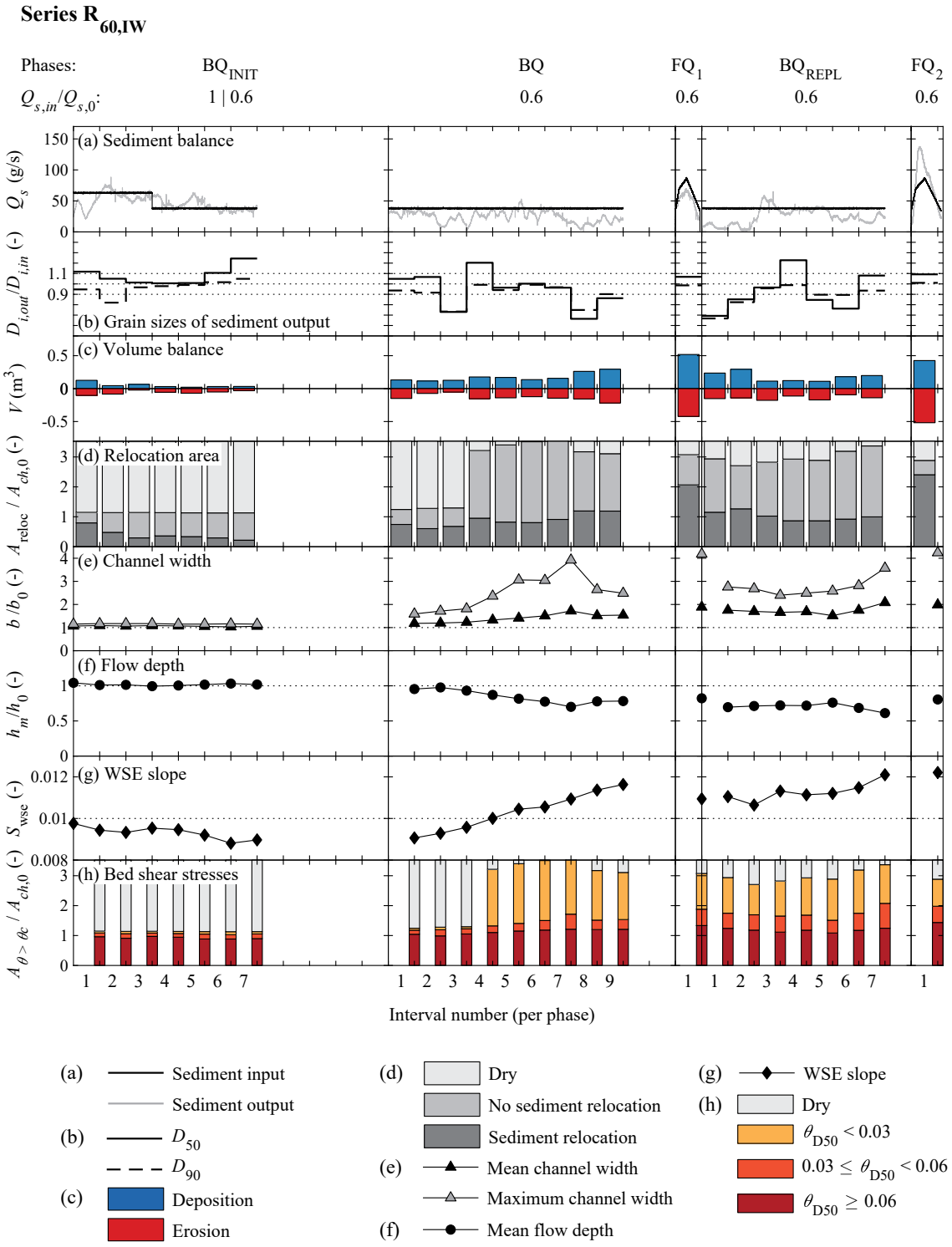

Figure 5.15 Series $R_{60,IW}$ with a sediment supply of $Q_{s,in}/Q_{s,0}$ = 1 and 0.6 and initial widening as bank erosion initiation measure at the start of phase BQ.

5.4 Alternate bars in initial channel

Results presented in this section: phase BQ_{INIT} of all series

Shortly after starting the first interval of phase BQ_{INIT}, steady alternate bars with roughly four submerged bar-scour units formed in the channel (Figure 5.16). Three of these bar-scour units were located in the widening perimeter (X = 3 to 25.5 m). The location of these bars was controlled by the fixed obstacle in the inlet (see Figure 4.4) and no bar migration was observed with the exception of minor upstream and downstream shifts. The bars are thus steady (see Section 3.3). The bar location at the end of the initial phase was similar among all series except for S_{INV} (Figure 5.16b), where two scours on the left and one scour on the right formed within the widening perimeter due to a slightly different inlet configuration. For all other series, a mirrored bar pattern with two scours on the right and one scour on the left side formed.

Figures 5.17 and 5.18 summarize the planimetric and altimetric dimensions of the alternate bars, respectively (see Section 4.5 for details on data analysis). For intervals with sediment supply of $Q_{s,in}/Q_{s,0} = 1$, mean bar wavelength was $L_B/b_0 = 16.9 \pm 2.1$ ($\pm\sigma$, $n = 57$; Figure 5.17b) and mean wave number $\lambda_B = (\pi b_0)/L_B = 0.19 \pm 0.03$ ($\pm\sigma$, $n = 57$; Figure 5.17c). These values correspond well to the predicted planimetric dimensions of $L_B/b_0 = 15.7$ and $\lambda_B = 0.20$ after Crosato and Mosselman (2009). They also fall within the typical range of wavelengths L_B/b_0 between 15 and 20 and wavenumbers λ_B between 0.15 and 0.2 specified for steady bars (Crosato and Mosselman 2020). The vertical dimensions also compared well with calculated values, with mean scour depth $\eta_B/h_0 = 0.8 \pm 0.25$ ($\pm\sigma$, $n = 90$; Figure 5.18a) and mean bar height $H_B/h_0 = 1.25 \pm 0.33$ ($\pm\sigma$, $n = 90$; Figure 5.18b). The corresponding values calculated after Ikeda (1984) are $\eta_B/h_0 = 0.78$ and $H_B/h_0 = 1.05$. The slight upstream and downstream shifts during phase BQ_{INIT} mentioned above as well as the inverse initial bar configuration of series S_{INV} are reflected in scattered riffle positions in the lowest panel of Figure 5.17a.

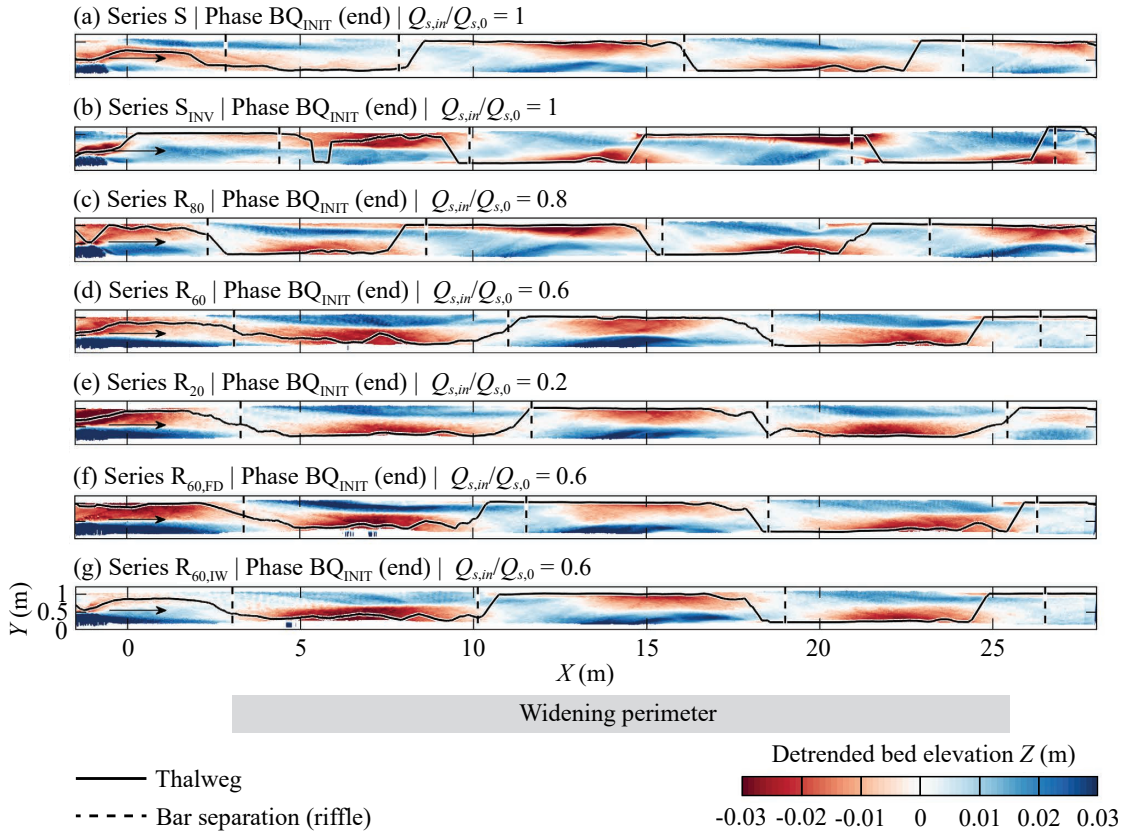

Figure 5.16 Detrended bed elevations after the last BQ_{INIT} interval of (a) series S with a sediment supply of $Q_{s,in}/Q_{s,0} = 1$, (b) series S_{INV} with $Q_{s,in}/Q_{s,0} = 1$ and an inverse bar pattern, (c) series R_{80} with $Q_{s,in}/Q_{s,0} = 0.8$, (d) series R_{60} with $Q_{s,in}/Q_{s,0} = 0.6$, (e) series R_{20} with $Q_{s,in}/Q_{s,0} = 0.2$, (f) series $R_{60,FD}$ with $Q_{s,in}/Q_{s,0} = 0.6$, and (g) series $R_{60,IW}$ with $Q_{s,in}/Q_{s,0} = 0.6$. Bar separation (see Section 4.5 for details on data analysis) and thalweg are indicated. The thalweg was determined as moving average (window size 0.5 m) of the location of the 5th percentile of cross-sectional bed elevations.

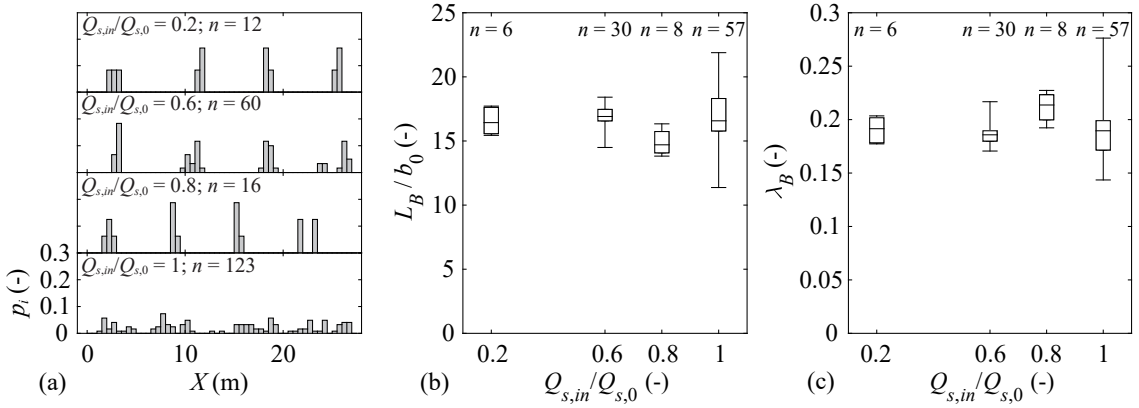

Figure 5.17 (a) Longitudinal frequency distribution of riffles (transition between bars) as a measure for bar location, (b) relative bar lengths L_B/b_0 (with b_0 = 0.89 m), and (c) wave numbers $\lambda_B = (\pi b_0)/L_B$ for different sediment supply levels. The boxes in (b) and (c) correspond to the interquartile range with the median value marked by a line. The whiskers represent the furthest outliers. All intervals of phase BQ_{INIT} are included in this analysis.

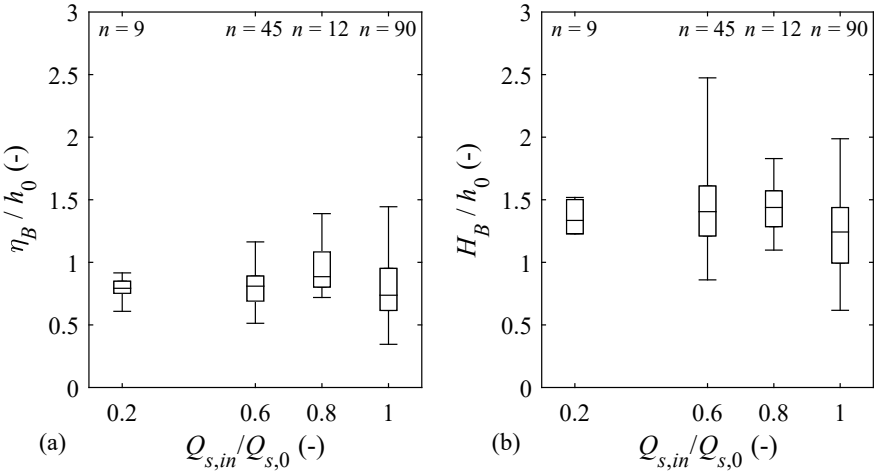

Figure 5.18 (a) Relative scour depths η_B/h_0 (with h_0 = 0.04 m), and (b) relative bar heights H_B/h_0 for different sediment supply levels. The boxes correspond to the interquartile range with the median value marked by a line. The whiskers represent the furthest outliers. All intervals of phase BQ_{INIT} are included in this analysis.

The decrease in sediment supply during phase BQ_{INIT} of all series except series S and S_{INV} led to rotational erosion around the fixed outlet sill. The longitudinal bed slope S_b remained stable with S_b = 0.0098±0.0003 (±σ, n = 7) for $Q_{s,in}/Q_{s,0}$ = 1 and S_b = 0.0099 (n = 1) for $Q_{s,in}/Q_{s,0}$ = 0.8 compared to the initial flat bed with $S_{b,0}$ = 0.0099±0.00005 (±σ, n = 7). In contrast, the slope decreased to S_b = 0.0091±0.0002 (±σ, n = 3) for $Q_{s,in}/Q_{s,0}$ = 0.6 and S_b = 0.0088 (n = 1) for $Q_{s,in}/Q_{s,0}$ = 0.2. The water surface slope evolved accordingly (cf. Figures 5.9g to 5.15g). The thalweg underwent some incision, especially in the upper part of the flume. However, no significant adjustment of the mean vertical bar dimensions was observed with scour depths and bar heights of η_B/h_0 = 0.78±0.1 (±σ, n = 9) and H_B/h_0 = 1.35±0.13 (±σ, n = 9), respectively, for series R_{20} with the lowest tested sediment supply (Figure 5.18). No significant correlation between wave lengths and numbers and sediment supply can be identified, either (Figures 5.17b,c). Riffle location was similar for $Q_{s,in}/Q_{s,0}$ = 0.6 and 0.2 and shifted somewhat upstream for $Q_{s,in}/Q_{s,0}$ = 0.8 (Figure 5.17a). It seems that, with the exception of series S_{INV}, bar position was similar for a sediment supply of $Q_{s,in}/Q_{s,0}$ = 1 and 0.8 (Figures 5.16a,c) as well as for $Q_{s,in}/Q_{s,0}$ = 0.6 and 0.2 (Figures 5.16d-g). A reduction of sediment supply may have therefore induced a slight downstream shift of the bars. However, it is not fully clear if these shifts are in fact related to sediment supply, as bar dynamics were rather sensitive to the inlet configuration.

5.5 Channel widening

5.5.1 Sediment supply control on widening progress

Results presented in this section: phases BQ and FQ_1 of series S, S_{INV}, R_{80}, R_{60}, and R_{20}

The widening process was initiated by removing the bank protection between channel and floodplain at the end of phase BQ_{INIT} (Figure 5.2). Bank erosion started at the location of the scours, that is, at the upstream and downstream end of the widening (except for series S_{INV}; see Section 5.4). Figures 5.19 and 5.20 show the resulting channel patterns after the last BQ interval as photographs and hillshade topographies with a DoD overlay. In series S, S_{INV}, and R_{80}, bank erosion progressed steadily, continuously widening the channel and increasing the WSE slope (see also Figures 5.9e-g to 5.11e-g). At the end of phase BQ of these series, the channel had significantly widened (Figures 5.19a-c) with a diverse pattern of sediment erosion and deposition along the entire perimeter (Figures 5.20a-c). Note how in series S, the channel at the upstream end of the widening seems to be rather narrow but the sediment pattern on the right side evidences the temporary channel shift that must have occurred during phase BQ (see also Figure 5.8a).

In contrast, limited bank erosion was observed in series R_{60} and R_{20} (Figures 5.19d,e), and the shape of the initial channel was largely conserved except at the downstream widening end in R_{20} (Figure 5.19e). By the end of phase BQ, sediment relocation activity had almost completely ceased (Figures 5.20d,e). The overall morphological stability can also be seen in Figures 5.12 and Figures 5.13. Flow depths, channel widths, and WSE slopes remained almost constant during phase BQ with the exception of maximum channel width increasing for R_{20} due to the erosion zone at the downstream end.

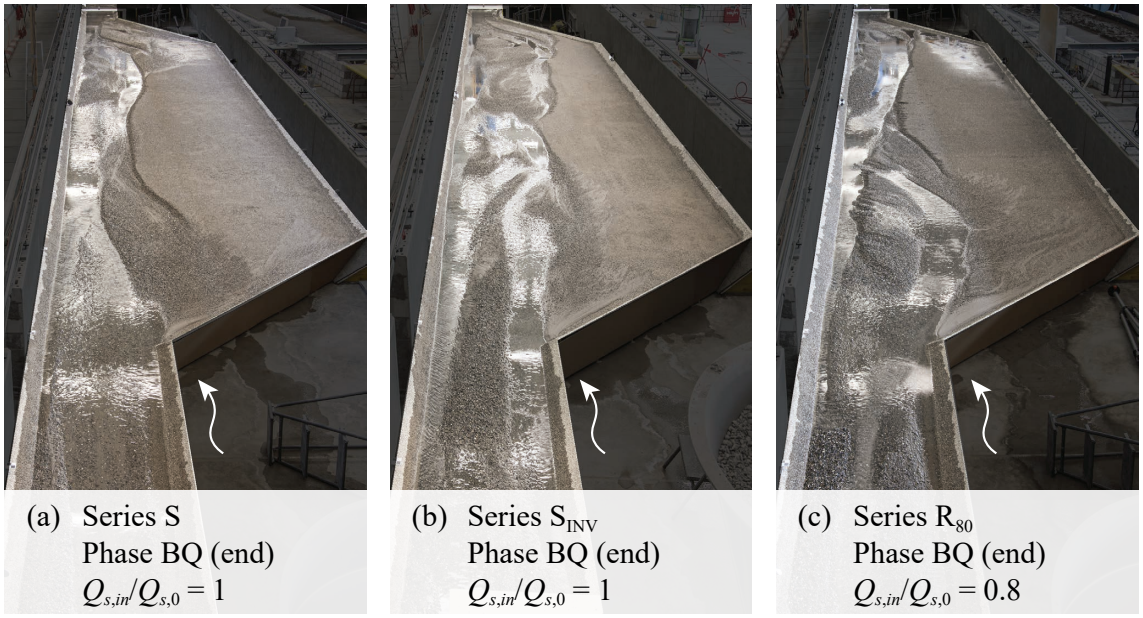

(a) Series S
Phase BQ (end)
$Q_{s,in}/Q_{s,0} = 1$

(b) Series S_{INV}
Phase BQ (end)
$Q_{s,in}/Q_{s,0} = 1$

(c) Series R_{80}
Phase BQ (end)
$Q_{s,in}/Q_{s,0} = 0.8$

(d) Series R_{60}
Phase BQ (end)
$Q_{s,in}/Q_{s,0} = 0.6$

(e) Series R_{20}
Phase BQ (end)
$Q_{s,in}/Q_{s,0} = 0.2$

Figure 5.19 Photographs of the topography at the end of phase BQ with a low discharge (1 l/s) for (a) series S with a sediment supply of $Q_{s,in}/Q_{s,0} = 1$, (b) series S_{INV} with $Q_{s,in}/Q_{s,0} = 1$ and an inverse initial bar pattern, (c) series R_{80} with $Q_{s,in}/Q_{s,0} = 0.8$, (d) series R_{60} with $Q_{s,in}/Q_{s,0} = 0.6$, and (e) series R_{20} with $Q_{s,in}/Q_{s,0} = 0.2$.

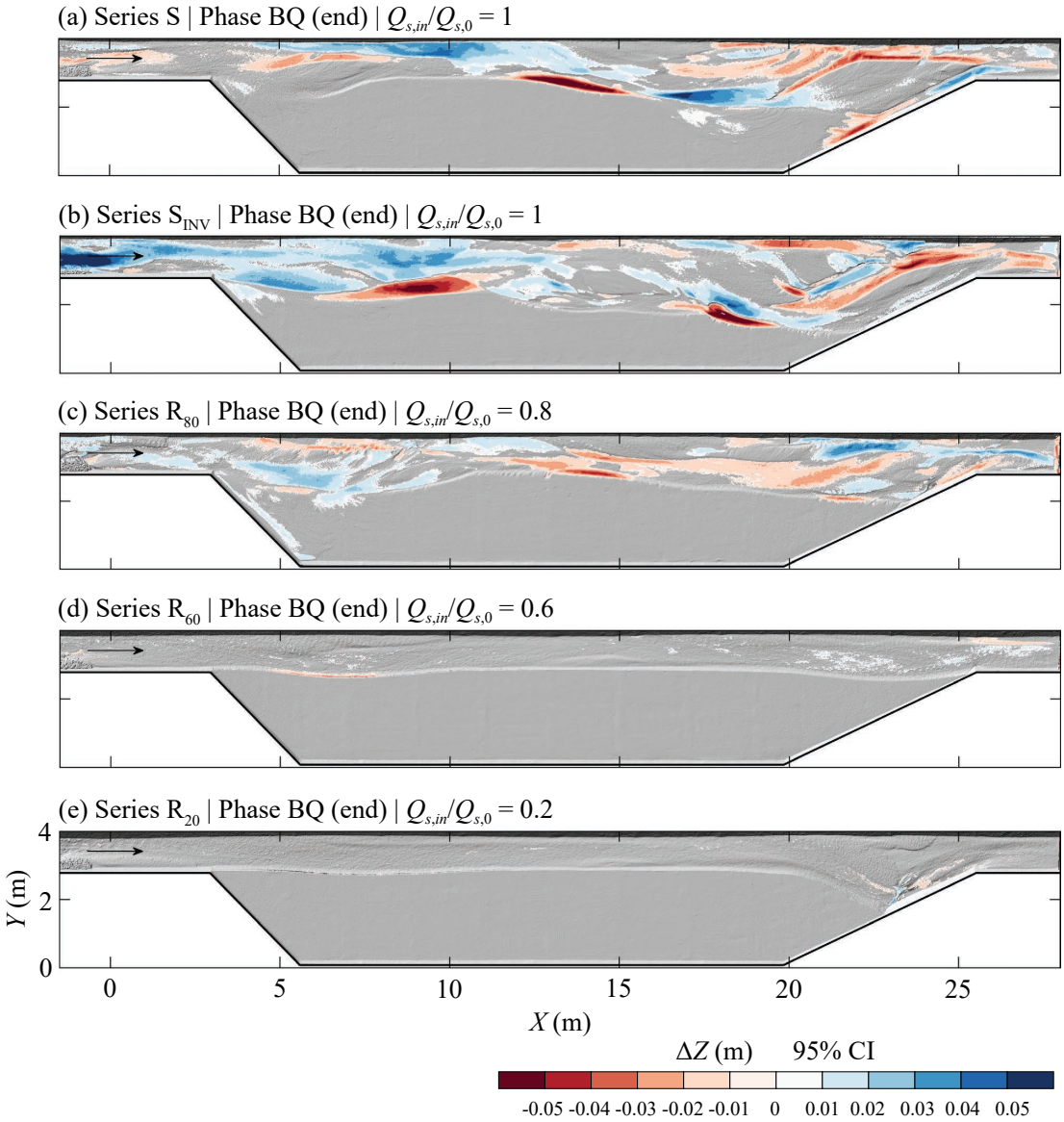

Figure 5.20 Bed elevation changes (95% confidence interval) during the last BQ interval shown on top of hillshade topographies at the end of phase BQ for (a) series S with a sediment supply of $Q_{s,in}/Q_{s,0} = 1$, (b) series S_{INV} with $Q_{s,in}/Q_{s,0} = 1$ and an inverse initial bar pattern, (c) series R_{80} with $Q_{s,in}/Q_{s,0} = 0.8$, (d) series R_{60} with $Q_{s,in}/Q_{s,0} = 0.6$, and (e) series R_{20} with $Q_{s,in}/Q_{s,0} = 0.2$.

Increased hydraulic forces during the subsequent unsteady phase FQ_1 caused channel shifting and sediment relocation for all series (Figure 5.21) but different patterns were observed (Figure 5.22). Series S, S_{INV}, and R_{80} continued to show a patchy pattern of erosion and deposition (Figures 5.22a-c). Deposition prevailed at the upstream end of the widening with large patches of shallow sediment deposition evidencing floodplain inundation (see also Figure 5.8b). Erosion was more prevalent at the downstream end of the perimeter where considerable channel widening occurred. WSE slopes remained largely stable (see Figures 5.9g to 5.11g).

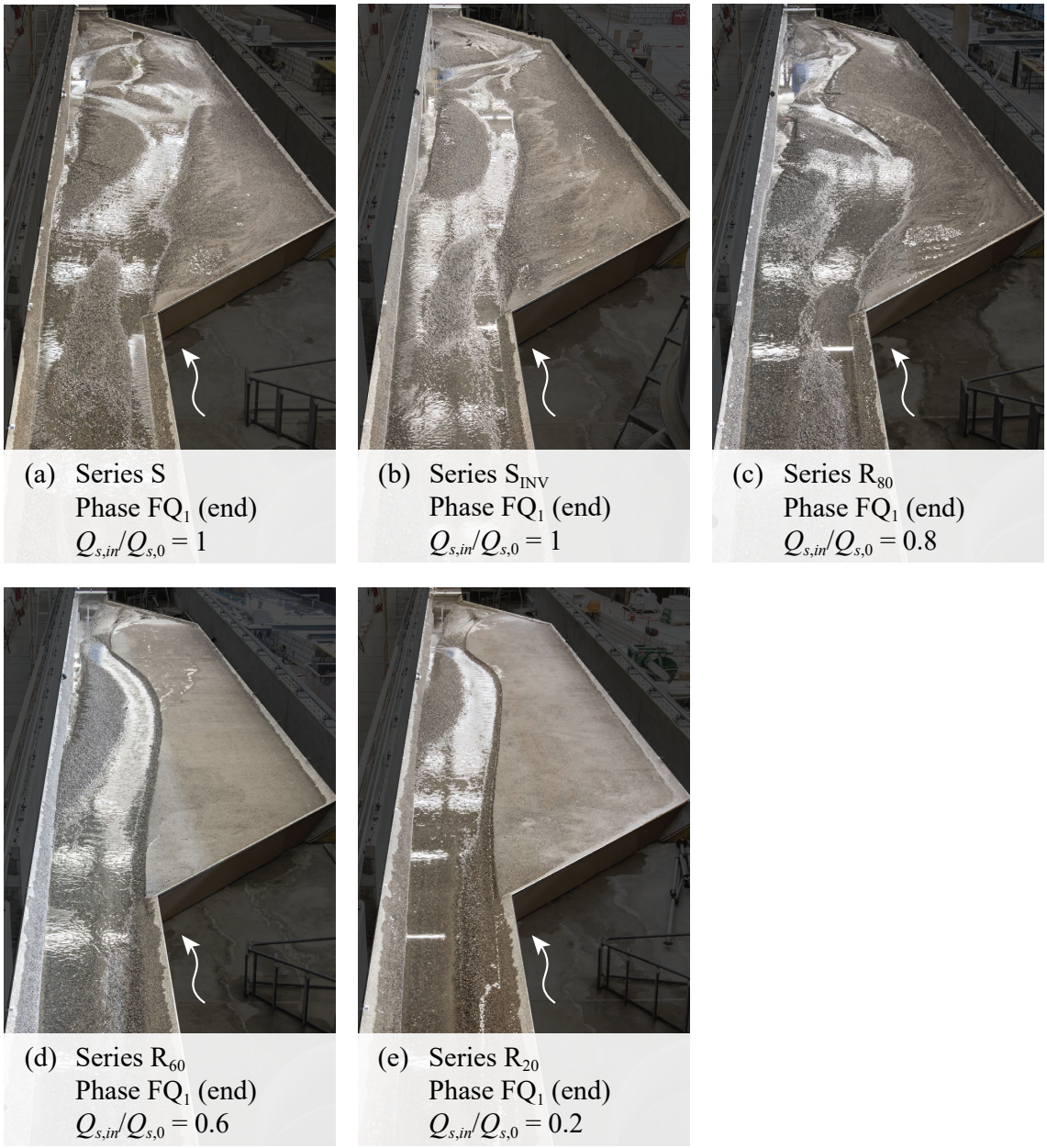

Figure 5.21 Photographs of the topography at the end of phase FQ_1 with a low discharge (1 l/s) for (a) series S with a sediment supply of $Q_{s,in}/Q_{s,0} = 1$, (b) series S_{INV} with $Q_{s,in}/Q_{s,0} = 1$ and an inverse initial bar pattern, (c) series R_{80} with $Q_{s,in}/Q_{s,0} = 0.8$, (d) series R_{60} with $Q_{s,in}/Q_{s,0} = 0.6$, and (e) series R_{20} with $Q_{s,in}/Q_{s,0} = 0.2$.

In contrast, the sinuous single-thread channel originating from the alternate bar morphology seems to be conserved in series R_{60} and R_{20} but with increased amplitude and wavelength (see also Figure 5.7). This led to pronounced floodplain erosion in the upstream half of the widening with flow subsequently being reflected at the fixed left bank near $X \approx 20$ m causing an elongated scour (Figures 5.22d,e). The next downstream floodplain erosion zone was limited by the fixed bank at the end of the widening. Erosion and

deposition were fairly balanced along the widening perimeter, and WSE remained stable (see Figures 5.12g and 5.13g).

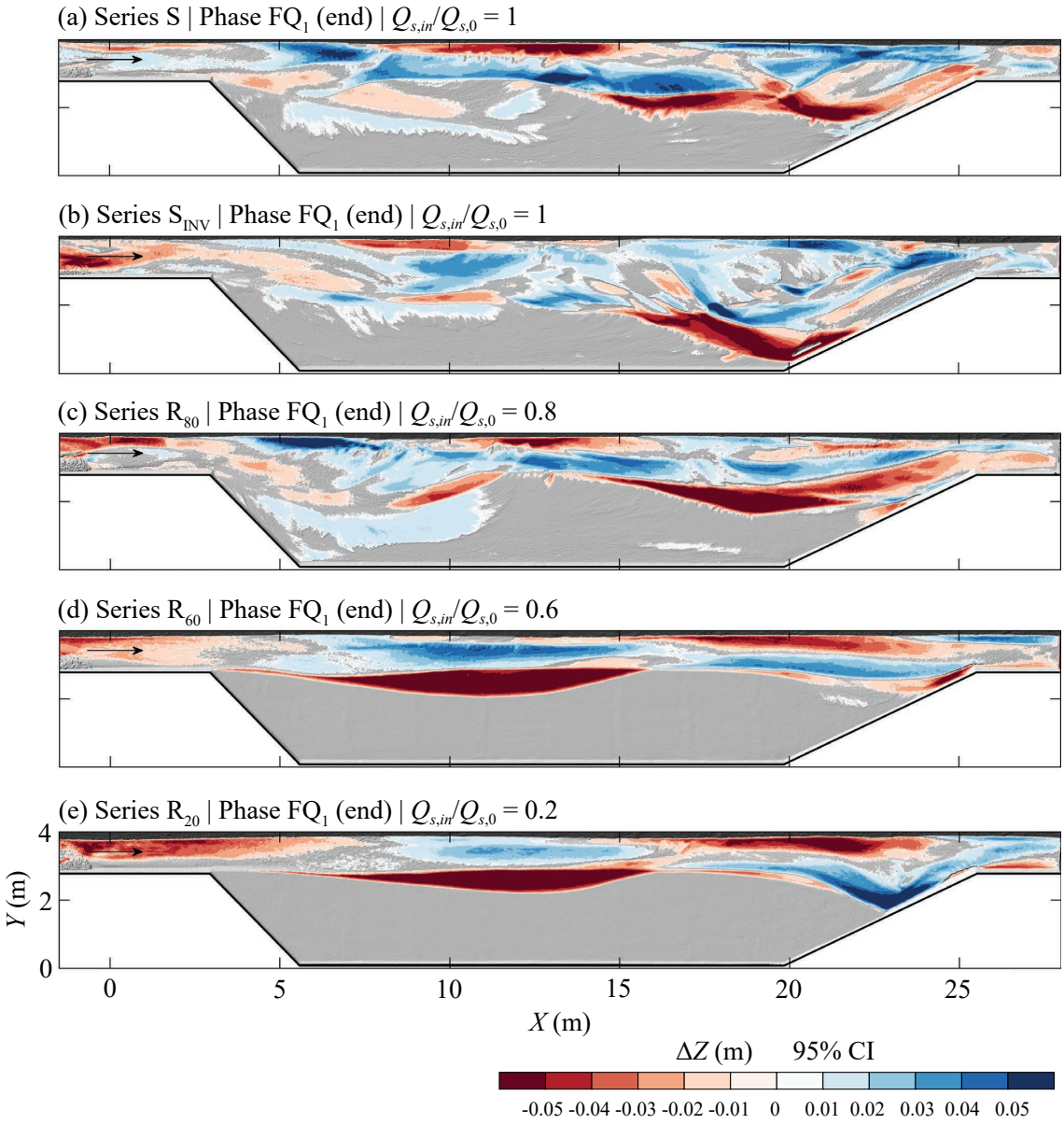

Figure 5.22 Bed elevation changes (95% confidence interval) during phase FQ_1 shown on top of hillshade topographies at the end of phase FQ_1 for (a) series S with a sediment supply of $Q_{s,in}/Q_{s,0} = 1$, (b) series S_{INV} with $Q_{s,in}/Q_{s,0} = 1$ and an inverse initial bar pattern, (c) series R_{80} with $Q_{s,in}/Q_{s,0} = 0.8$, (d) series R_{60} with $Q_{s,in}/Q_{s,0} = 0.6$, and (e) series R_{20} with $Q_{s,in}/Q_{s,0} = 0.2$.

5.5.2 Bank erosion initiation measures

Results presented in this section: phases BQ and FQ_1 of series $R_{60,FD}$ and $R_{60,IW}$

Two bank erosion initiation measures (flow deflector, initial widening; see Figures 4.8 and 4.9) were tested for a sediment supply of $Q_{s,in}/Q_{s,0} = 0.6$. This supply level was chosen based on the results described in the previous Section 5.5.1 suggesting that reaches with higher supply might not need additional measures to trigger channel widening. During phase BQ of series $R_{60,FD}$, limited widening was observed (Figures 5.23a and 5.24a). In contrast, the initial widening in $R_{60,IW}$ triggered local sediment deposition accompanied by significant floodplain erosion (Figures 5.23b and 5.24b; see also Figure 5.2b). Note how the patterns emerging in series $R_{60,IW}$ closely resemble those of series S, S_{INV}, and R_{80}, while the channel stability observed in series $R_{60,FD}$ is very similar to series R_{60} and R_{20} (see Section 5.5.1).

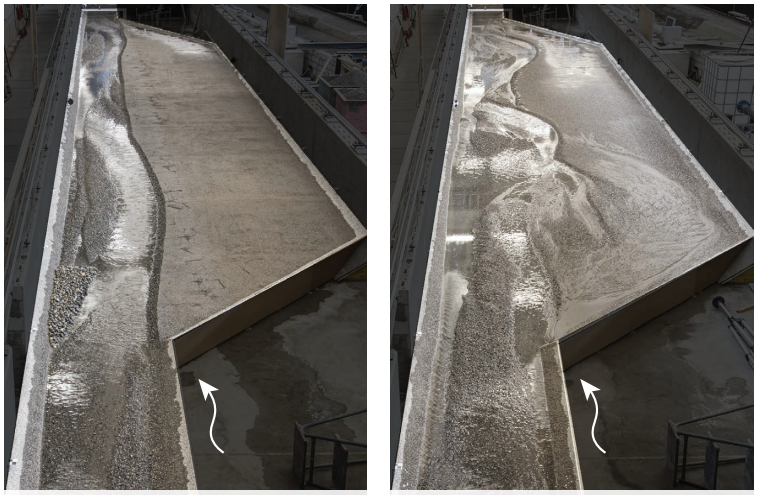

(a) Series $R_{60,FD}$ Phase BQ (end) $Q_{s,in}/Q_{s,0} = 0.6$

(b) Series $R_{60,IW}$ Phase BQ (end) $Q_{s,in}/Q_{s,0} = 0.6$

Figure 5.23 Photographs of the topography at the end of phase BQ with a low discharge (1 l/s) for (a) series $R_{60,FD}$ with a sediment supply of $Q_{s,in}/Q_{s,0} = 0.6$ and a flow deflector and (b) series $R_{60,IW}$ with $Q_{s,in}/Q_{s,0} = 0.6$ and initial widening.

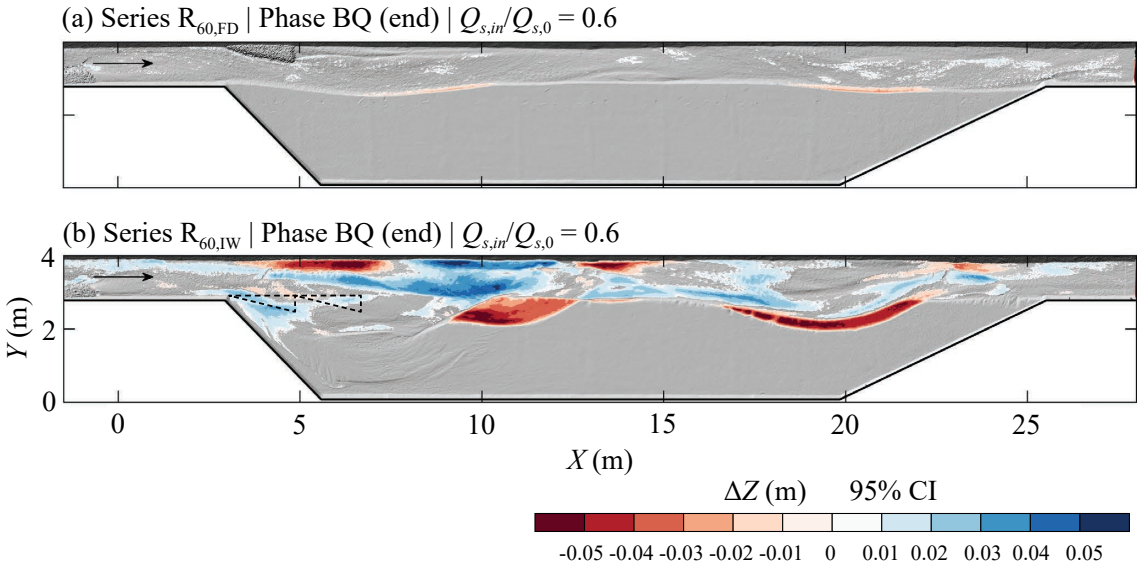

Figure 5.24 Bed elevation changes (95% confidence interval) during the last BQ interval shown on top of hillshade topographies at the end of phase BQ with a low discharge (1 l/s) for (a) series $R_{60,FD}$ with a sediment supply of $Q_{s,in}/Q_{s,0}$ = 0.6 and a flow deflector and (b) series $R_{60,IW}$ with $Q_{s,in}/Q_{s,0}$ = 0.6 and initial widening.

During the subsequent phase FQ_1 of series $R_{60,FD}$, the channel shifted into the floodplain (Figures 5.25a and 5.26a). Flow deflection and floodplain erosion were slightly stronger compared to series R_{60} and R_{20} but the single-thread channel was again preserved (cf. Figures 5.21d,e). In contrast, continued sediment relocation during phase FQ_1 of series $R_{60,IW}$ led to a thorough restructuring of the widening (Figures 5.25b and 5.26b). As for phase BQ, the morphological development during phase FQ_1 closely resembled series R_{60} and R_{20} in the case of series $R_{60,FD}$, and series S, S_{INV}, and R_{80} in the case of series $R_{60,IW}$ (compare also Figure 5.14 to Figures 5.12 and 5.13, and Figure 5.15 to Figures 5.9-5.11).

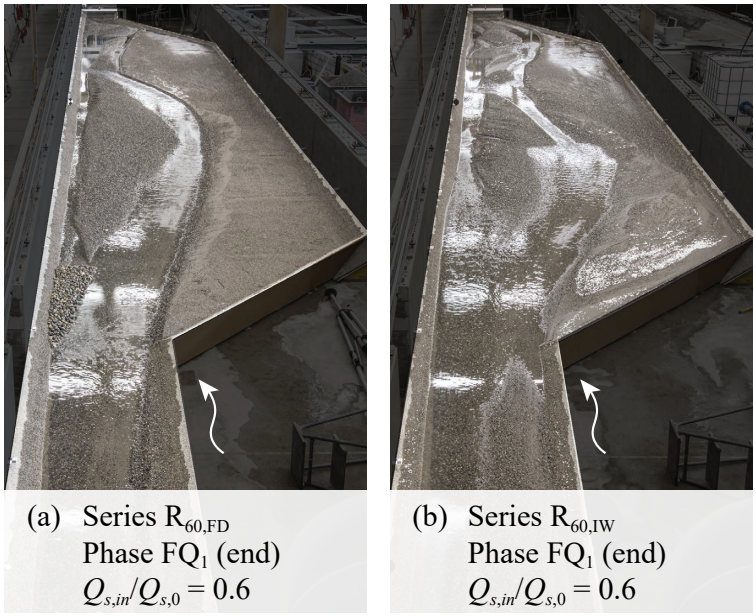

Figure 5.25 Photographs of the topography at the end of phase FQ_1 with a low discharge (1 l/s) for (a) series $R_{60,FD}$ with a sediment supply of $Q_{s,in}/Q_{s,0}$ = 0.6 and a flow deflector and (b) series $R_{60,IW}$ with $Q_{s,in}/Q_{s,0}$ = 0.6 and initial widening.

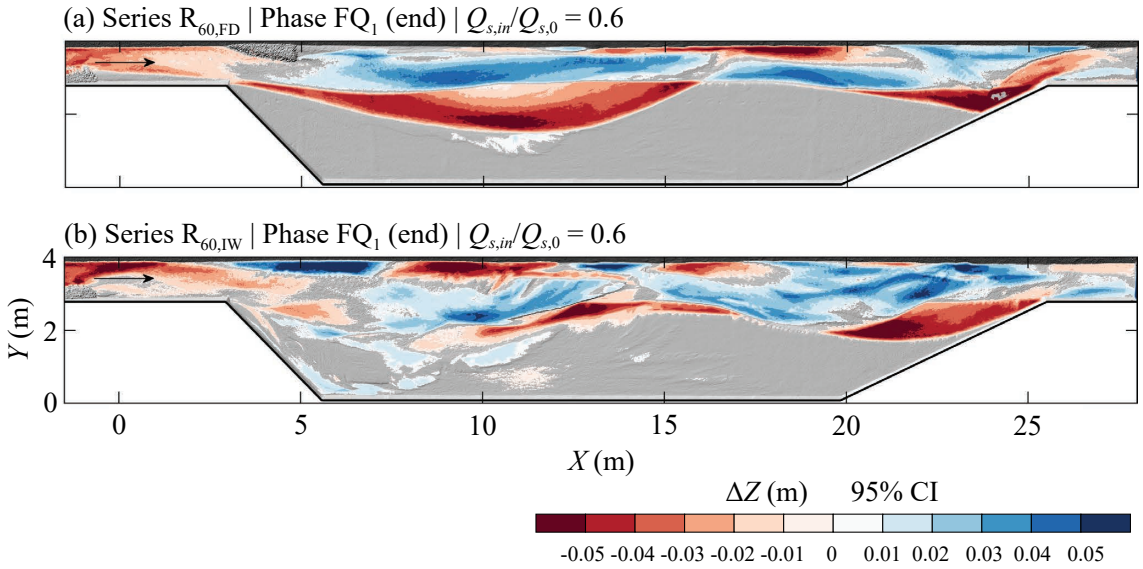

Figure 5.26 Bed elevation changes (95% confidence interval) during phase FQ_1 shown on top of hillshade topographies at the end of phase FQ_1 with a low discharge (1 l/s) for (a) series $R_{60,FD}$ with a sediment supply of $Q_{s,in}/Q_{s,0}$ = 0.6 and a flow deflector and (b) series $R_{60,IW}$ with $Q_{s,in}/Q_{s,0}$ = 0.6 and initial widening.

5.5.3 Widening response to sediment supply increase

Results presented in this section: phases BQ_{REPL} and FQ_2 of series R_{80}, R_{60}, and R_{20}

Sediment supply was increased to $Q_{s,in}/Q_{s,0}$ = 1 during phase BQ_{REPL} mimicking sediment replenishment measures. The following phase FQ_2 applied the same boundary conditions as phase FQ_1, but started from a topography adapted to higher sediment supply. During phases BQ_{REPL} and FQ_2, series R_{80} developed differently from series R_{60} and R_{20}. Because phases BQ_{INIT} to FQ_1 of series R_{80} were similar to series S and S_{INV} (see Sections 5.4 and 5.5.1), the sediment supply increase from $Q_{s,in}/Q_{s,0}$ = 0.8 to 1 did not induce clear changes in morphodynamic trends (Figures 5.27a to 5.30a). Figure 5.11 shows how WSE slope continued to increase, channel widening progressed further with no change in widening rate, and sediment relocation activity increased beyond the levels of phase BQ.

The increase in sediment supply had more pronounced effects on series R_{60} and R_{20} (Figures 5.27b,c to 5.30b,c). During phases BQ_{REPL} and FQ_2, all studied metrics displayed in Figures 5.12 and 5.13 showed some degree of adaptation to the higher sediment supply, similar to phase BQ of the $Q_{s,in}/Q_{s,0}$ = 1 and 0.8 series (see Figures 5.9 to 5.11). The adaptation to a sediment supply of $Q_{s,in}/Q_{s,0}$ = 1 sediment supply ultimately led to topographies and bed elevation changes at the end of phase BQ_{REPL} that strongly resembled phase BQ of series S, S_{INV}, and R_{80} (compare Figures 5.27b,c and 5.28b,c to Figures 5.19a-c and 5.20a-c). Phase FQ_2 with reduced sediment supply resulted in consistently high morphodynamic activity (Figures 5.29b,c and 5.30b,c), although there were signs of the main channel contracting (see also Figure 5.3).

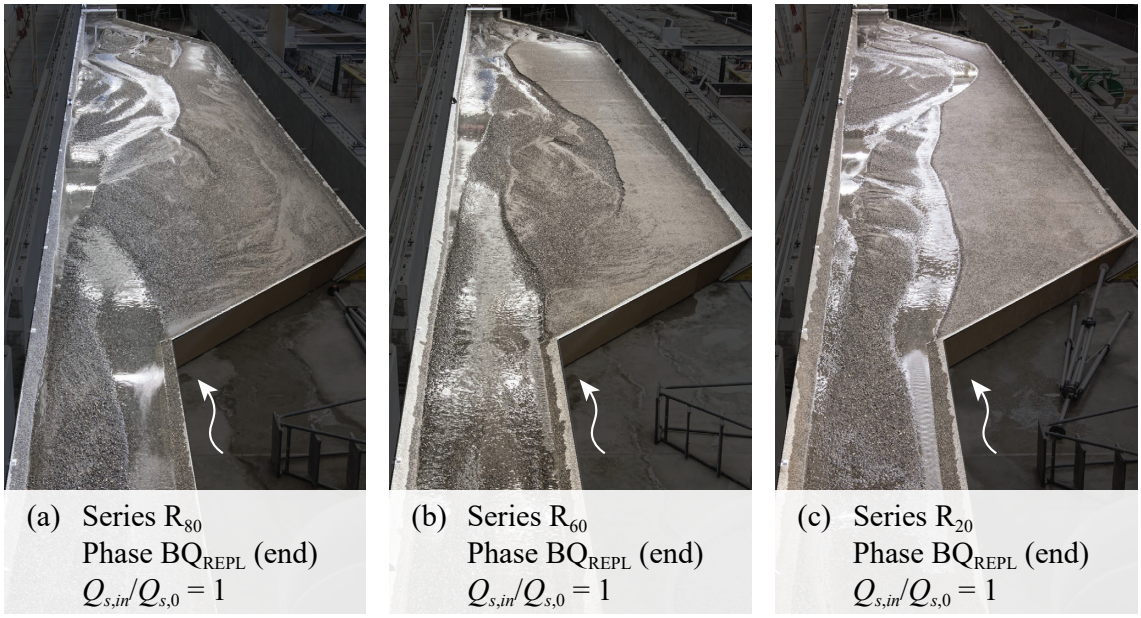

Figure 5.27 Photographs of the topography at the end of phase BQ_{REPL} with a low discharge (1 l/s) for (a) series R_{80}, (b) series R_{60}, and (c) series R_{20}, all with a sediment supply of $Q_{s,in}/Q_{s,0} = 1$.

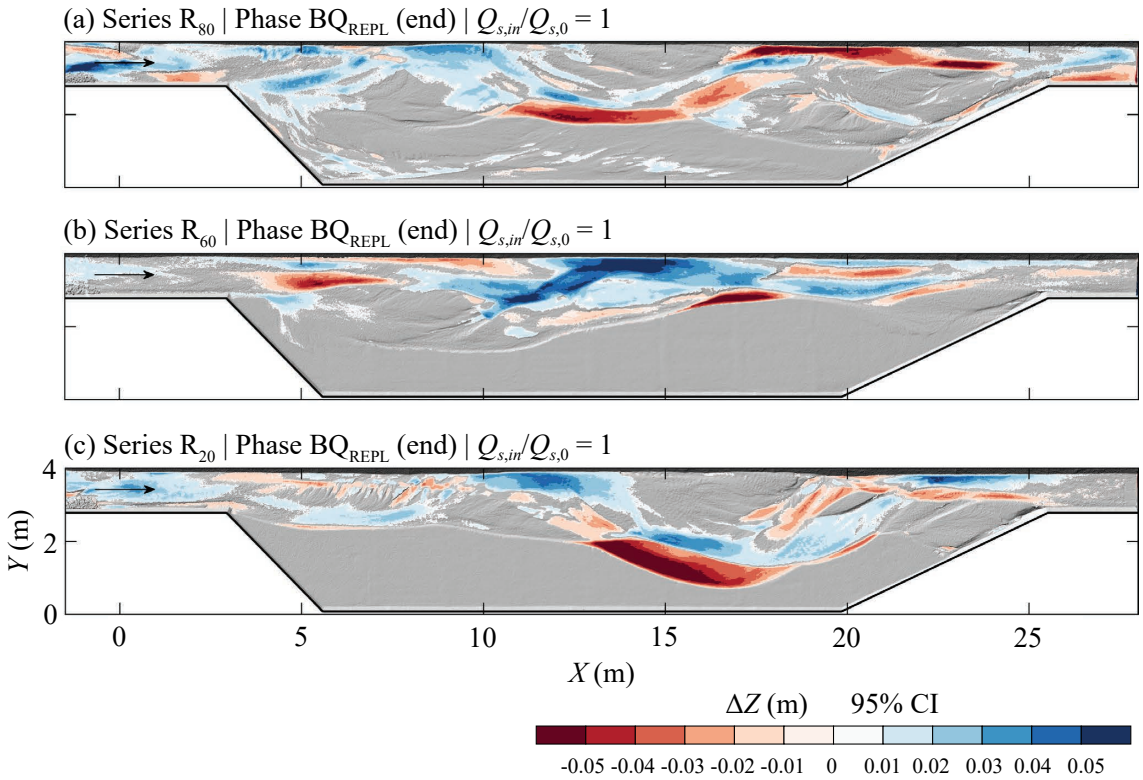

Figure 5.28 Bed elevation changes (95% confidence interval) during the last BQ_{REPL} interval shown on top of hillshade topographies at the end of phase BQ_{REPL} with a low discharge (1 l/s) for (a) series R_{80}, (b) series R_{60}, and (c) series R_{20}, all with a sediment supply of $Q_{s,in}/Q_{s,0} = 1$.

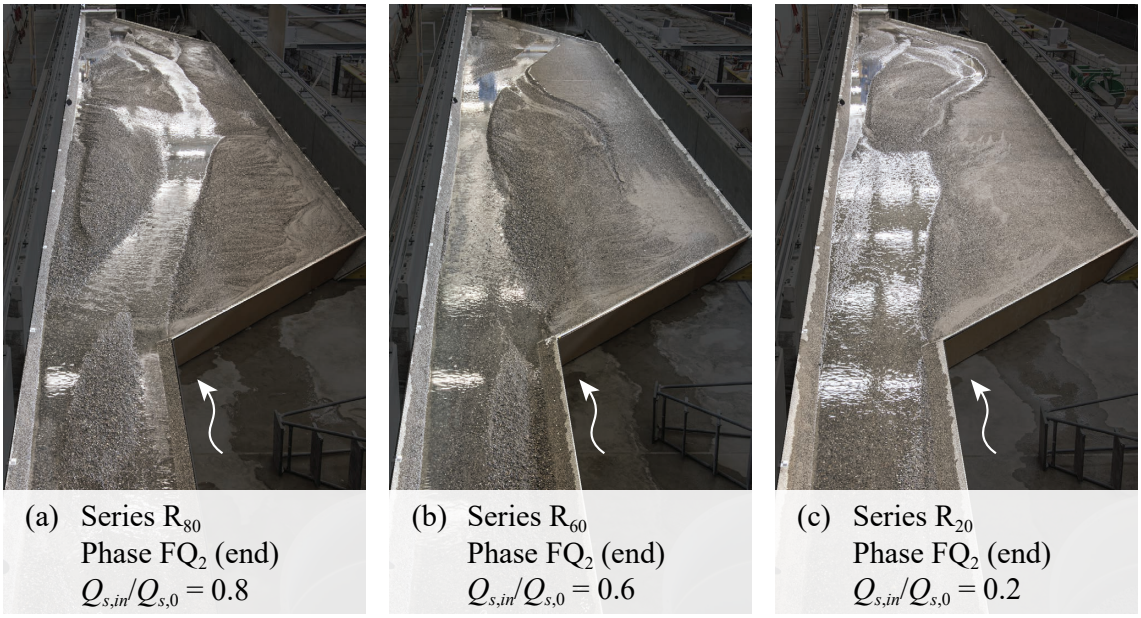

Figure 5.29 Photographs of the topography at the end of phase FQ_2 with a low discharge (1 l/s) for (a) series R_{80} with a sediment supply of $Q_{s,in}/Q_{s,0}$ = 0.8, (b) series R_{60} with $Q_{s,in}/Q_{s,0}$ = 0.6, and (c) series R_{20} with $Q_{s,in}/Q_{s,0}$ = 0.2.

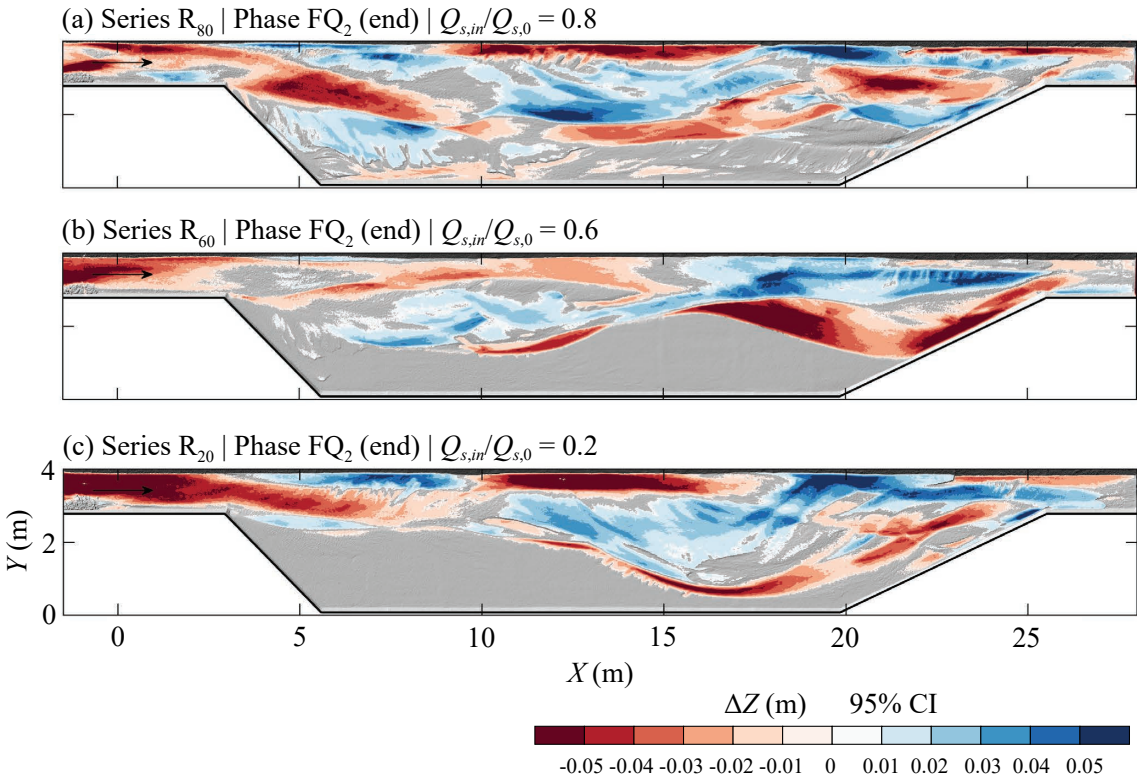

Figure 5.30 Bed elevation changes (95% confidence interval) during phase FQ_2 shown on top of hillshade topographies at the end of phase FQ_2 with a low discharge (1 l/s) for (a) series R_{80} with a sediment supply of $Q_{s,in}/Q_{s,0}$ = 0.8, (b) series R_{60} with $Q_{s,in}/Q_{s,0}$ = 0.6, and (c) series R_{20} with $Q_{s,in}/Q_{s,0}$ = 0.2.

5.6 Morphodynamic trajectories

To facilitate the comparison of the experimental series and to identify differences in their morphodynamic trajectories, bed elevation changes presented in Sections 5.4 and 5.5 are complemented with time series and boxplots of different quantitative metrics aggregated for all series (Figures 5.31 to 5.37). Some metrics are identical with those presented in Section 5.3. The legend below is valid for all figures in this section except Figure 5.38. Note that the values provided for phases FQ_1 and FQ_2 are based on the hydraulic conditions during peak flow (Q_F) but the topography was recorded at the end of the hydrograph.

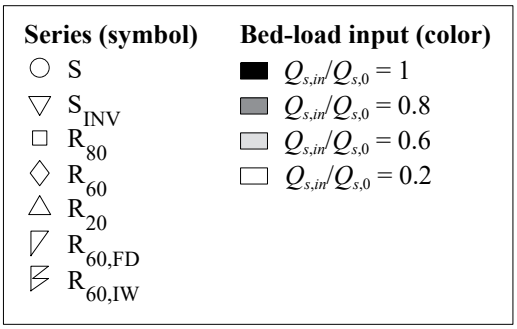

Figure 5.31 presents the trapping efficiency of the reach, that is, the amount of sediment retained relative to sediment input. At the start of phase BQ_{INIT}, sediment input was higher than sediment output with $(Q_{s,in} - Q_{s,out})/Q_{s,in} > 0$ due to alternate bar formation and some net parallel deposition. $(Q_{s,in} - Q_{s,out})/Q_{s,in} < 0$ were mostly recorded for series with a sediment supply reduction. Note, for example, the negative values for series R_{60} (Interval 3) or series R_{20} (Interval 6) showing the immediate response to reduced sediment input. The minimum value during interval 6 of series R_{20} indicates that about 2.5 times the input volume was evacuated from the reach and thus that significant erosion occurred. At the end of phase BQ_{INIT}, an equilibrium state was reached for all series except S_{INV} and R_{20} with $(Q_{s,in} - Q_{s,out})/Q_{s,in} = -0.06$ to -0.08 for the respective last intervals. $(Q_{s,in} - Q_{s,out})/Q_{s,in} = 0.42$ for series S_{INV} and $(Q_{s,in} - Q_{s,out})/Q_{s,in} = 0.29$ for series R_{20} indicate a disequilibrium during the last BQ_{INIT} interval. For series S_{INV}, this is indeed the case (see Figure 5.10a), but the entire phase BQ_{INIT} may be considered in equilibrium (see, e.g., WSE slopes in Figure 5.10g). Series R_{20} may also be considered in equilibrium at the end of phase BQ_{INIT} (see Figure 5.13) but the low sediment input rate causes the high $(Q_{s,in} - Q_{s,out})/Q_{s,in}$ value.

During phases BQ and BQ_{REPL}, trapping efficiency values mostly vary between 0 and

0.5 illustrating that depositional processes occurred. Values were never consistently close to $(Q_{s,in} - Q_{s,out})/Q_{s,in} = 1$ suggesting that there was always at least partial sediment conveyance through the widening perimeter. The flood hydrographs of phases FQ_1 and FQ_2 increased relative sediment evacuation for series with lower supply.

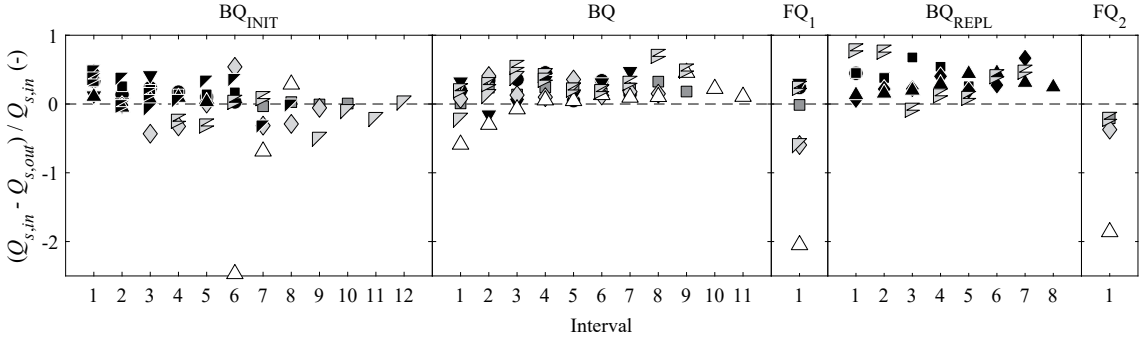

Figure 5.31 ***Trapping efficiency*****:** The ratio of sediment retained in the model perimeter to sediment input $(Q_{s,in} - Q_{s,out})/Q_{s,in}$ per interval for all experimental series. A value of 1 indicates that all sediment was retained while a value of 0 means that sediment input and output were balanced. If the value falls below 0, more sediment was evacuated than supplied during an interval.

Figure 5.32 compares the characteristic grain sizes of sediment input and output. The median D_{50} values are close to unity while the median D_{90} are slightly lower. The interquartile ranges indicate some variation in output grain sizes, especially for D_{50} (see also Figures 5.9b to 5.15b). Overall, however, no significant influence of sediment supply on transport conditions can be identified, that is, the experiments were conducted under equal mobility conditions.

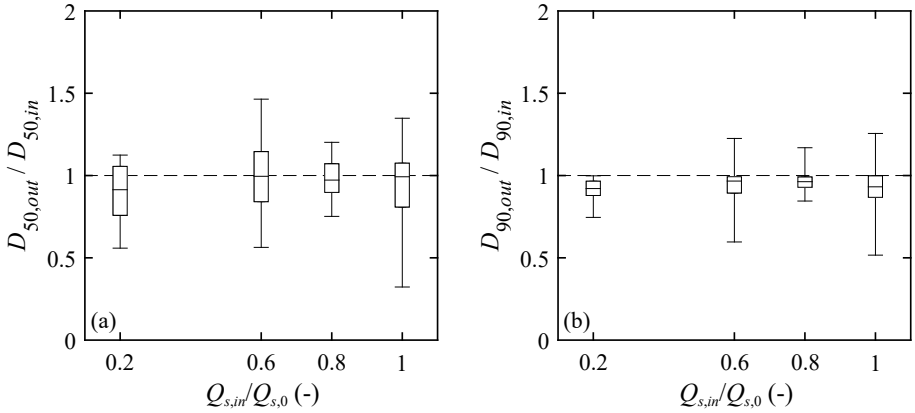

Figure 5.32 ***Grain mobility*****:** Output grain size relative to input grain size D_{out}/D_{in} as a function of sediment supply $Q_{s,in}/Q_{s,0}$ for the characteristic grain diameters (a) D_{50} and (b) D_{90} for phases BQ_{INIT}, BQ, and BQ_{REPL} of all experimental series (with $D_{50,in}$ = 1.9 mm and $D_{90,in}$ = 5.9 mm).

Figures 5.33 and 5.34 show various metrics related to altimetric adjustments of the widening. Although the data shows some scatter, WSE slopes during phase BQ_{INIT} re-

mained close to 0.01 for a supply of $Q_{s,in}/Q_{s,0}$ = 1 and 0.8, while they approached 0.009 for $Q_{s,in}/Q_{s,0}$ = 0.6 and 0.2 (Figure 5.33). In the following phase BQ, two different trajectories can clearly be identified. Series R_{20}, R_{60}, and $R_{60,FD}$ maintained relatively low WSE slopes, while the WSE slopes increased from 0.0095 to 0.01 to values between 0.0105 and 0.012 for the remaining series. During phase FQ_1 the respective WSE slopes were mostly unchanged. The replenishment phase BQ_{REPL} caused a WSE slope increase in series R_{20} and R_{60} with a rate similar to the high supply series in phase BQ. Both series seem to level off at S_{wse} = 0.011 to 0.012. Again, S_{wse} did not change considerably during phase FQ_2 but the values were overall higher than after phase FQ_1.

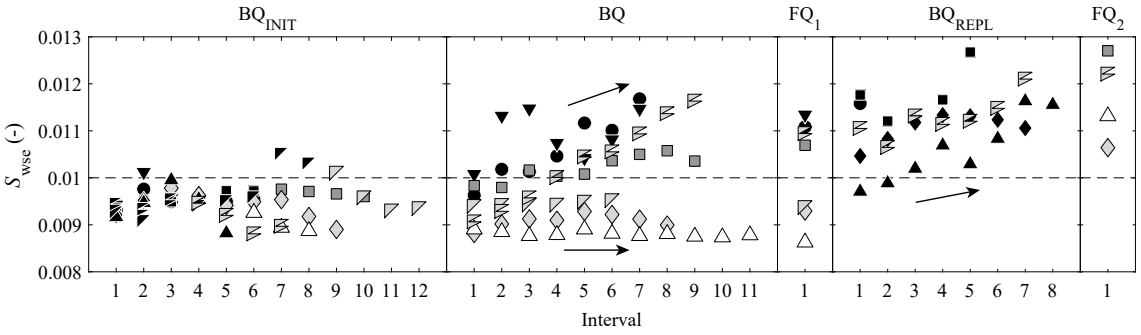

Figure 5.33 ***Altimetric adjustment*****:** Water surface slope S_{wse} at the end of each interval for all experimental series. Slopes were evaluated in the widening perimeter only.

Figure 5.34 relates widening metrics introduced by Hunzinger (1998; see Section 2.5.3) to sediment supply. Upstream bed aggradation Δz was defined as the mean elevation difference between the bed and the respective initial channel bed between X = 2.5 to 3 m (Figure 5.34a). The vertical bed offset s_z was determined as the mean elevation difference between a line connecting the bed at X = 3 m and X = 27.5 m and a linear fit of the bed elevation in the central widening between X = 5.64 to 19.8 m. Finally, the maximum constriction scour depth $t_{s,max}$ was defined as the maximum elevation difference between the minimum bed elevation and a linear fit of the bed elevation in the outlet section between X = 22.65 to 27.5 m.

While the bed upstream of the widening was degraded relative to the initial bed elevation by up to half the initial channel flow depth for $Q_{s,in}/Q_{s,0}$ = 0.2 and remained more or less stable for $Q_{s,in}/Q_{s,0}$ = 0.6, $Q_{s,in}/Q_{s,0}$ = 0.8 and 1 caused upstream aggradation of roughly half the channel flow depth (Figure 5.34b). No conclusive relation between vertical bed offset and sediment supply can be identified (Figure 5.34b) with values generally remaining low. Low sediment supply $Q_{s,in}/Q_{s,0}$ = 0.2 caused the deepest constric-

tion scours of more than one channel flow depth at the downstream widening end (Figure 5.34d). $Q_{s,in}/Q_{s,0}$ = 0.6, 0.8, and 1 caused scour depths of half to one full flow depth.

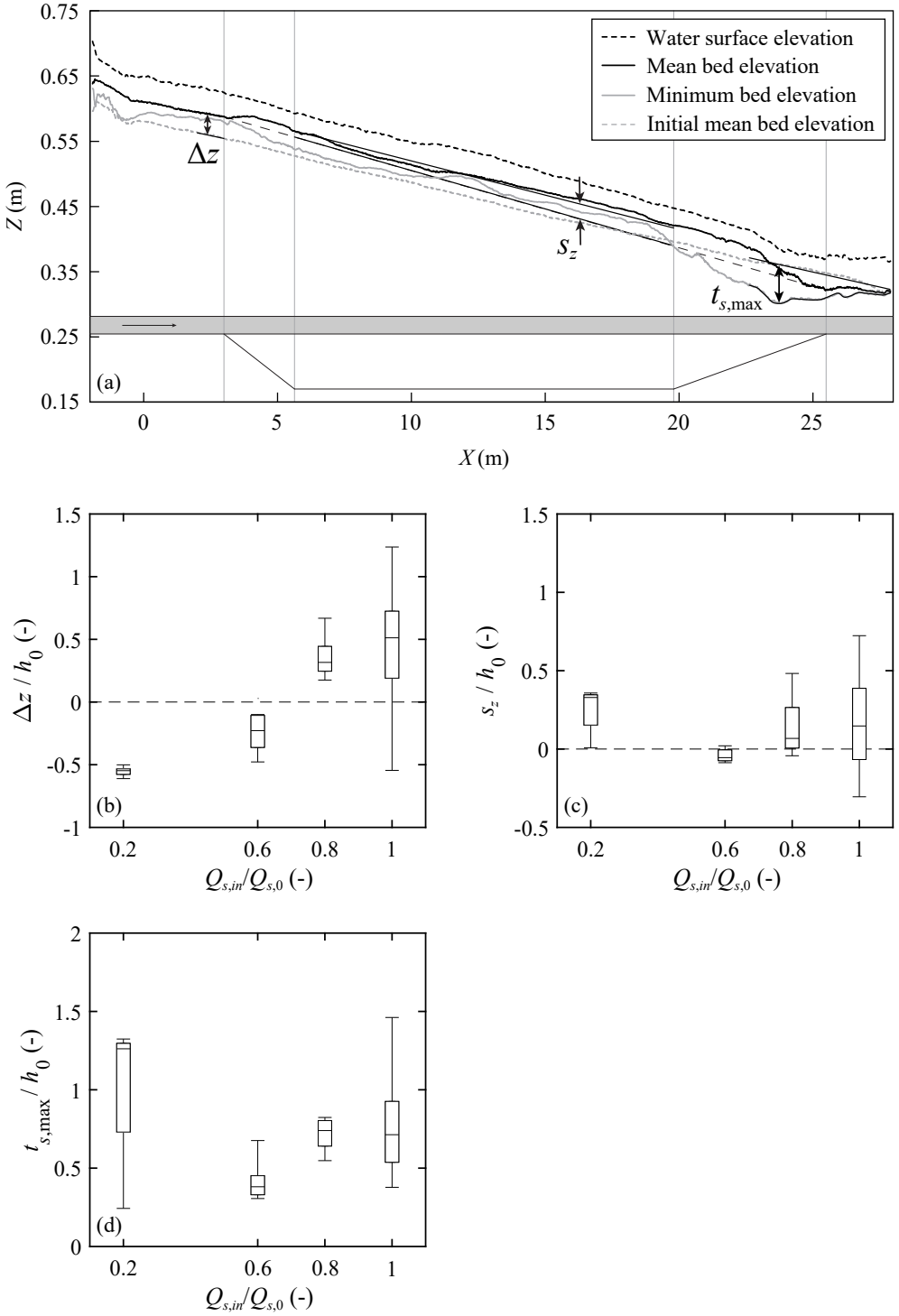

Figure 5.34 ***Altimetric adjustment*****:** (a) Example longitudinal profile illustrating the definition of the (b) relative upstream bed aggradation $\Delta z/h_0$ (with h_0 = 0.04 m), (c) relative vertical bed offset in the widening s_z/h_0, and (d) relative maximum scour depths $t_{s,\max}/h_0$ at the downstream end of the widening. Only data of phases BQ and BQ_{REPL} of series without initiation measures is shown in (b)-(d).

Figure 5.35 shows the development of channel width, flow depth, and resulting aspect ratio with the thresholds $b/h > 10$ for alternate bar formation and $b/h > 50$ for braiding according to Crosato and Mosselman (2020; Figure 5.35d). The respective values were calculated for the widening perimeter, only taking into account zones where $\theta_{D50} > 0.03$ (see Section 4.5). The values are constant during phase BQ_{INIT} due to the fixed channel width. Note that b_0 is lower than the data points because it corresponds to the initial bed width of the channel (0.89 m), while b_m and b_{max} are defined in relation to hydraulic properties ($\theta_{D50} > 0.03$). During phase BQ, opposing trends of channel width and flow depth can be observed for series S, S_{INV}, R_{80}, and $R_{60,IW}$ with channel width reaching $1.6b_0$ to $2b_0$ and flow depth decreasing to $0.65h_0$ to $0.8h_0$. As for WSE slopes (Figure 5.33), conditions remained largely stable for series R_{20}, R_{60}, and $R_{60,FD}$ while the aspect ratio gradually increased for all other series (Figure 5.35d). During phase FQ_1, aspect ratios were unchanged for series R_{20} and R_{60} while increasing for all other series. During phase BQ_{REPL}, the aspect ratios of all series further increased compared to phase BQ. Note how two subphases can be distinguished for series R_{20} with little change in aspect ratio during the first three to four intervals followed by a steeper increase. Finally, phase FQ_2 did not cause large changes in aspect ratio with all values remaining above the braiding threshold. Note how flow depths and channel widths are aligned during phase FQ_2 in contrast to phase FQ_1.

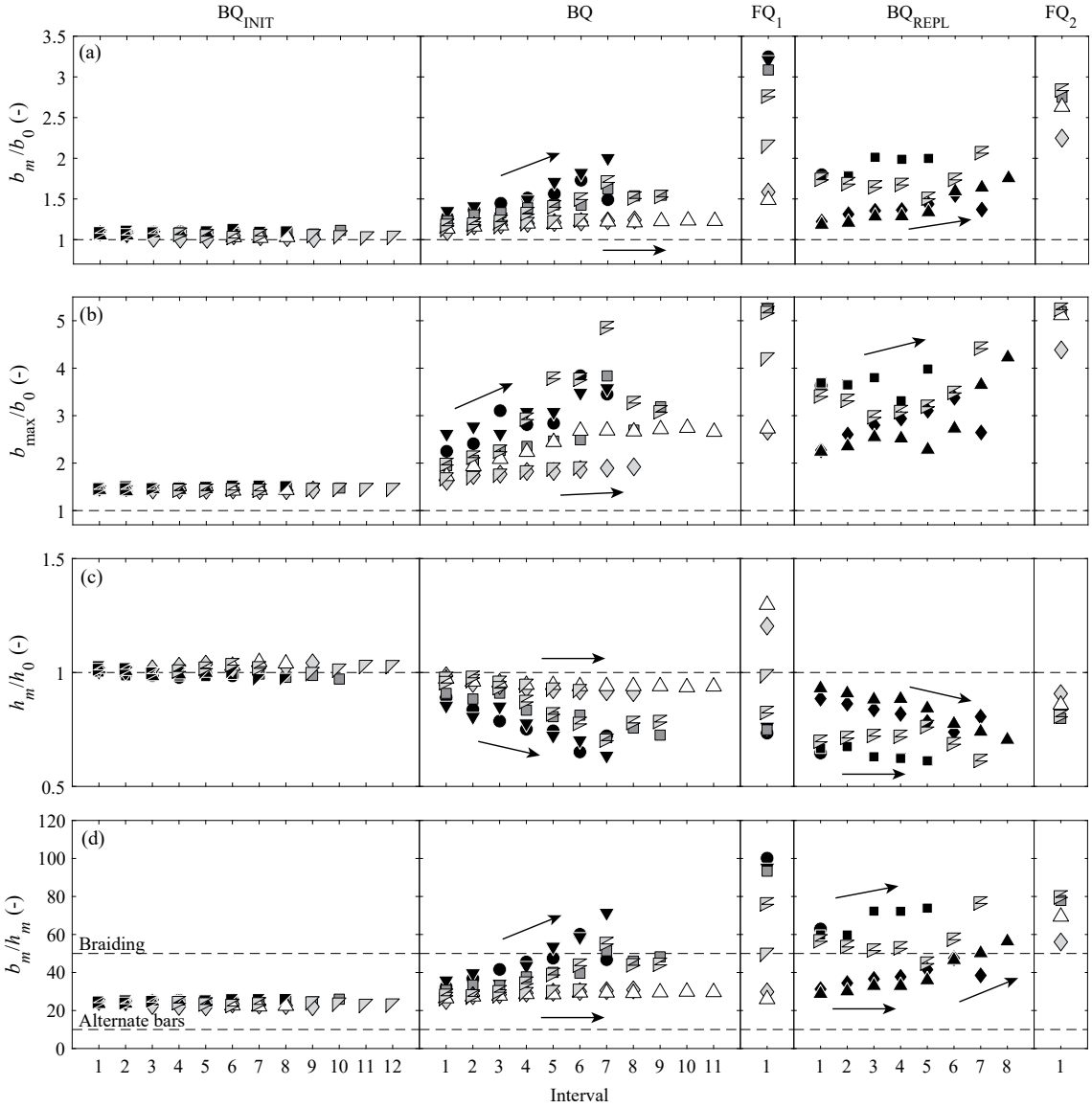

Figure 5.35 ***Channel widths and flow depths*****:** (a) Mean channel width relative to initial channel width b_m/b_0 (with b_0 = 0.89 m), (b) maximum channel width relative to initial channel width $b_{\max}/b_0$, (c) mean flow depth relative to initial flow depth h_m/h_0 (with h_0 = 0.04 m), and (d) mean aspect ratio b_m/h_m. All metrics were evaluated in the widening perimeter only (see Section 4.5 for further details on the data analysis).

Sediment relocation area A_{reloc}, defined as the sum of areas experiencing either erosion or deposition within the widening perimeter (see Section 4.5), is used as a measure for topographic stability (Figure 5.36). Due to alternate bar formation, the relocation area was almost equal to the channel area in the first interval of phase BQ_{INIT}. As the bars stabilized and possible erosion due to sediment deficit diminished, $A_{\text{reloc}}/A_{ch,0}$ approached 0, with values of 0.11 to 0.31 recorded for the respective last intervals of phase BQ_{INIT} (except for series S_{INV} with 0.88 due to bar shifting). Values remained low for series R_{20}, R_{60}, and

$R_{60,FD}$ during phase BQ but increased to $A_{reloc}/A_{ch,0} \geq 1$ for the other series. During each interval of these series, an area greater than the initial channel area was therefore subject to sediment relocation. The increased hydraulic forcing during phase FQ_1 caused even more sediment relocation in all series. In phase BQ_{REPL}, sediment relocation dipped during the first intervals of series R_{20} and R_{60} but after 3 to 4 intervals reached values similar to the high supply series during phase BQ. $A_{reloc}/A_{ch,0}$ further increased for all series in phase FQ_2 resulting in sediment relocation on approximately 2 to 3 times the initial channel area.

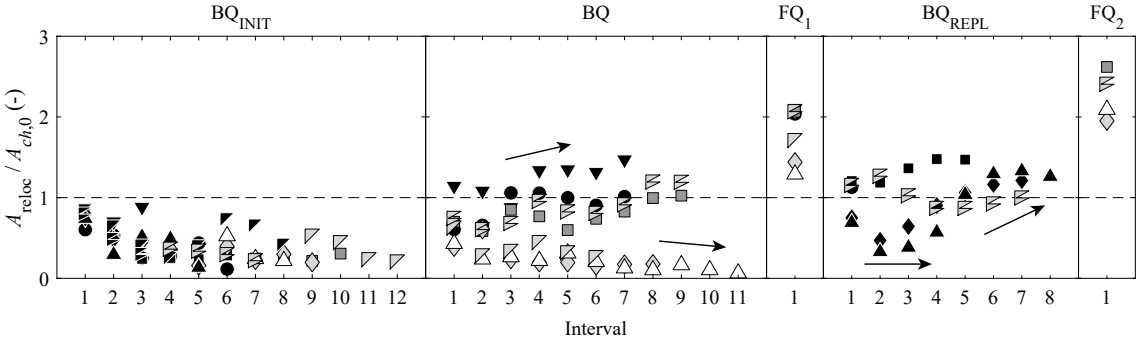

Figure 5.36 ***Sediment relocation*****:** Area with sediment relocation (erosion or deposition) relative to the initial channel area $A_{reloc}/A_{ch,0}$. Areas were evaluated in the widening perimeter only (see Section 4.5 for further details on the data analysis).

Two metrics for channel stability that were calculated based on the hydraulic and topographic characteristics of the individual intervals are shown in Figure 5.37. Figure 5.37a shows bar modes m after Crosato and Mosselman (2009; see Section 3.3) with the ranges for alternate bar formation ($0.5 \leq m < 1.5$), central bar formation ($1.5 \leq m < 2.5$), and braiding ($m \geq 2.5$). Figure 5.37b shows the detrended channel width b_* after Métivier *et al.* (2017; see Section 3.6.1) with the thresholds $b_* = 1$ for threshold channels (no sediment transport) and $b_* = 1.7$ for channel destabilization into braiding. Not unexpectedly, both metrics follow similar trends as, for example, the aspect ratio (Figure 5.35d), which is a major control on channel stability (cf. Abramian *et al.* 2020). A temporary reduction of these metrics, for example, during interval 7 of phase BQ in series S, can be explained by the abandonment of side channels on the former floodplain and an associated decrease in channel width (see also Figure 5.8a). If the widening were two-sided, this process presumably would not have decreased channel width but simply shifted the channel into the opposite floodplain.

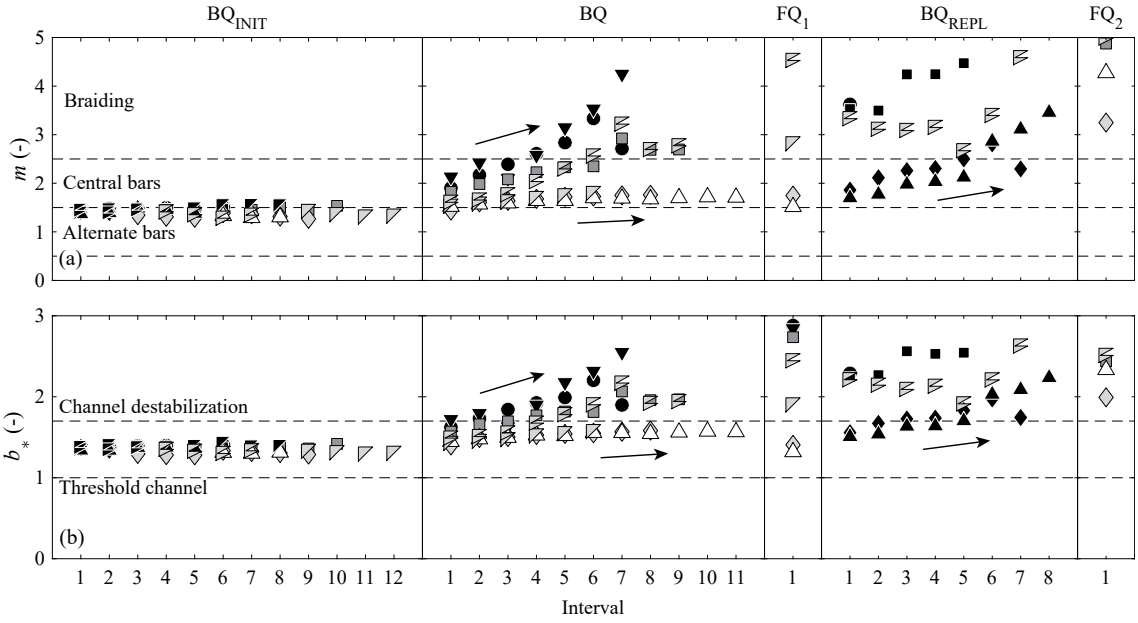

Figure 5.37 ***Channel stability*****:** (a) Bar modes *m* after Crosato and Mosselman (2009) and (b) detrended widths b_* after Métivier *et al.* (2017).

Figure 5.38 completes this section on morphodynamic trajectories by comparing the experimental results of all series without bank erosion initiation measures to the morphological region plan of Ahmari and da Silva (2011; see Section 3.3). The trajectories of all series except $R_{60,FD}$ suggest a transition from an alternate bar morphology towards the braiding region. Note that this transition may be caused by a sediment supply of $Q_{s,in}/Q_{s,0}$ = 1 or 0.8 (black and dark gray markers; Figures 5.38a-c), by elevated hydraulic stress (markers apart from the clusters are FQ intervals; Figures 5.38d,e), or by successful bank erosion initiation in series $R_{60,IW}$ (Figure 5.38g). For lower sediment supply of $Q_{s,in}/Q_{s,0}$ = 0.6 or 0.2 (light gray and white markers; Figures 5.38d,e) or unsuccessful bank erosion initiation in series $R_{60,FD}$ (Figure 5.38f), the widenings remain in the alternate bar region for bed-forming discharge. These results also suggest that even with high sediment supply, full braiding is unlikely to develop in the studied river widenings of limited length and width, a finding that corresponds well with the observed planforms (see Section 5.5).

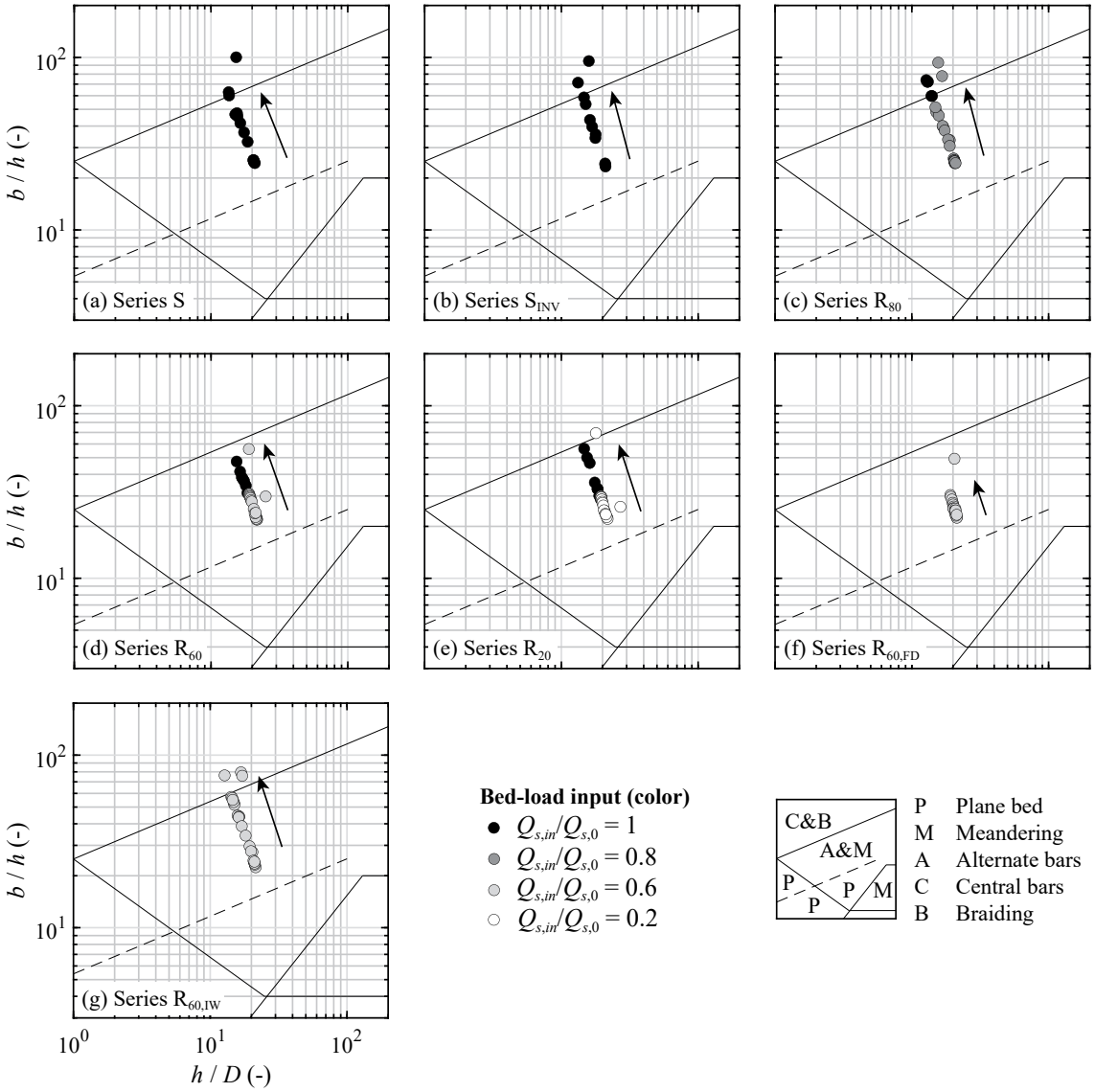

Figure 5.38 ***Morphology*****:** Trajectories in the Ahmari and da Silva (2011) diagram for phases BQ to FQ_2 of (a) series S, (b) series S_{INV}, (c) series R_{80}, (d) series R_{60}, (e) series R_{20}, (f) series $R_{60,FD}$, and (g) series $R_{60,IW}$.

5.7 Discussion

5.7.1 Alternate bar response to reduced sediment supply

Because the initial channel is laterally confined, the channel response to variable sediment supply is limited to changes in longitudinal slope and surface composition. The observed slope adjustments are similar to descriptions of alternate bar response to sediment supply variations in previous studies. Although the bars did not emerge as described by Lisle *et al.* (1993), thalweg incision was observed in response to sediment supply reduction. The longitudinal WSE slope decreased by −7.2% for −40% sediment supply and −10.2% for −80% sediment supply. Lisle *et al.* (1993) reported roughly −10% WSE slope in response to a sediment supply reduction of 68%. A further reduction to only 10% of the original feed rate had no additional effect on the longitudinal slope. The results of phase BQ_{INIT} are thus comparable with those of Lisle *et al.* (1993) although it must be noted that the initial slope and aspect ratio in their experiments was larger with $S = 0.03$ and $b/h = 39$. These conditions presumably resulted in bars of greater vertical dimensions that emerged already for relatively limited thalweg incision. A numerical modeling study on alternate bar response to reduced sediment supply by Vonwiller (2018) also resulted in thalweg incision and bar emergence. Bar erosion as reported by Venditti *et al.* (2012) was not observed in the laboratory experiments presented here. The contraction of the active bed-load transport zone and associated surface coarsening in response to reduced sediment supply has also been observed but cannot be quantified (cf. Dietrich *et al.* 1989; Lisle *et al.* 1993; Nelson *et al.* 2009).

5.7.2 Was channel widening predictable?

To examine the morphological state of the initial channel, different regime width approaches introduced in Section 3.4 were evaluated for discharges of 24 to 33 l/s (corresponding to $HQ_{1.5}$-HQ_5 in the reference system). Predicted channel widths of $b = 0.97$ to 1.14 m resulted after Lacey (1930), $b = 0.92$ to 2.16 m after Parker (1979) (using $D_{50,A} = D_{50}$ to D_{90}), $b = 1.06$ to 1.63 m after Millar (2005) (using $D_{50,A} = D_{90}$ and $\mu' = 1$ to 1.2), and $b = 4.03$ to 5.18 m after Ashmore *et al.* (2011). The first three approaches refer to the width of straight single-thread channels with active bed-load transport, thus to channels that did not destabilize into braiding. These are channels that have undergone *primary* lateral erosion as termed by Requena (2008). Conversely, the approach of Ashmore (2001)

refers to the total width of rivers that may have a braiding planform, thus corresponding to *secondary* lateral erosion after Requena (2008). Accordingly, greater widths result from this approach. Overall, it can be concluded that the initial channel in the experiments described here was expected to widen when bank protection is removed. But was widening to be expected for all sediment supply rates?

According to Métivier *et al.* (2017; see Section 3.6.1), threshold channel width is 0.74 to 0.87 m for Q = 24 to 33 l/s, D_{50} = 1.9 mm, and b_* = 1. The destabilization into braiding can be expected for channel widths of 1.26 to 1.48 m (b_* = 1.7). The initial channel width b_0 = 0.89 m is therefore slightly wider than the corresponding threshold channel, that is, this channel can only accommodate limited sediment supply without increasing its width. It can therefore be assumed that considerable sediment supply would lead to channel widening, as was observed for a supply of $Q_{s,in}/Q_{s,0}$ = 1 and 0.8 (see Section 5.5.1). Whether channel widening should have been expected for $Q_{s,in}/Q_{s,0}$ = 0.6, too, is difficult to determine because the initial channelized configuration does not correspond to an alluvial channel due to the fixed banks.

5.7.3 Morphodynamic activity

Two distinct morphodynamic trajectories emerge when considering the development of the widening during phases BQ to FQ_2. They can be distinguished by their *morphodynamic activity* (see Section 5.2):

- Series that were *morphodynamically active* throughout all phases include series S, S_{INV}, R_{80}, and $R_{60,IW}$. Series R_{20}, R_{60}, and $R_{60,FD}$ were partially morphologically active during phases FQ_1 to FQ_2.
- Series R_{20}, R_{60}, and $R_{60,FD}$ were *morphodynamically inactive* during phase BQ.

The sediment supply level seems to strongly influence morphodynamic activity. The destabilizing effect of higher sediment supply during the widening phase is in agreement with the general tendency for channels with sediment transport to be wider than threshold channels without sediment transport (e.g., Métivier *et al.* 2017; Baynes *et al.* 2020). Channel widening and steepening increases the reach-scale aspect ratio and decreases relative submergence, promoting a shift to a multi-thread morphology (e.g., Ahmari and da Silva 2011). Based on the laboratory observations, it can be assumed that localized flow perturbations may trigger local morphological adjustments that subsequently propagate to larger

scales and interact with each other. As a result, the process of concurrent bank accretion and bank erosion on the opposite channel side (cf. Klösch *et al.* 2015) seems to be more active for higher sediment supply. A similar mechanism seems to be responsible for the morphodynamic activity observed in series $R_{60,IW}$. The local floodplain lowering caused flow divergence and an associated decrease in transport capacity. Sediment was locally deposited and apparently triggered lateral erosion as described by Klösch *et al.* (2015). The growing central bar at the location of the initial widening can be seen in Figure 5.2b.

Based on these considerations, sediment supply seems to emerge as primary control of morphodynamic activity. One process that might obscure this relation is floodplain inundation. When the floodplain is partially inundated, as was the case in many experiments shown here, the reduction in transport capacity due to the reduction in specific discharge might lead to increased deposition in the main channel and associated lateral erosion. As the elevation difference between channel and floodplain and thus bankfull discharge can vary widely in heavily impacted rivers, this factor is a potential source of uncertainty. In the experiments presented here, floodplain inundation was more frequently observed in morphodynamically active widenings due to overall higher WSE slopes and thus decreased elevation difference between channel and floodplain (see Figure 5.39). It is therefore possible that floodplain inundation could be the triggering mechanism for morphodynamic activity. However, no conclusive relation between wetted area (as proxy for floodplain inundation) and morphodynamic activity can be identified (Figure 5.39). In several cases, the morphodynamic activity is high despite the floodplain not being inundated (Group II in Figure 5.39; see also Phase BQ in Figure 5.10 or Phase BQ_{REPL} in Figure 5.13). While floodplain inundation may certainly reinforce morphodynamic activity once a substantial part of the discharge is diverted, it cannot be identified as the decisive trigger for lateral erosion.

5.7.4 Sediment replenishment

It seems that the transformation of a stable, low sediment supply widening to a more dynamic, high sediment supply widening can be achieved by restoring sediment transport. However, this process is not linear. A delay of roughly four experimental intervals was identified in the laboratory experiments. Only after this delay all metrics indicated the reach was as dynamic as the high sediment supply widenings. During this delay, first the longitudinal slope increased to a value similar to high sediment supply systems, and only

afterwards did the lateral erosion and sediment relocation activity increase to match high sediment supply systems (cf. Venditti *et al.* 2012).

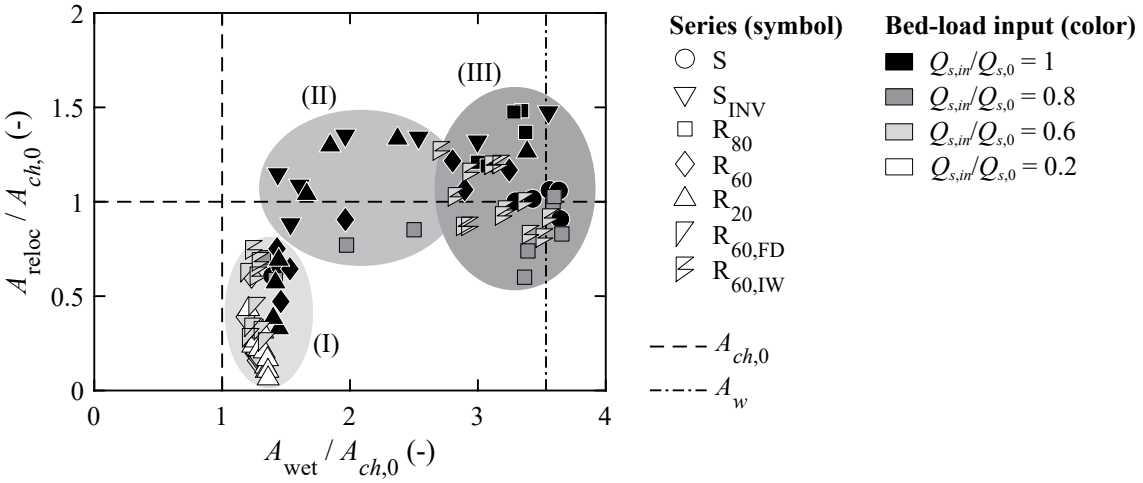

Figure 5.39 Relative relocation area as a function of relative wetted area for all intervals of phases BQ and BQ_{REPL} of all series. All areas refer to the widening perimeter only. Three groups of intervals can be identified: (I) floodplain not inundated / low to medium morphodynamic activity, (II) floodplain not or partially inundated / high morphodynamic activity, and (III) floodplain inundated / high morphodynamic activity.

5.7.5 Relevant time scales

To approximate the relevant time scale of the recovery described in the previous paragraph, all floods with a peak discharge of 118±10 m^3/s ($Q_B \approx 118$ m^3/s at field scale) were extracted from the discharge time series of the reference reach (FOEN 2019). Discarding discharges below the calculated threshold for bed-load transport (88 m^3/s), the median flood duration was 465 min. Comparing the downscaled flood duration (85 min) to the experimental interval duration (180 min) and considering the return period of 1.5 years, one experimental BQ interval can be estimated to represent the morphological change of roughly five years. The recovery period of four intervals observed in the laboratory experiments would thus correspond to approximately 20 years.

This rough estimation also holds if compared with bed-load transport. If the transport capacity $Q_{s,0}$ = 62.5 g/s identified in the laboratory experiments is upscaled and summed, a sediment volume of 10,720 m^3 was added during each interval. Compared with the modeled bed-load transport of 9000 m^3/a stated in HZP (2004), one interval would correspond to 1.2 years. But as many other Swiss rivers, the Kander River is in a state of sediment deficit (see Section 2.6; Schälchli and Kirchhofer 2012). If the effective bed-load transport rate for the bed-forming discharge Q_s = 0.04 m^3/s (pers. comm. HZP AG, 16.11.2020) is

compared to the upscaled $Q_{s,0}$ = 0.18 m^3/s, the laboratory transport capacity is higher by a factor of 4.5. Thus, one interval would roughly correspond to 1.2 · 4.5 = 5.4 years.

Evidently, these estimations are based on a significant simplification of hydrological and sedimentological conditions and in this form discount the effect of larger floods. The purpose of this exercise is solely to illustrate that an increase in sediment supply will not promptly transform a stable into a dynamic reach but rather initiate change that unfolds over years or decades (cf. Habersack *et al.* 2000). The consideration of relevant time scales, albeit as a rough estimation, is critical for restoration planning. In field settings, floodplain vegetation encroachment and maturation may further slow down or prevent the reactivation of bank erosion (e.g., Hafner *et al.* 2012), although erosion of vegetated floodplains after gravel mining cessation has also been reported (Moretto *et al.* 2014).

5.7.6 Comparison to excavated widenings

The reach-scale sediment balance of a widening is important to consider in the context of sediment continuity. The absence of trapping efficiency values close to 1 indicates that bed-load is at least partially transported through the widening reach studied here at all times (Figure 5.40). Indeed, the median values in Figure 5.40 suggest that only 10 to 20% of the sediment input is trapped in the widening. In contrast to excavated river widenings (Hunzinger 1998), dynamic river widenings cause more gradual changes in transport capacity due to channel widening. Note that in the case of excavated river widenings, complete sediment trapping may be prevented by anticipating the vertical bed offset (Hunzinger 1998).

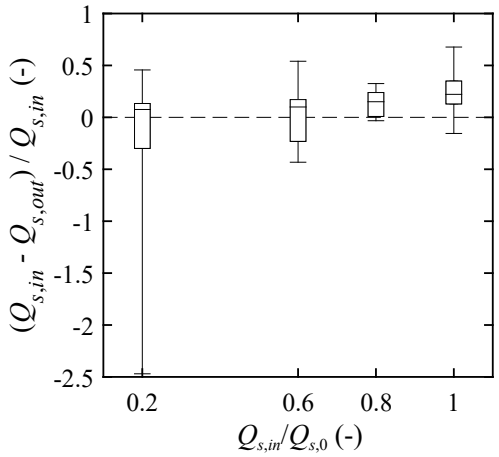

Figure 5.40 The ratio of sediment retained in the model perimeter to sediment input $(Q_{s,in} - Q_{s,out})/Q_{s,in}$ as a function of sediment supply $Q_{s,in}/Q_{s,0}$ for phases BQ_{INIT}, BQ, and BQ_{REPL} of all experimental series.

Measured and calculated values of metrics describing the altimetric widening adjustment proposed by Hunzinger (1998) (see Section 2.5.3) can also be compared for excavated and dynamic widenings. The comparison was restricted to high sediment supply widenings ($Q_{s,in}/Q_{s,0} = 1$) consistent with the experiments by Hunzinger (1998). Based on the data of intervals with $Q_{s,in}/Q_{s,0} = 1$ of phases BQ and BQ_{REPL}, the approaches by Hunzinger (1998) predict upstream bed aggradation of $\Delta z/h_0 = 0.36 \pm 0.26$ ($\pm\sigma$), vertical bed offsets of $s_z/h_0 = 0.33 \pm 0.13$ ($\pm\sigma$), and maximum scour depths of $t_{s,\max}/h_0 = 0.68 \pm 0.20$ ($\pm\sigma$).

Measured vertical bed aggradation was slightly higher with $\Delta z/h_0 \approx 0.5$ (Figure 5.34). The finding of previous studies according to which widenings in eroding rivers would not be able to stabilize the upstream river bed (Requena *et al.* 2005; Hafner *et al.* 2012; Berchtold 2015) can be confirmed based on the data shown in Figure 5.34a. Measured vertical bed offsets were lower than predicted values with s_z/h_0 close to 0. Measured scour depths were similar to predicted values with median values of $t_{s,\max}/h_0 \approx 0.7$ and maximum values almost reaching $t_{s,\max}/h_0 = 1.5$. Overall, this comparison reveals broad similarities for dynamic and excavated widenings in terms of their altimetric adjustments. The most significant difference occurs for the vertical bed offset, which is almost absent in dynamic widenings, and may be a result of less abrupt channel transitions.

5.7.7 Experimental limitations

Finally, there are some considerations to be made regarding study limitations: Due to the long series duration, it was not possible to repeat each experimental series a number of times. Statistically reliable statements on the widening process in relation to sediment supply can therefore not be provided at this stage. Nevertheless, one can evaluate the validity and reproducibility of the laboratory experiments based on several considerations. Firstly, the initial channel conditions with alternate bars proved reproducible with some minor deviations in bar location. The dimensions of the alternate bars compared well to literature values, and the initial channel slope of 0.01 was reproduced across all series. It follows that the strongly diverging topographic trajectories during the subsequent widening phase can be attributed to differences in sediment supply rate with reasonable certainty. Secondly, the effects of sediment supply reduction were also reproducible. Adding only 60% of the channel's transport capacity, for example, resulted in a significant slope reduction by the end of the channelized phase in all three series with this sediment supply. Thirdly,

the two series with sediment supply corresponding to the channel's transport capacity produced fairly similar widenings despite starting from mirrored alternate bar patterns. Ultimately, the channel patterns of either stable or dynamic widenings were remarkably similar across all experimental series. It can therefore be stated with reasonable confidence that the laboratory experiments represent a sound reproduction of morphodynamic processes in dynamic river widenings for the boundary conditions tested here. However, it is acknowledged that the expansion of the parameter range, e.g. to lower channel slopes, may result in a different relationship between widening and sediment supply.

5.8 Synthesis

The objective of the laboratory experiments was to relate the morphological evolution of one-sided dynamic river widenings to sediment supply. By closely tracking changes in riverbed topography, sediment supply was demonstrated to be a major control on the planimetric and altimetric widening evolution. Sediment supply roughly balanced with the channel's transport capacity led to faster and more extensive lateral erosion, higher bed and water surface elevation slopes, and more sediment relocation compared to lower sediment supply.

Based on the morphological response to variable sediment supply rates and structural bank erosion initiation measures, two morphodynamic states were identified: *morphodynamically active* and *morphodynamically inactive* widenings (Figure 5.41). Morphodynamic activity is thereby characterized by substantial channel shifting, channel widening, and/or sediment relocation.

The conceptual sketch in Figure 5.41 outlines the relative ranges of slope magnitude and morphodynamic activity for both bed-forming discharge and a 30-year flood resulting from high and low sediment supply. Low sediment supply cases showed considerable variability in morphodynamic activity depending on flood magnitude while consistently maintaining lower slopes compared to high sediment supply cases. High sediment supply produced higher slopes and morphodynamic activity, while being less sensitive to flood discharge. Flood magnitude seems to be a major driver of widening evolution, especially when sediment supply is low compared to transport capacity (Moretto *et al.* 2014; Eaton *et al.* 2020). Note that the influence of sediment supply may be somewhat weaker when bank erosion can successfully be initiated as was observed for initial floodplain lowering causing local flow deceleration.

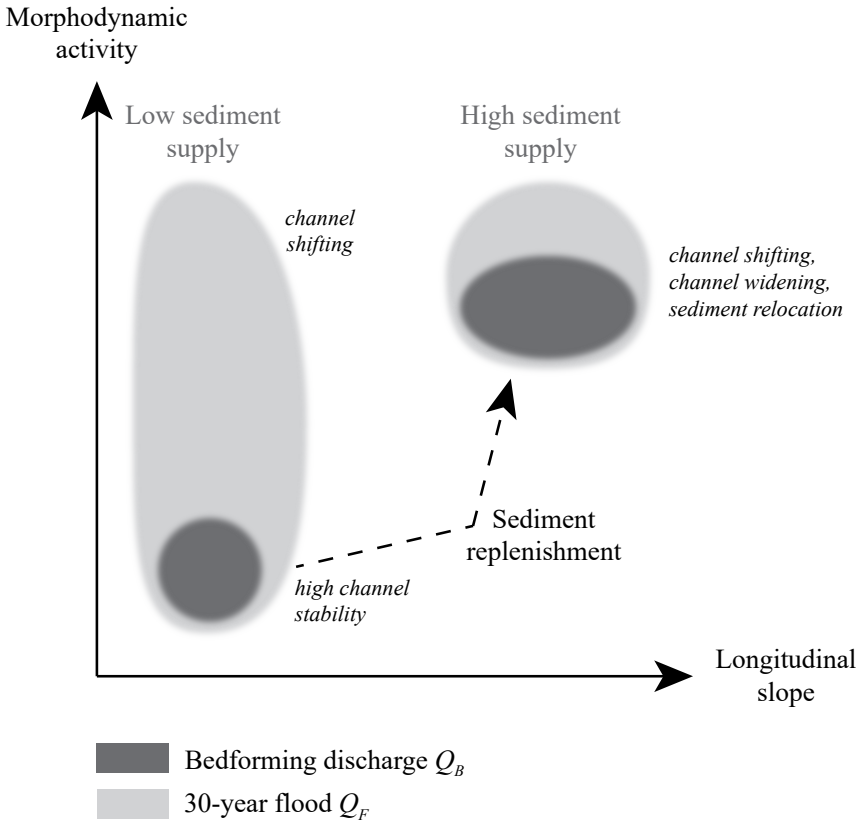

Figure 5.41 Distinct morphodynamic states of river widenings with dominant morphodynamic processes in italics identified for high and low sediment supply. High sediment supply thereby refers to $Q_{s,in}/Q_{s,0} \geq 0.8$ (close to channel transport capacity), while low sediment supply refers to $Q_{s,in}/Q_{s,0} \leq 0.6$ (significantly lower than channel transport capacity). Note that these quantitative values apply to the conditions studied here, that is, gravel-bed rivers with a longitudinal slope of approximately one percent. The transformation trajectory following sediment replenishment is indicated with an arrow.

6 Refugia availability in dynamic widenings

Parts of this chapter have been published in:

- *Rachelly* et al. *(2021b) How does sediment supply influence refugia availability in river widenings? Journal of Ecohydraulics.*

The results presented in Rachelly et al. *(2021b) were extended to include more experimental data and an additional analysis of high bed shear stress areas.*

6.1 Overview

The results of the laboratory experiments and hydrodynamic numerical simulations were evaluated with regard to various reach characteristics likely connected to refugia availability. Several reach-scale metrics were derived including hydraulic variability (Section 6.2), floodplain inundation dynamics (Section 6.3), bed shear stress distribution (Section 6.4), and the extent of the active bed-load transport zone (Section 6.5). The chapter is concluded with a discussion (Section 6.6) and a synthesis of the findings (Section 6.7).

To make the ecological implications of the results in this chapter more tangible, all results are presented at field scale using the Froude scale factor $\lambda = 30$ (cf. Section 4.2). Furthermore, the discharges applied in the numerical model are linked to the hydrological conditions of the Kander River reference reach (cf. Section 2.6 and Table 4.4). Note that results are presented for the end state of the respective experimental phases BQ to FQ_2.

6.2 Hydraulic variability

Figures 6.1 to 6.4 show simulated flow depths for topographies at the end of the four main experimental phases and a discharge of $Q_B = 118.3$ m^3/s ($\approx HQ_{1.5}$). The ratios of wetted area to total widening area A_{wet}/A_w and of high bed shear stress area to wetted area $A_{\theta>0.06}/A_{wet}$ are also provided. The hydraulic conditions are first described based on visual assessment of the flow field alone and then analyzed in quantitative terms. The floodplain inundation dynamics and bed shear stress distributions are presented in more detail in the following Sections 6.3 and 6.4.

Based on the flow depth distributions, it is evident that hydraulic variability at the end of phase BQ is significantly higher for a sediment supply of $Q_{s,in}/Q_{s,0} = 1$ and 0.8 (Figures 6.1a-c) than for $Q_{s,in}/Q_{s,0} = 0.6$ and 0.2 (Figures 6.1d,e). Not only is the floodplain inundated, thus providing extensive shallow areas, but the main channel is wider

and divided into multiple threads in some places. The shift from single-thread to multi-thread planform induces a higher topographic and hydraulic variability. Note that for $Q_{s,in}/Q_{s,0}$ = 1 and 0.8 almost the entire floodplain is inundated and 32 to 39% of the wetted area experience high bed shear stresses, whereas these numbers are almost inverse for $Q_{s,in}/Q_{s,0}$ = 0.6 and 0.2 indicating a significantly lower relative and absolute extent of low bed shear stress areas.

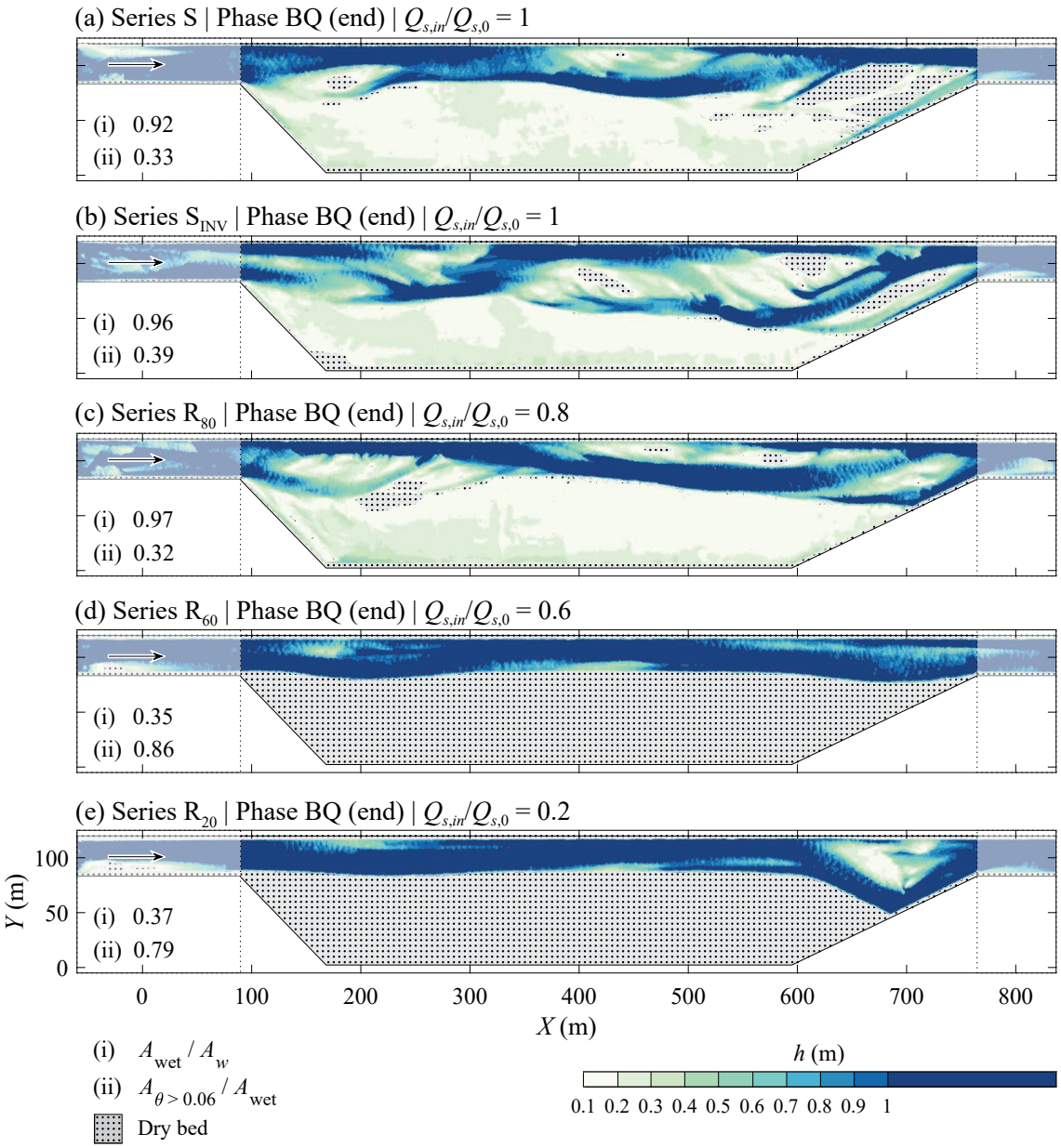

Figure 6.1 Simulated flow depths for topographies after phase BQ of series (a) S, (b) S_{INV}, (c) R_{80}, (d) R_{60}, and (e) R_{20} with discharge Q_B. The proportion of (i) wetted area to total widening area A_{wet}/A_w and (ii) high bed shear stress area to wetted area $A_{\theta>0.06}/A_{wet}$ are reported. The dimensionless bed shear stress θ is calculated for the median grain size D_{50}. The inlet and outlet sections (white overlay) do not contribute to the reported areas.

Similar conditions prevail after phase FQ_1 with the hydro-morphological diversity increasing further for $Q_{s,in}/Q_{s,0}$ = 1 and 0.8 (Figures 6.2a-c). The flow fields of series R_{60} and R_{20} also feature more shallow areas but the fundamental single-thread morphology and associated homogeneous hydraulic conditions persist (Figures 6.2d,e).

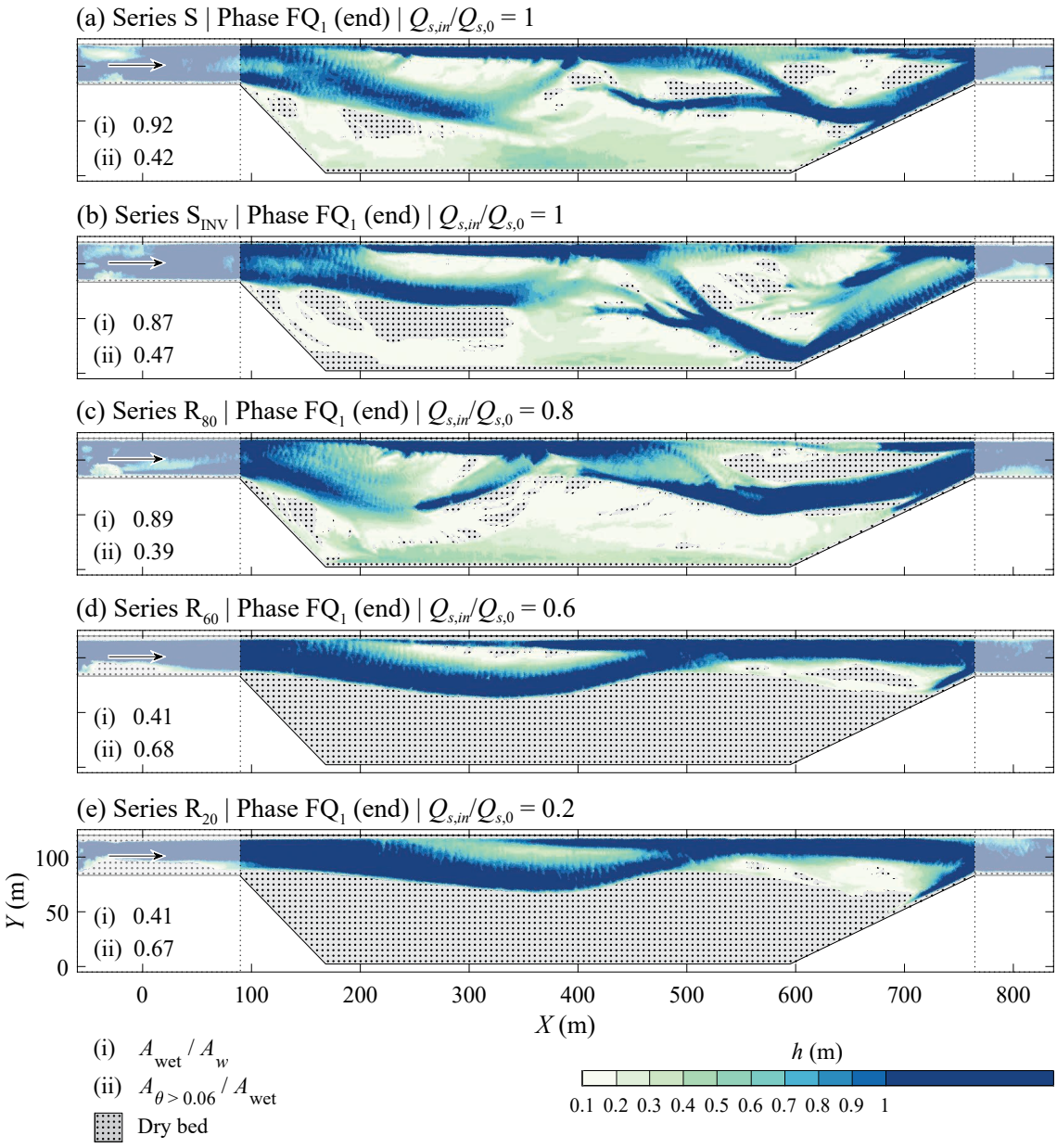

Figure 6.2 Simulated flow depths for topographies after phase FQ_1 of series (a) S, (b) S_{INV}, (c) R_{80}, (d) R_{60}, and (e) R_{20} with discharge Q_B. The proportion of (i) wetted area to total widening area A_{wet}/A_w and (ii) high bed shear stress area to wetted area $A_{\theta>0.06}/A_{wet}$ are reported. The dimensionless bed shear stress θ is calculated for the median grain size D_{50}. The inlet and outlet sections (white overlay) do not contribute to the reported areas.

The profound morphological changes triggered by sediment replenishment to a rate of $Q_{s,in}/Q_{s,0} = 1$ were translated to more diverse flow fields at the end of phase BQ_{REPL} for all series (Figure 6.3). Especially for R_{60} and R_{20}, the flow field is highly structured and features a more small-scale patchiness compared to phases BQ and FQ_1 (Figures 6.1 and 6.2).

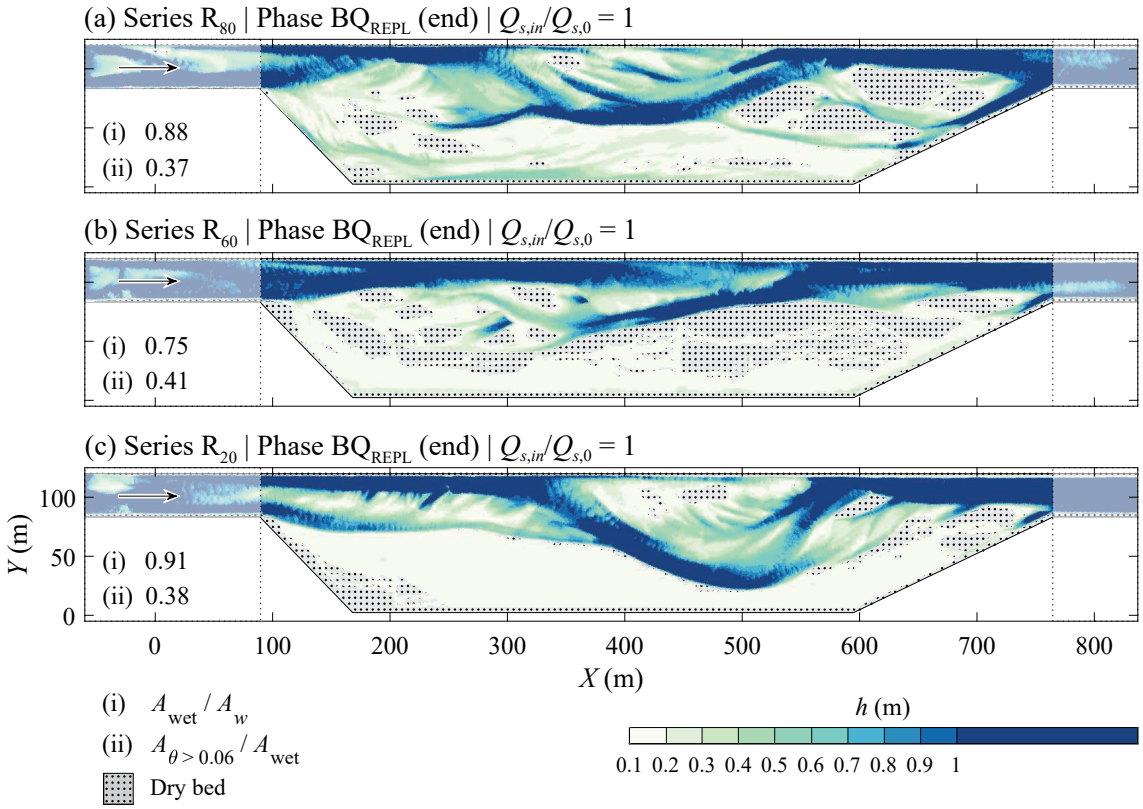

Figure 6.3 Simulated flow depths for topographies after phase BQ_{REPL} of series (a) R_{80}, (b) R_{60}, and (c) R_{20} with discharge Q_B. The proportion of (i) wetted area to total widening area A_{wet}/A_w and (ii) high bed shear stress area to wetted area $A_{\theta>0.06}/A_{wet}$ are reported. The dimensionless bed shear stress θ is calculated for the median grain size D_{50}. The inlet and outlet sections (white overlay) do not contribute to the reported areas.

A similar level of hydraulic variability can be observed after the final phase FQ_2 (Figure 6.4). Several substantial channel shifts can be observed, for example at the lower end of the widening in Figure 6.4b (cf. Figure 6.3b). However, especially during the flood hydrographs with a sediment supply of $Q_{s,in}/Q_{s,0} = 0.6$ and 0.2, the main channels seem to have slightly contracted, inching towards their low-supply single-thread morphology and reducing floodplain inundation for the bed-forming discharge Q_B shown here (Figures 6.4b,c).

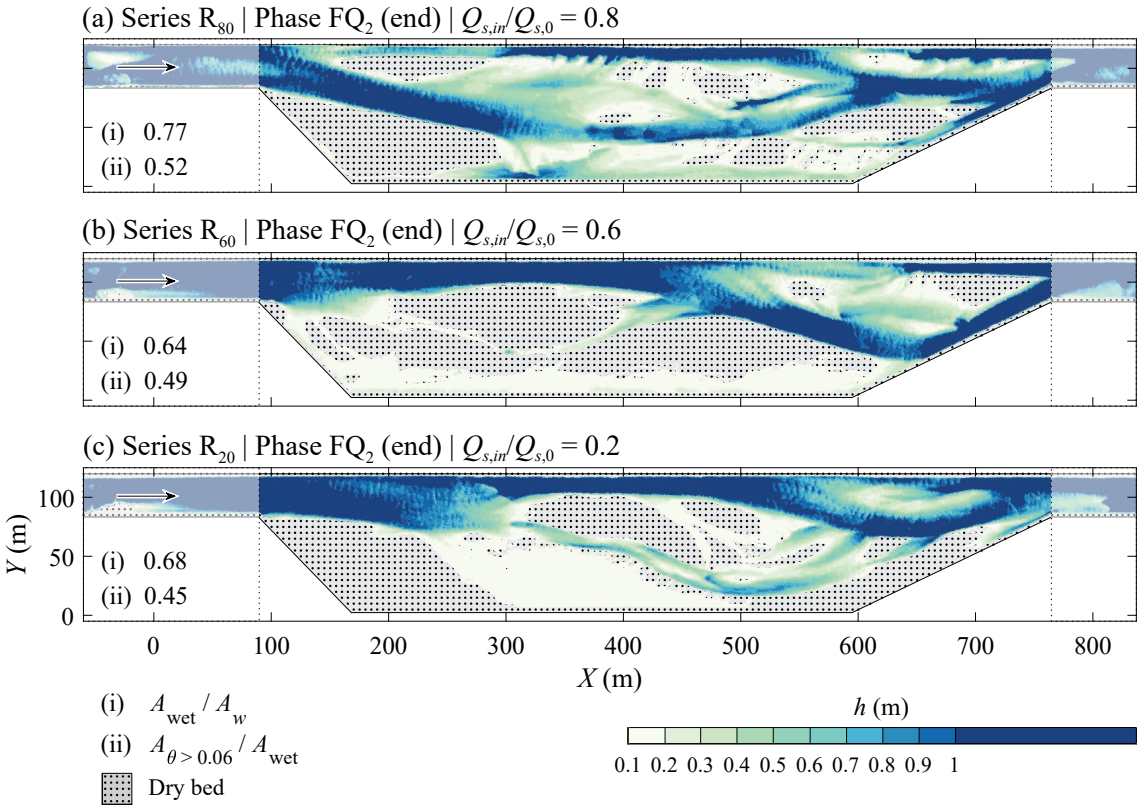

Figure 6.4 Simulated flow depths for topographies after phase FQ_2 of series (a) R_{80}, (b) R_{60}, and (c) R_{20} with discharge Q_B. The proportion of (i) wetted area to total widening area A_{wet}/A_w and (ii) high bed shear stress area to wetted area $A_{\theta>0.06}/A_{wet}$ are reported. The dimensionless bed shear stress θ is calculated for the median grain size D_{50}. The inlet and outlet sections (white overlay) do not contribute to the reported areas.

As described in Section 5.5.2, the trajectories of series $R_{60,FD}$ and $R_{60,IW}$ roughly follow the low and high supply scenarios, respectively. This is reflected in the resulting flow fields for Q_B after phases BQ and FQ_1 (Figure 6.5).

Figures 6.1 to 6.4 indicate that hydraulic variability is higher for $Q_{s,in}/Q_{s,0} = 1$ and 0.8 as opposed to $Q_{s,in}/Q_{s,0} = 0.6$ and 0.2. Topographic and hydraulic variability can be quantified as hydro-morphological index of diversity (HMID) (Gostner *et al.* 2013; see Section 4.5). Figures 6.6 and 6.7 present HMID values for a discharge range of 40 to 320 m^3/s and for series without and with bank erosion initiation measures, respectively. The subfigures display the values for the topographies resulting at the end of phases BQ, FQ_1, BQ_{REPL}, and FQ_2 of the respective series. Note that the discharge range is related to the hydrological regime of the reference reach.

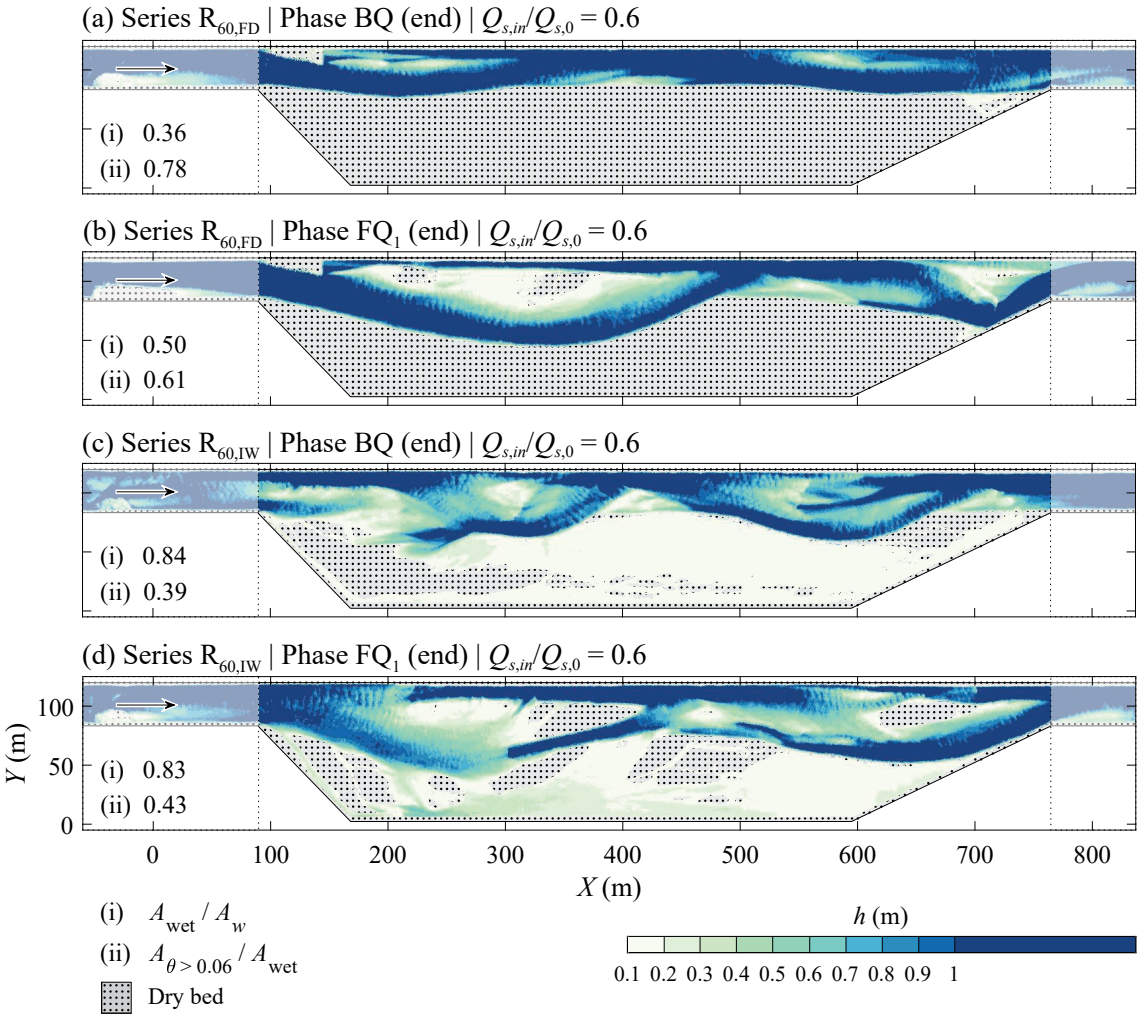

Figure 6.5 Simulated flow depths for topographies of series $R_{60,FD}$ after phases (a) BQ and (b) FQ_1 and of series $R_{60,IW}$ after phases (c) BQ and (d) FQ_1 with discharge Q_B. The proportion of (i) wetted area to total widening area A_{wet}/A_w and (ii) high bed shear stress area to wetted area $A_{\theta>0.06}/A_{wet}$ are reported. The dimensionless bed shear stress θ is calculated for the median grain size D_{50}. The inlet and outlet sections (white overlay) do not contribute to the reported areas.

For series without bank erosion initiation measures, maximum HMID values of 8 to 17 are attained for discharges < HQ_{30} and high sediment supply ($Q_{s,in}/Q_{s,0}$ = 1 and 0.8; Figure 6.6). Note that the general shape of the HMID curves for topographies at the end of phases BQ and BQ_{REPL} are similar (Figures 6.6a,c). However, the maximum values occur for slightly higher discharges in the case of BQ_{REPL} topographies previously supplied with $Q_{s,in}/Q_{s,0}$ = 0.6 and 0.2. Minimum values of 5 to 7 occur for the lowest and highest discharges of the tested range. For lower sediment supply ($Q_{s,in}/Q_{s,0}$ = 0.6 and 0.2), maximum values of 9 to 13 were reached for discharges > HQ_{30} and topographies after phases BQ and FQ_1 (Figures 6.6a,b). For topographies of phase FQ_2, the maximum values were shifted towards intermediate discharges of Q_1 to HQ_{10} (Figure 6.6d), presumably a

remnant of the replenishment during phase BQ_{REPL} (Figure 6.6c). Minimum HMID values for lower sediment supply lie around 2 to 5 for discharges < HQ_{30} (Figures 6.6a,b) and for discharges < Q_3 (Figures 6.6d). Overall, differences between the sediment supply levels are most pronounced at the end of phase BQ (Figure 6.6a) and less so in phases FQ_1 to FQ_2 (Figures 6.6b-d).

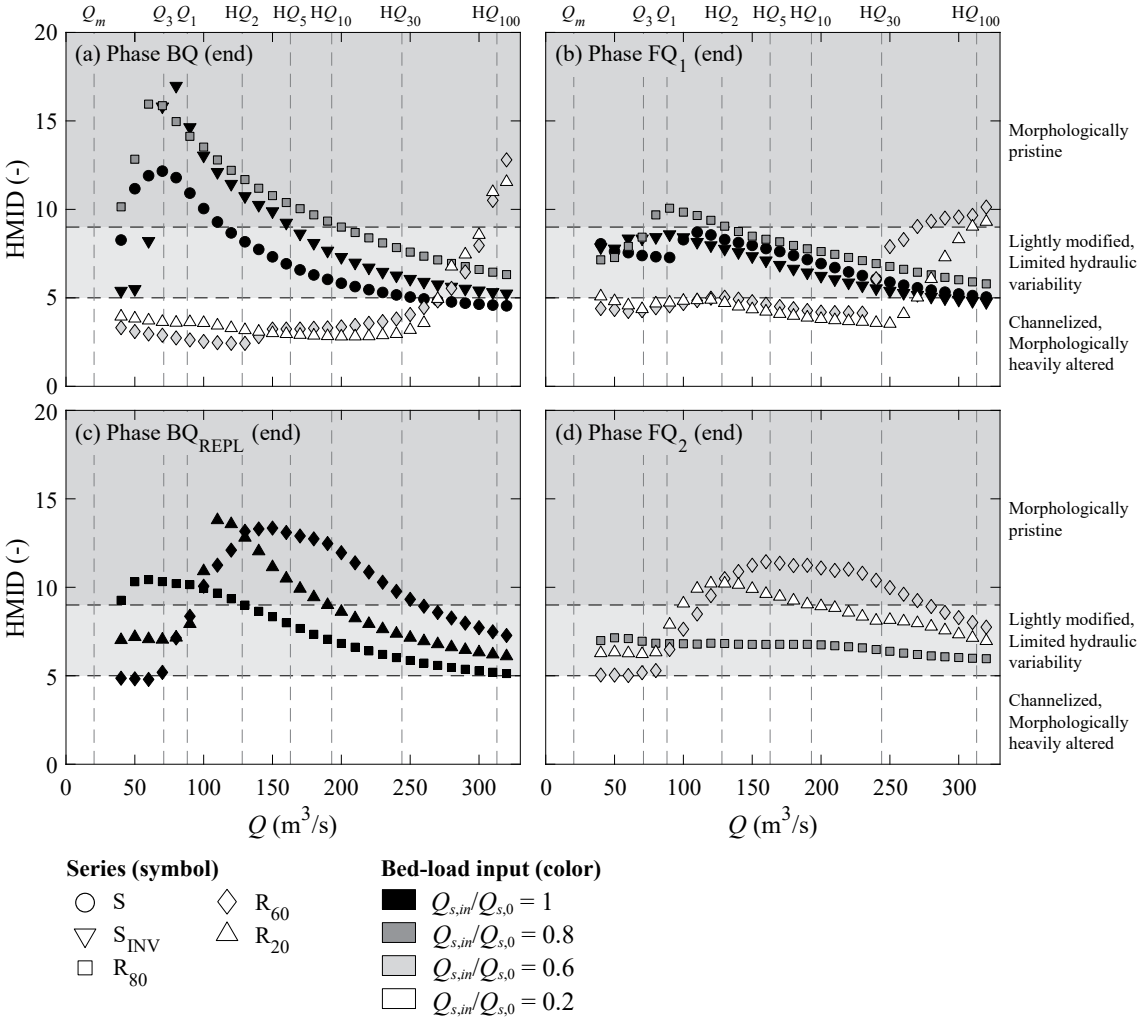

Figure 6.6 Hydro-morphological index of diversity (HMID) for topographies at the end of phases (a) BQ, (b) FQ_1, (c) BQ_{REPL}, and (d) FQ_2 of series without initiation measures and a discharge range of 40 to 320 m^3/s (Q_m = mean annual discharge, Q_x = reached and exceeded for x days per year, HQ_x = flood peak with return period of x years). The HMID classification after Gostner *et al.* (2013) is shown. Note that the classification was originally developed for mean flow conditions.

The HMID values for series $R_{60,FD}$ and $R_{60,IW}$ (Figure 6.7) reflect their respective similarity with the low ($Q_{s,in}/Q_{s,0}$ = 0.6 and 0.2) and high ($Q_{s,in}/Q_{s,0}$ = 1 and 0.8) sediment supply series (cf. Figure 6.6). The maximum and minimum HMID values lie in the same range as for the corresponding series without initiation measures. However, the position of

the maxima is slightly shifted. For the topography at the end of phase BQ of series $R_{60,IW}$, instead of reaching the maximum HMID for discharges < Q_1 (Figure 6.6a), the maximum HMID is reached at HQ_2 (Figure 6.7a). Similarly, the HMID maximum of series $R_{60,IW}$ is shifted to discharges around HQ_{10} (Figure 6.7a) compared to discharges clearly above HQ_{30} for series R_{60} and R_{20} (Figure 6.6a). The differences in HMID were again more pronounced for topographies after phase BQ (Figure 6.7a) as opposed to after phase FQ_1 (Figure 6.7b).

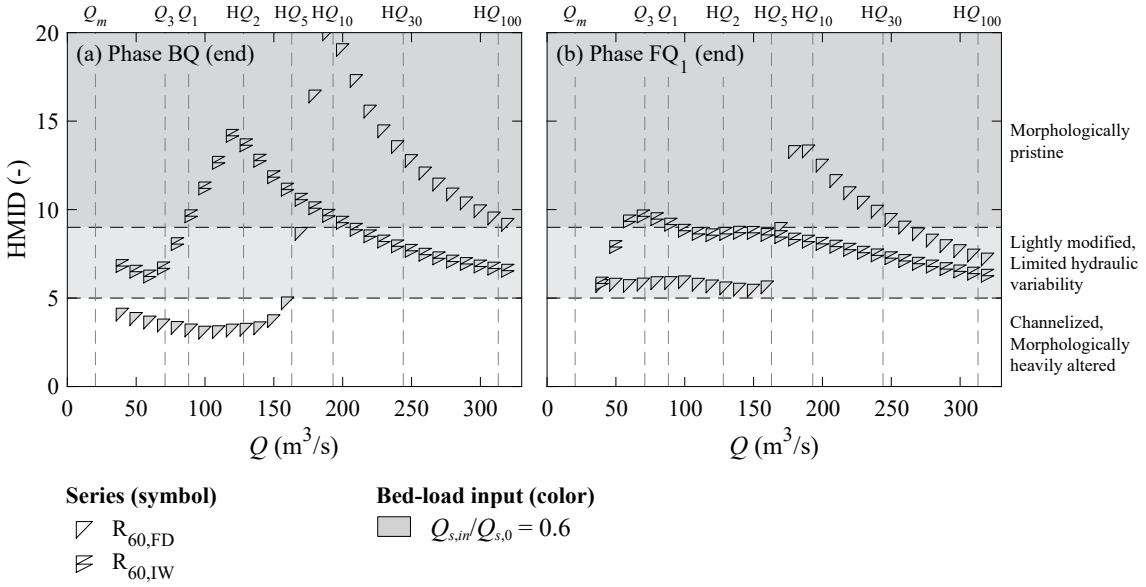

Figure 6.7 Hydro-morphological index of diversity (HMID) for topographies at the end of phases (a) BQ and (b) FQ_1 of series with initiation measures and a discharge range of 40 to 320 m^3/s (Q_m = mean annual discharge, Q_x = reached and exceeded for x days per year, HQ_x = flood peak with return period of x years). The HMID classification after Gostner *et al.* (2013) is shown. Note that the classification was originally developed for mean flow conditions.

6.3 Floodplain inundation

The previous section has established that pronounced differences in hydro-morphological diversity arise from different sediment supply levels and bank erosion initiation measures. Flow depth distributions also show that under high supply conditions (Figures 6.1a-c, 6.2a-c, and 6.3) or successful bank erosion initiation (Figures 6.5c,d), the floodplain is at least partially inundated and thus the wetted area A_{wet} is significantly larger in comparison to low supply conditions (Figures 6.1d,e, 6.2d,e) or unsuccessful bank erosion initiation (Figures 6.5a,b).

To visualize the discharge-dependent nature of floodplain inundation, Figure 6.8 displays the ratio of wetted to total widening area A_{wet}/A_w for discharges of 40 to 320 m^3/s and topographies of experimental series without bank erosion initiation measures. The inundation of the floodplain, visible as sharply increasing A_{wet}/A_w values over a limited discharge range, happens at distinctly different discharges for different sediment supply levels (Figure 6.8). For topographies developed with high sediment supply ($Q_{s,in}/Q_{s,0}$ = 1 and 0.8), the floodplain is fully inundated at discharges around HQ_2, for low sediment supply ($Q_{s,in}/Q_{s,0}$ = 0.6 and 0.2) at discharges above HQ_{100} (Figures 6.8a,b). No significant differences are apparent between the end of phases BQ (Figure 6.8a) and FQ_1 (Figure 6.8b), although the inundation process is slightly more sudden for BQ than for FQ_1 topographies, especially for high sediment supply. An increase in sediment supply aligns the floodplain inundation dynamics of previously low supply widenings with high supply widenings (Figure 6.8c). This alignment is mostly unchanged after the flood hydrograph of phase FQ_2, although the curves are slightly flattened (Figure 6.8d).

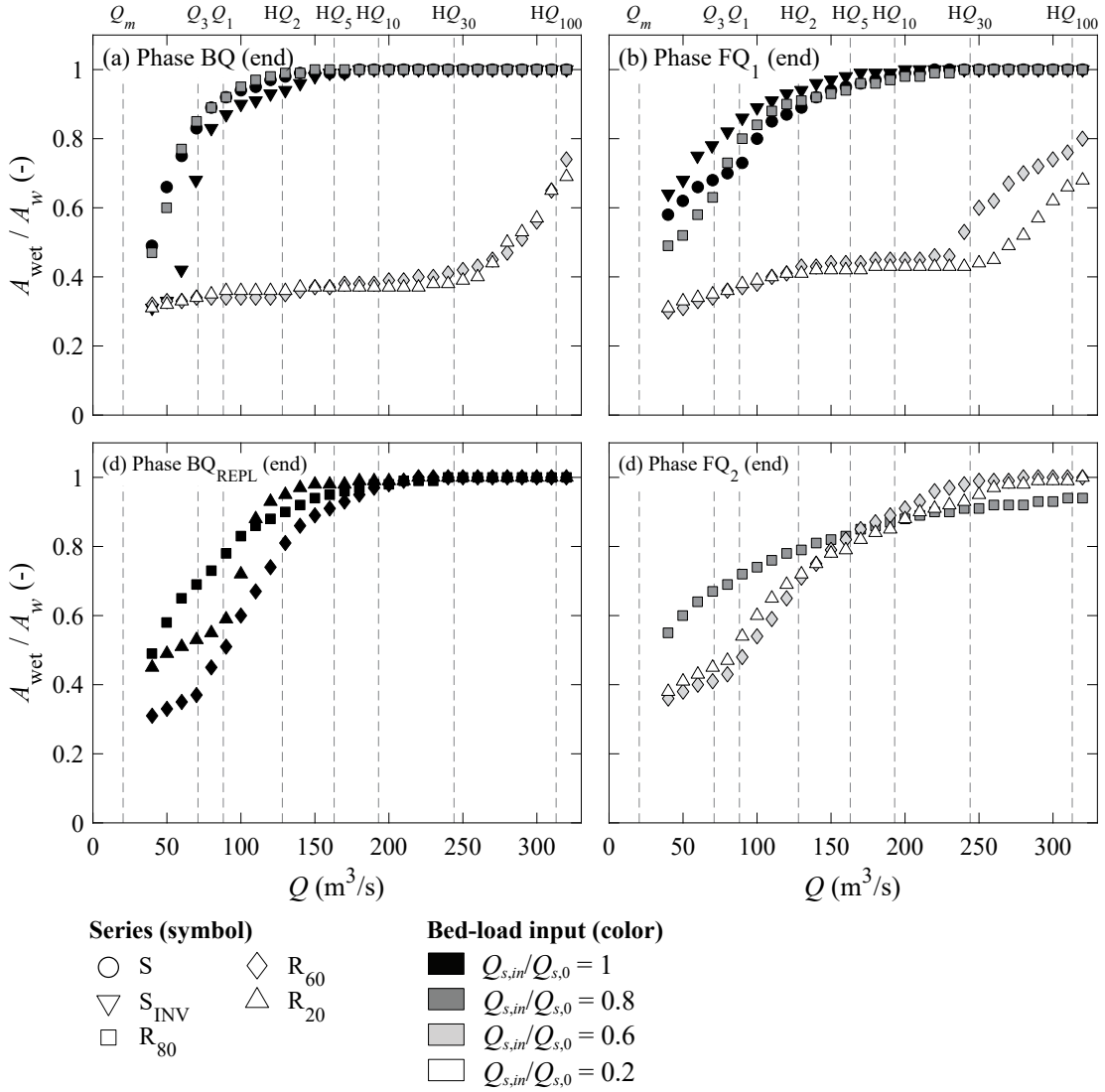

Figure 6.8 The ratio of wetted to total widening area A_{wet}/A_w for topographies at the end of phases (a) BQ, (b) FQ_1, (c) BQ_{REPL}, and (d) FQ_2 of series without initiation measures and a discharge range of 40 to 320 m^3/s (Q_m = mean annual discharge, Q_x = reached and exceeded for x days per year, HQ_x = flood peak with return period of x years).

Figure 6.9 presents the floodplain inundation dynamics for series $R_{60,FD}$ and $R_{60,IW}$ with bank erosion initiation measures. As was the case with HMID values (Figure 6.7), $R_{60,IW}$ is similar to the high supply series with almost complete inundation for discharges around HQ_2, while $R_{60,FD}$ shows an intermediate behaviour with complete inundation between HQ_5 and HQ_{10}.

Because flow depths on the inundated floodplain are shallow (Figures 6.1 to 6.5), A_{wet} is potentially sensitive to the threshold h_{dry} that was set to 0.1 m (see Section 4.4.2). However, a sensitivity analysis with h_{dry} = 0.05 m and 0.15 m showed no significant differences in the inundation process compared to h_{dry} = 0.1 m (Figure 6.10).

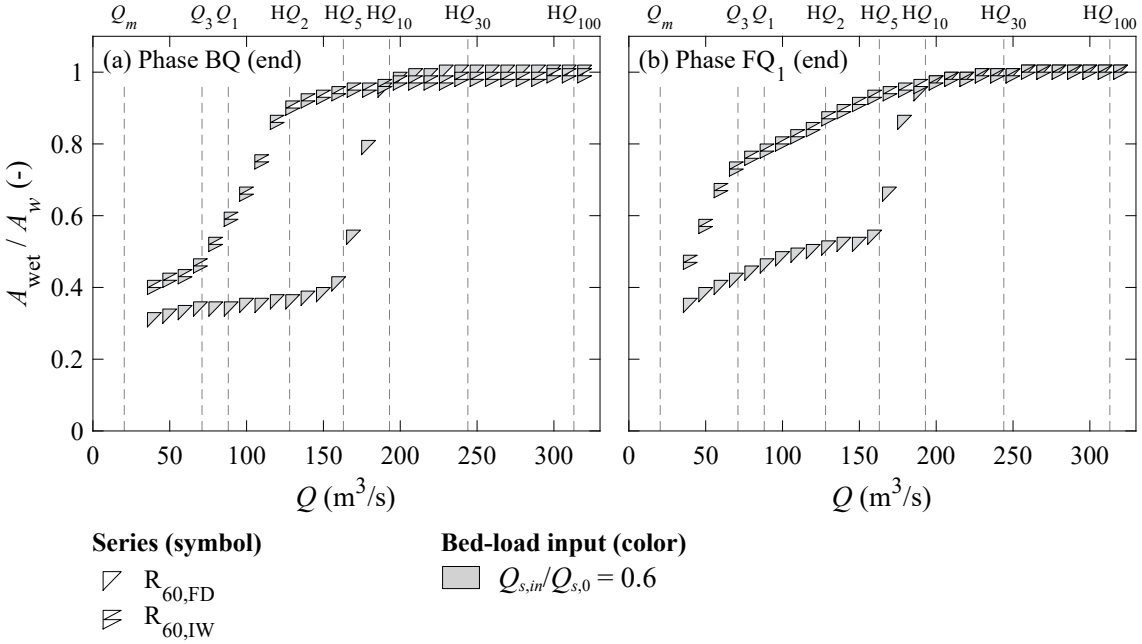

Figure 6.9 The ratio of wetted to total widening area A_{wet}/A_w for topographies at the end of phases (a) BQ and (b) FQ_1 of series with initiation measures and a discharge range of 40 to 320 m^3/s (Q_m = mean annual discharge, Q_x = reached and exceeded for x days per year, HQ_x = flood peak with return period of x years).

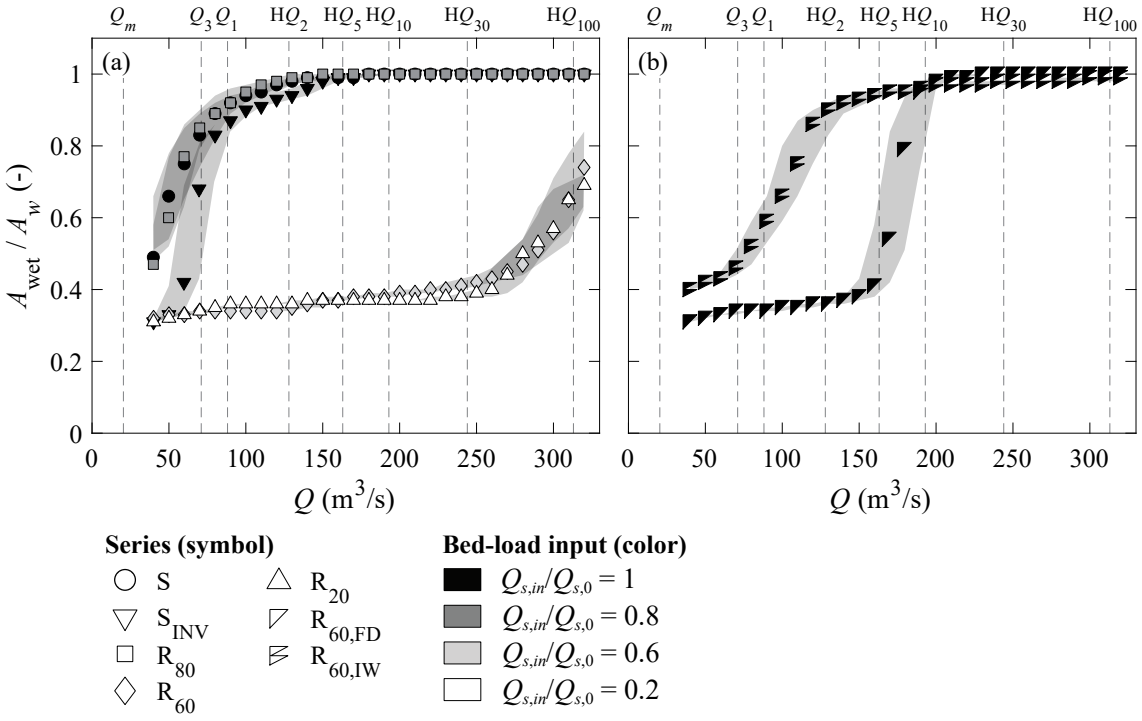

Figure 6.10 Sensitivity analysis of the ratio of wetted to total widening area A_{wet}/A_w for topographies at the end of phase BQ of series (a) without and (b) with bank erosion initiation measures versus the threshold h_{dry}. The shaded bands show the range of A_{wet}/A_w obtained for the variation of h_{dry} to 0.05 and 0.15 m, with the default value being h_{dry} = 0.1 m.

The inundation process is also reflected in the discharge-dependent shoreline length (Figure 6.11). The shoreline length is elevated and variable for the discharge range corresponding to partial floodplain inundation, and close to its minimum level of 2 km/km for lower and higher discharges, i.e., a completely dry or wet floodplain (cf. Figure 6.8). For example, shoreline length is 3 to 7 km/km for discharges below HQ_2 with $Q_{s,in}/Q_{s,0}$ = 1 and 0.8 supply at the end of phase BQ, whereas the minimum level of 2 km/km is maintained for discharges below HQ_{30} with $Q_{s,in}/Q_{s,0}$ = 0.6 and 0.2 supply (Figure 6.11a).

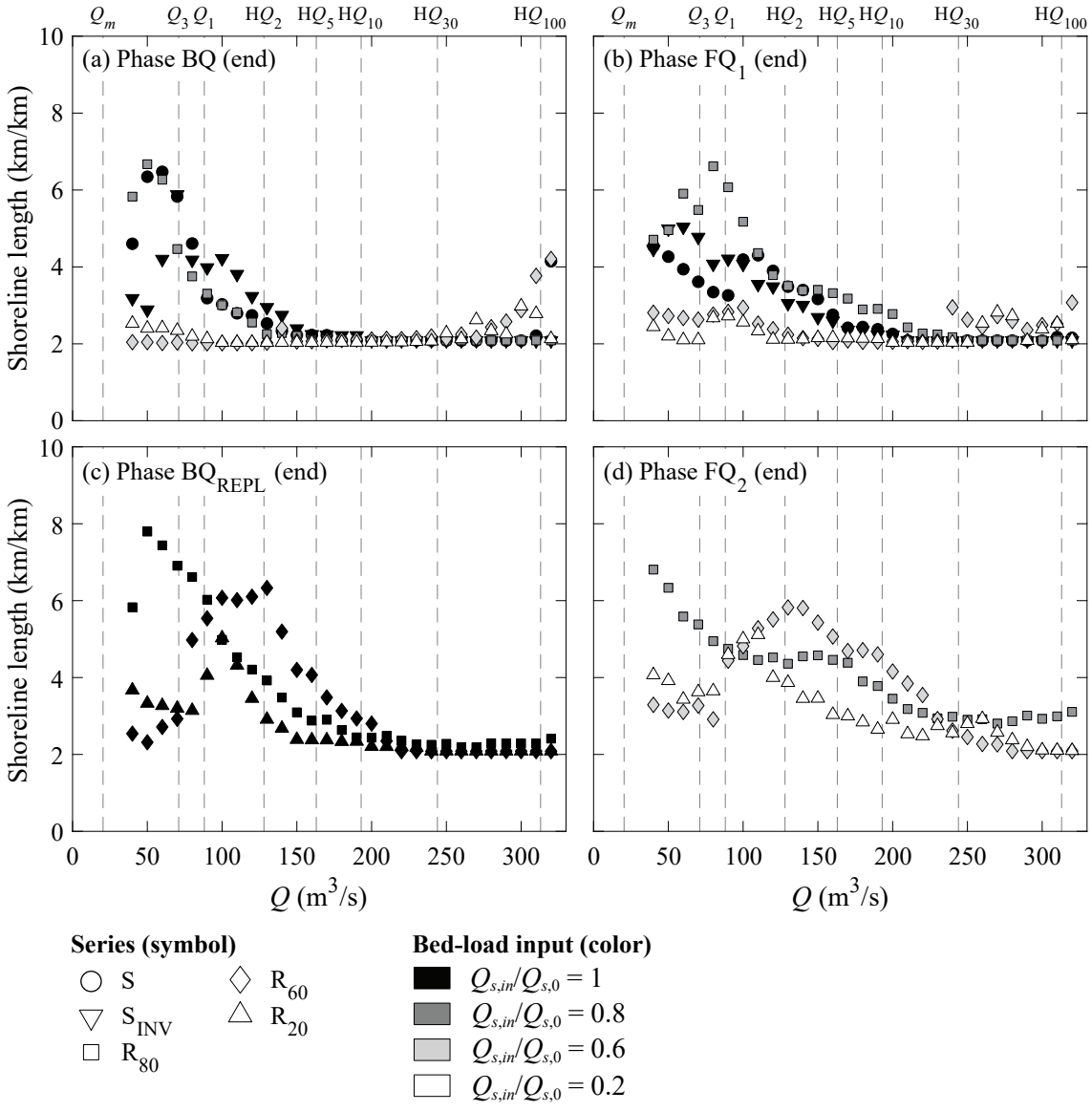

Figure 6.11 Shoreline length for topographies at the end of phases (a) BQ, (b) FQ$_1$, (c) BQ$_{REPL}$, and (d) FQ$_2$ of series without initiation measures and a discharge range of 40 to 320 m^3/s (Q_m = mean annual discharge, Q_x = reached and exceeded for x days per year, HQ_x = flood peak with return period of x years). The minimum value of the shoreline length is 2 km/km.

As for the HMID results (see Section 6.2), the differences between sediment supply levels is slightly less pronounced for topographies after phases FQ_1 to FQ_2 (Figure 6.11b-d) than for topographies after phase BQ (Figure 6.11a). Again, the shoreline length of series $R_{60,IW}$ develops similarly to the high supply series, while $R_{60,FD}$ exhibits the highest shoreline lengths at intermediate discharges of HQ_5 to HQ_{10} (Figure 6.12).

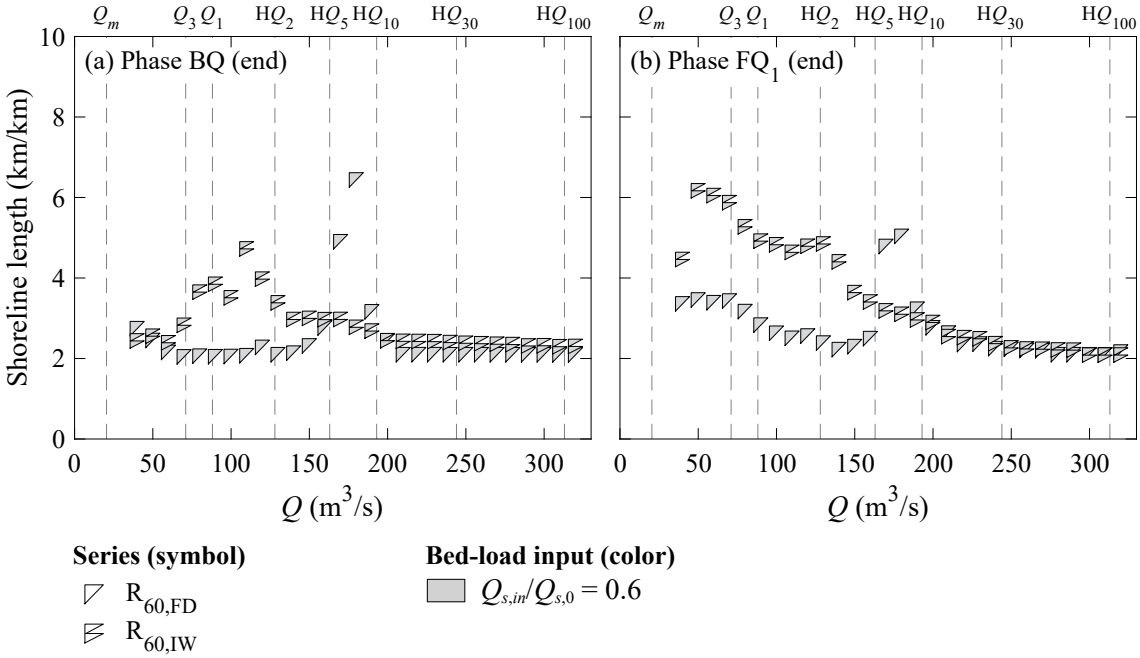

Figure 6.12 Shoreline length for topographies at the end of phases (a) BQ and (b) FQ_1 of series with initiation measures and a discharge range of 40 to 320 m^3/s (Q_m = mean annual discharge, Q_x = reached and exceeded for x days per year, HQ_x = flood peak with return period of x years). The minimum value of the shoreline length is 2 km/km.

6.4 Bed shear stresses

While the hydro-morphological diversity (see Section 6.2) and floodplain inundation dynamics (see Section 6.3) illustrate the extent of the wetted area and the hydraulic conditions likely to be encountered by organisms living in the water column, bed shear stresses provide indications of the conditions close to the river bed. This is in terms of hydraulic stress as experienced by organisms living on the bed surface and in terms of bed-load transport potentially affecting organisms on and below the bed surface. Here, the focus lies on bed-load transport. As elaborated in Section 6.2, the hydraulic conditions fall into two groups corresponding to morphodynamically active and inactive widenings (cf. Section 5.7.3). Bed shear stresses correlate with flow depth and velocity and bed shear stress results are thus only shown for selected topographies (see Figures 6.1 to 6.5 for all flow fields).

Figure 6.13 presents the simulated dimensionless bed shear stresses for the topographies of series without bank erosion initiation measures at the end of phase BQ with discharge Q_B. The dimensionless bed shear stresses were calculated for the median grain diameter D_{50} and classified according to commonly used thresholds for grain mobility. Critical bed shear stresses were assumed to be $\theta_c = 0.03$ for partial transport and $\theta_c = 0.06$ for full transport (Buffington and Montgomery 1997).

For all topographies, an extensive zone potentially experiencing full transport of D_{50} is visible (but see Section 6.5 for actual active bed-load transport zones). Indeed, if (i) A_{wet}/A_w is multiplied with (ii) $A_{\theta>0.06}/A_{\text{wet}}$ to receive the ratio of high bed shear stresses to total widening area $A_{\theta>0.06}/A_w$, similar values between 0.29 and 0.37 result for all topographies shown in Figure 6.13. However, the ratio of high bed shear stress areas to wetted area (ii) $A_{\theta>0.06}/A_{\text{wet}}$ is more relevant in the context of flood refugia because it captures the presence of wetted lower bed shear stress areas ($\theta_{\text{D50}} \leq 0.06$) as well. For $Q_{s,in}/Q_{s,0} = 0.6$ and 0.2, almost the entire wetted perimeter experiences high bed shear stresses, and low bed shear stress zones potentially functioning as refugia are scarce (Figures 6.13d,e). In contrast, extensive zones experiencing low bed shear stresses likely resulting in no or only intermittent transport of D_{50} show up in Figures 6.13a-c. Note how low bed shear stress zones are mostly present on the floodplain, especially along the channel-floodplain margin, and downstream of gravel bars.

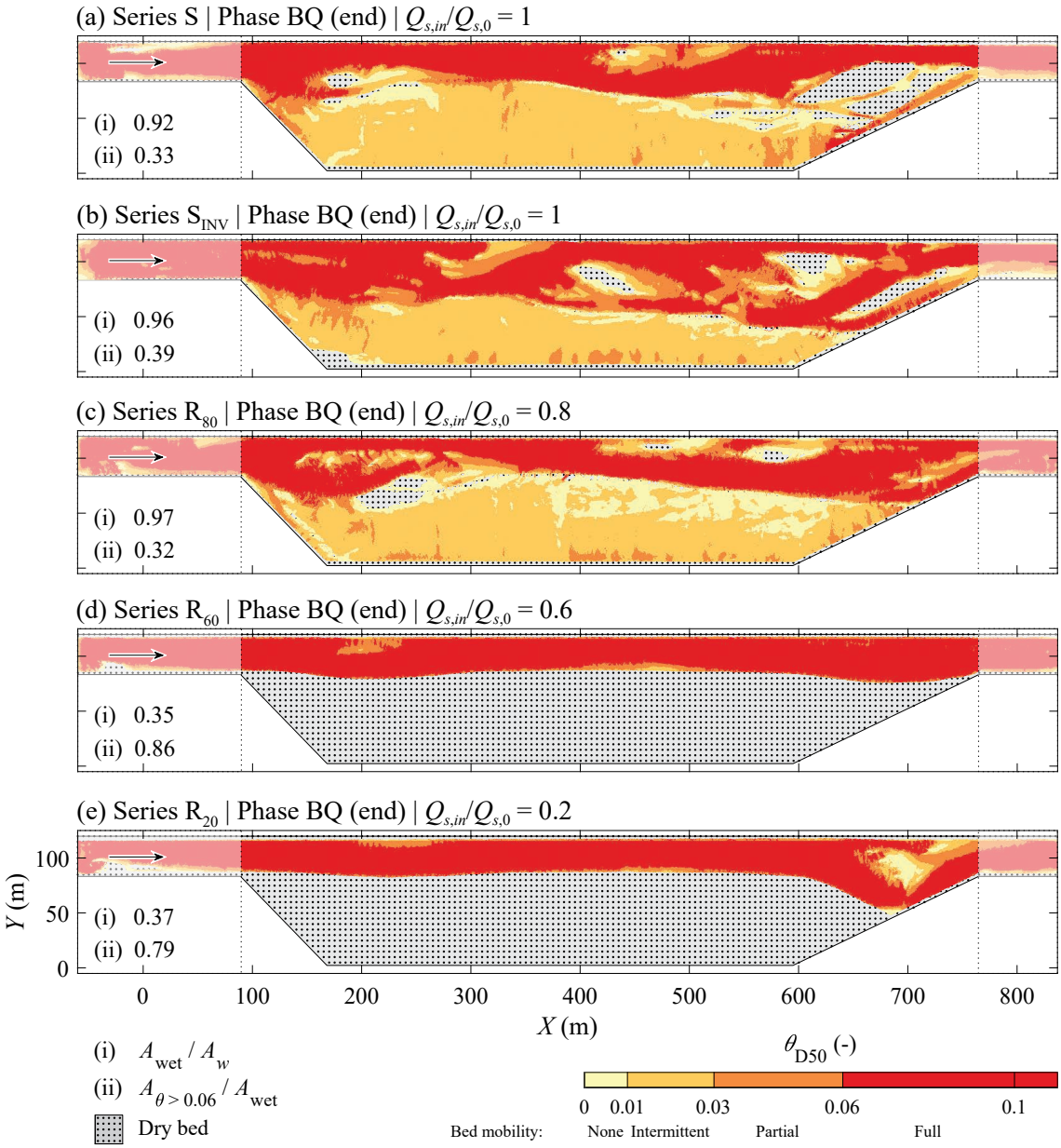

Figure 6.13 Simulated dimensionless bed shear stresses for topographies after phase BQ of series (a) S, (b) S_{INV}, (c) R_{80}, (d) R_{60}, and (e) R_{20} with discharge Q_B. The dimensionless bed shear stress θ_{D50} is calculated for the median grain size D_{50}. The color scale reflects the mobility of D_{50} based on commonly applied bed shear stress thresholds. The proportion of (i) wetted area to total widening area A_{wet}/A_w and (ii) high bed shear stress area to wetted area $A_{\theta>0.06}/A_{wet}$ are reported. The inlet and outlet sections (white overlay) do not contribute to the reported areas.

For the eight characteristic discharges listed in Table 4.4, bed shear stress distributions for topographies of series without initiation measures at the end of phases BQ and FQ_1 are shown in Figures 6.14 and 6.15, respectively. The shape of the gray area illustrates the distribution of bed shear stresses, while the relative size of the gray area represents the extent of the wetted area. For example, bed shear stresses below the critical value for full transport of D_{50} ($< \tau_{c,D50}$) occur for Q_1 in series R_{20} (Figure 6.14e), but they occupy a smaller area (9% of the total widening area) compared to series S (60% of the total widening area; Figure 6.14a). Symbolized by a black bar and a white circle, respectively, are the interquartile range and the median value. For the same example, the bed shear stress distribution is characterized by a higher median value and a lower interquartile range for series R_{20} (Figure 6.14e) compared to series S (Figure 6.14a). The display format used here allows the assessment of changes in bed shear stress distribution with discharge, that is, the susceptibility of the reach to high discharges in terms of bed shear stress intensity.

In the case of topographies resulting from a sediment supply of $Q_{s,in}/Q_{s,0}$ = 1 and 0.8, the median bed shear stress slowly increases over the entire discharge range (Figures 6.14a-c and 6.15a-c). In contrast, the median bed shear stress increases more sharply for the $Q_{s,in}/Q_{s,0}$ = 0.6 and 0.2 scenarios, before it drops for HQ_{100} (Figures 6.14d,e and 6.15d,e). The bed shear stress distribution and relative wetted areas A_{wet}/A_w indicate that the floodplain is inundated at lower discharges for $Q_{s,in}/Q_{s,0}$ = 1 and 0.8 compared to $Q_{s,in}/Q_{s,0}$ = 0.6 and 0.2 (cf. Section 6.3). As was also shown in Figure 6.13, floodplain inundation leads to a high proportion of low bed shear stress areas. Under sediment deficit conditions, only few low bed shear stress areas are available during flood events smaller than HQ_{100}, and the total wetted area remains limited (Figures 6.14d,e and 6.15d,e).

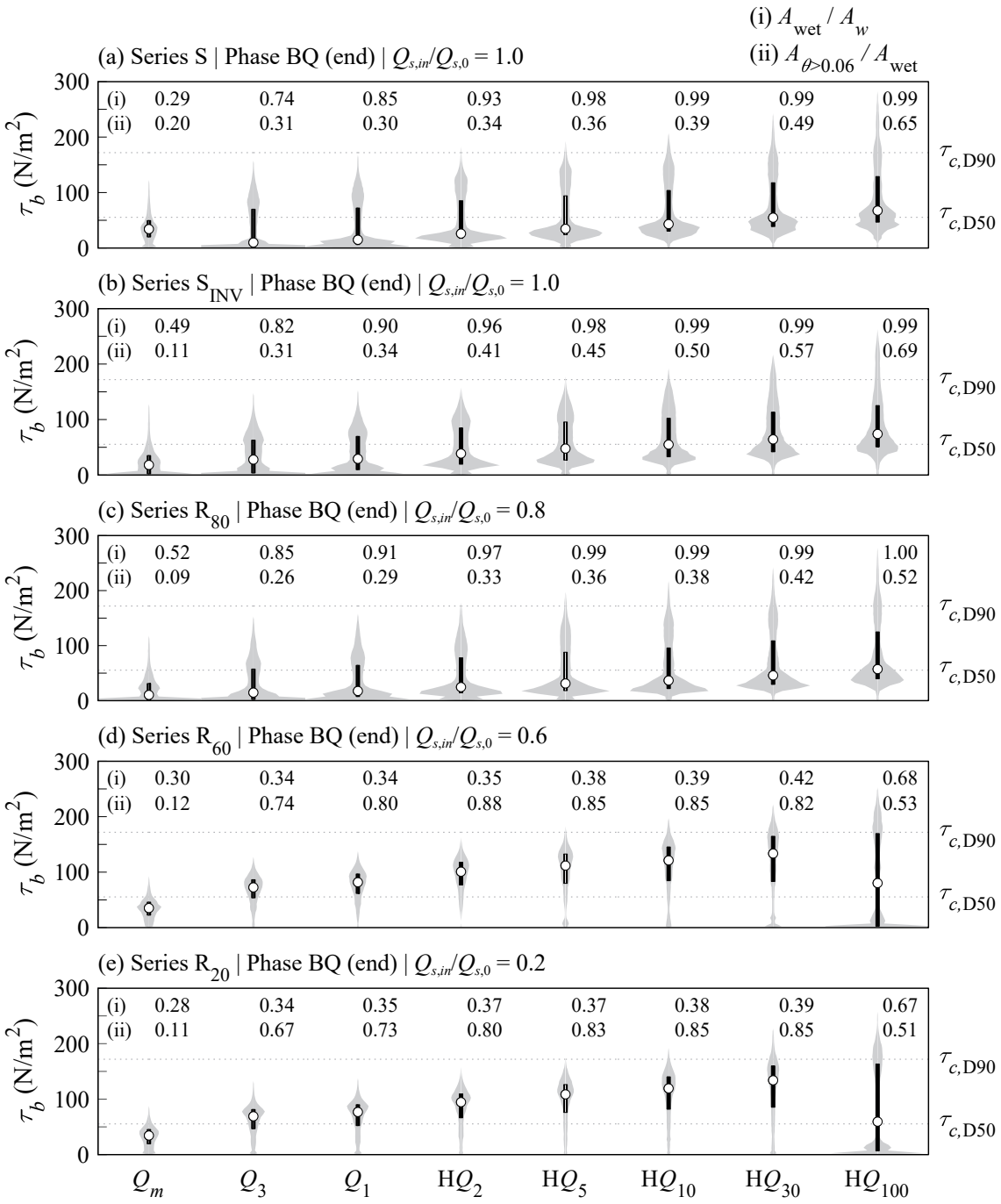

Figure 6.14 Simulated relative frequency of bed shear stresses τ_b in the widening for topographies after phase BQ of series (a) S, (b) S_{INV}, (c) R_{80}, (d) R_{60}, and (e) R_{20} for eight characteristic discharges (Q_m = mean annual discharge, Q_x = reached and exceeded for x days per year, HQ_x = flood peak with return period of x years). The gray area shows the distribution of bed shear stresses with its relative size representing the extent of the wetted area, the black bar the interquartile range, and the white circle the median value. The critical bed shear stress values for the entrainment of D_{50} ($\tau_{c,D50}$) and D_{90} ($\tau_{c,D90}$) grains calculated with a dimensionless critical bed shear stress of θ_c = 0.06 are shown for comparison. The ratio of wetted area to total widening area A_{wet}/A_w (i) and the ratio of high bed shear stress area (calculated for D_{50}) to wetted area $A_{\theta>0.06}/A_{wet}$ (ii) are reported.

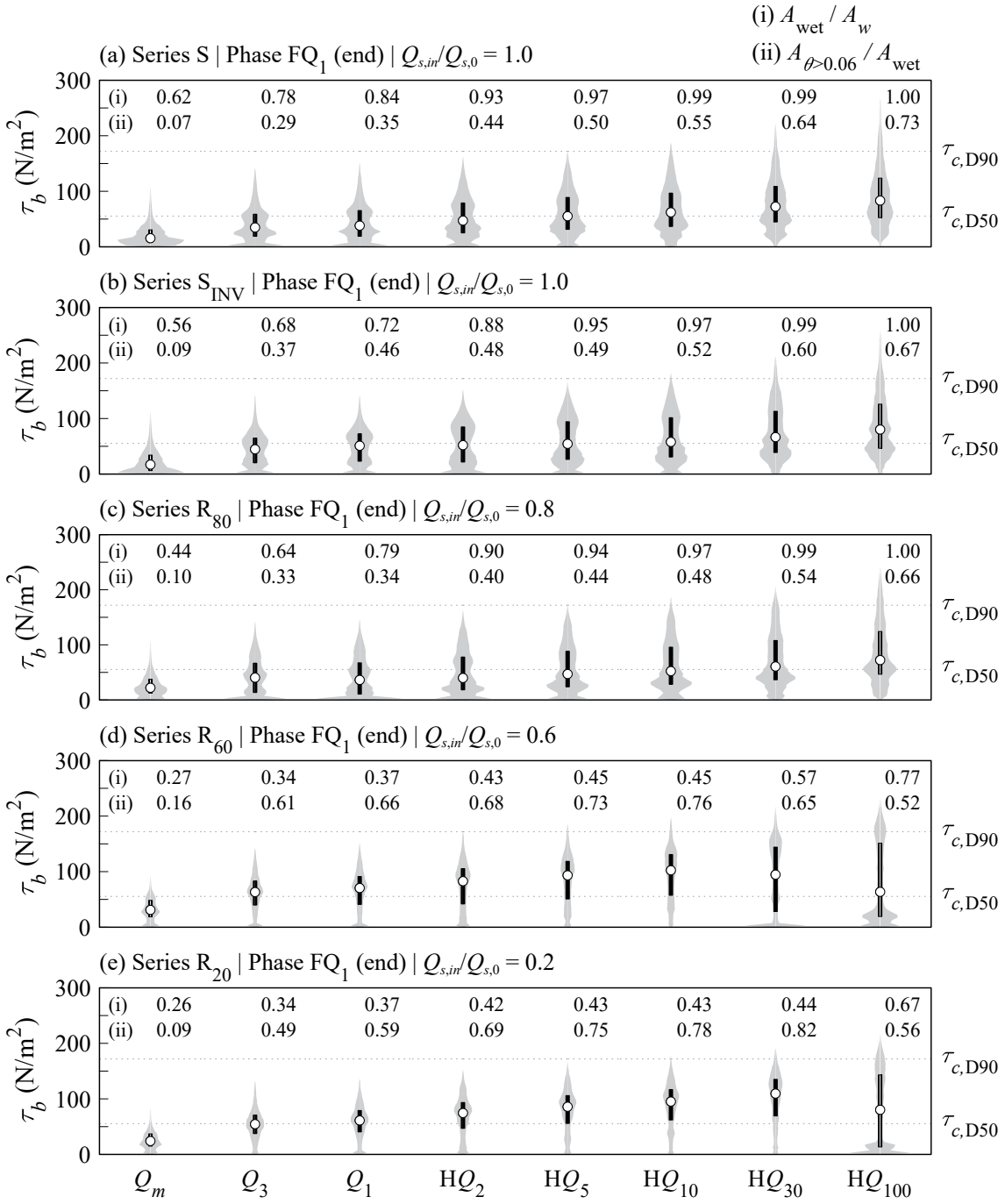

Figure 6.15 Simulated relative frequency of bed shear stresses τ_b in the widening for topographies after phase FQ_1 of series (a) S, (b) S_{INV}, (c) R_{80}, (d) R_{60}, and (e) R_{20} for eight characteristic discharges (Q_m = mean annual discharge, Q_x = reached and exceeded for x days per year, HQ_x = flood peak with return period of x years). The gray area shows the distribution of bed shear stresses with its relative size representing the extent of the wetted area, the black bar the interquartile range, and the white circle the median value. The critical bed shear stress values for the entrainment of D_{50} ($\tau_{c,D50}$) and D_{90} ($\tau_{c,D90}$) grains calculated with a dimensionless critical bed shear stress of θ_c = 0.06 are shown for comparison. The ratio of wetted area to total widening area A_{wet}/A_w (i) and the ratio of high bed shear stress area (calculated for D_{50}) to wetted area $A_{\theta>0.06}/A_{wet}$ (ii) are reported.

To assess the frequency of occurrence of high bed shear stresses and potential sediment relocation, the distributions detailed in Figures 6.14 and 6.15 are summarized for all series and phases as ratios of high bed shear stress areas to initial channel area $A_{\theta>\theta c}/A_{\mathrm{ch},0}$ (Figure 6.16) and wetted area $A_{\theta>\theta c}/A_{\mathrm{wet}}$ (Figure 6.17). The results are shown for critical bed shear stresses indicating partial ($\theta_c = 0.03$) and full ($\theta_c = 0.06$) transport of the median grain size D_{50}.

Morphodynamically active widenings show a steady increase of high bed shear stress areas ($\theta_{\mathrm{D50}} > \theta_c$) relative to the initial channel area with increasing discharge (Figure 6.16). Assuming $\theta_c = 0.03$, almost the entire widening perimeter may experience partial transport of D_{50} during large floods ($\mathrm{H}Q_{30}$, $\mathrm{H}Q_{100}$), whereas full transport can be expected on approximately twice the initial channel area ($\theta_c = 0.06$). In contrast, the proportion of high bed shear stress areas occurring in morphodynamically inactive widenings level off at approximately 130% of the initial channel area for discharges equal to or larger than $\mathrm{H}Q_2$ (Figures 6.16a-d).

The comparison of high bed shear stress areas with the respective wetted area reveals further differences between the two levels of morphodynamic activity (Figure 6.17). For morphodynamically active widenings, the area likely experiencing partial and full transport of D_{50} steadily increases with discharge to 80 to 100% and 40 to 60% of the wetted area, respectively. In morphodynamically inactive widenings, the ratio of high bed shear stress area reaches 70 to 90% of the wetted area except for Q_m and $\mathrm{H}Q_{100}$ (Figures 6.17a-d). These differences reflect contrasting floodplain inundation dynamics with morphodynamically active widenings experiencing floodplain inundation already for relatively small floods, while the floodplain is only inundated for very large floods in the case of morphologically inactive widenings (see Figures 6.8 and 6.9). Note that $\mathrm{R}_{60,\mathrm{FD}}$ shows an intermediate trajectory with floodplain inundation starting from $\mathrm{H}Q_2$ (Figures 6.17a-d).

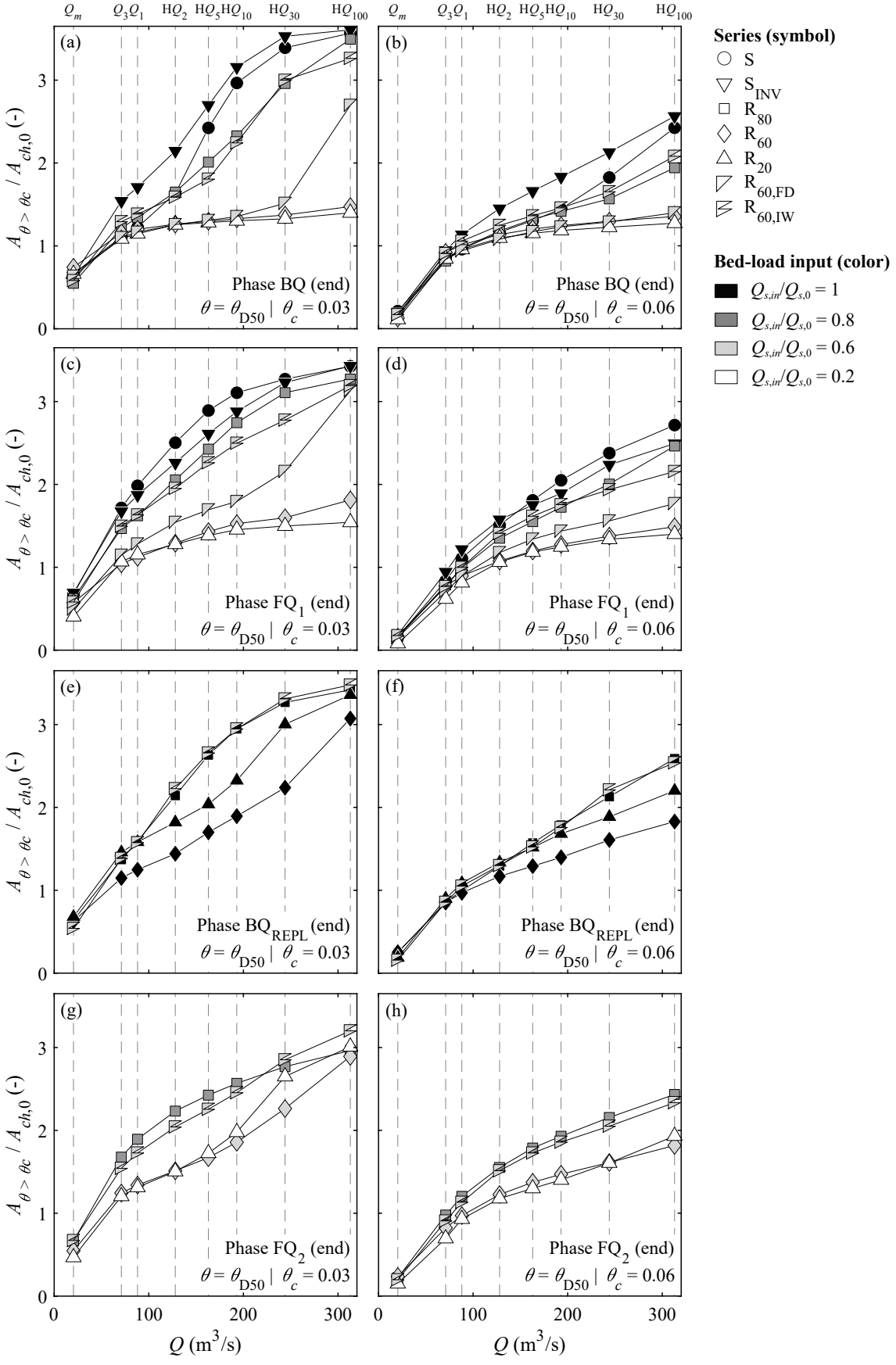

Figure 6.16 Areas with dimensionless bed shear stresses of $\theta_{D50} > 0.03$ and $\theta_{D50} > 0.06$ relative to the initial channel area $A_{ch,0}$ for all series at the end of phases (a,b) BQ, (c,d) FQ_1, (e,f) BQ_{REPL}, and (g,h) FQ_2. The areas were evaluated for a range of discharges with different frequencies of occurrence (Q_m = mean annual discharge, Q_x = reached and exceeded for x days per year, HQ_x = flood peak with return period of x years).

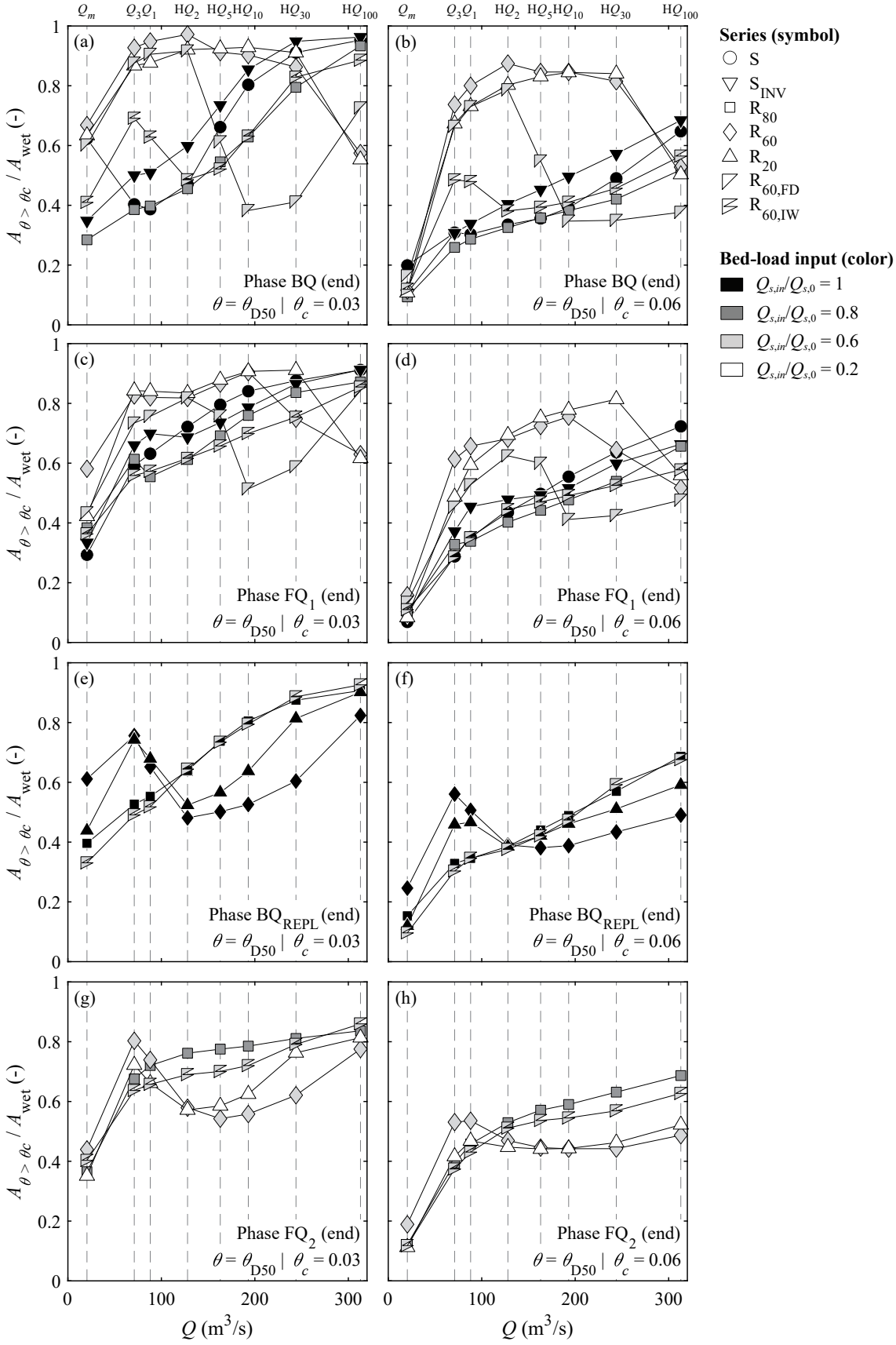

Figure 6.17 Areas with dimensionless bed shear stresses of $\theta_{D50} > 0.03$ and $\theta_{D50} > 0.06$ relative to the wetted area A_{wet} for all series at the end of phases (a,b) BQ, (c,d) FQ_1, (e,f) BQ_{REPL}, and (g,h) FQ_2. The areas were evaluated for a range of discharges with different frequencies of occurrence (Q_m = mean annual discharge, Q_x = reached and exceeded for x days per year, HQ_x = flood peak with return period of x years).

To appraise the implications of discharge-dependent high bed shear stresses zones on aquatic organisms, the results for topographies at the end of phase BQ of series without bank erosion initiation measures (Figures 6.16a and 6.17a) are displayed as plan views in Figure 6.18.

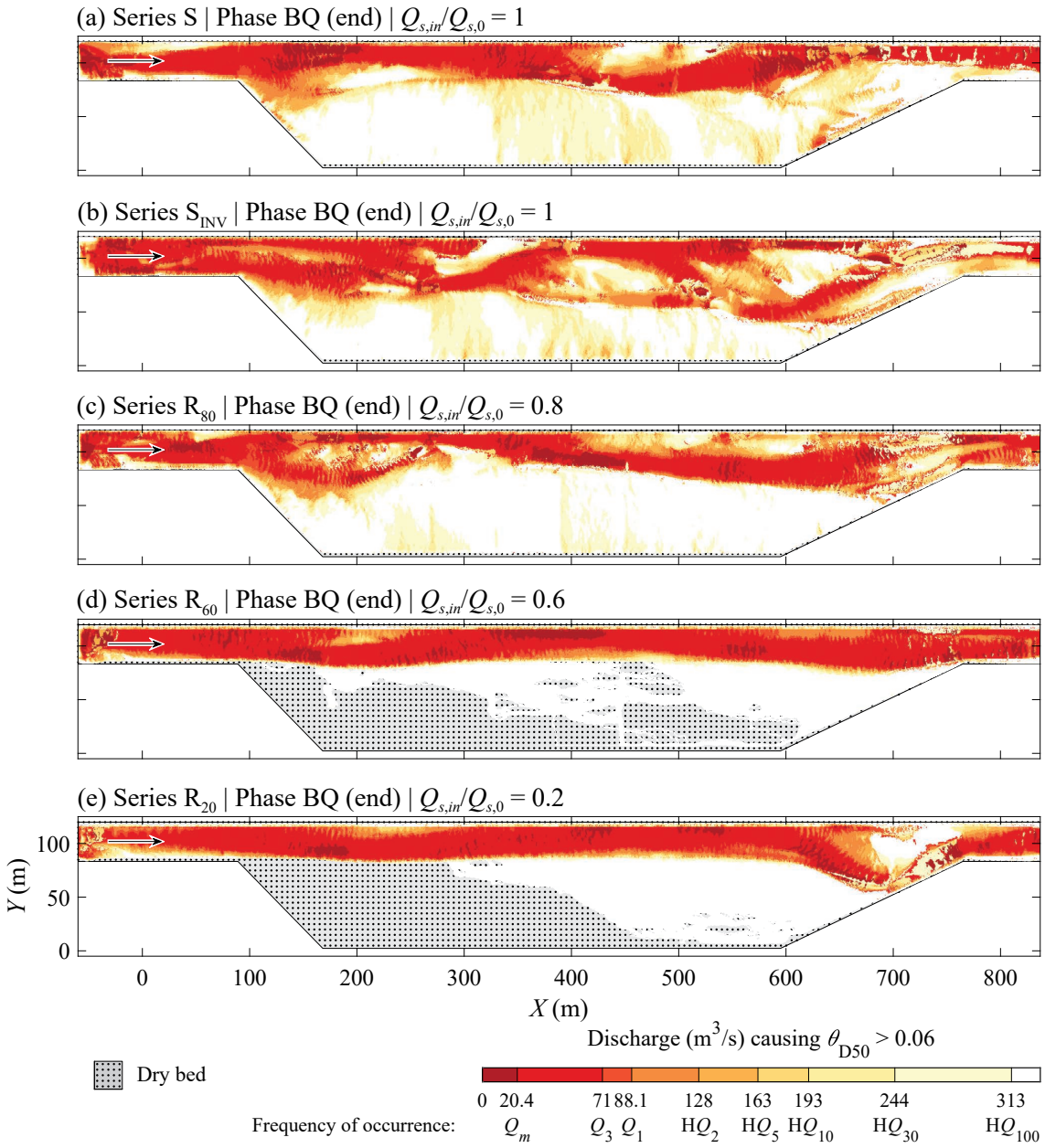

Figure 6.18 Areas with dimensionless bed shear stresses θ_{D50} > 0.06 for topographies after phase BQ of series (a) S, (b) S_{INV}, (c) R_{80}, (d) R_{60}, and (e) R_{20} and a range of discharges with different frequencies of occurrence (Q_m = mean annual discharge, Q_x = reached and exceeded for x days per year, HQ_x = flood peak with return period of x years). The dimensionless bed shear stress θ_{D50} is calculated for the median grain size D_{50}. The dry area corresponds to the zones that do not experience inundation for the highest discharge HQ_{100}.

For topographies developed with $Q_{s,in}/Q_{s,0}$ = 1 and 0.8, many patches show an even gradation of discharges causing high bed shear stresses, for example, areas near the channel-floodplain margins or gravel bars (Figures 6.18a-c). Aquatic organisms capable of active mobility may react to increasing discharges by moving along these gradients to zones with lower bed shear stresses or retreating into the interstitial. Organisms passively transported by drift may be retained in these zones, although bed shear stresses relevant for drift were not explicitly analyzed here (cf. Vanzo *et al.* 2016). In contrast, organisms in reaches developed with $Q_{s,in}/Q_{s,0}$ = 0.6 and 0.2 may not have the opportunity to escape high disturbance intensities or be retained in slow flowing zones. Hydraulic stress uniformly impacts almost the entire reach for discharges as low as the mean annual flow (Figures 6.18d,e).

6.5 Active bed-load transport zone

The combination of laboratory experiments and numerical modeling in this thesis provides an opportunity to compare high bed shear stress areas to areas actually experiencing sediment relocation. Figures 6.19 and 6.20 show the relative frequencies of bed shear stresses for topographies obtained at the end of phase BQ with bed-forming discharge Q_B. The inundated floodplain in morphodynamically active widenings is clearly visible as a pronounced peak with $\tau_b < 50$ N/m^2 in Figures 6.19a-c and 6.20b. Most of the floodplain experiences no elevation change, except for a small part of very low bed shear stress areas (light gray, $\tau_b < 20$ N/m^2). These are most likely floodplain zones where a shallow layer of fines was deposited. In contrast, the limited occurrence of low bed shear stresses ($\tau_b <$ 50 N/m^2) in morphodynamically inactive widenings (Figures 6.19d,e and 6.20a) indicates that the floodplain was not inundated at this discharge.

For $\tau_b > 50$ N/m^2, the bed shear stress distribution is rather similar for morphodynamically active (Figures 6.19a-c and 6.20b) and inactive widenings (Figures 6.19d,e and 6.20a), although the distribution is slightly wider for active widenings. However, the relative frequency of the wetted area experiencing bed elevation change is significantly higher for morphodynamically active widenings indicating that there is an extensive zone of active bed-load transport in the main channel. In contrast, most of the wetted area experienced no bed elevation change in morphodynamically inactive widenings. There may still be bed-load transport across the bed without bed elevation change (no net change). But due to low sediment supply and armoring of the bed surface, the extent of the active

bed-load transport zone is likely very limited (cf. Dietrich *et al.* 1989; Nelson *et al.* 2009).

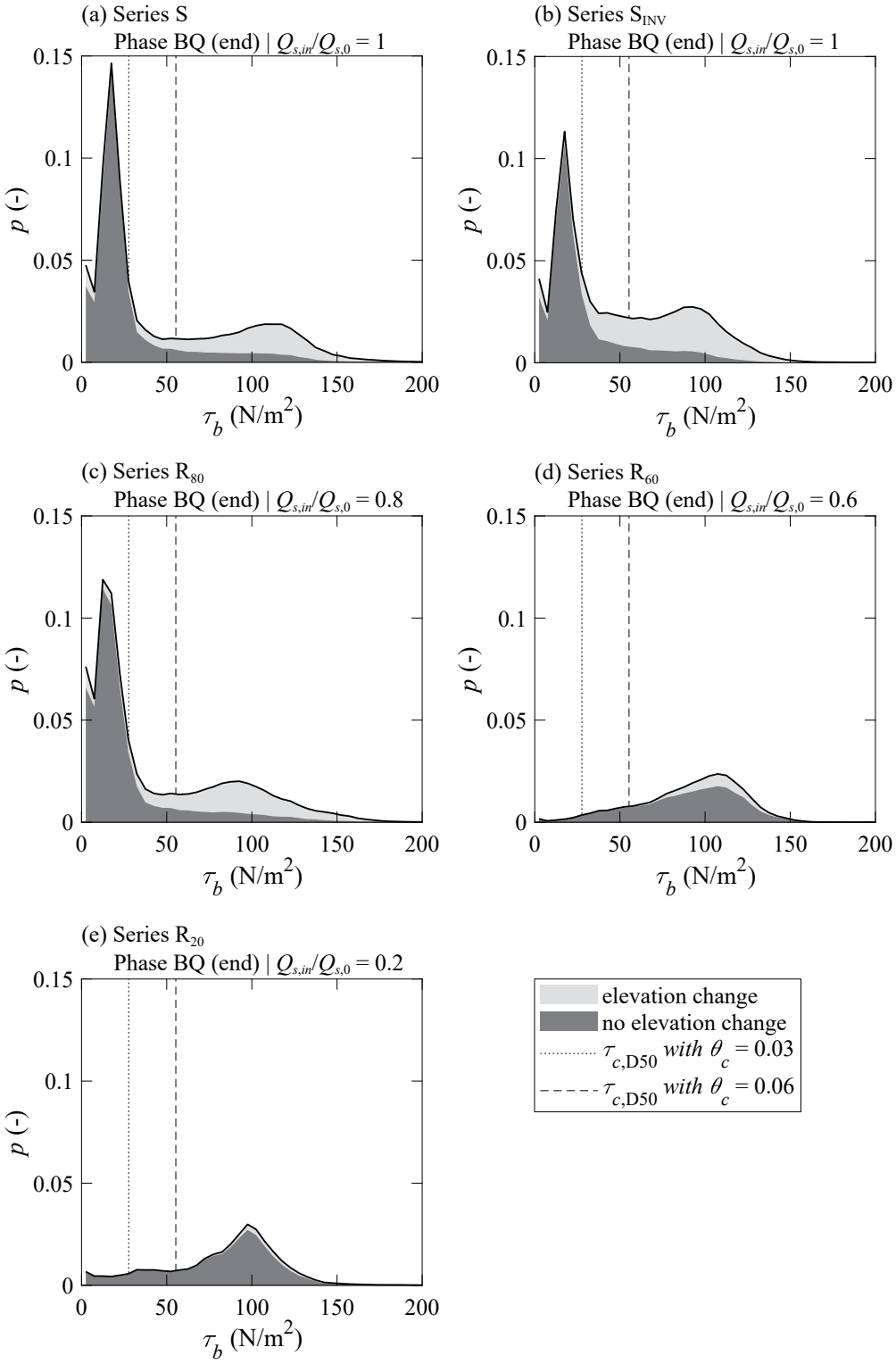

Figure 6.19 Relative frequency p of bed shear stresses and the partition into areas with and without elevation change for topographies after phase BQ of series (a) S, (b) S_{INV}, (c) R_{80}, (d) R_{60}, and (e) R_{20} and the bed-forming discharge Q_B. The area with elevation change (light gray) was determined from the respective last 3-hour experimental interval of phase BQ. Critical bed shear stresses for partial (θ_c = 0.03) and full (θ_c = 0.06) transport are displayed for comparison.

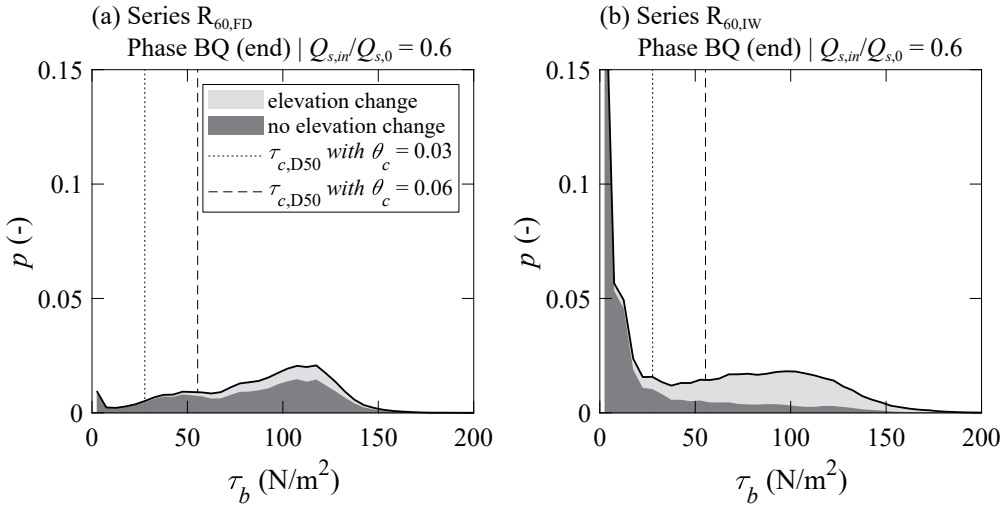

Figure 6.20 Relative frequency p of bed shear stresses and the partition into areas with and without elevation change for topographies after phase BQ of series (a) $R_{60,FD}$ and (b) $R_{60,IW}$ and the bed-forming discharge Q_B. The area with elevation change (light gray) was determined from the respective last 3-hour experimental interval of phase BQ. Critical bed shear stresses for partial (θ_c = 0.03) and full (θ_c = 0.06) transport are displayed for comparison.

Figures 6.19 and 6.20 also provide evidence as to whether the thresholds $\theta_c > 0.03$ and $\theta_c > 0.06$ applied to the median grain diameter D_{50} used here to assess the aggregated area of potential sediment relocation are appropriate. For morphodynamically active conditions, these thresholds seem to be applicable. For $\theta_c > 0.06$, most areas have experienced elevation change while for $\theta_c \leq 0.03$, areas without elevation change are dominant (e.g., Figure 6.19a). For $0.03 \leq \theta_c < 0.06$, the proportions are approximately balanced. It is recognized that these are not sharp thresholds, however. Deviations may arise due to the fact that integrated bed elevation changes of a 3-hour interval are compared to the bed shear stress distribution at the end of said interval. Further reasons could be differential initiation of transport for variable grain sizes or sorting processes. For morphodynamically inactive conditions, these thresholds fail to predict elevation change (e.g., Figure 6.19e). Strong sediment sorting and channel stability presumably led to bed-load being transported across the armored bed surface without causing extensive scour and fill. Overall, it can be concluded that the application of the bed shear stress thresholds $\theta_{c,D50} > 0.03$ and $\theta_{c,D50} > 0.06$ to identify areas of likely sediment relocation is only reasonable given that no significant armoring occurs (cf. Parker and Klingeman 1982).

6.6 Discussion

6.6.1 Interaction of sediment supply and hydro-morphological variability

The maximum shoreline lengths observed here are in the range of 5 to 9 km/km for morphodynamically active widenings and discharges < HQ_{30}. For inactive widenings and discharges > HQ_{30}, shoreline lengths of 3 to 5 km/km are reached. These values correspond to the lower end of the 5 to 15 km/km range reported for a constrained but not channelized reach of the Danube River in Austria (Tockner and Stanford 2002). In contrast, a natural river, such as the Tagliamento River in Italy, reaches shoreline lengths of 25 km/km (Tockner and Stanford 2002). While the shoreline length of the Danube River displays high dependence on discharge similar to this study, the Tagliamento River maintains consistently high shoreline lengths with the exception of very low and very high discharges (van der Nat *et al.* 2002).

The finding that shoreline length tends to decrease with reduced sediment supply is supported by field investigations. Bianchi (2018) found a significant negative linear relation between bed-load deficit and shoreline length for selected river reaches in Switzerland, although the data set was limited. Assuming that higher shoreline lengths result in more potential refuge areas in marginal zones (e.g., Rempel *et al.* 1999), morphodynamically active widenings thus show a higher refuge potential compared to inactive reaches. However, due to the limited length and width of the widenings described here, the attainable shoreline length remains limited.

While the general relation between shoreline length and sediment supply seems reasonable, absolute shoreline length values must be treated with caution. Although the hydrodynamic model has a high spatial resolution, it cannot represent the full complexity of marginal zones with crevices, indentations, etc., and absolute values of shoreline length generally depend on the observation scale. Furthermore, the floodplain in the laboratory experiment was unrealistically flat. This causes the shoreline length to drop to its minimum value of 2 km/km once the floodplain is completely inundated (e.g., Figure 6.11a). Although the shoreline length will likely decrease for high discharges, it will not drop to the minimum value in the case of a more structured floodplain, for example with patches of vegetation (Tockner and Stanford 2002).

The HMID values follow a similar trend as the shoreline length, with larger values

and thus higher hydro-morphological diversity in morphodynamically active compared to inactive widenings for all but the largest discharges. These differences are related to contrasting floodplain inundation dynamics, as discussed above. However, at discharges between HQ_{30} and HQ_{100}, similar HMID values of 4 to 7 result for all series at the end of phases BQ and FQ$_1$ (Figures 6.6a,b; similarly for HQ_5 in Figures 6.7a,b), implying that their respective flow fields are equally diverse. However, Figures 6.1 and 6.2 show that for high sediment supply and a discharge of H$Q_{1.5}$, the flow depth distribution consists of smaller patches and exhibits a more complex configuration than for low sediment supply. Comparable differences can be expected for higher discharges. The reason for equal HMID values despite apparent differences in the respective flow fields is that the HMID is a statistical bulk value to quantify hydro-morphological diversity. It does not, however, express the spatial arrangement of hydraulic patches (Gostner *et al.* 2013) which makes it suitable to measure the variability, but not the complexity of a hydraulic habitat mosaic.

For discharges up to HQ_{30}, both the shoreline length and HMID values are higher in morphodynamically active compared to inactive widenings. For discharges > HQ_{30} the relationship is inverse. Assuming that more refugia are potentially available in morphologically and hydraulically complex reaches (e.g., Pearsons *et al.* 1992; Gjerløv *et al.* 2003), both metrics imply higher refugia availability in morphodynamically active widenings up to HQ_{30}. This dynamic is closely linked to lateral channel-floodplain connectivity. Under high sediment supply conditions, stronger bed aggradation in the widened main channel led to reduced elevation differences between the main channel and the floodplain and, therefore, the floodplain was inundated at lower discharges (e.g., Hohensinner *et al.* 2004). Conversely, the incision of the main channel relative to the floodplain under low supply conditions prevented floodplain inundation except for high discharges (e.g., Surian and Rinaldi 2003).

However, increased lateral connectivity is only one of many factors that likely leads to a higher refugia availability in morphodynamically active widenings. Low bed shear stress zones that persist during high discharges provide potentially valuable refugia (e.g., Lancaster and Hildrew 1993; Winterbottom *et al.* 1997). In the widenings studied here, the discharge-dependent bed shear stress conditions in morphodynamically active widenings correspond to a type I shift as described by Lancaster and Hildrew (1993) (see Section 3.7.3) which is mainly associated with the inundation of the floodplain activating an ex-

tensive area of shallow flow depths, slow flow velocities, and low bed shear stress zones. Conversely, the conditions in morphodynamically inactive widenings resemble a type II shift with a narrow distribution of ever increasing bed shear stresses except for HQ_{100} when the floodplain is inundated and the distribution also resembles type I. The stronger increase of bed shear stresses in morphodynamically inactive widenings can be explained by their topographic characteristics (see Chapter 5). The homogeneous main channel that was preserved under low sediment supply conditions effectively concentrates the flow and leads to higher bed shear stresses with a more narrow distribution in comparison to high sediment supply conditions (Negishi *et al.* 2002; Czuba *et al.* 2018). Some benthic organisms may be able to retreat to the subsurface zone, but the refuge function of the hyporheic zone is highly variable (Dole-Olivier *et al.* 1997; Stubbington 2012).

Hydro-morphological diversity, bed shear stress distributions, and floodplain inundation have been shown to be highly interdependent. All metrics are discharge-dependent, but changes are more gradual in morphodynamically active compared to inactive widenings and thus more likely to provide organisms a chance to react to increasing disturbance intensity. In morphodynamically inactive widenings, disturbance intensity uniformly increases and habitats likely acting as flood refugia are only made accessible for the very large floods. Aggregating these findings, it can be concluded that the hydro-morphological conditions developed in morphodynamically inactive widenings are less likely to provide suitable flood refugia.

6.6.2 The floodplain as a refuge

The results shown in Figures 6.19 and 6.20 can be used to discuss the refuge function of the floodplain with special emphasis on flood dynamics. Under morphodynamically active conditions, the floodplain was inundated at comparably low discharges (Q_3 to HQ_2), suggesting that its shallow and slow flowing zones are readily accessible as refuge. But does the floodplain really assume refuge function? Schwartz and Herricks (2005) reported fish moving into the floodplain during high discharges and the same has been observed for macroinvertebrates (e.g., Negishi *et al.* 2002). However, the organisms must also be able to successfully return to the main channel once the flood receeds. A field study on macroinvertebrate refugia in a New Zealand stream investigated the refuge function of the floodplain by differentiating between the floodplain acting as a temporary shelter versus a permanent refuge (Matthaei and Townsend 2000). According to their study, the con-

ditions in the main channel during the falling limb of the hydrograph, that is, when the flow retreats from the floodplain and organisms return to the main channel, are decisive. Stranding on the drying floodplain does not seem to be a significant risk to macroinvertebrates (Matthaei and Townsend 2000) or fish (Mannes *et al.* 2008). However, if hydraulic conditions in the main channel remain unfavourable when organisms return, that is, if high bed shear stresses and active bed-load transport prevail, the temporary shelter on the floodplain does not offer any advantage regarding the persistence of organisms.

From the floodplain inundation dynamics (see Section 6.3), it was determined that the flow retreats from the floodplain for discharges < HQ_2 in morphodynamically active widenings, which corresponds to median bed shear stresses of 24 to 52 N/m^2 being present in the main channel (see Section 6.4). In contrast, the water almost entirely retreats from the floodplain around HQ_{30} in morphodynamically inactive widenings, with median bed shear stresses of 95 to 135 N/m^2 in the channel, thus presenting a higher risk for displacement. Note that a two-dimensional hydrodynamic model cannot accurately represent the detailed near-bed flow field (Rice *et al.* 2007) and shear forces at the scale of different organisms (Lancaster and Hildrew 1993), but rather allows the comparison of the relative magnitudes of hydraulic forces.

Another process to consider when evaluating floodplain refugia availability is bed-load transport activity in the main channel upon floodplain drying (Matthaei and Townsend 2000). In morphodynamically active widenings, the active bed-load transport zone determined from the laboratory experiments at Q_B is more extensive than in inactive widenings (e.g., Dietrich *et al.* 1989; Lisle *et al.* 1993; Nelson *et al.* 2009). Consequently, organisms returning from the floodplain to the main channel in morphodynamically active widenings are possibly subjected to destructive bed-load transport (e.g., Matthaei and Townsend 2000; Effenberger *et al.* 2006). However, even at Q_B, a significant portion of low bed shear stress areas without bed elevation change is present in the channel (Figures 6.19d,e and 6.20a). Considering that the floodplain only completely dries up for discharges close to Q_m and bed-load transport activity will have decreased further, one can therefore assume that in morphodynamically active widenings, organisms retreating from the floodplain will find plenty of potentially suitable habitat patches in the main channel.

6.6.3 Refugia availability versus use

The results presented in this chapter illustrate that morphodynamically active widenings have a higher refuge potential compared to inactive widenings. However, the availability of refugia does not necessarily imply positive effects on the biota (cf. Palmer *et al.* 2010). The use of refugia by aquatic organisms is dependent on a variety of factors that this study does not investigate. Organism characteristics such as their mobility (e.g., Williams and Hynes 1976; Rice *et al.* 2007) and their body size versus the spatial dimensions of the refuge (e.g., Lancaster 2000; Schwartz and Herricks 2005; Mathers *et al.* 2019) play an important role. Organisms seek out different refugia associated with varying suitability under differing discharge regimes. Sculpins, for example, are especially susceptible to scouring events as they hide in the interstitial pore spaces (Swanson *et al.* 1998). This refuge may therefore be suitable below a critical discharge, above which it is destroyed instantaneously.

The higher the flood severity, the more valuable large-scale refugia such as tributaries and floodplains may become (Sedell *et al.* 1990). The spatial configuration and hierarchy of refugia was not considered in this thesis, but may also have important implications for their use (e.g., Sedell *et al.* 1990; Lancaster and Belyea 1997). For example, the proximity and accessibility of a refuge to the residential habitat of an organism is crucial with regard to its energy expenditure (e.g., Weber *et al.* 2013; Sueyoshi *et al.* 2014). In the setting studied here, this means that possibly only the marginal floodplain areas close to the main channel may be used as a refuge and not the entire floodplain. This effect was observed by Matthaei and Townsend (2000) where floodplain areas close to the main channel were more likely to serve as a refuge compared to a backwater channel further away.

6.7 Synthesis

Figure 6.21 summarizes the findings of this chapter in the form of simplified relations between parameters relevant for the provision of potential flood refugia and discharge for morphodynamically active and inactive river widenings, respectively. The lines show the general relation and shaded regions represent approximate ranges of uncertainty.

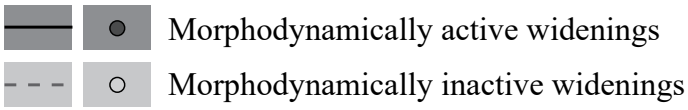

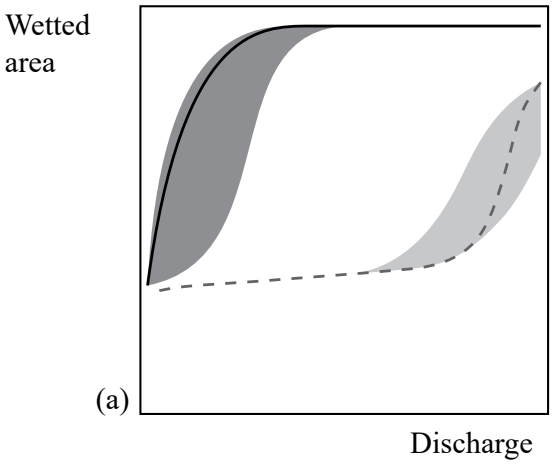

- The floodplain is inundated for relatively low discharges in morphodynamically active widenings.
- In morphodynamically inactive widenings, the floodplain is disconnected from the main channel for all but the highest discharges.

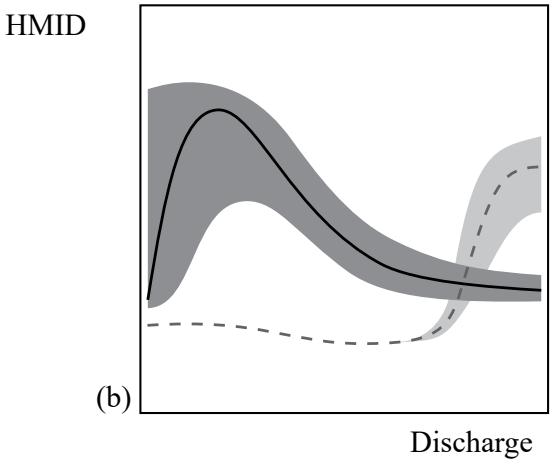

- Higher HMID values occur in morphodynamically active widenings, especially for low to medium discharges.
- HMID values are low in morphologically inactive widenings except for high discharges (delayed floodplain activation).

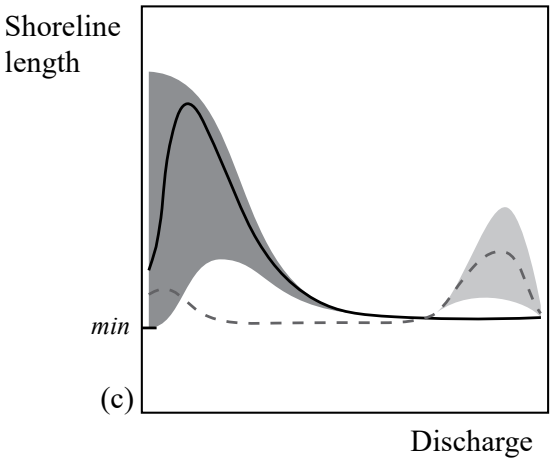

- Shoreline lengths are elevated for low to medium discharges in morphodynamically active widenings.
- Shoreline lengths close to the minimum value are maintained for all but the lowest and highest discharges in morphodynamically inactive widenings (delayed floodplain activation).

Figure 6.21 (a) Wetted area, (b) hydro-morphological index of diversity (HMID), and (c) shoreline length as a function of discharge. The theoretical minimum shoreline length is 2 km/km.

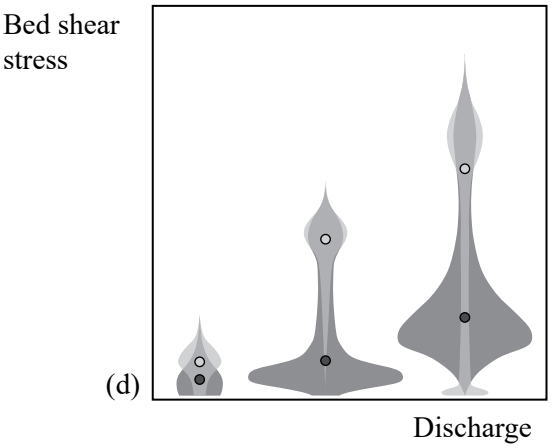

- The median bed shear stress increases less strongly with discharge in morphodynamically active compared to inactive widenings.
- The relative proportion and absolute extent of low bed shear stresses is greater in morphodynamically active compared to inactive widenings.

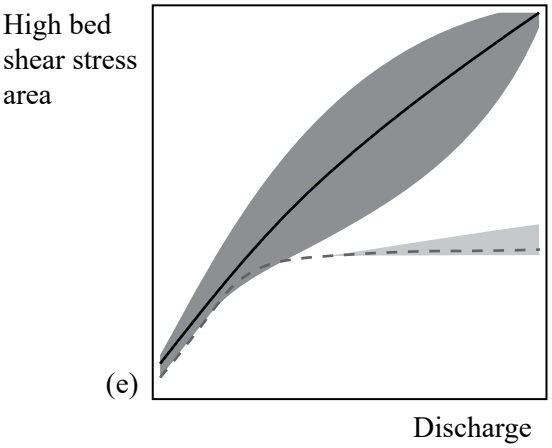

- High bed shear stress areas gradually expand with discharge in morphodynamically active widenings.
- In morphodynamically inactive widenings, high bed shear stress areas level off due to channel-floodplain disconnection.

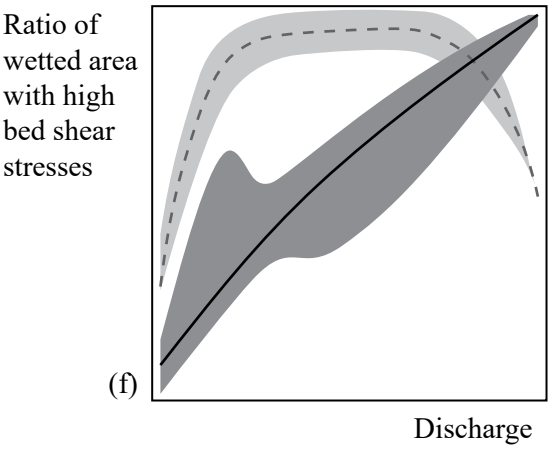

- The fraction of wetted area experiencing high bed shear stresses gradually increases with discharge in morphodynamically active widenings.
- For all but the lowest and highest discharges, almost the entire wetted area is affected by high bed shear stresses in morphodynamically inactive widenings.

Figure 6.21 (continued) (d) Bed shear stress distribution with median value (circles), (e) high bed shear stress area, and (f) ratio of wetted area experiencing high bed shear stresses and potentially bed-load transport as a function of discharge.

Based on the relations between these metrics and refugia function that were established in this chapter, it can be concluded that the availability of potential flood refugia is higher in morphodynamically active compared to inactive river widenings. The difference is especially pronounced for low to medium flood discharges but may be attenuated for very large floods. Incidentally, it also follows that the conditions in channelized river reaches are unfavorable with regard to refugia availability and thus the resistance and resilience of aquatic communities.

7 Management implications

While the experiments presented in this thesis illustrate that the goal of reactivating morphodynamic processes and increasing habitat heterogeneity (Rohde *et al.* 2005; Weber *et al.* 2009) may be attained on a reach scale given sediment supply is more or less balanced with flow competence, the findings also highlight the need to consider further management aspects. These include the initial channel topography, vertical adjustments and related stabilizing effects of widenings, flood hazards, bank erosion initiation measures, and widening length. Taking into account the hierarchical organization of fluvial environments (e.g., Gurnell *et al.* 2016; Polvi *et al.* 2020), these reach-scale considerations need to be aligned with larger-scale processes.

Initial topography

The initial topography of a channelized reach may strongly influence the widening evolution. The presence of bars will likely promote erosion of the opposite bank (cf. Requena 2008; Klösch *et al.* 2015; Crosato and Mosselman 2020), and similar initiating effects could also be caused by channel curvature and point bars (Aufleger and Niedermayr 2004). The position of the widening perimeter relative to bed forms in the channelized section thus defines bank zones predisposed for erosion. Similarly, whether the channel is widened on one or both sides will influence the initial widening shape. The effect of initial topography certainly diminishes with widening age, but may strongly influence the widening evolution during the first years after implementation. By correctly accounting for these initial effects, construction efforts may be optimized and public perception of the newly widened reach may be improved.

Vertical adjustments

Dynamic river widening may trigger varying degrees of vertical channel adjustments (Siviglia *et al.* 2008). For actively widening channels, water surface and bed slope increase within the widening perimeter, similar to the bed slope increase and vertical offset in constructed river widenings (Hunzinger 1998; Berchtold 2015). Channel widenings have thus been attributed with a stabilizing effect for the upstream channel bed by acting as a local fix point (Siviglia *et al.* 2008; Klösch *et al.* 2011). If the widened reach develops a steeper slope and higher bed elevation than the former channelized reach, the

resulting water surface elevation rise within and upstream of the widening must be considered in flood hazard management. However, the experiments presented here also support previous findings indicating that the stabilizing effect is absent or erosional tendencies may even be aggravated when sediment supply is too low to trigger significant channel widening (Requena *et al.* 2005; Hafner *et al.* 2012; Berchtold 2015).

Bank erosion initiation measures

To offset the stabilizing effect observed for low sediment supply, local initiation measures may be used to trigger lateral erosion (Die Moran *et al.* 2013; Friedl 2017; Williams *et al.* 2020). The principal objective of initiation measures is to induce flow perturbations and thus trigger local sediment deposition and bank erosion. Once the erosion-deposition interaction is initiated locally, it will likely prompt dynamic processes on a larger scale (Klösch *et al.* 2015). This thesis does not include systematic testing of initiation methods, their locations, and their interaction with different sediment supply levels. However, important differences were found between the effect of flow deflection (Figures 7.1a,b) versus initial widening (or floodplain lowering; Figures 7.1c,d) for the same sediment supply level ($Q_{s,in}/Q_{s,0} = 0.6$).

The experiments suggest that flow deflection alone may not be able to offset the impacts of low sediment supply, at least not for bed-forming discharges. The perturbation of the flow field was likely not strong enough, which may also be related to the location of the flow deflector at the apex of a bar. By positioning the structure in a scour ($X \approx 12$ to 15 m; see Figures 5.16 and 5.24a), a stronger perturbation might have been achieved. However, the limited ability of flow deflectors to trigger substantial bank erosion has also been shown before (Friedl 2017). Initial floodplain lowering seems to be a more promising strategy to overcome stabilizing effects, presumably due to a more instantaneous and localized perturbation of the flow field. Overall, it can be assumed that the lower sediment supply is in comparison with the transport capacity, the stronger the flow field perturbation necessary to trigger bank erosion and sustain morphodynamic activity. Local flow deceleration reducing transport capacity and triggering sediment deposition (Figures 7.1c,d) seems to be a more effective strategy than flow acceleration slightly increasing the hydraulic stress acting on the river banks (Figures 7.1a,b). However, further systematic tests would be necessary to confirm this hypothesis.

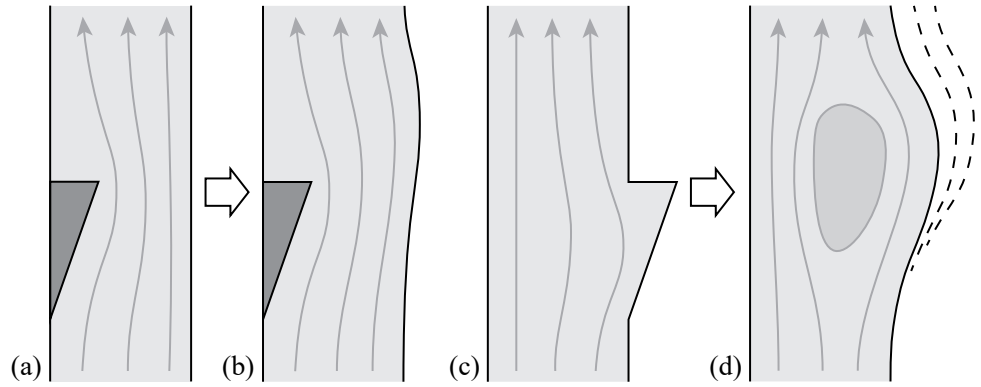

Figure 7.1 Plan view sketch showing the effects of local flow deflection with (a) flow acceleration leading to (b) limited lateral erosion in comparison to local floodplain lowering with (c) flow deceleration prompting (d) sediment deposition and associated channel widening.

Widening length

The experiments presented here correspond to a long widening according to Hunzinger (1998). It can therefore be assumed that a longer widening perimeter would not result in significantly different widening morphologies. Lateral erosion processes could potentially grow stronger with distance from the widening inlet (cf. Requena 2008; Aufleger *et al.* 2012), therefore disproportionately increasing the area subject to sediment relocation. Longer widenings have also been associated with more reliable bed stabilization effects (Hunzinger 1998), and higher ecological benefits (Weber *et al.* 2009). Regarding ecological benefits, however, the relation between the length of a restored reach and restoration success has not yet been conclusively resolved (e.g., Hering *et al.* 2015), and opportunities for longer widenings generally remain limited in heavily populated areas.

Restoring sediment supply

The experiments presented in this thesis demonstrate that increasing sediment supply to a morphodynamically inactive river reach may re-establish near-natural morphodynamic processes given enough space is available. One could conclude that the more sediment is added to a river reach, the better. However, increasing sediment supply beyond the transport capacity of a mainly channelized system is usually not desirable due to resulting sediment deposition and accompanying flood hazards. While sufficient sediment supply is vital for river ecosystem health, a long-term depositional state is usually not necessary in the context of river restoration. In many cases, it may also not be possible to restore sediment supply to a level close to the transport capacity. This is not to say

that a sediment supply increase to a value significantly lower than the transport capacity ($Q_{s,in} < 0.8Q_{s,0}$ in this study) is not beneficial for the fluvial ecosystem. Substrate composition may still be improved, however, no significant changes in overall morphology can be expected (cf. Rachelly *et al.* 2021a). It must be noted at this point that the definition of *sufficient* sediment supply is a difficult if not impossible task given the wide range of fluvial systems and associated natural sediment regimes (Wohl *et al.* 2015a, but see Yarnell *et al.* 2006). The results of this study can nevertheless support the definition of an appropriate sediment supply level by clarifying what degree of morphodynamic change can be expected.

Spatial organization of fluvial environments

Another important consideration for effective river restoration is the spatial organization of fluvial environments (e.g., Gurnell *et al.* 2016; Polvi *et al.* 2020). As long as significant deficits remain on a scale larger than the scale of a restoration project, the benefits of restoring small-scale features may be limited (e.g., Weber *et al.* 2009). This study illustrates how a large-scale process can impose limitations on a reach-scale restoration project, namely how sediment supply may play a fundamental role in defining the morphological evolution of river widenings. It is also worth mentioning here that river widenings should not be implemented by removing excavated floodplain sediment from the river system (except for reasons such as sediment contamination). Such removal would disrupt sediment continuity, thus creating a temporary sediment deficit for the downstream reach (Hunzinger 1998; Klösch *et al.* 2011).

This study provides an example of the conflicts that may arise if restoration measures do not target large-scale ecosystem processes but instead focus on habitat structure on a reach scale (e.g., Beechie *et al.* 2010; Polvi *et al.* 2020). In order for dynamic river widening to be an effective restoration measure, pressures on a larger scale such as impaired sediment and flow regimes (e.g., Vanzo *et al.* 2016), insufficient water quality, or land use changes must be addressed and, if possible, restored concurrently (Kondolf *et al.* 2006). Mitigation measures for sediment supply include various structural (e.g., sediment bypass tunnels), operational (e.g., reservoir drawdown), and replenishment measures (Kondolf *et al.* 2014). In Switzerland, a concerted effort to mitigate the effects of channel degradation, fish migration barriers, sediment deficit, and hydropeaking is ongoing (Bammatter *et al.* 2015; see Section 2.4.2). Regarding the disruption of sediment continuity, approx-

imately five hundred hydropower dams and weirs as well as other structures must be altered. This creates opportunities for downstream channel restoration measures, such as dynamic river widenings, to fulfil their ecological potential, for example by providing suitable flood refugia.

8 Conclusions and outlook

8.1 Conclusions

Mobile-bed laboratory experiments combined with 2D hydrodynamic numerical simulations were performed to identify the influence of sediment supply on morphodynamic processes in river widenings. The results were analyzed with regard to morphological characteristics and the availability of potential aquatic flood refugia. The main finding was that *morphodynamically active* and *inactive* widenings emerged as two distinct morphodynamic states. Their occurrence was shown to be a consequence of either sediment supply close to the initial channel's transport capacity ($Q_{s,in}/Q_{s,0}$ = 0.8 and 1) or structural bank initiation measures causing a local flow deceleration. Under these conditions, sediment is deposited locally and can initiate lateral erosion with associated bar growth. These local effects can then propagate along the perimeter leading to active morphodynamic processes in the entire widening. Morphodynamically inactive widenings resulted from sediment supply significantly lower than the transport capacity of the initial channel ($Q_{s,in}/Q_{s,0}$ = 0.2 and 0.6). The two identified morphodynamic states are described below in terms of their morphological characteristics and properties related to refugia availability. It must be noted that this study suggests that morphodynamic activity generally shows a binary rather than gradual response to sediment supply but the limited number of experiments does not allow definitive conclusions in this sense.

(1) Characteristics of *morphodynamically active* widenings:

- *Morphology*: The complexity of the widening morphology continuously increased with progressive lateral erosion and channel widening resulting in a morphology at the transition between alternate bars and braiding. Active sediment relocation continuously altered the specific morphological configuration during bed-forming discharge. With a discharge roughly twice as high, extensive morphological restructuring occurred.

- *Bed-load balance*: Although channel widening triggered sediment deposition within the widening perimeter, bed-load transport through the widening was maintained to a large extent. A severe sediment deficit in the downstream reach is therefore unlikely.

- *Bed and water surface elevation*: Sediment was deposited in the widening perimeter, increasing the water surface elevation and bed slope of the widened reach. The upstream bed elevation increased by about half a channel flow depth. Due to gradual channel transitions, the vertical bed offset relative to the upstream and downstream channel bed location was mostly absent or only up to half a channel flow depth thick. At the downstream end, scour depths between half and a full flow depth were observed.

- *Hydro-morphological diversity*: Due to the well-structured widening topography, hydro-morphological diversity and bed shear stress variability were generally high, resembling conditions in lightly modified natural reaches. A substantial part of the widening maintained low hydraulic stress during a flood thus both preventing the displacement of organisms and destructive bed-load transport. In addition, potential shelter was provided along the relatively complex shoreline separating the channel from the floodplain, especially during low to medium floods.

- *Channel-floodplain connectivity*: The floodplain was almost completely inundated at low to medium discharges, with the specific overbank flow depending on the elevation difference between channel and floodplain. The inundated floodplain provided extensive low flow areas potentially functioning as flood refugia for aquatic organisms, especially along the channel-floodplain margin. Importantly, when organisms are forced to return to the main channel during the receding limb of a hydrograph, low bed shear stress areas without bed-load transport would be available there.

(2) Characteristics of *morphodynamically inactive* widenings:

- *Morphology*: Initial lateral bank erosion quickly ceased and the alternate bar morphology of the initial channel was maintained. A flow deflector opposite of the floodplain was not effective in overcoming this stability. Sediment relocation at bed-forming discharge was very limited but extensive channel shifting was observed during a flood discharge roughly twice as high.

- *Bed-load balance*: Bed-load transport through the widening was largely maintained,

albeit on a low level. A further aggravation of the sediment deficit in the downstream reach is therefore unlikely.

- *Bed and water surface elevation*: With lateral erosion being limited, little sediment deposition occurred in the widening. Bed and water surface elevation thus remained largely stable or were lowered relative to initial conditions due to rotational erosion caused by the sediment deficit. The bed upstream of the widening was thereby eroded by up to half a flow depth, and the widening therefore does not provide the desired stabilizing function. At the downstream end, scour depths of up to one and a half flow depths occurred.

- *Hydro-morphological diversity:* Hydro-morphological diversity was generally low, suggesting these reaches remain morphologically heavily altered and will provide limited flood refugia. Only for the highest discharges can an increase in hydro-morphological diversity be expected due to overbank flow. Shoreline length was also low with most values close to the theoretical minimum of 2 km/km. This implies low structural complexity of the shoreline areas and thus low provision of marginal flood refugia for aquatic organisms.

- *Channel-floodplain connectivity:* Channel incision due to low sediment supply disconnected the channel from its floodplain, which was only inundated for high discharges. Floodplain zones are thus generally not accessible to aquatic organisms during floods, and aquatic organisms would be forced to remain in the main channel where conditions are very unfavorable for their survival.

8.2 Outlook

The findings presented in this thesis contribute to our understanding of the conditions under which dynamic river widenings show sustained morphodynamic activity and potentially offer ecological benefits. However, the following aspects would benefit from further research:

- The extension of the parameter range to lower channel slopes is strongly recommended. It is suspected that a lower sediment supply level might be sufficient to trigger lateral erosion and channel shifting for these conditions due to the underlying morphology tending towards meandering. However, the morphodynamic processes

might develop slower due to the inherently higher stability of meandering channels compared to braiding channels. An extension of the parameter range could also clarify whether the relation between sediment supply and morphodynamic activity has a binary or gradual character. Further parameter variations worth exploring could be sediment composition, widening configuration (two-sided or alternating), or floodplain erodibility. Variable floodplain erodibility is certainly challenging to implement in laboratory experiments but several studies using live (e.g., Tal and Paola 2010) or artificial (e.g., Vargas-Luna *et al.* 2019) vegetation have already been conducted.

- Morphodynamic numerical simulations of river widenings would allow a certain expansion of the parameter range just mentioned. However, the numerical modeling of such complex morphodynamic processes remains challenging. Promising first results on this issue have been obtained for the conditions studied here (Stadtmann 2020; Nieto Medina 2021) and will be further pursued.

- Systematic variation of the elevation difference between channel and floodplain would allow a clearer separation of floodplain inundation effects and the morphodynamic impact of variable sediment supply.

- The comparison of the findings of this thesis to field data is of greatest interest. There is evidence that a relation between sediment supply and reach characteristics such as habitat fragmentation or channel width variability exists, but more data are required to elaborate this relationship (Bianchi 2018). A more detailed habitat modeling applied to variable sediment supply conditions could further clarify the impact of sediment supply on aquatic habitats, for example, by explicitly considering their spatial arrangement or including information on habitat suitability.

- The topic of refugia generally deserves more attention. In addition to flood refugia, habitats that assume refugia function during droughts should also be considered. More biological data are needed to connect the hydro-morphological indicators of refugia availability such as the ones used here to real refuge function, especially for flood refugia.

Notation

Symbols

$A_{ch,0}$	Initial channel area (m^2)
A_{reloc}	Sediment relocation area (m^2; erosion + deposition)
A_w	Widening perimeter area (m^2)
A_{wet}	Wetted area (m^2)
$A_{\theta>\theta c}$	High bed shear stress area (m^2)
B	Degree of nonlinearity of sediment transport versus depth-averaged flow velocity (-)
b	Width (m)
b_{ch}	Channel width (m)
b_m	Mean widening width (m)
$b_{\max}$	Maximum widening width (m)
b_w	Maximum width of widening perimeter (m)
b_0	Initial channel width (m)
b_*	Detrended width (m)
c	Shallow water wave celerity (m/s)
C	Turbulent friction coefficient (-)
c_f	Dimensionless Chézy friction coefficient (-)
C_f	Dimensional Chézy friction coefficient ($m/s^{1/2}$)
D	Grain diameter (m)
D_m	Geometric mean of the grain size distribution (m)
D_i	i^{th} percentile of a grain size distribution (m; i.e., D_{50} is the median grain diameter)
$D_{i,A}$	D_i of the armor layer (m)
dz_{bw}	Difference between mean and wetted bed elevation (m)
F	Froude number (-)
g	Gravitational acceleration (m/s^2)
h	Flow depth (m)
H_B	Alternate bar height (m)
h_{ch}	Uniform flow depth in channel (m)

h_{dry}	Dry-wet threshold (m)
H_{FD}	Flow deflector height above mean bed level (m)
$h_{E,ch}$	Energy head elevation above channel bed (m)
$h_{E,w}$	Energy head elevation above widening bed (m)
h_m	Mean flow depth in widening (m)
$h_{\max}$	Maximum flow depth (m)
$\mathrm{H}Q_x$	Flood discharge with a return period of x years (m^3/s)
h_w	Uniform flow depth in widening (m)
h_0	Initial flow depth (m)
K_S	Bed roughness height (m)
k_{st}	Strickler coefficient ($m^{1/3}/s$)
L_B	Alternate bar wavelength (m)
L_c	Constriction length (m)
L_e	Expansion length (m)
L_r	Recirculation length (m)
L_w	Widening length (m)
$L_{w,\mathrm{tot}}$	Total length of widening perimeter (m)
m	Bar mode predictor (-)
p_i	Relative frequency (-)
Q	Discharge (m^3/s)
Q_B	Bed-forming discharge (m^3/s; $\approx \mathrm{H}Q_{1.5}$ in the reference reach)
Q_F	Flood discharge (m^3/s; $\approx \mathrm{H}Q_{30}$ in the reference reach)
Q_m	Mean annual discharge (m^3/s)
Q_s	Sediment transport rate (kg/s)
$Q_{s,in}$	Sediment input rate (kg/s)
$Q_{s,out}$	Sediment output rate (kg/s)
$Q_{s,0}$	Transport capacity of the initial channel (kg/s)
Q_x	Discharge reached and exceeded for x days per year (m^3/s)
Q_*	Dimensionless discharge (-)
R	Reynolds number (-)
R_h	Hydraulic radius (m)
r_i	Radius of mesh element incircle (m)

s	Relative sediment density ρ_s/ρ (-)
S	Longitudinal slope (-)
S_b	Longitudinal bed slope (-)
S^*_{bm}	Meandering-braiding threshold slope (-)
S_{ch}	Longitudinal bed slope in channel (-)
s_z	Vertical bed offset (m)
S_{wse}	Longitudinal water surface slope (-)
S_w	Longitudinal bed slope in widening (-)
S_0	Initial longitudinal slope (-)
t	Time (s)
$t_{s,\text{max}}$	Maximum scour depth (m)
U_*	Shear velocity (m/s)
v	Flow velocity magnitude (m/s)
v_{ch}	Mean flow velocity in channel (m/s)
v_w	Mean flow velocity in widening (m/s)
v_x	Flow velocity component in x-direction (m/s)
v_y	Flow velocity component in y-direction (m/s)
X	Streamwise coordinate (m)
Y	Transverse coordinate (m)
Z	Vertical coordinate (m)
z_{FP}	Vertical floodplain offset (m)
$Z_{m,i}$	Mean bed elevation per cross-section (m)
$Z_{5,i}$	5^{th} percentile of cross-section bed elevations (m)
$Z_{95,i}$	95^{th} percentile of cross-section bed elevations (m)
δ_c	Constriction angle (°)
δ_e	Expansion angle (°)
Δt	Time step (s)
Δz	Upstream bed aggradation (m)
ΔZ	Bed elevation difference (m)
η_B	Alternate bar scour depth (m)
θ	Dimensionless bed shear stress (-)
θ_c	Critical dimensionless bed shear stress (-)

θ_{Di}	Dimensionless bed shear stress for characteristic diameter (-; i.e., θ_{D50} for median grain diameter)
λ	Froude scale factor (-)
λ_B	Alternate bar wave number (-)
μ	Friction angle (-)
ν	Kinematic viscosity of water (m^2/s)
ρ	Water density (kg/m^3)
ρ_s	Sediment density (kg/m^3)
τ_b	Bed shear stress (N/m^2)
ω	Specific stream power (W/m^2)
ω^*	Dimensionless specific stream power (-)
ω_0^*	Critical dimensionless specific stream power (-)
ω_{bm}^*	Meandering-braiding threshold stream power (-)
ω_{ia}^*	Inactive-active threshold stream power (-)
ω_{sc}^*	Scroll bar-chute bar threshold stream power (-)

Abbrevations

CFL	Courant-Friedrichs-Lewy criterion
DEM	Digital elevation model
DoD	DEM of difference
FOEN	Federal Office for the Environment
GSD	Grain size distribution
HMID	Hydro-morphological index of diversity
LDS	Laser distance sensor
RMSE	Root mean square error
TLS	Terrestrial laser scanning
UDS	Ultrasonic distance sensor
VAW	Laboratory of Hydraulics, Hydrology and Glaciology
WSE	Water surface elevation

References

Abramian, A.; Devauchelle, O.; Lajeunesse, E. (2020). Laboratory rivers adjust their shape to sediment transport. *Physical Review E*, 102(5): 053101. https://doi.org/10.1103/PhysRevE.102.053101.

Addy, S.; Wilkinson, M.E. (2021). Embankment lowering and natural self-recovery improves river-floodplain hydro-geomorphic connectivity of a gravel bed river. *Science of The Total Environment*, 770: 144626. https://doi.org/10.1016/j.scitotenv.2020.144626.

Ahmari, H.; da Silva, A.M.F. (2011). Regions of bars, meandering and braiding in da Silva and Yalin's plan. *Journal of Hydraulic Research*, 49(6): 718–727. https://doi.org/10.1080/00221686.2011.614518.

Allan, J.D.; Castillo, M.M. (2007). Stream ecology: structure and function of running waters. ISBN 978-1-4020-5582-9. 2nd edn. *Springer*, Dordrecht, Netherlands.

ASCE (2000). Hydraulic Modeling: Concepts and Practice. ISBN 978-0-7844-7041-1. *American Society of Civil Engineers*, Reston, VA.

Ashmore, P. (2001). Braiding phenomena: statics and kinetics: 95–121. In: M. Mosley (ed.) Gravel Bed Rivers V. ISBN 0-473-07486-9. *New Zealand Hydrological Society*, Wellington, New Zealand.

Ashmore, P.E.; Bertoldi, W.; Gardner, J. (2011). Active width of gravel-bed braided rivers. *Earth Surface Processes and Landforms*, 36(11): 1510–1521. https://doi.org/10.1002/esp.2182.

Aufleger, M.; Gems, B.; Klar, R. (2012). Flussaufweitungen als flussbauliche Methode - Grundsätze und Werkzeuge. (Channel widening as river engineering method - principles and tools.). *Österreichische Wasser- und Abfallwirtschaft*, 64: 363–378. https://doi.org/10.1007/s00506-012-0006-x (in German).

Aufleger, M.; Niedermayr, A. (2004). Large scale tests for gravel-bed river widening. *Proc. Second International Conference on Fluvial Hydraulics*. *Taylor & Francis Group*, Napoli, Italy: 163–171. https://doi.org/10.1201/b16998.

Bammatter, L.; Baumgartner, M.; Greuter, L.; Haertel-Borer, S.; Huber Gysi, M.; Nitsche, M.; Thomas, G. (2015). Renaturierung der Schweizer Gewässer: Die Sanierungspläne der Kantone ab 2015 (Swiss river restoration: the cantonal restoration plans from 2015). *Technical Report*, Federal Office for the Environment (FOEN), Bern, Switzerland (in German).

Bankert, A.R.; Nelson, P.A. (2018). Alternate bar dynamics in response to increases and decreases of sediment supply. *Sedimentology*, 65(3): 702–720. https://doi.org/10.1111/sed.12399.

BASEmesh (2021). BASEmesh - tool for generation of computational meshes for numerical software BASEMENT, Versions 1.4.5 and 2.0.0. Laboratory of Hydraulics, Hydrology and Glaciology (VAW), ETH Zurich. https://basement.ethz.ch/download/tools/basemesh.html.

Baynes, E.R.; Lague, D.; Steer, P.; Bonnet, S.; Illien, L. (2020). Sediment flux-driven channel geometry adjustment of bedrock and mixed gravel–bedrock rivers. *Earth Surface Processes and Landforms*, 45(14): 3714–3731. https://doi.org/10.1002/esp.4996.

Beechie, T.J.; Sear, D.A.; Olden, J.D.; Pess, G.R.; Buffington, J.M.; Moir, H.; Roni, P.; Pollock, M.M. (2010). Process-based Principles for Restoring River Ecosystems. *BioScience*, 60(3): 209–222. https://doi.org/10.1525/bio.2010.60.3.7.

Berchtold, T. (2015). Numerische Modellierung von Flussaufweitungen (Numerical modeling of river widenings). *VAW-Mitteilung 231* (R.M. Boes, ed.). Laboratory of Hydraulics, Hydrology and Glaciology, ETH Zurich, Switzerland. https://doi.org/10.3929/ethz-a-010399877 (in German).

Bernhardt, E.S.; Palmer, M.A.; Allan, J.D.; Alexander, G.; Barnas, K.; Brooks, S.; Carr, J.; Clayton, S.; Dahm, C.; Follstad-Shah, J.; Galat, D.; Gloss, S.; Goodwin, P.; Hart, D.; Hassett, B.; Jenkinson, R.; Katz, S.; Kondolf, G.M.; Lake, P.S.; Lave, R.; Meyer, J.L.; O'Donnell, T.K.; Pagano, L.; Powell, B.; Sudduth, E. (2005). Synthesizing U.S. river restoration efforts. *Science*, 308(5722): 636–637. https://doi.org/10.1126/science.1109769.

Bertoldi, W.; Welber, M.; Gurnell, A.; Mao, L.; Comiti, F.; Tal, M. (2015). Physical

modelling of the combined effect of vegetation and wood on river morphology. *Geomorphology*, 246: 178–187. https://doi.org/10.1016/j.geomorph.2015.05.038.

Bianchi, A. (2018). Analyse ausgewählter Objekte des Bundesinventars der Auengebiete von nationaler Bedeutung (Analysis of selected objects of the Federal Floodplain Inventory). *Master Thesis*, VAW, ETH Zurich and Eawag, Switzerland (in German).

Biron, P.M.; Buffin-Bélanger, T.; Larocque, M.; Choné, G.; Cloutier, C.A.; Ouellet, M.A.; Demers, S.; Olsen, T.; Desjarlais, C.; Eyquem, J. (2014). Freedom Space for Rivers: A Sustainable Management Approach to Enhance River Resilience. *Environmental Management*, 54: 1056–1073. https://doi.org/10.1007/s00267-014-0366-z.

Blake, C.; Rhanor, A. (2020). The impact of channelization on macroinvertebrate bioindicators in small order Illinois streams: insights from long-term citizen science research. *Aquatic Sciences*, 82(35). https://doi.org/10.1007/s00027-020-0706-4.

Buffington, J.M.; Montgomery, D.R. (1997). A systematic analysis of eight decades of incipient motion studies, with special reference to gravel-bedded rivers. *Water Resources Research*, 33(8): 1993–2029. https://doi.org/10.1029/96WR03190.

Buffington, J.M.; Montgomery, D.R. (1999). Effects of sediment supply on surface textures of gravel-bed rivers. *Water Resources Research*, 35(11): 3523–3530. https://doi.org/10.1029/1999WR900232.

Bunte, K.; Abt, S.R. (2001). Sampling surface and subsurface particle-size distributions in wadable gravel- and cobble-bed streams for analysis in sediment transport, hydraulics, and streambed monitoring. *Technical Report RMRS-GTR-74*, U.S. Department of Agriculture, Forest Service, Rocky Mountain Research Station, Fort Collins, CO.

BUWAL/BWG (2003). Leitbild Fliessgewässer Schweiz. Für eine nachhaltige Gewässerpolitik. (Mission statement Swiss Watercourses. Towards sustainable water policy.). Bern, Switzerland (in German).

Böck, K.; Polt, R.; Schülting, L. (2018). Ecosystem Services in River Landscapes. Chap. 21: 413–433. In: S. Schmutz; J. Sendzimir (eds.) Riverine Ecosystem Management: Science for Governing Towards a Sustainable Future. ISBN 978-3-319-

73250-3. *Springer International Publishing*, Cham, Switzerland. https://doi.org/10.1007/978-3-319-73250-3_21.

Castro, J.M.; Thorne, C.R. (2019). The stream evolution triangle: Integrating geology, hydrology, and biology. *River Research and Applications*, 35(4): 315–326. https://doi.org/10.1002/rra.3421.

Chow, V.T. (1959). Open-Channel Hydraulics. ISBN 9781932846188. *The Blackburn Press*, Caldwell, NJ.

Church, M. (2006). Bed material transport and the morphology of alluvial river channels. *Annual Review of Earth and Planetary Sciences*, 34: 325–354. https://doi.org/10.1146/annurev.earth.33.092203.122721.

Conrad, O.; Bechtel, B.; Bock, M.; Dietrich, H.; Fischer, E.; Gerlitz, L.; Wehberg, J.; Wichmann, V.; Böhner, J. (2015). System for automated geoscientific analyses (SAGA) v. 2.1.4. *Geoscientific Model Development*, 8(7): 1991–2007. https://doi.org/10.5194/gmd-8-1991-2015.

Cordillot, F.; Klaus, G. (2011). Gefährdete Arten in der Schweiz - Synthese Rote Listen, Stand 2010 (Endangered species in Switzerland - red list synthesis, status 2010). *Technical Report 1120*, Federal Office for the Environment (FOEN), Bern, Switzerland (in German).

Crosato, A.; Mosselman, E. (2009). Simple physics-based predictor for the number of river bars and the transition between meandering and braiding. *Water Resources Research*, 45(3): W03424. https://doi.org/10.1029/2008WR007242.

Crosato, A.; Mosselman, E. (2020). An Integrated Review of River Bars for Engineering, Management and Transdisciplinary Research. *Water*, 12(2). https://doi.org/10.3390/w12020596.

Czuba, C.R.; Czuba, J.A.; Magirl, C.S.; Gendaszek, A.S.; Konrad, C.P. (2018). Effect of river confinement on depth and spatial extent of bed disturbance affecting salmon redds. *Journal of Ecohydraulics*, 3(1): 4–17. https://doi.org/10.1080/24705357.2018.1457986.

Demuth, P. (2020). Initiierung der Seitenerosion in eigendynamischen Flussaufweitungen (Bank erosion initiation measures in dynamic river widenings). *Master Thesis*, University of Natural Resources and Life Sciences, Vienna, Austria and VAW, ETH Zurich, Switzerland (unpublished, in German).

Detert, M. (2020). BASEGRAIN. Laboratory of Hydraulics, Hydrology and Glaciology (VAW), ETH Zurich. https://doi.org/10.5905/ethz-1007-347.

Die Moran, A.; El Kadi Abderrezzak, K.; Mosselman, E.; Habersack, H.; Lebert, F.; Aelbrecht, D.; Laperrousaz, E. (2013). Physical model experiments for sediment supply to the old Rhine through induced bank erosion. *International Journal of Sediment Research*, 28(4): 431–447. https://doi.org/10.1016/S1001-6279(14)60003-2.

Dietrich, W.E.; Kirchner, J.W.; Ikeda, H.; Iseya, F. (1989). Sediment supply and the development of the coarse surface layer in gravel-bedded rivers. *Nature*, 340: 215–217. https://doi.org/10.1038/340215a0.

Dole-Olivier, M.J.; Marmonier, P.; Beffy, J.L. (1997). Response of invertebrates to lotic disturbance: is the hyporheic zone a patchy refugium? *Freshwater Biology*, 37(2): 257–276. https://doi.org/10.1046/j.1365-2427.1997.00140.x.

Doretto, A.; Piano, E.; Larson, C.E. (2020). The River Continuum Concept: lessons from the past and perspectives for the future. *Canadian Journal of Fisheries and Aquatic Sciences*, 77(11): 1853–1864. https://doi.org/10.1139/cjfas-2020-0039.

Downs, P.W.; Piégay, H. (2019). Catchment-scale cumulative impact of human activities on river channels in the late Anthropocene: implications, limitations, prospect. *Geomorphology*, 338: 88–104. https://doi.org/10.1016/j.geomorph.2019.03.021.

Dudgeon, D.; Arthington, A.H.; Gessner, M.O.; Kawabata, Z.I.; Knowler, D.J.; Lévêque, C.; Naiman, R.J.; Prieur-Richard, A.H.; Soto, D.; Stiassny, M.L.; Sullivan, C.A. (2006). Freshwater biodiversity: importance, threats, status and conservation challenges. *Biological reviews*, 81(2): 163–182. https://doi.org/10.1017/S1464793105006950.

Dufour, S.; Piégay, H. (2009). From the myth of a lost paradise to targeted river restoration: forget natural references and focus on human benefits. *River Research and Applications*, 25(5): 568–581. https://doi.org/10.1002/rra.1239.

East, A.E.; Logan, J.B.; Mastin, M.C.; Ritchie, A.C.; Bountry, J.A.; Magirl, C.S.; Sankey, J.B. (2018). Geomorphic Evolution of a Gravel-Bed River Under Sediment-Starved Versus Sediment-Rich Conditions: River Response to the World's Largest Dam Removal. *Journal of Geophysical Research: Earth Surface*, 123(12): 3338–3369. https://doi.org/10.1029/2018JF004703.

Eaton, B.C.; Church, M. (2009). Channel stability in bed load–dominated streams with nonerodible banks: Inferences from experiments in a sinuous flume. *Journal of Geophysical Research: Earth Surface*, 114(F1): F01024. https://doi.org/10.1029/2007JF000902.

Eaton, B.C.; Church, M. (2011). A rational sediment transport scaling relation based on dimensionless stream power. *Earth Surface Processes and Landforms*, 36(7): 901–910. https://doi.org/10.1002/esp.2120.

Eaton, B.C.; Church, M.; Millar, R.G. (2004). Rational regime model of alluvial channel morphology and response. *Earth Surface Processes and Landforms*, 29(4): 511–529. https://doi.org/10.1002/esp.1062.

Eaton, B.C.; MacKenzie, L.G.; Booker, W.H. (2020). Channel stability in steep gravel–cobble streams is controlled by the coarse tail of the bed material distribution. *Earth Surface Processes and Landforms*, 45(14): 3639–3652. https://doi.org/10.1002/esp.4994.

Eaton, B.C.; Millar, R.G. (2017). Predicting gravel bed river response to environmental change: the strengths and limitations of a regime-based approach. *Earth Surface Processes and Landforms*, 42(6): 994–1008. https://doi.org/10.1002/esp.4058.

Eawag (2021). The Water Timeline: History of Swiss Water Protection since 1800. https://www.wassertimeline.ch/en/project/ (accessed December 7, 2021).

Effenberger, M.; Sailer, G.; Townsend, C.R.; Matthaei, C.D. (2006). Local disturbance history and habitat parameters influence the microdistribution of stream invertebrates. *Freshwater Biology*, 51(2): 312–332. https://doi.org/10.1111/j.1365-2427.2005.01502.x.

Ferguson, R. (1987). Hydraulic and sedimentary controls of channel pattern: 129–158. In: K.S. Richards (ed.) River channels: Environments and processes. ISBN 0-631-14577-X. *Basil, Blackwell*, Oxford, UK.

FOEN (2014). Generalised background map for the representation of hydrological data. Federal Office for the Environment (FOEN), Bern, Switzerland. https://opendata.swiss/en/dataset/generalisierte-hintergrundkarte-zur-darstellung-hydrologischer-daten (accessed August 14, 2017).

FOEN (2017). Federal Inventory of Floodplains of National Importance. Federal Office for the Environment (FOEN), Bern, Switzerland. https://opendata.swiss/en/dataset/bundesinventar-der-auengebiete-von-nationaler-bedeutung (accessed August 18, 2021).

FOEN (2019). Kander River, Switzerland. Hydrometric data of the station EDV 2469: Kander - Hondrich, data series 1981-2018. Federal Office for the Environment (FOEN), Bern, Switzerland. https://www.hydrodaten.admin.ch/de/2469.html (accessed August 15, 2019).

Friedl, F. (2017). Laboratory Experiments on Sediment Replenishment in Gravel-Bed Rivers. *VAW-Mitteilung 245* (R.M. Boes, ed.). Laboratory of Hydraulics, Hydrology and Glaciology, ETH Zurich, Switzerland. https://doi.org/10.3929/ethz-b-000479113.

Friedl, F.; Weitbrecht, V.; Boes, R.M. (2015). The role of bank erosion in restoration works in gravel-bed rivers. *Proc. E-Proceedings of the 36th IAHR World Congress, 28 June - 3 July, 2015, The Hague, Netherlands*. *International Association for Hydro-Environment Engineering and Research (IAHR)*, The Hague, Netherlands. ISBN 9789082484601.

Gabbud, C.; Bakker, M.; Clémençon, M.; Lane, S.N. (2019). Hydropower Flushing Events Cause Severe Loss of Macrozoobenthos in Alpine Streams. *Water Resources Research*, 55(12): 10056–10081. https://doi.org/10.1029/2019WR024758.

Gabbud, C.; Lane, S.N. (2016). Ecosystem impacts of Alpine water intakes for hydropower: the challenge of sediment management. *WIREs Water*, 3(1): 41–61. https://doi.org/10.1002/wat2.1124.

Garcia Lugo, G.A.; Bertoldi, W.; Henshaw, A.J.; Gurnell, A.M. (2015). The effect of lateral confinement on gravel bed river morphology. *Water Resources Research*, 51(9): 7145–7158. https://doi.org/10.1002/2015WR017081.

Gjerløv, C.; Hildrew, A.G.; Jones, J.I. (2003). Mobility of stream invertebrates in relation to disturbance and refugia: a test of habitat templet theory. *Journal of the North American Benthological Society*, 22(2): 207–223. https://doi.org/10.2307/1467993.

Gostner, W.; Alp, M.; Schleiss, A.; T. Robinson, C. (2013). The hydro-morphological index of diversity: a tool for describing habitat heterogeneity in river engineering projects. *Hydrobiologia*, 712: 43–60. https://doi.org/10.1007/s10750-012-1288-5.

Gurnell, A.; Rinaldi, M.; Belletti, B.; Bizzi, S.; Blamauer, B.; Braca, G.; Buijse, A.; Bussettini, M.; Camenen, B.; Comiti, F.; Demarchi, L.; García de Jalón, D.; González del Tánago, M.; Grabowski, R.; Gunn, I.; Habersack, H.; Hendriks, D.; Henshaw, A.; Klösch, M.; Lastoria, B.; Latapie, A.; Marcinkowski, P.; Martínez-Fernández, V.; Mosselman, E.; Mountford, J.; Nardi, L.; Okruszko, T.; M.T., O.; Palma, M.; Percopo, C.; Surian, N.; van de Bund, W.; Weissteiner, C.; Ziliani, L. (2016). A multi-scale hierarchical framework for developing understanding of river behaviour to support river management. *Aquatic sciences*, 78: 1–16. https://doi.org/10.1007/s00027-015-0424-5.

Habersack, H.; Klösch, M. (2012). Monitoring und Modellierung von eigendynamischen Aufweitungen an Drau, Mur und Donau (Monitoring and modeling of dynamic river widenings at the Drau, Mur, and Donau River). *Österreichische Wasser- und Abfallwirtschaft*, 64: 411–422. https://doi.org/10.1007/s00506-012-0007-9 (in German).

Habersack, H.; Koch, M.; Nachtnebel, H.P. (2000). Flussaufweitungen in Österreich - Entwicklung, Stand und Ausblick (River Bed Widening in Austria. Development, Present State, and Prospects). *Österreichische Wasser- und Abfallwirtschaft*, 52(7/8): 143–153 (in German).

Habersack, H.; Piégay, H. (2007). River restoration in the Alps and their surroundings: past experience and future challenges: 703–735. In: H. Habersack; H. Piégay; M. Rinaldi (eds.) Gravel-Bed Rivers VI: From Process Understanding to River Restoration. *Elsevier*. https://doi.org/10.1016/S0928-2025(07)11161-5.

HADES (2021). Hydrological Atlas of Switzerland (HADES). Federal Office for the Environment (FOEN). https://hydrologicalatlas.ch/.

Hafner, T.; Schaipp, B.; Wedding, S.; Schwaller, G. (2012). Erfahrungen mit dem Uferrückbau in Bayern (Experiences with bank protection removal in Bavaria). *Österreichische Wasser- und Abfallwirtschaft*, 64: 389–400. https://doi.org/10.1007/s00506-012-0008-8 (in German).

Hanus, E.; Roulier, C.; Paccaud, G.; Bonnard, L.; Fragnière, Y.; Ghilardi, T. (2021). Besoins de valorisation des zones alluviales d'importance nationale. Assainissement du charriage, des débits résiduels, des éclusées. Revitalisation. Mise à jour état 2018. (Restoration of the floodplains of the Federal Floodplain Inventory. Bed-load transport, environmental flow, and hydropeaking restoration. Reach-scale restoration. Update status 2018.). *Technical Report*, Federal Office for the Environment (FOEN) (in French).

Heller, V. (2011). Scale effects in physical hydraulic engineering models. *Journal of Hydraulic Research*, 49(3): 293–306. https://doi.org/10.1080/00221686.2011.578914.

Henderson, F.M. (1966). Open channel flow. ISBN 0023535105. *Macmillan*, New York, NY.

Hengl, M.; Aufleger, M.; de Mas, V.; Eggertsberger, J.; Hafner, T.; Michor, K.; Mühlbauer, M.; Raudaschl, S.; Schuardt, W.; Spannring, M.; Unterlercher, M.; Wiesenegger, C. (2012). Eigendynamische Aufweitungen an der Unteren Salzach – vom Konzept bis zu den ersten Erfahrungen (Self-forming widenings in the lower Salzach - from concept to initial experiences). *Österreichische Wasser- und Abfallwirtschaft*, 64: 401–410. https://doi.org/10.1007/s00506-012-0009-7 (in German).

Hering, D.; Aroviita, J.; Baattrup-Pedersen, A.; Brabec, K.; Buijse, T.; Ecke, F.; Friberg, N.; Gielczewski, M.; Januschke, K.; Köhler, J.; Kupilas, B.; Lorenz, A.W.; Muhar, S.; Paillex, A.; Poppe, M.; Schmidt, T.; Schmutz, S.; Vermaat, J.; Verdonschot, P.F.M.; Verdonschot, R.C.M.; Wolter, C.; Kail, J. (2015). Contrasting the roles of section length and instream habitat enhancement for river restoration success: a field study of 20 European restoration projects. *Journal of Applied Ecology*, 52(6): 1518–1527. https://doi.org/10.1111/1365-2664.12531.

Hohensinner, S.; Egger, G.; Muhar, S.; Vaudor, L.; Piégay, H. (2021). What remains today of pre-industrial Alpine rivers? Census of historical and current channel patterns in the Alps. *River Research and Applications*, 37(2): 128–149. https://doi.org/10.1002/rra.3751.

Hohensinner, S.; Habersack, H.; Jungwirth, M.; Zauner, G. (2004). Reconstruction of the characteristics of a natural alluvial river–floodplain system and hydromorphological changes following human modifications: the Danube River (1812–1991). *River Research and Applications*, 20: 25–41. https://doi.org/10.1002/RRA.719.

Hohensinner, S.; Jungwirth, M.; Muhar, S.; Schmutz, S. (2011). Spatio–temporal habitat dynamics in a changing Danube River landscape 1812 - 2006. *River Research and Applications*, 27(8): 939–955. https://doi.org/10.1002/rra.1407.

Hunziker, R. (2012). Erfahrungen mit der Aufweitung von Fließgewässern in der Schweiz (Experiences with river widening in Switzerland). *Österreichische Wasser- und Abfallwirtschaft*, 64: 379–388. https://doi.org/10.1007/s00506-012-0010-1 (in German).

Hunzinger, L. (1998). Flussaufweitungen - Morphologie, Geschiebehaushalt und Grundsätze zur Bemessung (River widenings - morphology, bed-load balance, and design guidelines). *VAW-Mitteilung 159* (H.E. Minor, ed.). Laboratory of Hydraulics, Hydrology and Glaciology, ETH Zurich, Switzerland (in German).

Hunzinger, L. (2004). Flussaufweitungen: Möglichkeiten und Grenzen (River widenings: Opportunities and limitations). *Wasser Energie Luft*, 96(9/10): 243–249 (in German).

HZP (2004). Geschiebehaushalt Kander (Bed-load balance Kander River). *Technical Report*, Tiefbauamt des Kantons Bern, Amt für Landwirtschaft und Natur des Kantons Bern (unpublished, in German).

Ikeda, S. (1984). Prediction of Alternate Bar Wavelength and Height. *Journal of Hydraulic Engineering*, 110(4): 371–386. https://doi.org/10.1061/(ASCE)0733-9429(1984)110:4(371).

Janssen, P.; Stella, J.C.; Piégay, H.; Räpple, B.; Pont, B.; Faton, J.M.; Cornelissen, J.H.C.; Evette, A. (2020). Divergence of riparian forest composition and functional traits from

natural succession along a degraded river with multiple stressor legacies. *Science of The Total Environment*, 721: 137730. https://doi.org/10.1016/j.scitotenv.2020.137730.

Jungwirth, M.; Muhar, S.; Schmutz, S. (2002). Re–establishing and assessing ecological integrity in riverine landscapes. *Freshwater Biology*, 47(4): 867–887. https://doi.org/10.1046/j.1365-2427.2002.00914.x.

Jäggi, M.N.R. (1983). Alternierende Kiesbänke (Alternate gravel bars). *VAW-Mitteilung 62* (D. Vischer, ed.). Laboratory of Hydraulics, Hydrology and Glaciology, ETH Zurich, Switzerland (in German).

Jäggi, M.N.R. (1986). Non distorted models for research on river morphology. *Proc. Symposium on Scale Effects in Modelling Sediment Transport Phenomena*. *International Association for Hydro-Environment Engineering and Research (IAHR)*, Toronto, Canada: 70–84.

Jähnig, S.C.; Brunzel, S.; Gacek, S.; Lorenz, A.W.; Hering, D. (2009). Effects of Re-Braiding Measures on Hydromorphology, Floodplain Vegetation, Ground Beetles and Benthic Invertebrates in Mountain Rivers. *Journal of Applied Ecology*, 46(2): 406–416. https://doi.org/10.1111/j.1365-2664.2009.01611.x.

Kleinhans, M.G.; van den Berg, J.H. (2011). River channel and bar patterns explained and predicted by an empirical and a physics-based method. *Earth Surface Processes and Landforms*, 36(6): 721–738. https://doi.org/10.1002/esp.2090.

Klösch, M.; Blamauer, B.; Habersack, H. (2015). Intra-event scale bar–bank interactions and their role in channel widening. *Earth Surface Processes and Landforms*, 40(11): 1506–1523. https://doi.org/10.1002/esp.3732.

Klösch, M.; Hornich, R.; Baumann, N.; Puchner, G.; Habersack, H. (2011). Mitigating Channel Incision Via Sediment Input and Self-Initiated Riverbank Erosion at the Mur River, Austria: 319–336. In: A. Simon; S.J. Bennett (eds.) Stream Restoration in Dynamic Fluvial Systems. ISBN 978-11-186666-7-8. *American Geophysical Union (AGU)*. https://doi.org/10.1029/2010GM000977.

Kondolf, G. (1997). Hungry water: Effects of dams and gravel mining on river channels. *Environmental Management*, 21(4): 533–551. https://doi.org/10.1007/s002679900048.

Kondolf, G.M.; Boulton, A.J.; O'Daniel, S.; Poole, G.C.; Rahel, F.J.; Stanley, E.H.; Wohl, E.; Bång, A.; Carlstrom, J.; Cristoni, C.; Huber, H.; Koljonen, S.; Louhi, P.; Nakamura, K. (2006). Process-Based Ecological River Restoration: Visualizing Three-Dimensional Connectivity and Dynamic Vectors to Recover Lost Linkages. *Ecology and Society*, 11(2). https://www.jstor.org/stable/26266026.

Kondolf, G.M.; Gao, Y.; Annandale, G.W.; Morris, G.L.; Jiang, E.; Zhang, J.; Cao, Y.; Carling, P.; Fu, K.; Guo, Q.; Hotchkiss, R.; Peteuil, C.; Sumi, T.; Wang, H.W.; Wang, Z.; Wei, Z.; Wu, B.; Wu, C.; Yang, C.T. (2014). Sustainable sediment management in reservoirs and regulated rivers: Experiences from five continents. *Earth's Future*, 2(5): 256–280. https://doi.org/10.1002/2013EF000184.

Kurth, A.; Schirmer, M. (2014). Thirty years of river restoration in Switzerland: implemented measures and lessons learned. *Environmental Earth Sciences*, 72: 2065–2079. https://doi.org/10.1007/s12665-014-3115-y.

Künzi, R.; Kimmerle, R. (2017). Kander Augand. Erfahrungen und Lehren aus dem Festlegen von Interventionslinien (Kander Augand. Experiences and lessons learned from setting intervention lines). *Ingenieurbiologie*, 27(2): 27–30 (in German).

Lacey, G. (1930). Stable Channels in Alluvium. *Minutes of the Proceedings of the Institution of Civil Engineers*, 229(1930): 259–292. 10.1680/imotp.1930.15592.

Lachat, T.; Pauli, D.; Gonseth, Y.; Klaus, G.; Scheidegger, C.; Vittoz, P.; Walter T. (Eds.) (2010). Wandel der Biodiversität in der Schweiz seit 1900. Ist die Talsohle erreicht? (Biodiversity changes in Switzerland since 1900. Has a bottom been reached?). ISBN 978-3-258-07569-3. *Haupt Verlag*, Bern, Switzerland (in German).

Lake, P.S. (2000). Disturbance, patchiness, and diversity in streams. *Journal of the North American Benthological Society*, 19(4): 573–592. https://doi.org/10.2307/1468118.

Lancaster, J. (2000). Geometric scaling of microhabitat patches and their efficacy as refugia during disturbance. *Journal of Animal Ecology*, 69(3): 442–457. https://doi.org/10.1046/j.1365-2656.2000.00407.x.

Lancaster, J.; Belyea, L.R. (1997). Nested Hierarchies and Scale-Dependence of Mech-

anisms of Flow Refugium Use. *Journal of the North American Benthological Society*, 16(1): 221–238. https://doi.org/10.2307/1468253.

Lancaster, J.; Hildrew, A.G. (1993). Characterizing In-stream Flow Refugia. *Canadian Journal of Fisheries and Aquatic Sciences*, 50(8): 1663–1675. https://doi.org/10.1139/f93-187.

Lane, E. (1955). The importance of fluvial morphology in hydraulic engineering. *Proceedings of the American Society of Civil Engineers*, 81.

Lane, S.N.; Westaway, R.M.; Murray Hicks, D. (2003). Estimation of erosion and deposition volumes in a large, gravel-bed, braided river using synoptic remote sensing. *Earth Surface Processes and Landforms*, 28(3): 249–271. https://doi.org/10.1002/esp.483.

Lave, R. (2009). The Controversy Over Natural Channel Design: Substantive Explanations and Potential Avenues for Resolution. *Journal of the American Water Resources Association*, 45(6): 1519–1532. https://doi.org/10.1111/j.1752-1688.2009.00385.x.

Leopold, L.B.; Maddock, T. (1953). *The hydraulic geometry of stream channels and some physiographic implicationsUSGS Numbered Series 252*. *US Government Printing Office*, Washington, D.C..

Leopold, L.B.; Wolman, M.G. (1957). *River channel patterns: braided, meandering, and straightUSGS Numbered Series 282*. *US Government Printing Office*, Washington, D.C..

Lepori, F.; Hjerdt, N. (2006). Disturbance and Aquatic Biodiversity: Reconciling Contrasting Views. *BioScience*, 56(10): 809–818. https://doi.org/10.1641/0006-3568(2006)56[809:DAABRC]2.0.CO;2.

Lisle, T.E.; Iseya, F.; Ikeda, H. (1993). Response of a channel with alternate bars to a decrease in supply of mixed-size bed load: A flume experiment. *Water Resources Research*, 29(11): 3623–3629. https://doi.org/10.1029/93WR01673.

MacKenzie, L.G.; Eaton, B.C. (2017). Large grains matter: contrasting bed stability and morphodynamics during two nearly identical experiments. *Earth Surface Processes and Landforms*, 42(8): 1287–1295. https://doi.org/10.1002/esp.4122.

Madej, M.A.; Sutherland, D.G.; Lisle, T.E.; Pryor, B. (2009). Channel responses to varying sediment input: A flume experiment modeled after Redwood Creek, California. *Geomorphology*, 103(4): 507–519. https://doi.org/10.1016/j.geomorph.2008.07.017.

Makaske, B.; Smith, D.G.; Berendsen, H.J.; de Boer, A.G.; van Nielen-Kiezebrink, M.F.; Locking, T. (2009). Hydraulic and sedimentary processes causing anastomosing morphology of the upper Columbia River, British Columbia, Canada. *Geomorphology*, 111(3): 194–205. https://doi.org/10.1016/j.geomorph.2009.04.019.

Mannes, S.; Robinson, C.T.; Uehlinger, U.; Scheurer, T.; Ortlepp, J.; Mürle, U.; Molinari, P. (2008). Ecological effects of a long-term flood program in a flow-regulated river. *Journal of alpine research*, 96(1): 125–134. https://doi.org/10.4000/rga.450.

Marti, C. (2006). Morphologie von verzweigten Gerinnen - Ansätze zur Abfluss-, Geschiebetransport- und Kolktiefenberechnung (Morphology of braided rivers - Approaches for discharge, bed-load transport, and scour depth estimation). *VAW-Mitteilung 199* (H.E. Minor, ed.). Laboratory of Hydraulics, Hydrology and Glaciology, ETH Zurich, Switzerland (in German).

Martínez-Fernández, V.; González, E.; López-Almansa, J.C.; González, S.M.; García de Jalón, D. (2017). Dismantling artificial levees and channel revetments promotes channel widening and regeneration of riparian vegetation over long river segments. *Ecological Engineering*, 108: 132–142. https://doi.org/10.1016/j.ecoleng.2017.08.005.

Mathers, K.L.; Hill, M.J.; Wood, C.D.; Wood, P.J. (2019). The role of fine sediment characteristics and body size on the vertical movement of a freshwater amphipod. *Freshwater Biology*, 64(1): 152–163. https://doi.org/10.1111/fwb.13202.

Mathers, K.L.; Kowarik, C.; Rachelly, C.; Robinson, C.T.; Weber, C. (2021). The effects of sediment traps on instream habitat and macroinvertebrates of mountain streams. *Journal of Environmental Management*, 295: 113066. https://doi.org/10.1016/j.jenvman.2021.113066.

Matthaei, C.D.; Arbuckle, C.J.; Townsend, C.R. (2000). Stable surface stones as refugia for invertebrates during disturbance in a New Zealand stream. *Journal of the North American Benthological Society*, 19(1): 82–93. https://doi.org/10.2307/1468283.

Matthaei, C.D.; Townsend, C.R. (2000). Inundated floodplain gravels in a stream with an unstable bed: Temporary shelter or true invertebrate refugium? *New Zealand Journal of Marine and Freshwater Research*, 34(1): 147–156. https://doi.org/10.1080/00288330.2000.9516922.

McDonald, A.; Lane, S.N.; Haycock, N.E.; Chalk, E.A. (2004). Rivers of dreams: on the gulf between theoretical and practical aspects of an upland river restoration. *Transactions of the Institute of British Geographers*, 29(3): 257–281. https://doi.org/10.1111/j.0020-2754.2004.00314.x.

Millar, R.G. (2005). Theoretical regime equations for mobile gravel-bed rivers with stable banks. *Geomorphology*, 64(3): 207–220. https://doi.org/10.1016/j.geomorph.2004.07.001.

Moretto, J.; Rigon, E.; Mao, L.; Picco, L.; Delai, F.; Lenzi, M.A. (2014). Channel adjustments and island dynamics in the Brenta River (Italy) over the last 30 years. *River Research and Applications*, 30(6): 719–732. https://doi.org/10.1002/rra.2676.

Morgan, J.A.; Nelson, P.A. (2021). Experimental investigation of the morphodynamic response of riffles and pools to unsteady flow and increased sediment supply. *Earth Surface Processes and Landforms*, 46(4): 869–886. https://doi.org/10.1002/esp.5072.

Métivier, F.; Devauchelle, O.; Chauvet, H.; Lajeunesse, E.; Meunier, P.; Blanckaert, K.; Ashmore, P.; Zhang, Z.; Fan, Y.; Liu, Y.; Dong, Z.; Ye, B. (2016). Geometry of meandering and braided gravel-bed threads from the Bayanbulak Grassland, Tianshan, P. R. China. *Earth Surface Dynamics*, 4(1): 273–283. https://doi.org/10.5194/esurf-4-273-2016.

Métivier, F.; Lajeunesse, E.; Devauchelle, O. (2017). Laboratory rivers: Lacey's law, threshold theory, and channel stability. *Earth Surface Dynamics*, 5(1): 187–198. https://doi.org/10.5194/esurf-5-187-2017.

Naiman, R.; Decamps, H.; Pollock, M. (1993). The Role of Riparian Corridors in Maintaining Regional Biodiversity. *Ecological Applications*, 3(2): 209–212. https://doi.org/10.2307/1941822.

National Research Council (1992). Restoration of aquatic ecosystems; science, technology, and public policy. *Technical Report*, National Academy Press, Washington, D.C.

Negishi, J.N.; Inoue, M.; Nunokawa, M. (2002). Effects of channelisation on stream habitat in relation to a spate and flow refugia for macroinvertebrates in northern Japan. *Freshwater Biology*, 47(8): 1515–1529. https://doi.org/10.1046/j.1365-2427.2002.00877.x.

Nelson, P.A.; Brew, A.K.; Morgan, J.A. (2015). Morphodynamic response of a variable-width channel to changes in sediment supply. *Water Resources Research*, 51(7): 5717–5734. https://doi.org/10.1002/2014WR016806.

Nelson, P.A.; Morgan, J.A. (2018). Flume experiments on flow and sediment supply controls on gravel bedform dynamics. *Geomorphology*, 323: 98–105. https://doi.org/10.1016/j.geomorph.2018.09.011.

Nelson, P.A.; Venditti, J.G.; Dietrich, W.E.; Kirchner, J.W.; Ikeda, H.; Iseya, F.; Sklar, L.S. (2009). Response of bed surface patchiness to reductions in sediment supply. *Journal of Geophysical Research: Earth Surface*, 114(F2): F02005. https://doi.org/10.1029/2008JF001144.

Nieto Medina, M. (2021). Numerical simulation of dynamic river widenings induced by alternate bars. *Project Thesis*, VAW, ETH Zurich, Switzerland (unpublished).

Palmer, M.; Bernhardt, E.; Allan, J.D.; Lake, P.; Alexander, G.; Brooks, S.; Carr, J.; Clayton, S.; Dahm, C.N.; Follstad Shah, J.; Galat, D.L.; Loss, S.G.; Goodwin, P.; Hart, D.; Hassett, B.; Jenkinson, R.; Kondolf, G.; Lave, R.; Meyer, J.; O'Donnell, T.; Pagano, L.; Sudduth, E. (2005). Standards for ecologically successful river restoration: Ecological success in river restoration. *Journal of Applied Ecology*, 42(2): 208–217. https://doi.org/10.1111/j.1365-2664.2005.01004.x.

Palmer, M.A.; Menninger, H.L.; Bernhardt, E. (2010). River restoration, habitat heterogeneity and biodiversity: a failure of theory or practice? *Freshwater Biology*, 55(s1): 205–222. https://doi.org/10.1111/j.1365-2427.2009.02372.x.

Parker, G. (1979). Hydraulic Geometry of Active Gravel Rivers. *Journal of the Hydraulics Division*, 105(9): 1185–1201. https://doi.org/10.1061/JYCEAJ.0005275.

Parker, G.; Klingeman, P.C. (1982). On why gravel bed streams are paved. *Water Resources Research*, 18(5): 1409–1423. https://doi.org/10.1029/WR018i005p01409.

Pearsons, T.N.; Li, H.W.; Lamberti, G.A. (1992). Influence of Habitat Complexity on Resistance to Flooding and Resilience of Stream Fish Assemblages. *Transactions of the American Fisheries Society*, 121(4): 427–436. https://doi.org/10.1577/1548-8659(1992)121<0427:IOHCOR>2.3.CO;2.

Pfeiffer, A.M.; Finnegan, N.J.; Willenbring, J.K. (2017). Sediment supply controls equilibrium channel geometry in gravel rivers. *Proceedings of the National Academy of Sciences*, 114(13): 3346–3351. https://doi.org/10.1073/pnas.1612907114.

Piton, G.; Recking, A. (2016). Design of Sediment Traps with Open Check Dams. I: Hydraulic and Deposition Processes. *Journal of Hydraulic Engineering*, 142(2): 04015045. https://doi.org/10.1061/(ASCE)HY.1943-7900.0001048.

Piégay, H.; Darby, S.E.; Mosselman, E.; Surian, N. (2005). A review of techniques available for delimiting the erodible river corridor: a sustainable approach to managing bank erosion. *River Research and Applications*, 21(7): 773–789. https://doi.org/10.1002/rra.881.

PL-LCH (2010). Aménagement de la Broye à Villeneuve - Hydraulique, morphologie et sécurité. (Development of the Broye River at Villeneuve - Hydraulics, Morphology, and flood safety.). *Technical Report 05/2010*, Platform of Hydraulic Constructions, EPFL Lausanne, Switzerland (unpublished, in French).

Podolak, C.J.P.; Wilcock, P.R. (2013). Experimental study of the response of a gravel streambed to increased sediment supply. *Earth Surface Processes and Landforms*, 38(14): 1748–1764. https://doi.org/10.1002/esp.3468.

Poff, N.L.; Allan, J.D.; Bain, M.B.; Karr, J.R.; Prestegaard, K.L.; Richter, B.D.; Sparks, R.E.; Stromberg, J.C. (1997). The natural flow regime: a paradigm for river conservation and restoration. *BioScience*, 47(11): 769. https://doi.org/10.2307/1313099.

Polvi, L.E.; Lind, L.; Persson, H.; Miranda-Melo, A.; Pilotto, F.; Su, X.; Nilsson, C. (2020). Facets and scales in river restoration: Nestedness and interdependence of hy-

drological, geomorphic, ecological, and biogeochemical processes. *Journal of Environmental Management*, 265: 110288. https://doi.org/10.1016/j.jenvman.2020.110288.

QGIS (2021). QGIS Geographic Information System. Open Source Geospatial Foundation Project. https://qgis.org.

Rachelly, C.; Friedl, F.; Boes, R.M.; Weitbrecht, V. (2021a). Morphological Response of Channelized, Sinuous Gravel-Bed Rivers to Sediment Replenishment. *Water Resources Research*, 57(6): e2020WR029178. https://doi.org/10.1029/2020WR029178.

Rachelly, C.; Mathers, K.L.; Weber, C.; Weitbrecht, V.; Boes, R.M.; Vetsch, D.F. (2021b). How does sediment supply influence refugia availability in river widenings? *Journal of Ecohydraulics*, 6(2): 121–138. https://doi.org/10.1080/24705357.2020.1831415.

Rachelly, C.; Vetsch, D.F.; Boes, R.M.; Weitbrecht, V. (2021c). Dataset for the research project "Sediment supply control on river widening morphodynamics". ETH Research Collection. https://doi.org/10.3929/ethz-b-000509319.

Rachelly, C.; Vetsch, D.F.; Boes, R.M.; Weitbrecht, V. (2022). Sediment supply control on morphodynamic processes in gravel-bed river widenings [Manuscript submitted for publication.].

Rachelly, C.; Weitbrecht, V.; Vetsch, D.F.; Boes, R.M. (2018). Morphological development of river widenings with variable sediment supply. *E3S Web Conf.*, 40: 02007. https://10.1051/e3sconf/20184002007.

Reid, D.A.; Hassan, M.A.; Bird, S.; Pike, R.; Tschaplinski, P. (2020). Does variable channel morphology lead to dynamic salmon habitat? *Earth Surface Processes and Landforms*, 45(2): 295–311. https://doi.org/10.1002/esp.4726.

Rempel, L.L.; Richardson, J.S.; Healey, M.C. (1999). Flow Refugia for Benthic Macroinvertebrates during Flooding of a Large River. *Journal of the North American Benthological Society*, 18(1): 34–48. https://doi.org/10.2307/1468007.

Requena, P. (2008). Seitenerosion in kiesführenden Flüssen, Prozessverständnis und quantitative Beschreibung (Lateral erosion in gravel-bed rivers, process and quantitative description). *VAW-Mitteilung 210* (H.E. Minor, ed.). Laboratory of Hy-

draulics, Hydrology and Glaciology, ETH Zurich, Switzerland. https://doi.org/10.3929/ethz-a-005714430 (in German).

Requena, P.; Bezzola, G.R.; Minor, H.E. (2005). Aufweitungen in erodierenden Flüssen (Widenings in eroding rivers). *Wasser Energie Luft*, 97(7/8): 183–189 (in German).

Resh, V.H.; Brown, A.V.; Covich, A.P.; Gurtz, M.E.; Li, H.W.; Minshall, G.W.; Reice, S.R.; Sheldon, A.L.; Wallace, J.B.; Wissmar, R.C. (1988). The Role of Disturbance in Stream Ecology. *Journal of the North American Benthological Society*, 7(4): 433–455. https://doi.org/10.2307/1467300.

Reynolds, C.; Carling, P.; Beven, K. (1991). Flow in River Channels - New Insights into Hydraulic Retention. *Archive for Hydrobiology*, 121(2): 171–179.

Rice, S.P.; Buffin-Bélanger, T.; Lancaster, J.; Reid, I. (2007). Movements of a macroinvertebrate (Potamophylax latipennis) across a gravel-bed substrate: effects of local hydraulics and micro-topography under increasing discharge: 637–659. In: H. Habersack; H. Piégay; M. Rinaldi (eds.) Gravel-Bed Rivers VI: From Process Understanding to River Restoration. *Elsevier*. https://doi.org/10.1016/S0928-2025(07)11152-4.

Ritchie, A.; Warrick, J.; East, A.; Magirl, C.; Stevens, A.; Bountry, J.; Randle, T.; Curran, C.; Hilldale, R.; Duda, J.; Gelfenbaum, G.; Miller, I.; Pess, G.; Foley, M.; McCoy, R.; Ogston, A. (2018). Morphodynamic evolution following sediment release from the world's largest dam removal. *Scientific Reports*, 8: 13279. https://doi.org/10.1038/s41598-018-30817-8.

Rohde, S.; Schütz, M.; Kienast, F.; Englmaier, P. (2005). River widening: an approach to restoring riparian habitats and plant species. *River Research and Applications*, 21(10): 1075–1094. https://doi.org/10.1002/rra.870.

Roni, P.; Hanson, K.; Beechie, T. (2008). Global Review of the Physical and Biological Effectiveness of Stream Habitat Rehabilitation Techniques. *North American Journal of Fisheries Management*, 28(3): 856–890. https://doi.org/10.1577/M06-169.1.

Schalko, I.; Wohl, E.; Nepf, H. (2021). Flow and wake characteristics associated with large wood to inform river restoration. *Scientific Reports*, 11: 8644. https://doi.org/10.1038/s41598-021-87892-7.

Schinegger, R.; Trautwein, C.; Melcher, A.; Schmutz, S. (2012). Multiple human pressures and their spatial patterns in European running waters. *Water and Environment Journal*, 26(2): 261–273. https://doi.org/10.1111/j.1747-6593.2011.00285.x.

Schmocker-Fackel, P.; Hüsler, F.; Oosenbrug, E.; Lanz, K.; Zahner, S.; Wieser, E. (2021). Effects of climate change on Swiss water bodies. Hydrology, water ecology and water management. *Technical Report 2101*, Federal Office for the Environment (FOEN), Bern, Switzerland.

Schwartz, J.S.; Herricks, E.E. (2005). Fish use of stage-specific fluvial habitats as refuge patches during a flood in a low-gradient Illinois stream. *Canadian Journal of Fisheries and Aquatic Sciences*, 62(7): 1540–1552. https://doi.org/10.1139/f05-060.

Schälchli, U.; Kirchhofer, A. (2012). Sanierung Geschiebehaushalt. Strategische Planung. Ein Modul der Vollzugshilfe Renaturierung der Gewässer. (Restoration bed-load transport. Strategical Planning. A module of the implementation guide for river restoration.). *Technical Report 1226*, Federal Office for the Environment (FOEN), Bern, Switzerland (in German).

Scorpio, V.; Zen, S.; Bertoldi, W.; Surian, N.; Mastronunzio, M.; Prá, E.D.; Zolezzi, G.; Comiti, F. (2018). Channelization of a large alpine river: What is left of its original morphodynamics? *Earth Surface Processes and Landforms*, 43(5): 1044–1062. https://doi.org/10.1002/esp.4303.

Sedell, J.R.; Reeves, G.H.; Hauer, F.R.; Stanford, J.A.; Hawkins, C.P. (1990). Role of refugia in recovery from disturbances: modern fragmented and disconnected river systems. *Environmental Management*, 14(5): 711–724. https://doi.org/10.1007/BF02394720.

Siviglia, A.; Repetto, R.; Zolezzi, G.; Tubino, M. (2008). River bed evolution due to channel expansion: general behaviour and application to a case study (Kugart River, Kyrgyz Republic). *River Research and Applications*, 24(9): 1271–1287. https://doi.org/10.1002/rra.1095.

Smith, N.D.; Smith, D.G. (1984). William River: An outstanding example of channel widening and braiding caused by bed-load addition. *Geology*, 12(2): 78–82. https://doi.org/10.1130/0091-7613(1984)12<78:WRAOEO>2.0.CO;2.

Stadtmann, P. (2020). Numerische Simulation von Seitenerosionsprozessen in Flussaufweitungen (Numerical simulation of lateral erosion processes in river widenings). *Master Thesis*, VAW, ETH Zurich, Switzerland (in German).

Stanford, J.A.; Lorang, M.S.; Hauer, F.R. (2005). The shifting habitat mosaic of river ecosystems. *SIL Proceedings, 1922-2010*, 29(1): 123–136. https://doi.org/10.1080/03680770.2005.11901979.

Stanford, J.A.; Ward, J.V. (1983). The serial discontinuity concept of lotic ecosystems: 29–42. In: T.D. Fontaine; S.M. Bartell (eds.) Dynamics of lotic ecosystems. *Ann Arbor Science Publishers*, Ann Arbor, MI.

Stanford, J.A.; Ward, J.V. (1993). An Ecosystem Perspective of Alluvial Rivers: Connectivity and the Hyporheic Corridor. *Journal of the North American Benthological Society*, 12(1): 48–60. https://doi.org/10.2307/1467685.

Stevenson, J.A.; Sun, X.; Mitchell, N.C. (2010). Despeckling SRTM and other topographic data with a denoising algorithm. *Geomorphology*, 114(3): 238–252. https://doi.org/10.1016/j.geomorph.2009.07.006.

Stocker, B. (2019). Eigendynamische Flussaufweitungen: Entwicklung eines bildbasierten Algorithmus zur Uferdetektion im hydraulischen Modellversuch (Dynamic river widenings: Development of an image-based edge detection algorithm for hydraulic laboratory experiments). *Master Thesis*, VAW, ETH Zurich, Switzerland (unpublished, in German).

Strickler, A. (1923). Beiträge zur Frage der Geschwindigkeitsformel und der Rauhigkeitszahlen für Ströme, Kanäle und geschlossene Leitungen (Contributions to the Question of a Velocity Formula and Roughness Data for Streams, Channels and Closed Pipelines). *Mitteilungen des Eidgenössischen Amtes für Wasserwirtschaft 16*. Bern, Switzerland (in German).

Stubbington, R. (2012). The hyporheic zone as an invertebrate refuge: a review of variability in space, time, taxa and behaviour. *Marine and Freshwater Research*, 63(4): 293–311. https://doi.org/10.1071/MF11196.

Sueyoshi, M.; Nakano, D.; Nakamura, F. (2014). The relative contributions of refugium types to the persistence of benthic invertebrates in a seasonal snowmelt flood. *Freshwater Biology*, 59(2): 257–271. https://doi.org/10.1111/fwb.12262.

Sun, X.; Rosin, P.L.; Martin, R.; Langbein, F. (2007). Fast and Effective Feature-Preserving Mesh Denoising. *IEEE Transactions on Visualization and Computer Graphics*, 13(5): 925–938. https://doi.org/10.1109/TVCG.2007.1065.

Surian, N.; Rinaldi, M. (2003). Morphological response to river engineering and management in alluvial channels in Italy. *Geomorphology*, 50(4): 307–326. https://doi.org/10.1016/S0169-555X(02)00219-2.

Swanson, F.J.; Johnson, S.L.; Gregory, S.V.; Acker, S.A. (1998). Flood Disturbance in a Forested Mountain Landscape. *BioScience*, 48(9): 681–689. https://doi.org/10.2307/1313331.

swisstopo (2018). swissBOUNDARIES3D. Federal Office of Topography (swisstopo). https://opendata.swiss/en/dataset/swissboundaries3d-landesgrenzen (accessed October 22, 2018).

Syvitski, J.P.M.; Vörösmarty, C.J.; Kettner, A.J.; Green, P. (2005). Impact of Humans on the Flux of Terrestrial Sediment to the Global Coastal Ocean. *Science*, 308(5720): 376–380. https://doi.org/10.1126/science.1109454.

Tal, M.; Paola, C. (2010). Effects of vegetation on channel morphodynamics: results and insights from laboratory experiments. *Earth Surface Processes and Landforms*, 35(9): 1014–1028. https://doi.org/10.1002/esp.1908.

Tockner, K.; Stanford, J.A. (2002). Riverine flood plains: present state and future trends. *Environmental Conservation*, 29(3): 308–330. https://doi.org/10.1017/S037689290200022X.

Toro, E.F. (2001). Shock-Capturing Methods for Free-Surface Shallow Flows. *Wiley and Sons Ltd*, Chichester, UK.

Townsend, C.R. (1989). The Patch Dynamics Concept of Stream Community Ecology. *Journal of the North American Benthological Society*, 8(1): 36–50. https://doi.org/10.2307/1467400.

Townsend, C.R.; Scarsbrook, M.R.; Dolédec, S. (1997). The intermediate disturbance hypothesis, refugia, and biodiversity in streams. *Limnology and Oceanography*, 42(5): 938–949. https://doi.org/10.4319/lo.1997.42.5.0938.

van den Berg, J.H. (1995). Prediction of alluvial channel pattern of perennial rivers. *Geomorphology*, 12(4): 259–279. https://doi.org/10.1016/0169-555X(95)00014-V.

van der Nat, D.; Schmidt, A.P.; Tockner, K.; Edwards, P.J.; Ward, J.V. (2002). Inundation Dynamics in Braided Floodplains: Tagliamento River, Northeast Italy. *Ecosystems*, 5: 0636–0647. https://doi.org/10.1007/s10021-002-0170-0.

Vannote, R.L.; Minshall, G.W.; Cummins, K.W.; Sedell, J.R.; Cushing, C.E. (1980). The river continuum concept. *Canadian journal of fisheries and aquatic sciences*, 37(1): 130–137. https://doi.org/10.1139/f80-017.

Vanzo, D.; Peter, S.; Vonwiller, L.; Bürgler, M.; Weberndorfer, M.; Siviglia, A.; Conde, D.; Vetsch, D.F. (2021). Basement v3: a modular freeware for river process modelling over multiple computational backends. *Environmental Modelling & Software*: 105102. https://doi.org/10.1016/j.envsoft.2021.105102.

Vanzo, D.; Zolezzi, G.; Siviglia, A. (2016). Eco-hydraulic modelling of the interactions between hydropeaking and river morphology. *Ecohydrology*, 9(3): 421–437. https://doi.org/10.1002/eco.1647.

Vargas-Luna, A.; Duró, G.; Crosato, A.; Uijttewaal, W. (2019). Morphological adaptation of river channels to vegetation establishment: A laboratory study. *Journal of Geophysical Research: Earth Surface*, 124(7): 1981–1995. https://doi.org/10.1029/2018JF004878.

VAW (1993). Strada. Flussmorphologisches Gutachten zur geplanten lnnrevitalisierung im Zusammenhang mit der Umfahrungsstrasse Strada (Strada. Morphological report on the planned restoration of the Inn River in connection with the bypass Strada). *Technical Report 4064*, Laboratory of Hydraulics, Hydrology and Glaciology, ETH Zurich, Switzerland (unpublished, in German).

VAW (2006). Flussaufweitungen - Möglichkeiten und Grenzen, Workshop der VAW vom 4. Oktober 2006 (River widenings - opportunities and limitations, workshop at VAW

held October 4 2006). *VAW-Mitteilung 200* (H.E. Minor, ed.). Laboratory of Hydraulics, Hydrology and Glaciology, ETH Zurich, Switzerland (in German).

VAW (2007). Morphologische Entwicklungen in Flussaufweitungen. Analyse von 14 Aufweitungen hinsichtlich der Auswirkungen auf die Sohlenentwicklung (Morphological developments in river widenings. Analysis of 14 widenings with regard to their impact on the bed evolution). *Technical Report 4234*, Laboratory of Hydraulics, Hydrology and Glaciology, ETH Zurich, Switzerland (unpublished, in German).

VAW (2008). Blockrampen Landquart. Hydraulische Modellversuche zu klassischen und aufgelösten Blockrampen. (Block ramps Landquart. Hydraulic model tests on classic and unstructured block ramps.). *Technical Report 4236*, Laboratory of Hydraulics, Hydrology and Glaciology, ETH Zurich, Switzerland (unpublished, in German).

VAW (2009). Hochwasserschutz Linth 2000, Flussaufweitung Chli Gäsitschachen. (Flood protection Linth 2000, river widening Chli Gäsitschachen.). *Technical Report 4245*, Laboratory of Hydraulics, Hydrology and Glaciology, ETH Zurich, Switzerland (unpublished, in German).

VAW (2019). Flussbauliches Monitoring Dynamisierung Töss 'Mittlere Aue'. (Montitoring of dynamization Töss River 'Mittlere Aue'.). *Technical Report 4291*, Laboratory of Hydraulics, Hydrology and Glaciology, ETH Zurich, Switzerland (unpublished, in German).

Venditti, J.G.; Nelson, P.A.; Bradley, R.W.; Haught, D.; Gitto, A.B. (2017). Bedforms, Structures, Patches, and Sediment Supply in Gravel-Bed Rivers: 439–466. In: D. Tsutsumi; J.B. Laronne (eds.) Gravel-Bed Rivers: Processes and Disasters. ISBN 978-1-118-97140-6. *John Wiley & Sons, Ltd*. https://doi.org/10.1002/9781118971437.ch16.

Venditti, J.G.; Nelson, P.A.; Minear, J.T.; Wooster, J.; Dietrich, W.E. (2012). Alternate bar response to sediment supply termination. *Journal of Geophysical Research: Earth Surface*, 117(F2): F02039. https://doi.org/10.1029/2011JF002254.

Vetsch, D.F.; Allen, J.; Belser, A.; Boes, R.M.; Brodersen, J.; Fink, S.; Franca, M.J.; Juez, C.; Nadyeina, O.; Robinson, C.T.; Scheidegger, C.; Schleiss, A.; Siviglia, A.; Weber, C.; Weitbrecht, V. (2018). Lebensraum Gewässer - Sedimentdynamik und Vernetzung:

Forschungsprogramm *Wasserbau und Ökologie* (Riverscapes - Sediment dynamics and lateral connectivity: Research program *Hydraulic engineering and ecology*). *Wasser Energie Luft*, 110(1): 19–24 (in German).

Vetsch, D.F.; Siviglia, A.; Bacigaluppi, P.; Bürgler, M.; Caponi, F.; Conde, D.; Gerke, E.; Kammerer, S.; Koch, A.; Peter, S.; Vanzo, D.; Vonwiller, L.; Weberndorfer, M. (2021). System Manuals of BASEMENT, Version 3.1.1. Laboratory of Hydraulics, Hydrology and Glaciology (VAW), ETH Zurich. https://basement.ethz.ch/download/documentation/docu3.html.

Vonwiller, L. (2018). Numerical Modeling of Morphological Response of Gravel-Bed Rivers to Sediment Supply. *VAW-Mitteilung 246* (R.M. Boes, ed.). Laboratory of Hydraulics, Hydrology and Glaciology, ETH Zurich, Switzerland. https://doi.org/10.3929/ethz-b-000267914.

Ward, J.V. (1989). The four-dimensional nature of lotic ecosystems. *Journal of the North American Benthological Society*, 8(1): 2–8. https://doi.org/10.2307/1467397.

Ward, J.V.; Tockner, K.; Schiemer, F. (1999). Biodiversity of floodplain river ecosystems: ecotones and connectivity. *Regulated Rivers: Research & Management*, 15(1-3): 125–139. https://doi.org/10.1002/(SICI)1099-1646(199901/06)15:1/3<125::AID-RRR523>3.0.CO;2-E.

Ward, J.W.; Stanford, J.A. (1983). Intermediate-disturbance hypothesis: an explanation for biotic diversity patterns in lotic ecosystems: 347–356. In: T. Fontaine; S. Bartell (eds.) Dynamics of Lotic Systems. *Ann Arbor Science Publishers*, Ann Arbor, MI.

Weber, C.; Nilsson, C.; Lind, L.; Alfredsen, K.T.; Polvi, L.E. (2013). Winter Disturbances and Riverine Fish in Temperate and Cold Regions. *BioScience*, 63(3): 199–210. https://doi.org/10.1525/bio.2013.63.3.8.

Weber, C.; Schager, E.; Peter, A. (2009). Habitat diversity and fish assemblage structure in local river widenings: A case study on a Swiss river. *River Research and Applications*, 25(6): 687–701. https://doi.org/10.1002/rra.1176.

Weber, C.; Sprecher, L.; Åberg, U.; Thomas, G.; Baumgartner, S.; Haertel-Borer, S. (2019). Zusammenfassung und Inhalt. In: Wirkungskontrolle Revitalisierung - Gemein-

sam lernen für die Zukunft. (Summary and content. In: Impact monitoring restoration - Collaborative learning for the future.). *Technical Report 0, V1.02.*, Federal Office for the Environment (FOEN), Bern, Switzerland (in German).

Williams, D.D.; Hynes, H.B.N. (1976). The Recolonization Mechanisms of Stream Benthos. *Oikos*, 27(2): 265–272. https://doi.org/10.2307/3543905.

Williams, R.; Bangen, S.; Gillies, E.; Kramer, N.; Moir, H.; Wheaton, J. (2020). Let the river erode! Enabling lateral migration increases geomorphic unit diversity. *Science of The Total Environment*, 715: 136817. https://doi.org/10.1016/j.scitotenv.2020.136817.

Winterbottom, J.; Orton, S.; Hildrew, A.; Lancaster, J. (1997). Field experiments on flow refugia in streams. *Freshwater Biology*, 37: 569–580. https://doi.org/10.1046/J.1365-2427.1997.00184.X.

Wohl, E. (2017). Connectivity in rivers. *Progress in Physical Geography: Earth and Environment*, 41(3): 345–362. https://doi.org/10.1177/0309133317714972.

Wohl, E.; Bledsoe, B.P.; Jacobson, R.B.; Poff, N.L.; Rathburn, S.L.; Walters, D.M.; Wilcox, A.C. (2015a). The Natural Sediment Regime in Rivers: Broadening the Foundation for Ecosystem Management. *BioScience*, 65(4): 358–371. https://doi.org/10.1093/biosci/biv002.

Wohl, E.; Kramer, N.; Ruiz-Villanueva, V.; Scott, D.N.; Comiti, F.; Gurnell, A.M.; Piegay, H.; Lininger, K.B.; Jaeger, K.L.; Walters, D.M.; Fausch, K.D. (2019). The Natural Wood Regime in Rivers. *BioScience*, 69(4): 259–273. https://doi.org/10.1093/biosci/biz013.

Wohl, E.; Lane, S.N.; Wilcox, A.C. (2015b). The science and practice of river restoration. *Water Resources Research*, 51(8): 5974–5997. https://doi.org/10.1002/2014WR016874.

Wong, M.; Parker, G. (2006). Reanalysis and Correction of Bed-Load Relation of Meyer-Peter and Müller Using Their Own Database. *Journal of Hydraulic Engineering*, 132(11): 1159–1168. https://doi.org/10.1061/(ASCE)0733-9429(2006)132:11(1159).

Wood, P.J.; Boulton, A.J.; Little, S.; Stubbington, R. (2010). Is the hyporheic zone a refugium for aquatic macroinvertebrates during severe low flow conditions? *Fundamental and Applied Limnology*, 176(4): 377–390. https://doi.org/10.1127/1863-9135/2010/0176-0377.

Woolsey, S.; Weber, C.; Gonser, T.; Hoehn, E.; Hostmann, M.; Junker, B.; Roulier, C.; Schweizer, S.; Tiegs, S.; Tockner, K.; Peter, A. (2005). Handbuch für die Erfolgskontrolle bei Fliessgewässerrevitalisierungen. *Technical Report*, Eawag, WSL, LCH-EPFL, VAW-ETHZ, Federal Office for the Environment (FOEN) (in German).

Yalin, M.; da Silva, A. (2001). Fluvial processes. *International Association for Hydro-Environment Engineering and Research (IAHR)*, Delft, Netherlands.

Yarnell, S.M.; Mount, J.F.; Larsen, E.W. (2006). The influence of relative sediment supply on riverine habitat heterogeneity. *Geomorphology*, 80(3): 310–324. https://doi.org/10.1016/j.geomorph.2006.03.005.

Zarn, B. (1992). Lokale Gerinneaufweitung - eine Massnahme zur Sohlenstabilisierung der Emme bei Utzenstorf (Local channel widening - a bed stabilization measure in the Emme River near Utzenstorf). *VAW-Mitteilung 118* (D. Vischer, ed.). Laboratory of Hydraulics, Hydrology and Glaciology, ETH Zurich, Switzerland (in German).

Zarn, B. (1997). Einfluss der Flussbettbreite auf die Wechselwirkung zwischen Abfluss, Morphologie und Geschiebetransportkapazitat (Influence of channel width on the interaction of discharge, morphology, and bed-load transport capacity). *VAW-Mitteilung 154* (D. Vischer, ed.). Laboratory of Hydraulics, Hydrology and Glaciology, ETH Zurich, Switzerland (in German).

Zarn, B.; Oplatka, M.; Pellandini, S.; Mikos, M.; Hunziker, R.; Jäggi, M. (1995). Geschiebehaushalt Alpenrhein. Neue Erkenntnisse und Prognosen über die Sohlenveränderungen und den Geschiebetransport (Bed-load budget Alpine Rhine. New findings and forecasts on bed elevation changes and bed-load transport). *VAW-Mitteilung 139* (D. Vischer, ed.). Laboratory of Hydraulics, Hydrology and Glaciology, ETH Zurich, Switzerland (in German).

A Appendix

A.1 River widenings in Switzerland

Töss River, Mittlere Au

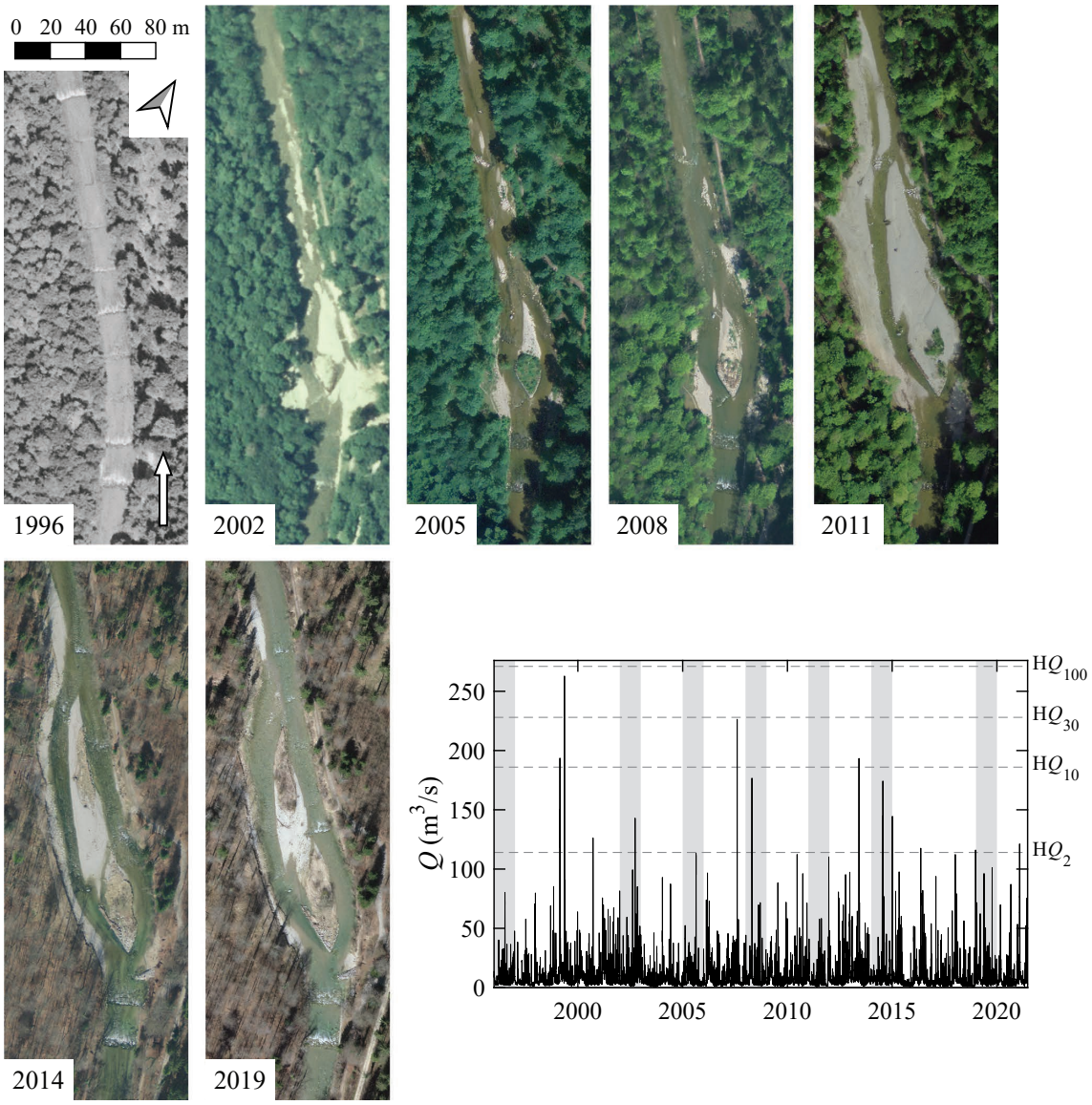

Figure A.1 Temporal evolution of the river widening Mittlere Au, Töss River (47°27′50.215″N 8°43′40.027″E), and discharge time series with orthophoto acquisition years marked in gray (Photos: Federal Office of Topography; discharge data: Federal Office for the Environment)

Table A.1 Characteristics of the river widening Mittlere Au, Töss River

Width (channel → widening)	19 m → 60 m
Slope	0.0062
D_m, D_{90} *	2.5-4 cm, 6-9 cm
Discharge+	no specifications
Bed-load[x]	no specifications
Morphodynamics	Limited morphodynamic activity

*VAW (2019), +HADES (2021), [x]Schälchli and Kirchhofer (2012)

Inn River, Strada

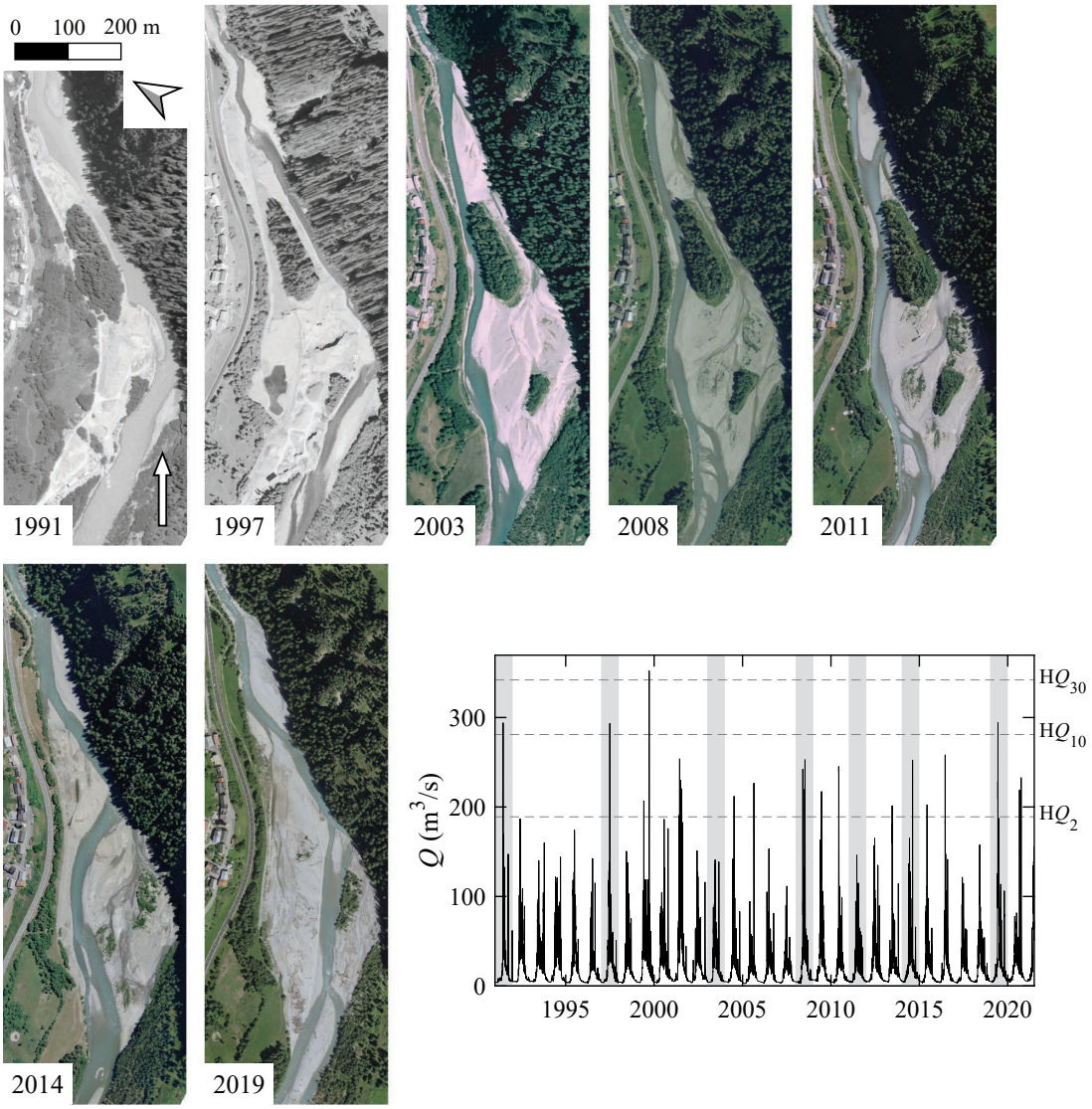

Figure A.2 Temporal evolution of the river widening Strada, Inn River (46°51′37.725″N 10°26′02.998″E), and discharge time series with orthophoto acquisition years marked in gray (Photos: Federal Office of Topography; discharge data: Federal Office for the Environment)

Table A.2 Characteristics of the river widening Strada, Inn River

Width (channel → widening)	35 m → 220 m
Slope	0.0053
D_m, D_{90} *	7.8 cm, 18.9 cm
Discharge$^+$	21-40% of natural yearly discharge remaining
Bed-load^x	50-80% of the natural bed-load remaining
Morphodynamics	Moderate channel widening shifting, evidence of erosion of vegetated areas

*VAW (1993), $^+$HADES (2021), ^{x}Hanus *et al.* (2021)

Moesa River, Gravéra

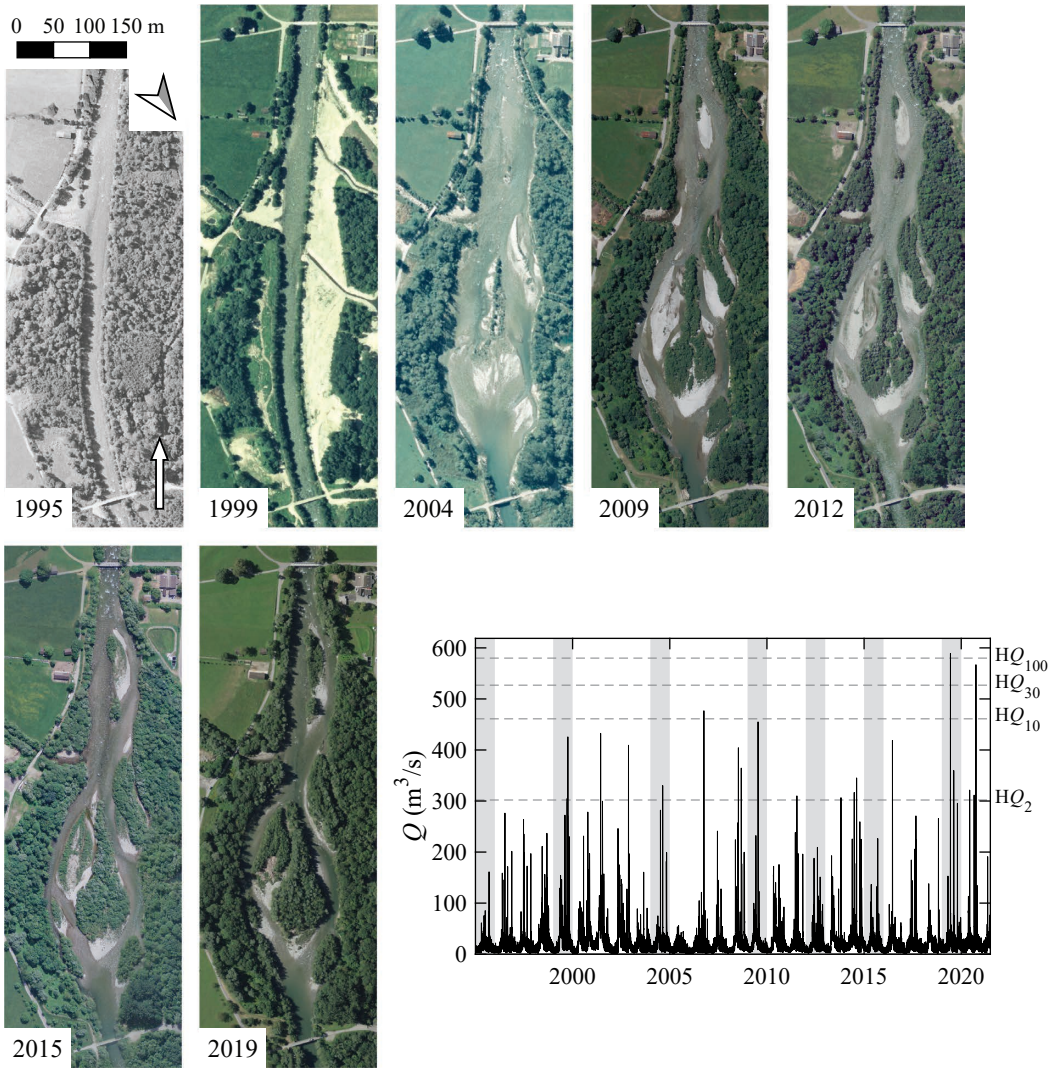

Figure A.3 Temporal evolution of the river widening Gravéra, Moesa River (46°14′53.466″N 9°09′26.584″E), and discharge time series with orthophoto acquisition years marked in gray (Photos: Federal Office of Topography; discharge data: Federal Office for the Environment)

Table A.3 Characteristics of the river widening Gravéra, Moesa River

Width (channel → widening)	30 m → 130 m
Slope	0.006
D_m, D_{90} *	7.9 cm, 19.3 cm
Discharge+	> 80% of natural yearly discharge remaining; hydropeaking
Bed-loadx	50-80% of the natural bed-load remaining
Morphodynamics	Limited channel shifting, stabilization by vegetation growth

*VAW (2007), +HADES (2021), xHanus *et al.* (2021)

Moesa River, Rosera

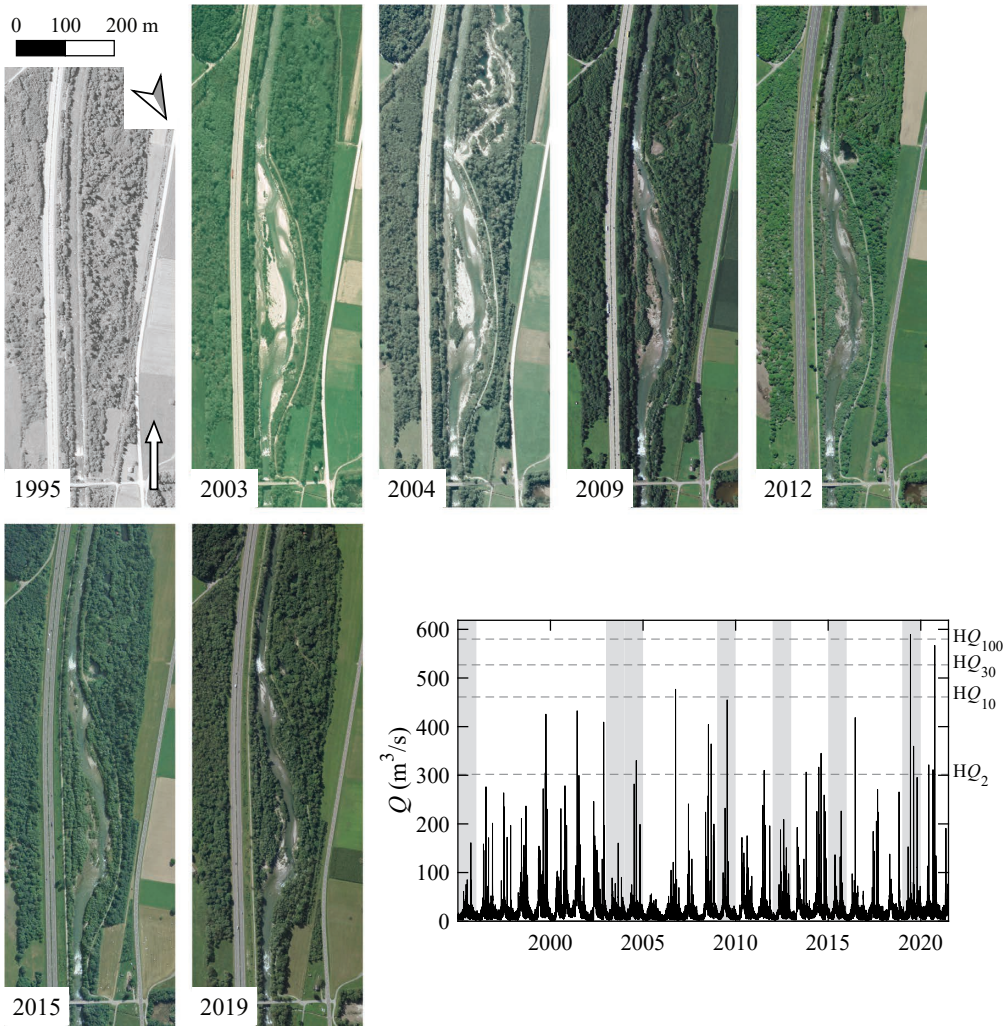

Figure A.4 Temporal evolution of the river widening Rosera, Moesa River (46°18′06.616″N 9°11′20.536″E), and discharge time series with orthophoto acquisition years marked in gray (Photos: Federal Office of Topography; discharge data: Federal Office for the Environment)

Table A.4 Characteristics of the river widening Rosera, Moesa River

Width (channel → widening)	20 m → 60 m
Slope	0.0093
D_m, D_{90} *	7.9 cm, 19.3 cm
Discharge+	> 80% of natural yearly discharge remaining; at least 20% discharge increase in winter; hydropeaking
Bed-loadx	50-80% of the natural bed-load remaining
Morphodynamics	Limited channel shifting, stabilization by vegetation growth

*VAW (2007), +HADES (2021), xHanus *et al.* (2021)

Linth River, Chli Gäsitschachen

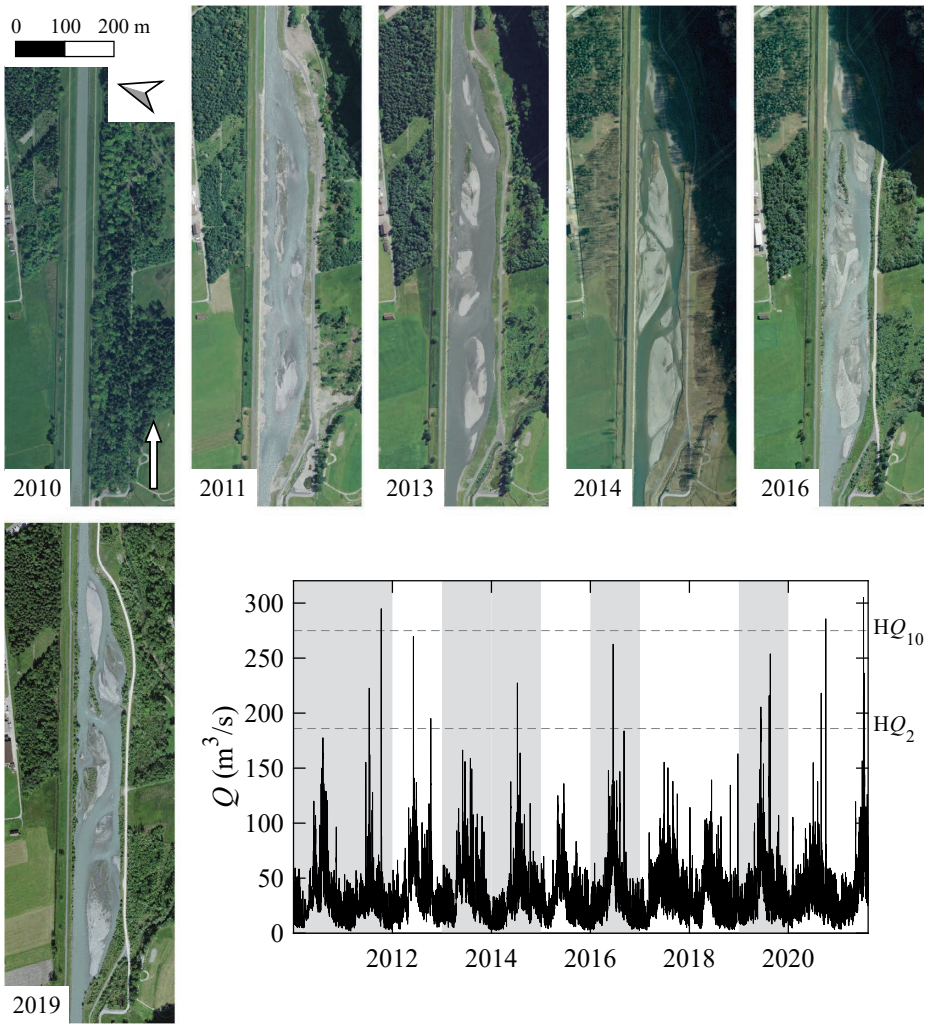

Figure A.5 Temporal evolution of the river widening Chli Gäsitschachen, Linth River (47°07′10.558″N 9°05′44.149″E), and discharge time series with orthophoto acquisition years marked in gray (Photos: Federal Office of Topography; discharge data: Federal Office for the Environment)

Table A.5 Characteristics of the river widening Chli Gäsitschachen, Linth River

Width (channel → widening)	23 m → 60 m
Slope	0.0032
D_m, D_{90} *	10 cm, 23.2 cm
Discharge+	> 80% of natural yearly discharge remaining; at least 20% discharge increase in winter; hydropeaking
Bed-loadx	50-80% of the natural bed-load remaining
Morphodynamics	Regular channel shifting

*VAW (2009), +HADES (2021), xSchälchli and Kirchhofer (2012)

La Broye River, Les Iles de Villeneuve

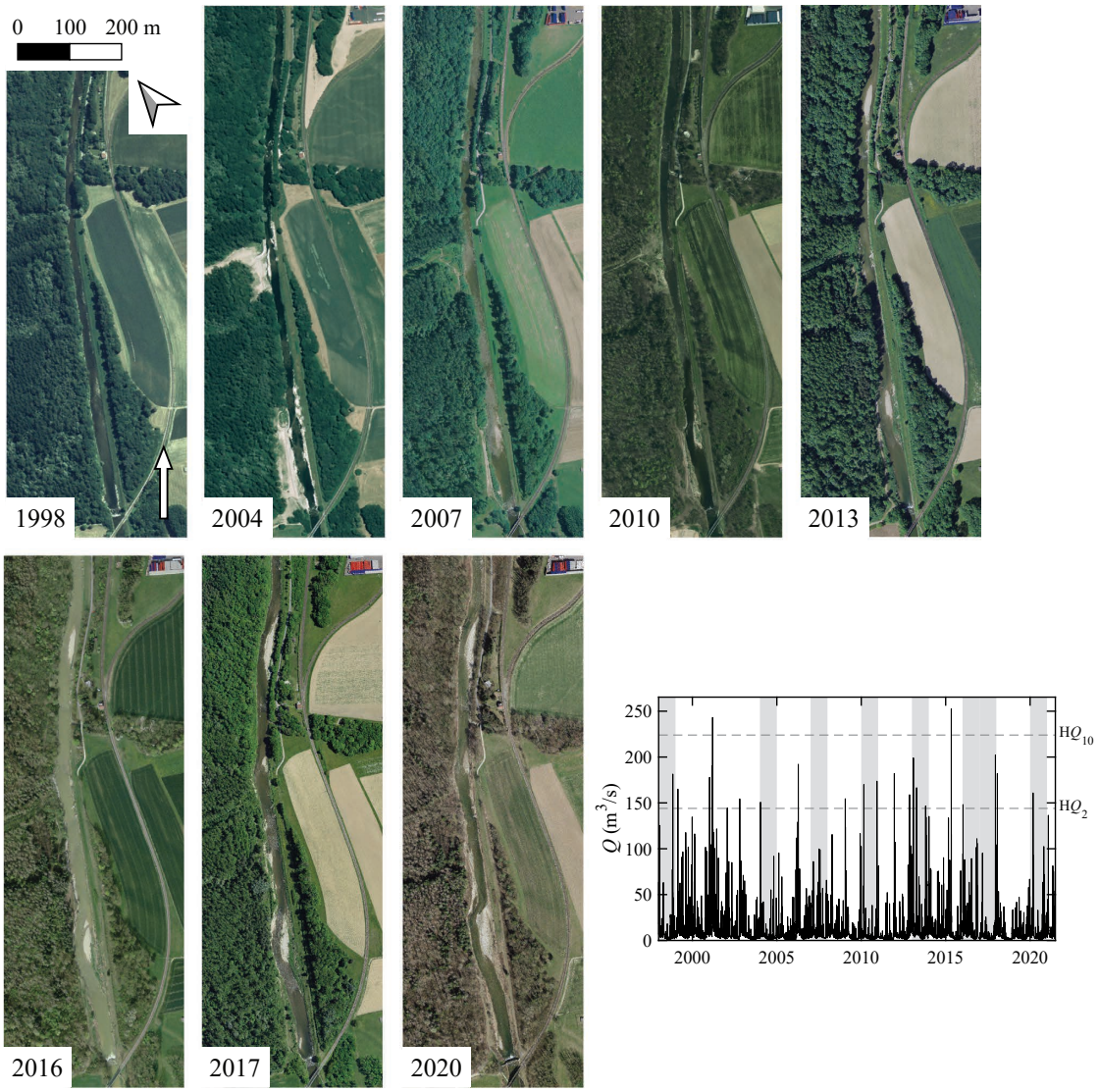

Figure A.6 Temporal evolution of the river widening Les Iles de Villeneuve, La Broye River (46°43′39.629″N 6°51′35.537″E), and discharge time series with orthophoto acquisition years marked in gray (Photos: Federal Office of Topography; discharge data: Federal Office for the Environment)

Table A.6 Characteristics of the river widening Les Iles de Villneuve, La Broye River

Width (channel → widening)	17 m → 48 m
Slope	0.0035
D_m, D_{90} *	5 cm, 12-15 cm
Discharge+	no specifications
Bed-loadx	20-50% of the natural bed-load remaining
Morphodynamics	Limited channel widening

*PL-LCH (2010), +HADES (2021), xHanus *et al.* (2021)

Kander River, Schwandi-Ey

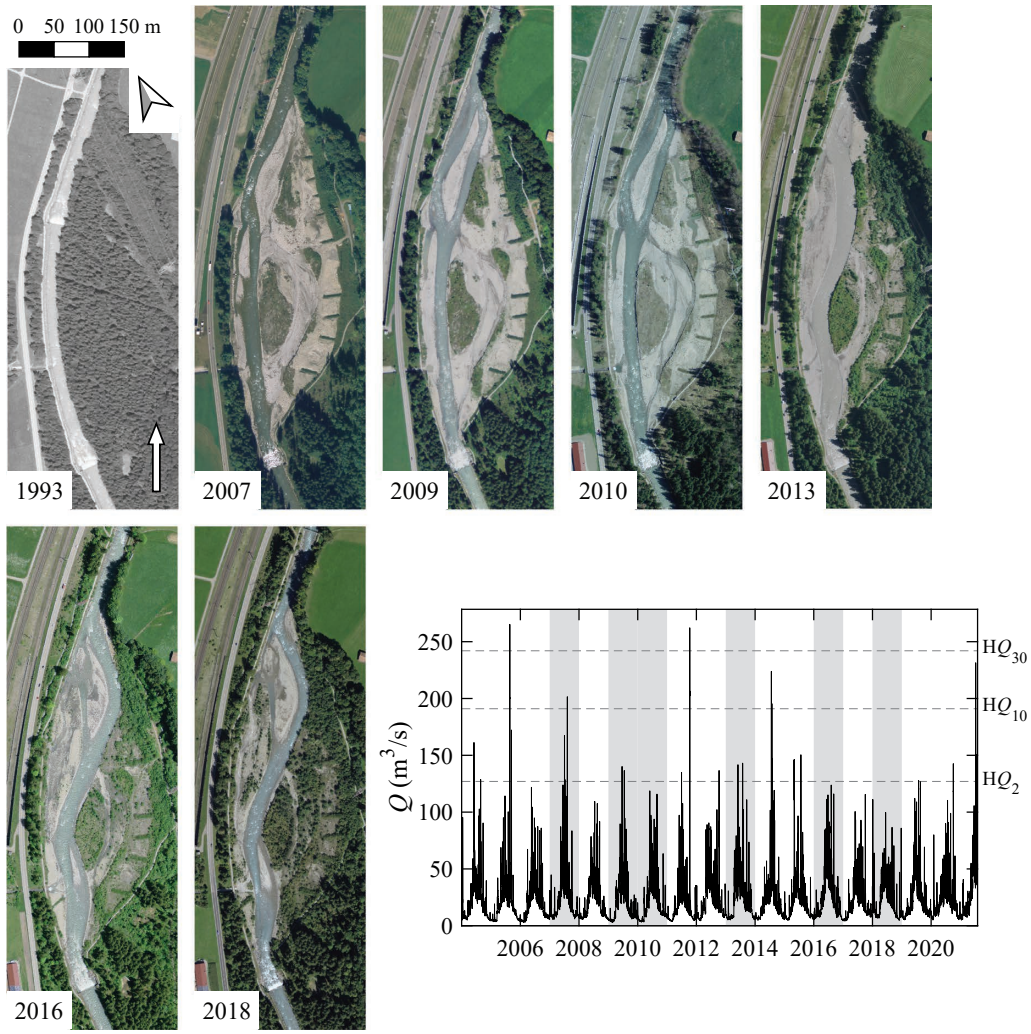

Figure A.7 Temporal evolution of the river widening Schwandi-Ey, Kander River (46°36′12.366″N 7°39′50.662″E), and discharge time series with orthophoto acquisition years marked in gray (Photos: Federal Office of Topography; discharge data: Federal Office for the Environment)

Table A.7 Characteristics of the river widening Schwandi-Ey, Kander River

Width (channel → widening)	20 m → 90 m
Slope	0.013
D_m, D_{90} *	10-14 cm, 27-35 cm
Discharge+	no specifications
Bed-loadx	0-20% of the natural bed-load remaining
Morphodynamics	Some channel shifting, potential stabilization due to vegetation growth and the absence of large floods in recent years

*HZP (2004), +HADES (2021), xSchälchli and Kirchhofer (2012)

Kander River, Augand

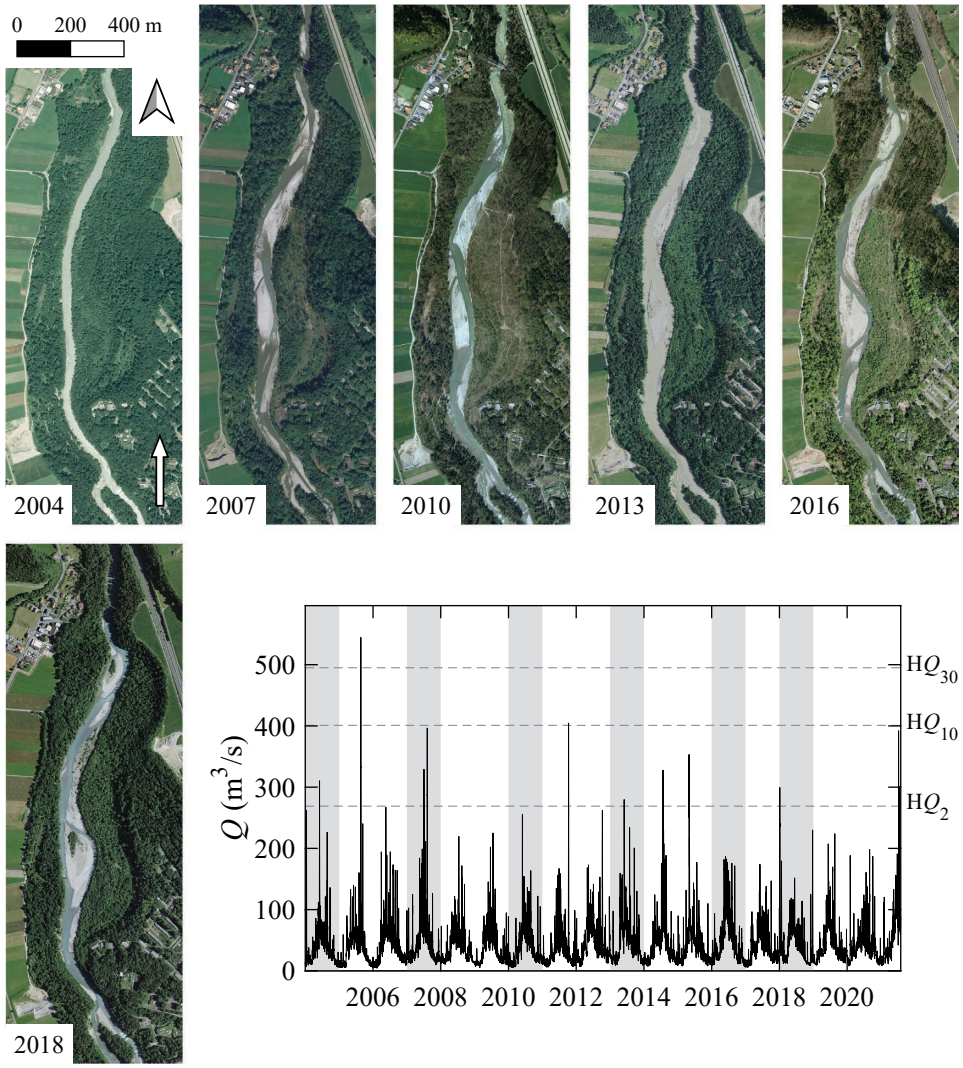

Figure A.8 Temporal evolution of the river widening Augand, Kander River (46°41′56.164″N 7°37′54.114″E), and discharge time series with orthophoto acquisition years marked in gray (Photos: Federal Office of Topography; discharge data: Federal Office for the Environment)

Table A.8 Characteristics of the river widening Augand, Kander River

Width (channel → widening)	32 m → 140 m
Slope	0.0065
D_m, D_{90} *	10-11 cm, 27-35 cm
Discharge+	> 41-60% of natural yearly discharge remaining
Bed-loadx	20-50% of the natural bed-load remaining
Morphodynamics	Regular channel shifting, potential stabilization due to vegetation growth and the absence of large floods in recent years

*HZP (2004), +HADES (2021), xSchälchli and Kirchhofer (2012)

Landquart River, Schierser Sand

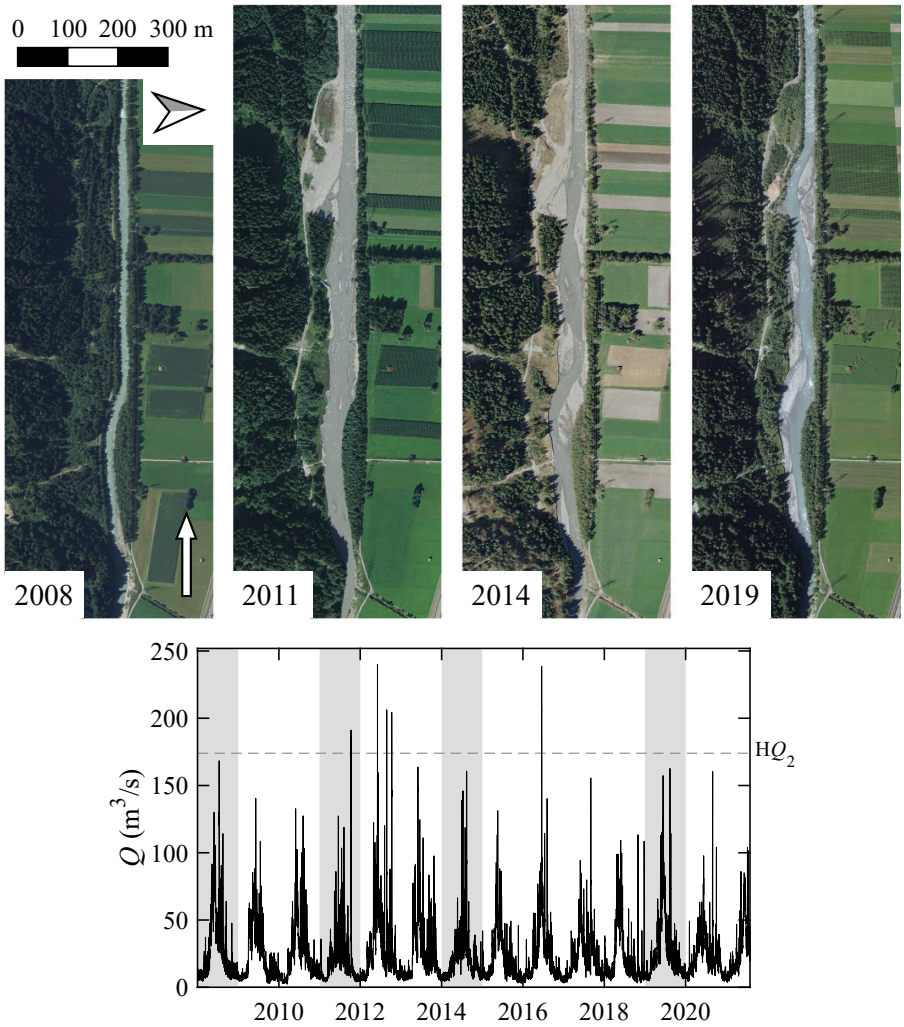

Figure A.9 Temporal evolution of the river widening Schierser Sand, Landquart River (46°58′21.912″N 9°39′46.178″E), and discharge time series with orthophoto acquisition years marked in gray (Photos: Federal Office of Topography; discharge data: Federal Office for the Environment)

Table A.9 Characteristics of the river widening Schierser Sand, Landquart River

Width (channel → widening)	25 m → 65 m
Slope	0.01
D_{50}, D_{90} *	6.6 cm, 25 cm
Discharge+	> 80% of natural yearly discharge remaining
Bed-loadx	50-80% of natural bed-load remaining
Morphodynamics	Limited channel shifting, mostly maintaining single-thread morphology, vegetation growth on stable areas

*VAW (2008), +HADES (2021), xSchälchli and Kirchhofer (2012)